Characterization of capacitance soil moisture sensors for the automated scheduling of drip irrigation in orchards

Jesús María Dominguéz Niño

Universitat de Lleida

TESI DOCTORAL

Characterization of capacitance soil moisture sensors for the automated scheduling of drip irrigation in orchards

Jesús María Domínguez Niño

Memòria presentada per optar al grau de Doctor
per la Universitat de Lleida
Programa de Doctorat en Ciència i Tecnologia Agrària i Alimentària

Director/a
Jaume Casadesús Brugués

Tutor/a
Alexandre Escolà Agustí

Lleida, juliol 2020

This thesis research was carried out in the Efficient Use of Water in Agriculture programme of the Institute for Food and Agricultural Research and Technology (IRTA) Lleida.

The Doctoral Thesis was supported by Spain's National Institute for Agricultural and Food Research and Technology (INIA) (RTA 2013-00045-C04-01).

The funding allowed pre-doctoral stays at:
Instituto de Tierras, Agua y Medio Ambiente (ITAMA), Universidad Nacional del Comahue, Argentina (2017).
Agrosphere Institute (IBG-3), Forschungszentrum Jülich GmbH, Germany (2018).
Department of Land, Air, and Water Resources, University of California (UC Davis), United States (2019).

Quan surts per fer el viatge cap a Ítaca,
has de pregar que el camí sigui llarg,
ple d'aventures, ple de coneixences.
Has de pregar que el camí sigui llarg,
que siguin moltes les matinades
que entraràs en un port que els teus ulls ignoraven,
i vagis a ciutats per aprendre dels que saben.
Tingues sempre al cor la idea d'Itaca.
Has d'arribar-hi, és el teu destí,
però no forcis gens la travessia.
És preferible que duri molts anys,
que siguis vell quan fondegis l'illa,
ric de tot el que hauràs guanyat fent el camí,
sense esperar que et doni més riqueses.
Ítaca t'ha donat el bell viatge,
sense ella no hauries sortit.

Lluís Llach, Ítaca, 1975

Acknowledgements

Parece mentira, pero estos años han pasado volando y me siento afortunado de poder haber contado con un gran equipo de personas durante este viaje y toda la riqueza personal y laboral que me han aportado, como bien dice la canción Itaca de Lluis Llach "Que seas rico de todo lo que habrás ganado haciendo el camino".

En primer lugar, quiero agradecer mi director de tesis, el Dr. Jaume Casadesús, por permitirme embarcar en este reto, por su paciencia, dedicación y perseverancia. También a mi tutor de la UdL, el Dr. Alexandre Escolà por acompañarme e implicarse en esta aventura.
A mis compañeros Maite Prats y Jordi Oliver por su generosidad y ayuda desinteresada cuando lo he necesitado. Al resto del equipo de Uso Eficiente del Agua: Xavi, Ana, Gemma, Christian, Omar, Quim, David, Joan, Mercè, Carles, Jesús, J. Virgili, J. Ballber, J. Rufat, Arnau, Aurica, Amadeu, Héctor, Aurora y Dolors.

Al Dr. Gerard Arbat de la UdG por compartir su experiencia y conocimiento en HYDRUS.
Al Dr. Federico Horne y Dra. Gabriela Polla del ITAMA por su colaboración, aportaciones y sobre todo por hacerme sentir como en casa.
To Dr. Heye Bogena and Dr. Sander Huisman for granting me the opportunity to join their lab at Forschungszentrum Jülich and for dedicating their time and knowledge during my stay in Germany.
To Dr. Isaya Kisekka and Dr. Iael Raij-Hoffman from UC Davis for their guidance and advice in the simulation world.

A todas las personas que conocí durante las estancias y compartieron su tiempo y aventuras conmigo: Analía, Gustavo, Vanina, Guillermina, Juan Pablo, Carol, Santi, Flor, Estela, Nuria, Irene, Neda, Ivan, Mauricio, Florian, Philipp, Sylvain, Apurv, Mrinal, Srini, Floyid, Usama, Tibin, Kelley, Jingyuan, Kim, Mui, Silvia, María, Xavi, Sergio, Christian, Andry…¡Gracias!

A Ilan y Anabel, porque seis años después, por cosas del destino llegamos el mismo día a California y habéis sido como mi familia durante mi estancia allí.

A mis amigos de siempre y en especial a Frantxu, Fanny, Miguel, Marcelo, Pablo, Rober, Silvia, Andrea, Estefanía, Álvaro, Cris, Lety, Alberto y Laura porque, aunque el tiempo pase y nos veamos dos veces al año, siempre estamos ahí dando guerra.

A tota la gent que s'ha creuat amb mi durant la meva estada a Lleida, per compartir el seu temps i bons moments amb mi: Camila, Adelaida, Marc, Carmen, Mari, Jaume, Adrià, Eva, Cris (x2), Josep, Esther, Soraya, Vicente, Iván, Héctor… i sobretot a tu Kiko, pel teu altruisme, estar sempre a peu del canó, per ensenyar-me els racons d'aquesta magnífica terra i ser un compi d'aventures de deu.

A mis padres y mi hermana, por ser la luz de mi camino, por su apoyo incondicional y estar siempre a mi lado a pesar de la distancia, pero sobre todo por enseñarme que a la palabra imposible le sobran dos letras, porque gracias a vosotros he llegado aquí.

RESUM

La sostenibilitat econòmica i ambiental de l'agricultura en regadiu requereix la millora dels sistemes de reg. L'optimització del reg en una parcel·la requereix proporcionar la dosi adequada d'aigua al moment adequat per a satisfer les necessitats del cultiu, que varien espacialment i amb el pas del temps. Un dels factors més importants a considerar és la humitat del sòl, que es pot mesurar de moltes maneres. Els sensors que es basen en la capacitància són dispositius interessants per a controlar i programar el reg. Aquests sensors són populars perquè proporcionen mesures contínues del contingut d'aigua del sòl, són robustos, de baix cost i requereixen poc manteniment. Tot i que les mesures d'aquests sensors tenen bona exactitud al laboratori, quan s'instal·len en plantacions amb reg per degoteig mostren grans diferències entre sensors. Això dificulta fer valoracions i prendre decisions. Per tant, és interessant conèixer i comprendre quines són les incerteses pràctiques d'aquestes mesures respecte a la variabilitat real del contingut d'aigua del sòl en una plantació regada per degoteig. El coneixement dels factors implicats permetrà optimitzar l'ús d'aquests sensors, quant a aspectes com el seu nombre i ubicació en el sòl, així com la seva interpretació i integració en el flux de treball de la programació automatitzada del reg. La tesi s'estructura en quatre capítols. Els resultats mostren que les diferències entre els sensors individuals en condicions de laboratori són insignificants i que un calibratge específic considerant el sòl local millora la precisió de les mesures. Independentment dels sensors, la dinàmica 3D de l'aigua del sòl en aquest tipus d'escenari es pot simular adequadament en tres dimensions mitjançant el model HYDRUS-3D, utilitzant paràmetres hidràulics determinats pel mètode HYPROP + WP4 i específics per al sòl de cada parcel·la. Tanmateix, la dinàmica de l'aigua del sòl prevista per HYDRUS-3D només pot explicar una fracció de les diferències observades entre sensors. La variació addicional es podria explicar pels patrons més arbitraris i de grans contrastos que es donen en la superfície de sòl mullat pels emissors. Malgrat aquestes limitacions pràctiques, l'ús de sensors que es basen en la capacitància per a la programació automatitzada del reg per degoteig es demostra factible, sempre que es segueixin els enfocaments adequats quant a la ubicació dels sensors, la seva interpretació i el mètode de programació del reg.

Paraules clau: Reg per degoteig, contingut d'aigua en sòl, sensor de capacitància, calibratge, HYDRUS-3D, IRRIX, automatització

.

RESUMEN

La sostenibilidad económica y ambiental de la agricultura de regadío requiere la mejora de los sistemas de riego. La optimización del riego en una parcela debe proporcionar la dosis adecuada de agua en el momento adecuado para satisfacer las necesidades del cultivo, que varían espacialmente y con el paso del tiempo. Uno de los factores más importantes a considerar es la humedad del suelo, que se puede medir de diversas maneras. Los sensores de capacitancia son dispositivos interesantes para controlar y programar el riego. Estos sensores son populares porque proporcionan mediciones continuas del contenido de agua del suelo, son robustos, de bajo coste y requieren poco mantenimiento. Aunque las mediciones efectuadas por estos sensores tienen buena exactitud en el laboratorio, cuando se instalan en plantaciones con riego por goteo muestran grandes diferencias entre sensores. Esto dificulta establecer consignas y tomar decisiones. Por lo tanto, es interesante conocer y comprender cuáles son las incertidumbres prácticas de estas mediciones respecto a la variabilidad real del contenido de agua del suelo en una plantación regada por goteo. El conocimiento de los factores implicados permitirá optimizar el uso de estos sensores, en cuanto a aspectos como su número y ubicación en el suelo, así como su interpretación e integración en el flujo de trabajo de la programación automatizada del riego. La tesis se estructura en cuatro capítulos. Los resultados muestran que las diferencias entre los sensores individuales en condiciones de laboratorio son insignificantes y que un calibrado específico con el suelo local mejora la precisión de las mediciones. Independientemente de los sensores, la dinámica del agua del suelo en este tipo de escenario se puede simular adecuadamente en tres dimensiones mediante el modelo HYDRUS-3D, utilizando parámetros hidráulicos determinados por el método HYPROP + WP4 y específicos para el suelo de cada parcela. Sin embargo, la dinámica del agua del suelo prevista por HYDRUS-3D sólo puede explicar una fracción de las diferencias observadas entre sensores. La variación adicional se podría explicar por los patrones más arbitrarios y de grandes contrastes que se dan en la superficie de suelo mojado por los goteros. A pesar de estas limitaciones prácticas, el uso de sensores de capacitancia para la programación automatizada del riego por goteo se demuestra factible, siempre que se sigan los enfoques adecuados en cuanto a su instalación, interpretación y método de programación del riego.

Palabras clave: Riego por goteo, contenido de agua en suelo, sensor de capacitancia, calibración, HYDRUS-3D, IRRIX, automatización

ABSTRACT

The economic and environmental sustainability of irrigation agriculture requires the improvement of irrigation systems. The optimization of irrigation on a plot of land requires providing the right dose of water at the right time to meet the water needs of the crop, which vary spatially and over time. One of the most important factors to consider is soil moisture, which can be measured in many ways. Capacitance soil moisture sensors are interesting devices for monitoring and scheduling irrigation. These sensors are popular because they provide continuous measurements of soil water content, are robust, low cost and require little maintenance. Although the measurements by these sensors are accurate in the laboratory, when they are installed in drip-irrigated orchards they show large sensor-to-sensor differences. This makes it difficult to establish guidelines and make decisions. Therefore, it is interesting to know and understand which are the practical uncertainties of such measurements with regard to the actual variability of soil water content in a drip-irrigated orchard. Knowledge of the factors involved will allow to optimize their use, regarding aspects such as the number and location of the sensors as well as their interpretation and integration in the workflow of automated irrigation scheduling. The thesis is structured in four chapters. The results show that the differences between individual sensors in laboratory conditions are negligible and that a site-specific calibration considering the local soil improves the accuracy of the measurements. Independently of the sensors, the 3D dynamics of soil water in a drip irrigated orchard can be simulated adequately by HYDRUS-3D model, using site-specific soil hydraulic parameters determined by the method of HYPROP + WP4. However, the soil water dynamics predicted by HYDRUS-3D can only explain a fraction of the observed sensor-to-sensor differences. Additional variations can be explained by the more arbitrary and sharply defined patterns of soil surface wetted by the drippers. Despite these practical limitations, the use of capacitance sensors for automated irrigation scheduling in orchards is proven feasible, provided that the adequate approaches are followed regarding sensor location, interpretation and irrigation scheduling method.

Keywords: Drip irrigation, soil water content, capacitance sensor, calibration, HYDRUS-3D, IRRIX, automation

INTRODUCTION

Water as a resource

Water is essential for socioeconomic development, energy and food production, healthy ecosystems and for the survival of humans (United Nations - Water, 2020). The most important uses of water are related to agriculture, industry and domestic consumption (Mateo-Sagasta and Burke, 2010). The increase in the world's population and the consequent increase in water consumption makes it necessary to manage water resources properly (Ashofteh et al., 2015). World agriculture consumes approximately 70% of freshwater withdrawn per year (UNESCO, 2015) and approximately 17% of the world's cropland is irrigated but produces 40% of the world's food (FAO, 2002). This situation may be intensified by climate change, which will affect the availability of water resources for both rain-fed and irrigated agriculture. Also, due to rising temperatures and extreme events such as drought and more intense and longer-lasting floods, causing fluctuations of food production and important effects on global food security (Parry et al., 1999; Stocker et al., 2013). In addition, in 2018, the United Nations asserted that people should seek to find a solution to overcome the water problems of the 21st century and efficiently address global challenges such as climate change, food and water security, disaster risk reduction and economic and social development (Boretti and Rosa, 2019). Traditionally, irrigation has been increased to augment agricultural production, , but currently, due to the decrease in water resources, the use of efficient irrigation systems is necessary (Hagin et al., 2003).

Apple crop

The Mediterranean basin has long been a site of temperate fruit and nut production (Tous and Ferguson, 1996). Among the fruit crops, the apple tree stands out. The apple (*Malus domestica* Mill.) is native to Central Asia. Most apple trees are grown in temperate zones due to their need for a minimum number of cold hours for proper bud break in the spring season. There are more than 7500 known varieties, which differ in fruit size, color, taste and final tree size, even when planted with the same rootstock (Steduto et al., 2012). The apple, which grows in areas characterized by water scarcity is the fruit crop with the largest surface area in the world after grape (Girona et al., 2010), and in terms of production it ranks third after banana and grape. In 2018, total apple production was 125.3 million tons, with a harvested area exceeding 6.9 million hectares and an average yield of 16.4 t/ha. In Spain, the harvested area was around 30000 hectares, production was 0.56 million tons and yield was 18.8 t/ha (FAO, 2020). The water requirements of the apple tree are determined by the evaporative demand of the atmosphere and the amount of energy intercepted by the canopy. Trees with low crop loads use less water than trees with commercial loads (Girona et al., 2011).

Crop water requirements

The usual method for determining crop water requirements is based on the water balance (Doorenbos and Pruit, 1977, Allen et al., 1998). The most relevant component of the balance to determine irrigation is crop evapotranspiration (ET_C), which is estimated from the evapotranspiration of a reference crop (ET_O) and a crop coefficient (K_C) according to:

$$ET_C = ET_O \times K_C \quad \text{(Eq. 1)}$$

where ET_O represents the demand imposed by meteorological conditions and K_C integrates the physical and biophysical differences between the reference crop and the crop whose evapotranspiration is to be estimated.

However, in fruit crops, this approach may be uncertain because different conditions vary and event occur from one plot to another within the same crop variety. For example, irrigation requirements can vary between plots due to differences in the planting pattern and row orientation (Intrieri et al., 1998), in the particular variety (Higgins et al., 1992), in the rootstock (Li et al., 2002) or the shape and size of the canopy, where a crop coefficient adjustment based on the soil cover fraction can be used (Fereres et al., 1981; Allen and Pereira, 2009). In addition, radiation interception by the crop is one of the processes with the greatest impact on water needs and production in crops with discontinuous canopies (Green et al. 2006; Lakso, 2008). The relationship between K_C and radiation interception is not constant and varies between phenological stages of the crop (Girona et al., 2011; Auzmendi et al., 2011; Marsal et al. 2013). Therefore, in order to schedule irrigation, it is necessary to undertake differential management and provide different amounts of water in the different subzones according to their water requirements. In this sense, it is necessary consider the precision agriculture, which is the mechanism that controls the land productivity, maximizing the yield and minimizing the impact by automating the complete agriculture processes (Keswani et al., 2019).

Drip irrigation

In many agricultural scenarios, drip irrigation is preferred over other irrigation methods due to its high application efficiency, as it provides water to a limited volume of soil in the region where the greatest water extraction by plants occurs, reducing losses by surface evaporation and deep percolation (Naglic et al., 2014).

Surface drip irrigation is much more widespread than subsurface drip irrigation partly due to the more easily observable indicators of operation and performance, but mainly because growers think that subsurface drip irrigation has a higher economic risk, especially when managing large irrigated areas (Lamm et al., 2012). The distribution of moisture within a volume of wet soil is known as the wet bulb (Arraes et al., 2019). The

factors that affect wet bulb formation are soil physical properties (texture, bulk density, initial water content…), crop absorption by root system, soil surface evaporation and the intensity of the irrigation rate. These factors are in turn affected by, amongst many others, solar radiation, air temperature, air humidity and crop growing conditions (Lazarovitch et al., 2007; Hao et al., 2007; Kandelous et al., 2011). This wet soil volume is one of the most important factors that need to be taken into account in the design of drip irrigation systems, especially the wetted depth in the soil profile and the radius on the soil surface (Kilic, 2020).

Soil water dynamics and simulation

In irrigated crops, the wetting profile in the root zone is dynamic and is influenced by crop characteristics, the irrigation system and soil hydraulic properties (Soulis et al., 2015). Drip irrigation is one of the technologies increasingly being used in modern irrigated agriculture, with a high potential for water use efficiency and good economic viability (Lei et al., 2003). Drip irrigation is an irrigation method that allows accurately controlled application of water, allowing water to drip slowly near the plant roots, generating wet bulbs (Moncef and Khemaies, 2016). Wetting patterns can be obtained either directly by field measurements or by simulation using suitable mathematical models. In most of these models, the Richards equation, which governs water flow under unsaturated flow conditions is used to simulate the soil water matric potential or soil water distribution (Elmaloglou et al., 2013; Berardi et al., 2016). Thanks to the simulations, the effect of the soil properties on the moisture pattern around the emitters can be seen. WetUP (Cook et al., 2003), FUSSIM (Heinen, 2001), or HYDRUS (Simunek et al., 2016) are some of the models used to simulate soil water dynamics.

Soil moisture sensors

Water content (also known as moisture content) is the quantity of water contained in a material, such as soil, called soil moisture. Water content can be expressed as a ratio, ranging from 0 (completely dry) to the value of the material's porosity at saturation (Kumar et al., 2016). The volumetric water content (VWC) is a key parameter for the study of precision agriculture (Deng et al., 2019). Besides destructive gravimetric sampling, electromagnetic methods (EM) such as time domain reflectometry (TDR), time domain transmission (TDT) and capacitance sensors and impedance sensors are commonly used to measure the soil water content (SWC) at the point scale (Bogena et al., 2017). Capacitance soil sensors, such as the 10HS and EC-5 sensors, are frequency domain reflectometry (FDR)-based electrical sensors, whose operating principle consists of measuring the dielectric constant or permittivity of the soil to calculate its moisture content (Lopez-Aldaba et al., 2018). Capacitance soil sensors are preferred because they are reasonably robust, precise, consume little energy, provide real-time SWC at a low cost and require low maintenance (Domínguez-Niño et al., 2019). However, although in

laboratory conditions the accuracy of these sensors is good (Spelman et al., 2013), when they are installed in drip-irrigated orchards they show large sensor-to-sensor variability. This variability may be due to the size, shape and alignment of the wet bulb to the dripper as well as factors such as texture, gravels, roots, bulk density, macropores, etc (Dane and Hopmans, 2002). For this reason, it is necessary to know and understand what sources of variability are involved in the soil water content measurements. This is additionally of interest because it allows identification of the positions and depths that show the most relevant information to support making decisions in irrigation scheduling.

Moisture sensor irrigation

A disadvantage of irrigation scheduling based only on the water balance method is that the balance estimate may not be representing the real situation for a particular case. Inaccuracy in the inputs or outputs of the water balance will produce a systematic error that will cumulate over the course of the crop cycle.

Moisture sensor irrigation control is an alternative, which makes it possible to adjust irrigation to the precise needs of a particular plot and to the actual water availability of the plants, without relying on external reference values. The simplest versions of control with soil water sensors consist of triggering / inhibiting irrigation when measurements cross above or below pre-set threshold values (Muñoz-Carpena et al., 2005; Cáceres et al., 2007; Dukes et al., 2010). Other systems can modulate the daily irrigation intensity taking into account the effect observed in previous irrigation events (Singh et al., 1995). Water balance and control in response to sensors have complementary advantages and disadvantages, but their combination does allow the advantages of both to be exploited. One way of combining them is to periodically apply an irrigation whose dose is predetermined by an estimate of ET_C, but with a system that turns off the irrigation when the soil moisture exceeds a certain threshold (Muñoz-Carpena et al, 2005). Another advanced way consists of combining a water balance based on the estimation of ET_C, with the soil water status sensors' measurements, which can be used to readjust the ET_C estimation (Bacci et al., 2008, Casadesús et al., 2012). Capacitance-type moisture sensors are the most commonly used type to measure the soil water content due to their low cost and maintenance and their lower energy consumption compared to TDR sensors (Visconti et al., 2014; Domínguez-Niño et al., 2019). Capacitive sensors measure the dielectric permittivity of the soil, which depends mainly on the water content (Campbell, 1990; Bogena et al., 2007; Kizito et al., 2008). The dielectric properties of water depend on temperature and electrical conductivity, so the accuracy of measurements is affected by these factors (Kizito et al, 2008; Kargas and Soulis, 2019). In localized irrigation, the difficulty in using soil moisture sensors is due to the complex spatial distribution that occurs in this type of irrigation. Drip irrigation is characterized by the formation of wet bulbs under the drippers while the rest of the soil may be only slightly affected or not at all by the irrigation (Millán et al., 2020). Therefore, it is necessary to consider where and

how to install the sensors and how to interpret the measurements given the spatial variability.

The optimal location of the sensors within the frame of a dripper – regarding depth and position relative to the dripper- must not be confused with the optimal location of monitored spots within a plot -regarding their representativeness of the whole cropped area-. One problem that affects the efficient management of irrigation is the heterogeneity of the plots. One solution is to adjust the design of the irrigation sectors to make them homogeneous units (Poh-Kok, 1987). However, this approach has limitations and it is common to find in the same sector areas that behave differently in terms of water balance. These differences may be in the vegetation cover or variations in the depth or other properties of the soil. The location of the monitored spots for soil moisture -typically several sensors- have to provide a representative view of the whole irrigation sector to be controlled. Therefore, the problem is to decide the ideal location and the optimal number of monitored spots to install (Soulis et al., 2015; Adeyemi et al., 2017).

Automated irrigation with soil moisture sensors

The most common use of these sensors in crops has been for the supervision of the irrigation through a human operator. However, there are also examples where it has been used to automatically adjust irrigation (Fernández et al., 2008; Casadesús et al., 2012). The main limitations of manual irrigation with moisture sensors is the large amount of data that are generated, which, alternatively, can easily be processed by automated systems. These data must be filtered, analysed and interpreted to be useful. For the irrigator, all the information from the moisture sensors means additional work due to the analysis and time required. Consequently, it is necessary to automate irrigation through Information and Communication Technologies (ICTs). Regarding the scheduling algorithm, the approach of a water balance tuned by feedback from sensors combines the reliability and predictability of water balance with the spontaneous site-specific adjustment by sensors (Casadesús et al., 2012; Casadesús et al., 2014). This approach allows applying more sophisticated interpretation mechanisms to the series of soil moisture data. For instance, it can apply fuzzy logic to interpret data from moisture sensors using a series of rules.

In addition, it is important to consider how the position and accuracy of sensors can affect irrigation efficiency in soil moisture-based automated irrigation scheduling. This is especially true in drip irrigation where non-uniform water distribution patterns below drippers make the placement of moisture sensors in the soil a key factor in the performance of irrigation scheduling schemes (Coelho and Or, 1996).

Overall, in numerous studies, capacitance-type moisture sensors have been used in laboratory conditions, as well as in field conditions, in scenarios where the spatial heterogeneity of soil moisture is low (rainfed and sprinkler or flood-irrigated crops). However, drip irrigated orchards show great interest for the application of smart

irrigation approaches. Then, given the heterogeneity in soil moisture in this type of orchards, it is necessary to know and understand the phenomena that originate variability in the sensor readings. In this context, this thesis focuses on the problems that affect the use of capacitance moisture sensors in the automation of irrigation in a drip-irrigated orchard.

Literature cited

Adeyemi, O.; Grove, I.; Peets, S.; Norton, T. Advanced monitoring and management systems for improving sustainability in precision irrigation. Sustainability. 2017, 9, 353.

Allen, R.G.; Pereira, L.S.; Raes, D.; Smith, M. Crop evapotranspiration. Guidelines for computing crop water requirements. FAO Irrigation and Drainage Paper No. 56, 1998, Rome.

Allen, R. G.; Pereira, L. S. Estimating crop coefficients from fraction of ground cover and height. Irrig. Sci., 2009, 28, 17-34.

Arraes, F. D.; Miranda, J. H. D.; Duarte, S. N. Modeling soil water redistribution under surface drip irrigation. Eng. Agricola, 2019, 39, 55-64.

Ashofteh, P. S.; Haddad, O. B.; Akbari-Alashti, H.; Marino, M. A. Determination of irrigation allocation policy under climate change by genetic programming. J. Irrig. Drain. Eng. 2015, 141, 04014059.

Auzmendi, I.; Mata, M.; Lopez, G.; Girona, J.; Marsal, J. Intercepted radiation by apple canopy can be used as a basis for irrigation scheduling. Agric. Water Manag. 2011, 98, 886-892.

Bacci, L.; Battista, P.; Rapi, B. An integrated method for irrigation scheduling of potted plants. Sci. Hortic. 2008, 116, 89-97.

Berardi, M.; Andrisani, A.; Lopez, L.; Vurro, M. A new data assimilation technique based on ensemble Kalman filter and Brownian bridges: an application to Richards' equation. Comput. Phys. Commun. 2016, 208, 43-53.

Bogena, H.R.; Huisman, J.A.; Schilling, B.; Weuthen, A.; Vereecken, H. Effective calibration of low-cost soil water content sensors. Sensors 2017, 17, 208.

Bogena, H. R.; Huisman, J. A.; Oberdörster, C.; Vereecken, H. Evaluation of a low-cost soil water content sensor for wireless network applications. J. Hydrol. 2007, 344, 32-42.

Boretti, A.; Rosa, L. Reassessing the projections of the World Water Development Report. NPJ Clean Water. 2019, 2, 1-6.

Cáceres, R.; Casadesús, J.; Marfà, O. Adaptation of an automatic irrigation-control tray

system for outdoor nurseries. Biosyst. Eng. 2007, 96, 419-425.

Campbell, J. E. Dielectric properties and influence of conductivity in soils at one to fifty megahertz. Soil Sci. Soc. Am. J. 1990, 54, 332-341.

Casadesús, J.; Mata, M.; Marsal, J.; Girona, J. A general algorithm for automated scheduling of drip irrigation in tree crops. Comput. Electron. Agric. 2012, 83, 11-20.

Casadesus, J., Mata, M., Marsal, J., Girona, J. Spontaneous Accommodation of Irrigation Scheduling to Groundwater through Feedback from Soil Water Sensors in Drip Irrigated Peach. Acta Horticulturae. 2014, 1038, 207-213.

Coelho, E. F.; Or, D. Flow and uptake patterns affecting soil water sensor placement for drip irrigation management. Trans. ASAE. 1996, 39, 2007-2016.

Cook, F. J.; Thorburn, P. J.; Fitch, P.; Bristow, K. L. WetUp: a software tool to display approximate wetting patterns from drippers. Irrig. Sci. 2003, 22, 129-134.

Dane, J.H.; Hopmans, J.W. Water retention and storage. In: Dane, J.H., Topp, G.C. (Eds.), Methods of Soil Analysis. Part 4, SSSA Book Series No. 5. 2002, Soil Science Society of America Journal, Madison WI.

Deng, X.; Gu, H.; Yang, L.; Lyu, H.; Cheng, Y.; Pan, L.; Fu, Z; Cui, L; Zhang, L. A method of electrical conductivity compensation in a low-cost soil moisture sensing measurement based on capacitance. Measurement. 2020, 150, 107052.

Domínguez-Niño, J. M.; Bogena, H. R.; Huisman, J. A.; Schilling, B.; Casadesús, J. On the accuracy of factory-calibrated low-cost soil water content sensors. Sensors. 2019, 19, 3101.

Doorenbos, J.; Pruitt, W.O. Guidelines for predicting crop water requirements. FAO Irrigation and Drainage Paper No. 24, 1977, Rome.

Dukes, M. D.; Zotarelli, L.; Morgan, K. T. Use of irrigation technologies for vegetable crops in Florida. Horttechnology. 2010, 20, 133-142.

Elmaloglou, S.; Soulis, K. X.; Dercas, N. Simulation of soil water dynamics under surface drip irrigation from equidistant line sources. Water Resour. Manag. 2013, 27, 4131-4148.

FAO. Crops and Drops: Making the Best Use of Water in Agriculture; Food and Agriculture Organization of the United Nations: Rome, Italy, 2000.

FAO. Online database FAOSTAT 2020, available in http://www.fao.org/faostat/en/.

Fereres, E.; Pruitt, W. O.; Beutel, J. A.; Henderson, D. W.; Holzapfel, E.; Shulbach, H.; Uriu, K. Evapotranspiration and drip irrigation scheduling. In Drip irrigation management. Fereres E. Tech. Ed., Division of Agricultural Sciences, University of California, CA, USA, 1981: pp. 8-13.

Fernández, J. E.; Green, S. R.; Caspari, H. W.; Diaz-Espejo, A.; Cuevas, M. V. The use of sap flow measurements for scheduling irrigation in olive, apple and Asian pear trees and in grapevines. Plant Soil, 2008, 305, 91-104.

Girona, J.; Behboudian, M. H.; Mata, M.; Del Campo, J.; Marsal, J. Exploring six reduced irrigation options under water shortage for 'Golden Smoothee' apple: responses of yield components over three years. Agric. Water Manag. 2010, 98, 370-375.

Girona, J.; Del Campo, J.; Mata, M.; Lopez, G.; Marsal, J. A comparative study of apple and pear tree water consumption measured with two weighing lysimeters. Irrig. Sci. 2011, 29, 55-63.

Green, S. R.; Kirkham, M. B.; Clothier, B. E. Root uptake and transpiration: From measurements and models to sustainable irrigation. Agric. Water Manag. 2006, 86, 165-176.

Hao, A.; Marui, A.; Haraguchi, T.; Nakano, Y. Estimation of wet bulb formation in various soil during drip irrigation. J. Fac. Agr. Kyushu U. 2007, 52, 187.

Hagin, J.; Sneh, M.; Lowengart-Aycicegi, A. Fertigation - Fertilization through Irrigation. International Potash Institute, IPI Research Topics no. 23. Ed. by A.E- Johnston. Basel, Switzerland, 2002.

Heinen, M. FUSSIM2: brief description of the simulation model and application to fertigation scenarios Agronomie. 2001, 21, 285-296.

Higgins, S. S.; Larsen, F. E.; Bendel, R. B.; Radamaker, G. K.; Bassman, J. H.; Bidlake, W. R.; Al Wir, A. Comparative gas exchange characteristics of potted, glasshouse-grown almond, apple, fig, grape, olive, peach and Asian pear. Sci. Hortic. 1992, 52, 313-329.

Intrieri, C.; Poni, S.; Rebucci, B.; Magnanini, E. Row orientation effects on whole-canopy gas exchange of potted and field-grown grapevines. Vitis. 2015, 37, 147.

Kandelous, M. M.; Simunek, J.; Van Genuchten, M. T.; Malek, K. Soil water content distributions between two emitters of a subsurface drip irrigation system. Soil Sci. Soc. Am. J. 2011, 75, 488-497.

Kargas, G.; Soulis, K. X. Performance evaluation of a recently developed soil water content, dielectric permittivity, and bulk electrical conductivity electromagnetic sensor. Agric. Water Manag. 2019, 213, 568-579.

Keswani, B.; Mohapatra, A. G.; Mohanty, A.; Khanna, A.; Rodrigues, J. J.; Gupta, D.; de Albuquerque, V. H. C. Adapting weather conditions based IoT enabled smart irrigation technique in precision agriculture mechanisms. Neural Comput Appl. 2019, 31, 277-292.

Kilic, M. A new analytical method for estimating the 3D volumetric wetting pattern

under drip irrigation system. Agric. Water Manag. 2020, 228, 105898.
Kizito, F.; Campbell, C. S.; Campbell, G. S.; Cobos, D. R.; Teare, B. L.; Carter, B.; Hopmans, J. W. Frequency, electrical conductivity and temperature analysis of a low-cost capacitance soil moisture sensor. J. Hydrol. 2008, 352, 367-378.

Kumar, M. S.; Chandra, T. R.; Kumar, D. P.; Manikandan, M. S. (2016, January). Monitoring moisture of soil using low cost homemade Soil moisture sensor and Arduino UNO. In Proceedings of the 2016 3rd International Conference on Advanced Computing and Communication Systems (ICACCS); Coimbatore, India, 22-23 January 2016; pp. 1-4.

Lazarovitch, N.; Warrick, A. W.; Furman, A.; Simunek, J. Subsurface water distribution from drip irrigation described by moment analyses. Vadose Zone J. 2007, 6, 116-123.

Lakso, A. N. Water relations of apples. In Apples: Botany, Production and Uses. Ferree, D.C. and I.J. Warrington Eds. CAB Interntional, 2003, USA.

Lamm, F. R.; Bordovsky, J. P.; Schwankl, L. J.; Grabow, G. L.; Enciso-Medina, J.; Peters, R. T., Colaizzi, P. D.; Trooien T. P.; Porter, D. O. Subsurface drip irrigation: Status of the technology in 2010. T. ASABE. 2012, 55, 483-491.

Lei, T. W.; Xiao, J.; Li, G. Y.; Mao, J. H.; Wang, J. P.; Liu, Z. Z.; Zhang, J. G. Effect of drip irrigation with saline water on water use efficiency and quality of watermelons. Water Resour. Manag. 2003, 17, 395–408.

Li, F.; Cohen, S.; Naor, A.; Shaozong, K.; Erez, A. Studies of canopy structure and water use of apple trees on three rootstocks. Agric. Water Manag. 2002, 55, 1-14.

Lopez Aldaba, A.; Lopez-Torres, D.; Campo-Bescós, M. A.; López, J. J.; Yerro, D.; Elosua, C.; Arregui, F.J., Auguste, J.-L.; Jamier, R.; Roy, P., López-Amo, M. Comparison between capacitive and microstructured optical fiber soil moisture sensors. Appl. Sci. 2018, 8, 1499.

Marsal, J.; Johnson, S.; Casadesus, J.; Lopez, G.; Girona, J.; Stöckle, C. Fraction of canopy intercepted radiation relates differently with crop coefficient depending on the season and the fruit tree species. Agr. Forest Meteorol. 2014, 184, 1-11.

Mateo-Sagasta, J; Burke, J. Agriculture and water quality interactions: A global overview. SOLAW Background Thematic Report - TR08. Food and Agriculture Organization of the United Nations (FAO). Rome, 2010.

Millán, S.M; Campillo, C.; Casadesús, J.; Pérez-Rodríguez, J. M.; Prieto, M. H. Automatic irrigation scheduling on a hedgerow olive orchard using an algorithm of water balance readjusted with soil moisture sensors. Sensors. 2020, 20, 2526.

Moncef, H.; Khemaies, Z. An analytical approach to predict the moistened bulb volume beneath a surface point source. Agric. Water Manag. 2016, 166, 123-129.

Muñoz-Carpena, R.; Li, Y. C.; Klassen, W.; Dukes, M. D. Field comparison of tensiometer

and granular matrix sensor automatic drip irrigation on tomato. Horttechnology, 2005, 15, 584-590.

Parry, M.; Rosenzweig, C.; Iglesias, A.; Fischer, G.; Livermore, M. Climate change and world food security: a new assessment. Global Environ. Change. 1999, 9, S51-S67.

Poh-Kok, Ng. Irrigation design: A conceptual framework. In Proceedings of the Asian Regional Symposium on Irrigation Design for Management, Kandy, Sri Lanka, 1987; pp. 61–78.

Soulis, K. X.; Elmaloglou, S.; Dercas, N. Investigating the effects of soil moisture sensors positioning and accuracy on soil moisture-based drip irrigation scheduling systems. Agric. Water Manag. 2015, 148, 258-268.

Spelman, D.; Kinzli, K. D.; Kunberger, T. Calibration of the 10HS soil moisture sensor for southwest Florida agricultural soils. J Irrig. Drain Eng. 2013, 139, 965-971.

Steduto, P.; Hsiao, T.C.; Fereres, E.; Raes, D. Yield response to water of fruit Trees and vines: Guidelines. In Crop yield response to water. FAO Irrigation and drainage paper 66. Food and Agriculture Organization of the United Nations, Rome, Italy, 2012.

Stocker, T. F; Qin, D.; Plattner, G.-K.; Alexander, L. V.; Allen, S. K.; Bindoff, N. L.; Bréon, F.-M.; Church, J. A.; Cubasch, U.; Emori, S.; Forster, P.; Friedlingstein, P.; Gillett, N.; Gregory, J. M.; Hartmann, D. L.; Jansen, E.; Kirtman, B.; Knutti, R.; Kumar, K. K.; Lemke, P.; Marotzke, J.; Masson-Delmotte, V; Meehl, G.A.; Mokhov, I.I.; Piao, S; Ramaswamy, V., Randall, D.; Rhein, M.; Rojas, M.; Sabine, C.; Shindell, D., Talley, L.D.; Vaughan, D.G., Xie, S.P. Technical summary. In Climate change 2013: The physical science basis. Contribution of Working Group I to the Fifth Assessment Report of the Intergovernmental Panel on Climate Change, Cambridge University Press, 2013; pp. 33-115.

Simunek, J.; Van Genuchten, M. T; Sejna, M. Recent developments and applications of the HYDRUS computer software packages. Vadose Zone J. 2016, 15, 25.

Tous, J.; Ferguson, L. Mediterranean fruits. In: Progress in new crops. Janick J. (ed.). ASHS. Alexandria. 1996, 416-430.

UNESCO. The United Nations World Water Development Report 2015: Water for a sustainable world; United Nations Educational, Scientific and Cultural Organization: Paris, France, 2015.

United Nations. Water. Available online: https://www.un.org/es/sections/issues-depth/water/index.html (accessed on 20th January 2020).

Visconti, F.; de Paz, J. M.; Martínez, D.; Molina, M. J. Laboratory and field assessment of the capacitance sensors Decagon 10HS and 5TE for estimating the water content of irrigated soils. Agric. Water Manag. 2014, 132, 111–119.

PRESENTATION OF THE WORK

This PhD thesis considers the characterization and simulation of soil water dynamics for the purpose of automated irrigation scheduling in woody crops. The field work for this PhD thesis was carried out in an apple orchard with loamy soil.

The PhD thesis consist of four chapters, which are summarized below (Fig. 1).

Chapter I analyses the response of 10HS sensors to soil moisture in laboratory conditions and discusses the relevance of the two steps of a soil-specific calibration of the sensors. In the first step, the response of individual sensors is related to the dielectric permittivity around them, using well-known permittivity media. In the second step, the permittivity is related to the soil water content (SWC) of a specific soil of interest, using undisturbed soil samples and time domain reflectometry (TDR) measurements. The two-step calibration improves the accuracy of the measurements, at least in laboratory conditions.

Chapter II characterizes the soil water dynamics in a drip-irrigated apple orchard and analyses the most appropriate HYDRUS-3D configuration to simulate the dynamics of water in the soil in a drip irrigated orchard. For this, the parameterization of the HYDRUS 3D model is studied, considering soil hydraulic parameters obtained with Rosetta and HYPROP + WP4C method from undisturbed soil samples. One of the hydraulic parameters is empirically calibrated from a subset of the soil water measurements by neutron probe. The simulations are finally validated at different positions around the dripper on a daily and hourly basis using neutron probe and tensiometers.

Chapter III analyses the performance of capacitance-type moisture sensors installed at different soil locations relative to the drippers in a drip-irrigated orchard under semi-arid conditions. The study compares the variability observed in the sensor measurements with the estimated potential perturbation by factors such as variability in the wetted area below the drippers, soil temperature, sensor calibration and patterns of SWC within a wet bulb expected by HYDRUS-3D simulations.

Chapter IV demonstrates the use of capacitance soil moisture sensors as an input to automated scheduling of irrigation in a drip-irrigated orchard. The approach consists of empirical adjustment of the FAO water balance using soil moisture sensors through the IRRIX web application in an apple orchard with heterogeneous vigour. The automated system is compared with the evapotranspiration determined by a weighing lysimeter located in the same orchard and with the manual scheduling determined by an experienced irrigator using a classical water balance.

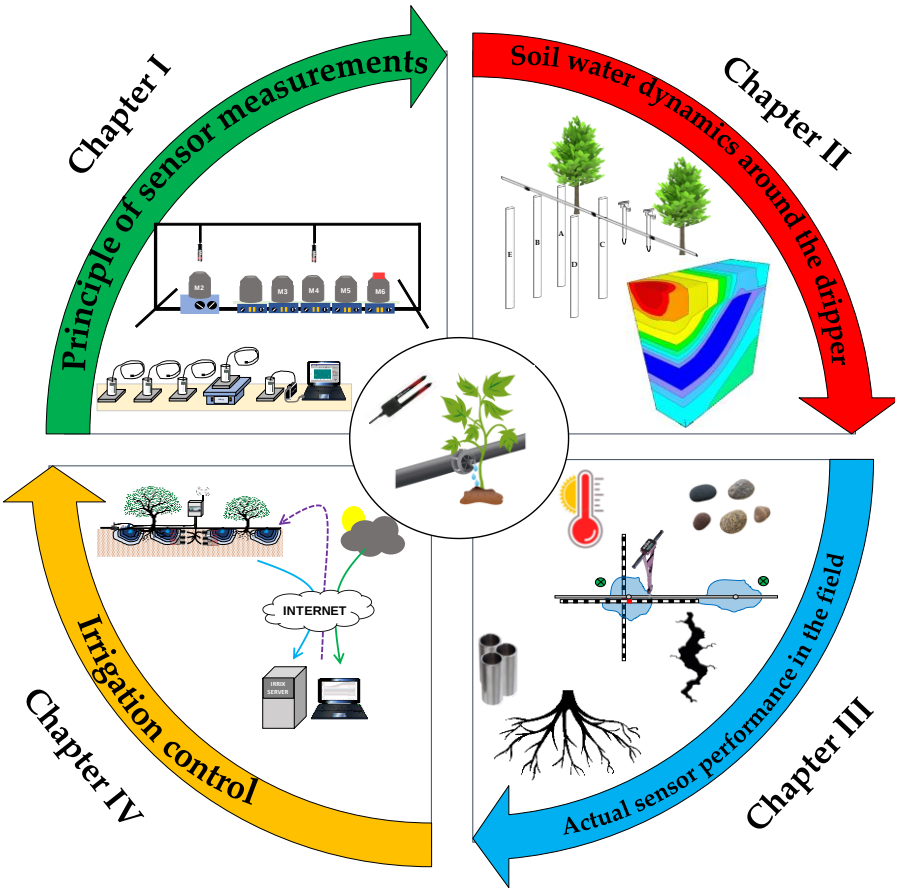

Figure 1. Representative diagram of the thesis.

OBJECTIVES

The main objective of this thesis is:

To understand the response of capacitance-type soil moisture sensors with regard to the soil water dynamics in a drip-irrigated orchard, in order to optimize the usage of these sensors in automated irrigation scheduling.

To attain the main objective, the following sub-objectives were established:

1. To test the degree of improvement of various sensor- and soil-specific calibration options compared to factory calibrations by taking the 10HS sensor as an example.

2. To characterize and understand the soil water dynamics and configure the HYDRUS-3D model in a drip-irrigated apple orchard, calibrating and validating the simulations with soil water measurements from neutron probe and tensiometers.

3. To analyse why soil capacitance sensors in laboratory conditions provide accurate soil water content (SWC) measurements and why, when they are installed in drip-irrigated orchards, their measurements show large sensor-to-sensor differences.

4. To demonstrate the feasibility of using capacitance soil moisture sensors in automated scheduling irrigation in orchards, where these sensors can spontaneously provide site-specific adjustment, in this case to size and structure of the canopy.

METHODOLOGY

This section will describe the methodology used during the elaboration of this thesis. Each chapter of the thesis will also explain in more detail some relevant aspects that will be of interest.

Location and description of the treatments

The study was carried out in an apple orchard (*Malus domestica* Borkh. cv 'Golden Reinders') located at the IRTA-Lleida Experimental Station in Mollerussa (41.6° N, 0.8° E, 260 m above sea level), Lleida, Spain. The orchard planted in 2011 was oriented north-south and spaced at 3.63 m x 1.2 m. In the plantation there were three experimental treatments (Fig. 1).

1. **Manual treatment:** in which irrigation application was based on the FAO water balance (Allen et al., 1998), calculated on a weekly basis, by an experienced irrigator, using the ET_O from the previous week recorded by a weather station located in the same farm and crop coefficients (K_C) determined in previous years using a weighing lysimeter included in the same orchard. Manual treatment was addressed in *Chapter IV*.

2. **Automated treatment:** in which soil moisture sensors were installed and the irrigation was automatically scheduled daily by the IRRIX web platform (Casadesús et al., 2012). IRRIX applied a daily irrigation dose calculated from $ET_{OH} \times K_X$, where ET_{OH} is an estimate of the ET_O calculated from the Hargreaves formula, and K_X is an irrigation coefficient, similar to the crop coefficient, but automatically readjusted by IRRX in response to the sensors. Automated treatment was addressed in *Chapter IV*.

3. **Simulation treatment:** in which apple trees were irrigated daily to meet crop water needs, with daily irrigation doses (DID) determined on a weekly basis according to the FAO water balance (Allen et al., 1998): $DID = ET_O \times K_C$, where ET_O was the reference evapotranspiration from the previous week recorded by a weather station located in the same farm and Kc was the crop coefficient determined in previous years using the weighing lysimeter included in the same orchard (Girona et al., 2004). However, alterations to this irrigation pattern were applied in order to challenge the simulations at reproducing some temporary imbalances in the soil water budget, typically consisting of interruptions of irrigation for a period around one week, followed by recovery of soil water content, as well as the application of arbitrary periods of overirrigation and drought. Simulation treatment was addressed in *Chapters II* and *III*.

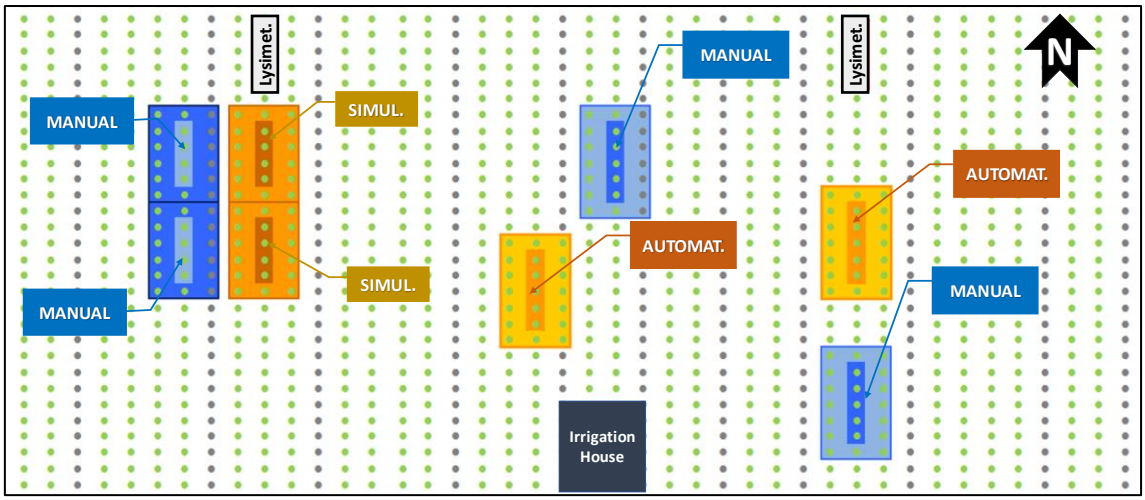

Figure 1. Scheme of Mollerussa orchard and its different treatments and repetitions.

Data collection

1. Datalogger

The different soil moisture measurements were collected by dataloggers, electronic devices capable of storing data from soil moisture sensors. The datalogger used in this thesis were the models CR1000 (Fig. 2) and CR800 (Campbell Scientific Inc., Logan, UT, USA). Their basic operation is based on reading the voltage difference between the terminals where the sensors are connected. The dataloggers required 12V DC power for their operation but were equipped with an internal lithium battery that prevented loss of memory data when the device had no power. The data stored by the datalogger was downloaded *in situ* through a cable connected to a computer or, if the installation had a modem, telematically.

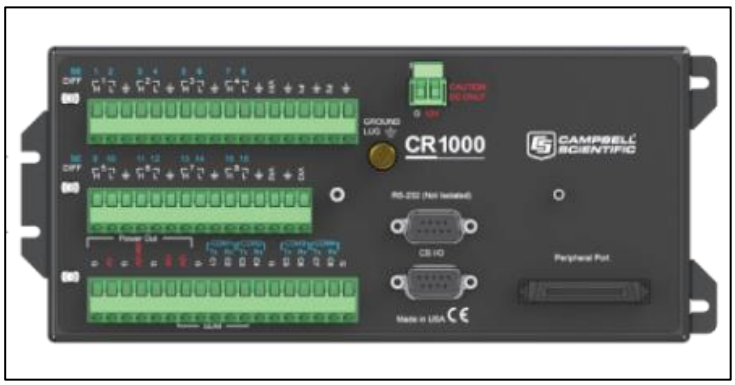

Figure 2. Datalogger CR1000 from Campbell Scientific Inc.

2. Capacitance sensors

The capacitance sensors used in this thesis were the 10HS sensors and EC-5 sensors. The 10HS sensor (Fig. 3) (METER Group Inc., Pullman, WA, USA) is an analog output sensor that uses the soil and water electrical properties to estimate the volumetric water content in the soil. The sensor requires an excitation of between 3 and 15 VDC and has a

theoretical exploring volume of about 1.3 L. The direct measurement of the sensor is the dielectric permittivity that arrives as a voltage difference to the datalogger.

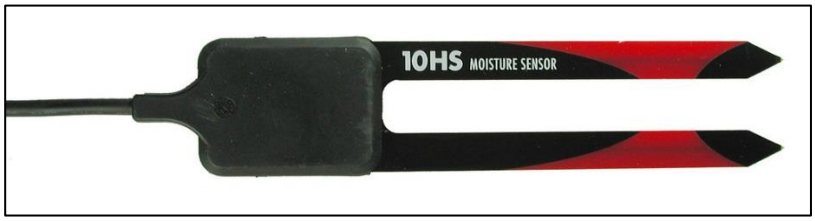

Figure 3. 10HS sensor from METER Group Inc.

The EC-5 sensor (METER Group Inc., Pullman, WA, USA) (Fig. 4) as well as 10HS sensor is an analog output sensor that uses the soil and water electrical properties to estimate the volumetric water content in the soil. The sensor requires an excitation of between 2.5 and 3.6 VDC and has a theoretical exploring volume of about 0.3 L.

Figure 4. EC-5 sensor from METER Group Inc.

3. Tensiometers

The type RSU-C tensiometer (Irrometer, Riverside, CA, USA) (Fig. 5) measures the tension exerted by the soil when the liquid inside it dries. It is in contact with the soil through a porous ceramic tip. When the soil dries, the soil matrix strains the liquid content of the tensiometer, and when the soil moisture increases the column is tightened. The tension was measured with a transducer. Tensiometers were located in different positions around the dripper as described in *Chapter II*.

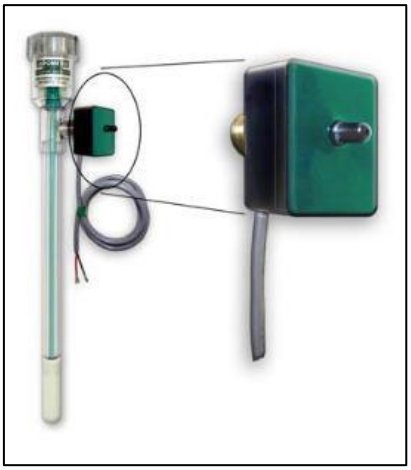

Figure 5. RSU-C tensiometer from Irrometer Group Inc.

4. Neutron probe

The neutron probes access tubes were installed in the ground in different positions around the drippers to 180 cm depth. The neutron probe tubes used were PVC because this material has little effect on the reading of the measurements. To measure the soil moisture, a neutron probe (Hydroprobe 503DR, Campbell Pacific Nuclear Corp., Martinez, CA, USA) (Fig. 6) was employed which uses radioactive material and contains an electronic gauge, a connecting cable, and a source tube containing both nuclear source and detector tube. The source tube was lowered into the tube to the different measurement depths. Neutron probe was employed during growing season in *Chapters II and III*.

Figure 6. Hydroprobe 503DR from Campbell Pacific Nuclear Corp.

5. Weather station

The weather data was obtained from a weather station (Fig. 7) located in the Experimental Station at Mollerussa and integrated into the Xarxa d'Estacions Meteorolològiques Automátiques (XEMA) operated by the Catalan Meteorological Service. The data obtained from the weather station were the rainfall and reference evapotranspiration (ETo).

Figure 7. Weather station.

The measurement of solar radiation was obtained from a pyranometer (SKYE Instruments Ltd, Llandrindod Wells, Powys, UK) (Fig. 8) installed in the plot, which measures solar radiation with wavelengths between 350 nm and 1100 nm.

Figure 8. Pyranometer from SKYE Instruments Ltd.

6. Lysimeters

The apple orchard had two weighing lysimeters (Fig. 9), which provide a continuous measurement of crop evapotranspiration (ET_C). The lysimeters installed in the orchard consist of a steel tank containing four apple trees with their soil volume and supported by four load cells resting on a concrete support. The signal from the load cells was read and stored in a datalogger, where the ET_C, its radiation interception and its drainage were continuously recorded (Girona et al., 2014). The lysimeters were used to provide the ET_C used as input of HYDRUS-3D simulations of the *Chapters II* and *III* and to contrast the irrigation applied in *Chapter IV*.

Figure 9. Weighing lysimeter located in Mollerussa Experimental Station.

Physiological and agronomical measurements

1. Stem Water Potential (SWP)

Stem water potential (SWP) was measured using a pressure chamber (3005-series portable plant water status console, Soil Moisture Equipment Corp., Santa Barbara, CA, USA) (Fig. 10) and following the protocol established by McCutchan and Shackel (1992). Measurements were made at solar noon on leaves located close to the main trunk. Previously, the leaves were covered with plastic sheathes with aluminium foil bags to minimize transpiration and maintain balance with the xylem of the tree. SWP was determined once a week in *Chapter IV.*

Figure 10. 3005-series portable plant water status console from Soil Moisture Equipment Corp.

2. Fraction of Intercepted Photosynthetically Active Radiation (FIPAR)

The method used to measure the fraction of intercepted photosynthetically active radiation (FIPAR) was related to that for fisheye photography described by Wüsnsche et al. (1995) and consisted of taking hemispheric photographs from below the tree, following a pattern that covered the entire planting space. The photos were taken with a Nikon digital camera and a 10-17 mm AT-X Tokina fish-eye lens on a self-levelling support that held the camera 10 cm above the ground (Fig. 11). Later, the photographs were processed to calculate the daily solar path on each picture and analyse the fraction between treetop pixels and background at the different sun positions along the day. FIPAR was used to see the differences in tree vigour in Chapter IV

Figure 11. Digital camera on a self-levelling support.

3. Extent and position of wetted area

The extent and position of the area wetted by the drippers were measured using the Fieldscout TDR 300 (Spectrum Technologies Inc., Aurora, IL, USA) with 12 cm length rods (Fig. 12). The characterization of the extent of the wetted area consisted of measuring the soil water content (SWC) at intervals of 10 cm, parallel and perpendicular to the dripline. The position of the wetting pattern referred to the centering of the wet bulb relative to the dripper and was determined as the point with the highest soil water content between two drippers. To determine the variability in the extent and position of the wetted area, a "reference wetting pattern", was defined as the wetting pattern most frequently observed during the measurements. Then, all transects included in the dataset were compared with this "reference wetting pattern". The extent of the wetted pattern at the soil surface under the dripper was measured in *Chapter II* and *III.*

Figure 12. Fieldscout TDR 300 from Spectrum Technologies Inc.

4. Soil hydraulic characterization

The characterization and description of the soil hydraulic properties is of fundamental importance for the application and optimization of the irrigation water. For this purpose, there are different methodologies in which measurements can be taken with disturbed or undisturbed samples, continuously or punctually, and in the laboratory or field. The bulk density (BD), field capacity (FC) and wilting point (WP) were determined in each position and depth where the moisture sensors were installed. To calculate BD, first undisturbed soil samples were taken using Kopecky rings (Eijkelkamp, Giesbeek, The Netherlands) of 5.1 cm length and 5.3 – 5.0 cm diameter (Fig. 13). The cylinder was covered with two lids to avoid moisture losses and weighed in the laboratory. Later, the sample was dried in an oven (105 °C) for 24 h or until the sample reached a constant weight. Finally, the moisture was determined by dividing the dry weight by the volume of the cylinder. The cylinders were used to take undisturbed soil samples in *Chapters I* and *II.*

Figure 13. Kopecky rings from Eijkelkamp.

Soil water content at -33 kPa (FC) and -1500 kPa (WP) were determined from dry and sieved samples using a porous ceramic pressure plate with compressed air (Soil Moisture Equipment Corp., Santa Barbara, CA, USA) (Fig. 14) (Dane and Hopmans, 2002). Pressure plates allowed to obtain the FC and WP that were used in *Chapter II.*

Figure 14. Pressure plates with compressed air from Soil Moisture Equipment Corp.

In addition, the combination of the HYPROP (METER Group, Pullman, WA, USA) and WP4C (METER Group, Pullman, WA, USA) systems (Fig. 15) provide complete soil hydraulic characterization from undisturbed samples through continuous laboratory measurements. The fact that the soil sample is undisturbed adds quality to the measurements, making the characterization more representative. The soil hydraulic characterizations were used to estimate the FC and WP values and the soil hydraulic parameters (θr = residual water content; θs = saturated water content; Ks = saturated hydraulic conductivity; α, n and l are van Genuchten shape parameters), which were later used in the HYDRUS-3D simulation model. Data obtained from HYPROP and WP4C was used in *Chapter II* and *III*.

Figure 15. HYPROP (right) and WP4C (left) systems.

Characterization of capacitance sensors and two-step calibration

The factory calibration of the capacitance sensors is often criticized for its limited accuracy. To improve their precision a two-step calibration procedure can be used (Bogena et al., 2017; Seyfried and Murdock, 2004). In the first step (Fig. 16), media with well-known dielectric properties, such as air, glass beads, and 2-isopropoxyethanol are used. The advantages of using these reference media are: (a) the avoidance of air gaps and density variations, (b) the possibility to separate sensor- and soil-specific effects, and (c) the ability to quickly calibrate multiple sensors for a wide range of dielectric permittivity.

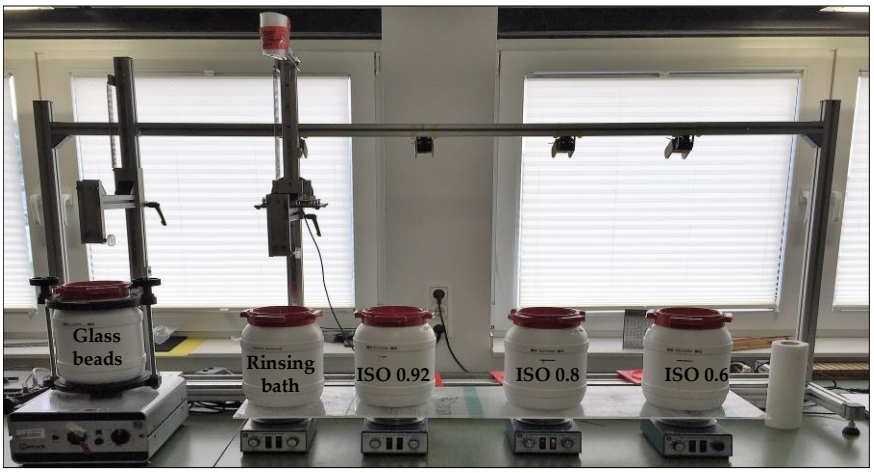

Figure 16. Different known permittivity media where the capacitance sensor response was characterized.

In the second step (Fig. 17), an appropriate relationship between permittivity and SWC needs to be established. One possibility is to use available empirical or semi-empirical models that relate permittivity and SWC. To obtain more accurate SWC measurements, a site-specific calibration accounting for variations in key soil properties can also be established using a limited number of soil samples. Here, the use of TDR measurements was preferred because of its ability to directly provide dielectric permittivity and higher accuracy of the permittivity measurements.

Figure 17. Local relationship between SWC and permittivity using TDR sensor.

HYDRUS-3D model

The soil water distribution and root water uptake were modelled with Richards equation in 3 dimensions, which incorporated a sink term to contemplate the evapotranspiration. The simulations made in this PhD thesis were carried out using the HYDRUS-3D (Simunek et al., 2016) model, which is a software that simulates water flow and root water uptake (RWU) in homogeneous and isotropic soils. HYDRUS-3D solves Richards equation (Eq. 1) using the Galerkin finite element method from the initial and boundary conditions.

$$\frac{\partial \theta}{\partial t} = \frac{\partial}{\partial x}\left[K(h)\frac{\partial h}{\partial x}\right] + \frac{\partial}{\partial y}\left[K(h)\frac{\partial h}{\partial y}\right] + \frac{\partial}{\partial z}\left[K(h)\left(\frac{\partial h}{\partial z} + 1\right)\right] - S \qquad \text{(Eq. 1)}$$

where θ is volumetric water content (L^3L^{-3}), t is the time (T), x and y the horizontal space coordinates, h is soil water pressure head (L), K is hydraulic conductivity, z is the vertical space coordinate, and S is the sink term (T^{-1}).

The HYDRUS model solves Richards equation using van Genuchten's parametric function (1980), which relates moisture and soil potential using the following equation (Eq. 2):

$$\theta(h) = \begin{cases} \theta_r + \dfrac{\theta_s - \theta_r}{[1 + |\alpha \cdot h|^n]^m} & h < 0 \\ \theta_s & h \geq 0 \end{cases} \qquad \text{(Eq. 2)}$$

where θs = saturated water content; θr = residual water content; and m, n and α are empirical values that affect the shape of the retention curve, and for the purposes of simplification it is assumed that $m = 1 - (1/n)$ (Eq. 3)

$$S_e = \frac{\theta - \theta_r}{\theta_s - \theta_r}, \qquad m = 1 - 1/n \tag{Eq. 3}$$

where S_e is the dimensionless effective water content.

The unsaturated hydraulic conductivity *K(h)* is determined by the following expression (Mualen, 1976) (Eq. 4)

$$K(h) = K_s S_e^l \left[1 - (1 - S_e^{1/m})^m\right]^2 \tag{Eq. 4}$$

where K_s is the saturated hydraulic conductivity of the soil and l is an empirical parameter related to the connectivity between the pores.

The application of a three-dimensional model made it possible to simulate the evolution of soil water content in different positions and depths, including sensors, tensiometers and neutron probe access tubes.

HYDRUS-3D simulations were validated with soil moisture measurements by neutron probe -at different dates on two irrigation seasons- and by tensiometers -on the course of several days-. The volumetric SWC at different depths on an array of access tubes was measured using a neutron probe (Hydroprobe 503DR, Campbell Pacific Nuclear Corp., Martinez, CA, USA) on specific days of the growing season. The tensiometers measured the soil water tension every 10 seconds and the average reading over 5 minutes was stored in a datalogger.

Characterization of sensor performance in a real orchard

In this thesis, as described in *Chapter III*, capacitance soil moisture sensors (10HS and EC-5) were located in two plots, with one sensor type in each plot. There repetitions of 9 or 10 sensors were installed in each plot in different positions and depths around the dripper (Fig. 18). All repetitions were within the same tree row and separated by a distance of less than 5 m. The 10HS sensors of Plot II, which were deployed in equivalent positions and depths as EC-5 sensors in Plot I, additionally included position D at a depth of 30 cm.

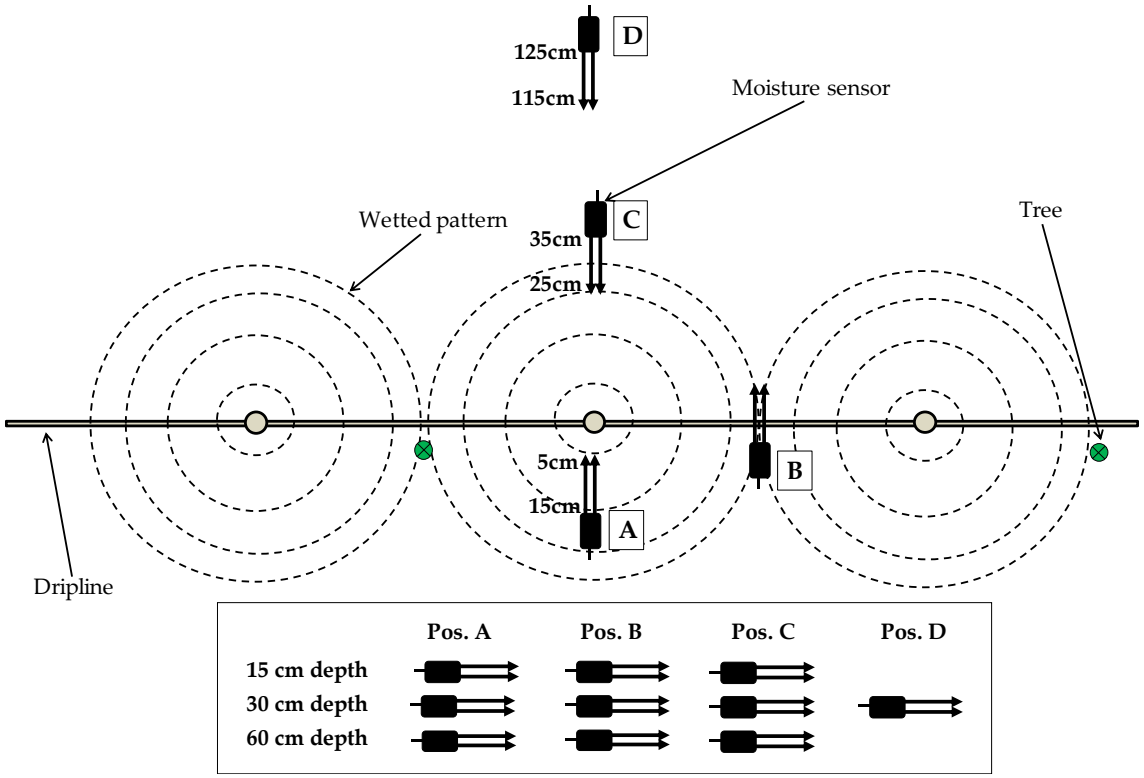

Figure 18. Moisture sensors installed at three depths (15, 30 and 60 cm) in four positions relative to the dripper (Pos. A: centre of wet bulb, Pos. B: mid-point between two drippers (30 cm), Pos. C: perimeter of the wet area, Pos. D: outside the influence of the dripper.

In this study, one concept of interest regarding the performance of sensors in real orchard conditions is the practical uncertainty of monitoring SWC with a setup of several sensors, each of which is reporting a different value. Here, uncertainty refers to the degree of precision with which a quantity is measured while variability refers to natural variation in some quantity (Van Belle, 2008). When comparing the output of several soil sensors, the observed differences between sensors can be caused by uncertainties in the measuring process, by actual variability in the physical property being measured, or by both. Since in a practical usage of the sensors we cannot distinguish between them, here we treat them all as practical uncertainties, expressed in terms of the root mean square error (RMSE). The conversion of uncertainties or variabilities to a common expression allows their comparison.

IRRIX web platform

In this thesis, the use of capacitive sensors for automated irrigation scheduling was conducted with IRRIX. IRRIX is an experimental web platform for automated irrigation monitoring and control, which implements automatic localised irrigation algorithms and methods for unmanned interpretation of capacitance sensors (Casadesús et al., 2012).

IRRIX is capable of creating predictions of irrigation needs and executing decisions autonomously. The system works by collecting data through different sensors installed

in the field, which are crossed with reference meteorological data and the water resources available in the plot. With this information, the platform designs the seasonal plan in an efficient and adjusted way in each case, without the need for intervention from the operators. With this information, the platform designs the seasonal plan in an efficient and adjusted way in each case, without the need for intervention from the operators. Every day, the system adjusts automatically according to the indications of the sensors, within the limits that the pre-established planning at the beginning of the seasonal plan allows.

IRRIX is a complement to the irrigation controllers currently available on the market which offer the possibility of optimizing the scheduling on a daily basis without the need for user intervention, as well as supervising the correct operation of the irrigation system based on real observations from the sensors. The operation of IRRIX requires an irrigation controller, in which a water meter and two or more soil moisture sensors per irrigation sector can be remotely controlled and installed. The irrigator can interact with the system through any device connected to the Internet.

Literature cited

Allen, R. G.; Pereira, L. S.; Raes, D.; Smith, M. Crop evapotranspiration. Guidelines for computing crop water requirements. FAO irrigation and drainage paper 56, 1998. Rome.

Bogena, H.R.; Huisman, J.A.; Oberdörster, C.; Vereecken, H. Evaluation of a low-cost soil water content sensor for wireless network applications. J. Hydrol. 2007, 344, 32–42.

Casadesús, J.; Mata, M.; Marsal, J.; Girona, J. A general algorithm for automated scheduling of drip irrigation in tree crops. Comput. Electron. Agric. 2012, 83, 11-20.

Dane, J.H.; Hopmans, J.W. Water retention and storage. In: Dane, J.H., Topp, G.C. (Eds.), Methods of Soil Analysis. Part 4, SSSA Book Series No. 5. 2002, Soil Science Society of America Journal, Madison WI.

Girona, J.; Marsal, J.; Mata, M.; del Campo, J. Pear crop coefficients obtained in a large weighing lysimeter. Acta Hortic. 2004, 664, 277-281

McCutchan, H.; Shackel, K.A. Stem water potential as a sensitive indicator of water stress in prune trees (Prunus domestica L. Cv. French.). J. Am. Soc. Hortic. Sci. 1992, 117, 607–611.

Mualem, Y. A new model for predicting the hydraulic conductivity of unsaturated porous media. Water Resour. Res. 1976,12, 513–522.

Seyfried, M.S.; Murdock, M.D. Measurement of Soil Water Content with a 50-MHz Soil Dielectric Sensor. Soil Sci. Soc. Am. J. 2004, 68, 394.

Simunek, J.; Van Genuchten, M. T; Sejna, M. Recent developments and applications of the HYDRUS computer software packages. Vadose Zone J. 2016, 15, 25.

Van Belle, G. Statistical Rules of Thumb (2nd edition), John Wiley and Sons, Hoboken, 2008, New Jersey.

Van Genuchten, M. T. A closed-form equation for predicting the hydraulic conductivity of unsaturated flow, Soil Sci. Soc. Am. J. 1980, 44, 892-898.

Wu̇nsche, J. N.; Lakso, A. N.; Robinson, T. L. Comparison of four methods for estimating total light interception by apple trees of varying forms. HortScience. 1995, 30, 272-276.

CHAPTERS

Chapter I: Principle of sensor measurements

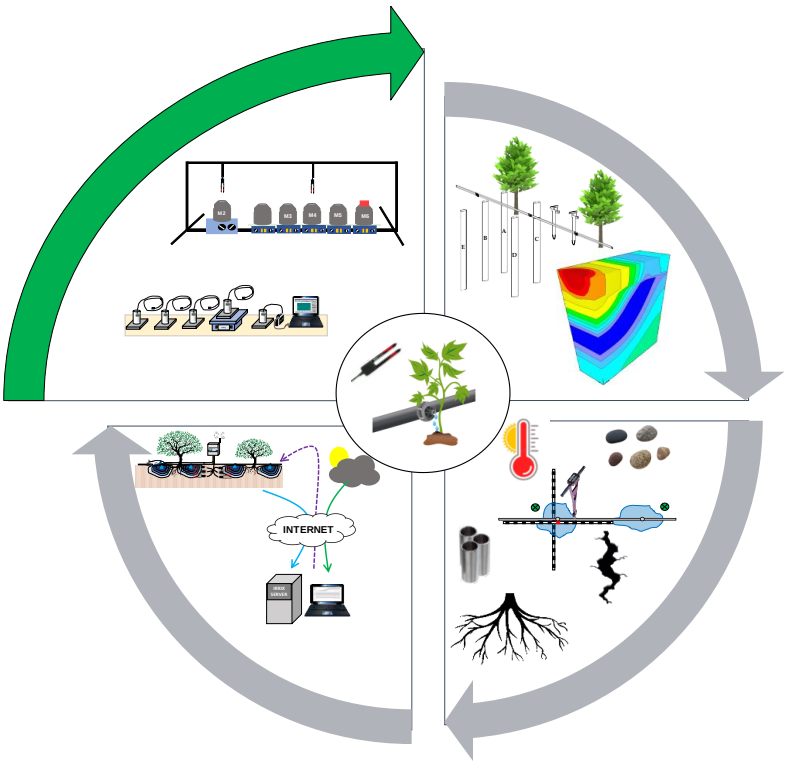

On the accuracy of factory-calibrated low-cost soil water content sensors

Jesús María Domínguez-Niño[1], Heye Reemt Bogena[2], Johan Alexander Huisman[2], Bernd Schilling[2], Jaume Casadesús[1].

[1] Programme on Efficient Use of Water in Agriculture, Institute of Agrifood Research and Technology (IRTA), Parc de Gardeny (PCiTAL), Fruitcentre, 25003, Lleida, Spain; jesus.dominguez@irta.cat; jaume.casadesus@irta.cat

[2] Institute of Bio- and Geosciences, Agrosphere Institute (IBG-3), Forschungszentrum Jülich GmbH, 52425, Jülich, Germany; h.bogena@fz-juelich.de; s.huisman@fz-juelich.de; b.schilling@fz-juelich.de

Sensors (2019), 19-14, 3101 DOI: 10.3390/s19143101

Abstract

Soil water content (SWC) monitoring is often used to optimize agricultural irrigation. Commonly, capacitance sensors are used for this task. However, the factory calibrations have been often criticised for their limited accuracy. The aim of this paper is to test the degree of improvement of various sensor- and soil-specific calibration options compared to factory calibrations by taking the 10HS sensor as an example. To this end, a two-step sensor calibration was carried out. In the first step, the sensor response was related to dielectric permittivity using calibration in media with well-defined permittivity. The second step involved the establishment of a site-specific relationship between permittivity and soil water content using undisturbed soil samples and time domain reflectometry (TDR) measurements. Our results showed that a model, which considered the mean porosity and a fitted dielectric permittivity of the solid phase for each soil and depth, provided the best fit between bulk permittivity and SWC. Most importantly, it was found that the two-step calibration approach (RMSE: 1.03 vol.%) provided more accurate SWC estimates compared to the factory calibration (RMSE: 5.33 vol.%). Finally, we used these calibrations on data from drip-irrigated almond and apple orchards and compared the factory calibration with our two-step calibration approach.

Keywords: Soil water content; 10HS sensor; calibration; sensor variability; specific calibration; CRIM model.

1. Introduction

Efficient irrigation management is essential for reducing water consumption. To this end, real-time monitoring of soil water content (SWC) is essential to optimize the amount and timing of water irrigation (Nolz et al., 2013; Soulis et al., 2018). Electromagnetic (EM) methods, such as time domain reflectometry (TDR) (e.g. Robinson et al., 2003) and capacitance sensors (Kojima et al., 2016; Bogena et al., 2017), are most commonly used for soil water content measurements at the point scale. Capacitance sensors are often preferred over TDR sensors as they provide real-time SWC at a lower cost. In addition, they were shown to be reasonably robust and precise, and consume less energy compared to TDR sensors (Rosenbaum et al., 2010; Spelman et al., 2013; Visconti et al., 2014). Both TDR and capacitance methods make use of the strong dependence of the soil dielectric permittivity on volumetric SWC. As the dielectric permittivity of liquid water is much higher than the dielectric permittivity of the other soil components, SWC is the principal factor governing the apparent soil permittivity (Topp et al., 2000). However, other soil properties such as salinity and texture may cause dielectric losses and disturb the SWC measurements with EM sensors (Jones et al., 2000). These dielectric losses depend on the frequency of the electric field generated by the sensors and are especially important for sensors that work at frequencies between 1 and 200 MHz (Hilhorst et al., 1994). In addition, capacitance sensors can show substantial sensor-to-sensor variability, which affects the accuracy of the soil water content measurements if this is not considered (Sakaki et al., 2008; Rosenbaum et al., 2013). One solution to compensate for this effect would be to directly calibrate each sensor individually with soil samples (Vaz et al., 2013). However, this procedure is time consuming and thus often not viable in case of a high number of sensors (Rosenbaum et al., 2010; Bogena et al., 2017). Alternatively, a two-step calibration procedure can be used (Robinson et al., 1998; Seyfried et al., 2004; Jones et al., 2005; Bogena et al., 2007). In a first step, a calibration between sensor response and permittivity is established for each of the sensors. In this step, media with well-known dielectric properties (referred to as reference permittivity), such as air, glass beads (Kögler et al., 2013) and 2-isopropoxyethanol (Kaatze et al., 2016), are used. The advantages of using these reference media are: (i) the avoidance of air gaps and density variations, (ii) the possibility to separate sensor- and soil-specific effects, and (iii) the ability to quickly calibrate multiple sensors for a wide range of dielectric permittivity. In a second step, an appropriate relationship between permittivity and SWC needs to be established. One possibility is to use available empirical or semi-empirical models that relate permittivity and SWC (Topp et al., 1980; Roth et al., 1990). To obtain more accurate SWC measurements, a site-specific calibration accounting for variations in key soil properties can also be established using a limited number of soil samples. Here, the use of TDR measurements should be preferred because of its ability to directly provide dielectric permittivity and the higher accuracy of the permittivity measurements.

In this study, we focused on the low-cost capacitance SWC sensor 10HS (METER Group Inc., 2018). The main goal was to analyse whether it is worthwhile to perform sophisticated sensor- and soil-specific calibrations instead of using the factory calibration suggested by the manufacturer. To this end, we carried out sensor-specific calibrations with 10HS sensors using reference media with well-known dielectric properties and determined permittivity-SWC relationships using undisturbed soil samples and TDR measurements. The permittivity of the undisturbed samples was related to SWC taking into account different properties such as porosity and permittivity of the solid phase. We then compared the factory and the two-step calibration approach using i) packed sand samples with known SWC in a laboratory experiments and ii) SWC time series obtained at two test sites.

2. Materials and Methods

2.1. Sensor Technology

In this study, we used the 10HS SWC sensor manufactured by METER Group Inc., USA. This sensor has a prong length of 10.0 cm and a distance between the prongs of 2.2 cm (Figure 1). The 10HS sensor determines SWC using the capacitance method. According to the manufacturer, it has a probing volume of about 1 dm^3, which is much larger than other low-cost SWC sensors like the EC-5 and EC-20, which have a volume of influence of 0.3 dm^3 (Rosenbaum et al., 2011).

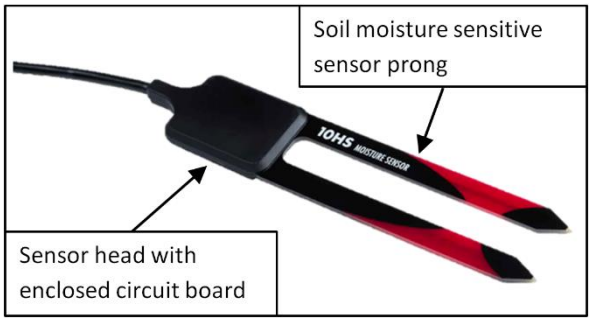

Figure 1. The 10HS sensor from METER Group Inc., USA

The 10HS sensor determines SWC by measuring the charge time of a capacitor (i.e. the soil-probe system), which is related to the permittivity of the soil surrounding the sensor (Bogena et al., 2007). The manufacturer provides a factory calibration to obtain SWC from the sensor response:

$$SWC\ (vol.\%) = (1.16 \times 10^{-9}\ (RAW^3) - 3.95 \times 10^{-6}\ (RAW^2) + 4.89 \times 10^{-3}\ (RAW) - 1.92) \times 100 \quad \text{(Eq. 1)}$$

where RAW is the raw sensor count. According to the manufacturer, this calibration equation is valid for SWC in the range between 0 and 57 vol.%. Like all ECH_2O SWC sensors of the METER Group, the 10HS sensor uses an oscillation frequency of 70 MHz.

Therefore, the SWC measurements with the 10HS sensor may be affected by temperature and soil bulk electrical conductivity variations (Rosenbaum et al., 2011).

2.2. Study area

We used 16 10HS sensors to measure SWC in an almond and apple orchard located in Menàrguens and Mollerussa (Lleida, Spain), respectively. Both orchards were equipped with a drip irrigation system. The almond plants were planted in ridges of 200 cm width and 50 cm height on top of the original soil. The soil material used to create the ridges consisted of a mixture of local soil and an organic amendment. The irrigation system of the almond orchard was located on the top of the ridge and consisted of a double tube system separated by 40 cm with drippers spaced at 100 cm intervals. The sensors were installed in the middle of the ridge at depths of 20 and 50 cm. The apple orchard had a single tube system with drippers spaced every 60 cm and the sensors were located under and between the drippers at depths of 15 and 30 cm. The properties of the soils are summarized in Table 1.

Table 1. Characteristics of the soils at different deeps in almond and apple crop.

Depth (m)	**Menàrguens**		**Mollerussa**	
	0 - 0.5 (Ridge)	0.5 - 1 (Under ridge)	0 - 0.2	0.2 - 0.4
Silt (0.002 < d < 0.05 mm) %	37.2	37.0	40.7	40.6
Clay (d < 0.002 mm) %	21.2	24.3	23.5	23.9
Sand (0.05 < d < 2 mm) %	41.6	38.7	35.8	35.5
USDA Soil Classification	Loam	Loam	Loam	Loam
Bulk density (kg m^{-3})	1370	1700	1480	1500

2.3. Laboratory experiments

In this study, we relied on a two-step calibration approach to relate sensor response to SWC. In a first step, the relationship between sensor response and permittivity was established for each sensor (i.e. a sensor-specific calibration). In a second step, a site-specific relationship between permittivity and soil water content was developed using a limited number of soil samples using the TDR method (soil-specific calibration).

2.3.1. Sensor response – permittivity calibration for the 10HS sensor

For the first calibration step, we used the approach of Bogena et al. (Bogena et al., 2017) and calibrated 16 sensors. We used five calibration standards for sensor calibration (air, glass beads and three mixtures of 2-isopropoxyethanol (i-C_3E_1) and deionized water with a defined volume fraction of i-C_3E_1). The properties of these reference media are described in Table 2. We used soda lime glass beads (type: Silibeads 4501, Sigmund Lindner GmBH, Germany) with a grain size between 0.25 and 0.50 mm and a dielectric permittivity of 3.34 (Kögler et al., 2013). The sensor response for all reference media was measured at 25°C using the ProCheck device (Meter Group Inc., USA). The permittivity

range from 1.0 to 34.8 covers most of the dielectric permittivity values found in natural soils. Table 2 shows that there is a considerable gap between 4 and 32%. Initially, pure I-C_3E_1 with an equivalent water content of 24% was also considered. However, pure I-C_3E_1 is highly hydrophilic. Therefore, these measurements were unreliable and not stable during calibration. For this reason, we decided to discard this solution from the analysis. Future studies should investigate alternative reference liquids to fill this gap.

Each of the 16 sensors was calibrated taking into account two immersions variants. In the first variant, only the sensor prongs were inserted in the reference media (i.e. incomplete immersion). In the second variant, the entire sensor including the sensor head with the electronics (see Figure 1) was fully immersed in the reference media. This second variant mimics a typical field installation where the sensor head is fully surrounded by soil, whereas the first variant represents a typical situation for crops planted in bags of growing media and laboratory SWC measurements. If the sensor electronics in the sensor head are not influenced by the permittivity of the surrounding media, both variants should provide the same sensor reading for a given dielectric permittivity.

Table 2. Properties of the calibration media as well as the equivalent soil water content (SWC) calculated with the Topp equation (Topp et al., 1980).

Calibration standard	Medium	Reference Permittivity	Volume fraction i-C_3E_1	Volume fraction water	Equivalent SWC
		-	-	-	vol. %
M1	Air	1.00	-	-	-
M2	Glass beads	3.34	-	-	4.0
M3	I-C_3E_1/water mixture	18.14	0.92	0.08	32.0
M4	I-C_3E_1/water mixture	26.26	0.80	0.20	41.0
M5	I-C_3E_1/water mixture	34.82	0.68	0.32	48.0

Several precautions were considered to obtain precise calibrations. First, we used sufficiently large (6.4 dm^3) polyethylene bottles (diameter of 19.5 cm, height of 23.0 cm) to fully include the sensing volume of the 10HS sensor (1 dm^3). Second, the sensor was fixed and centrally immersed in the reference media to reduce the effects of sensor position on the measurements. Finally, possible degrading effects of the reference media on the plastic body of the sensor were minimized by carefully cleaning the sensor after each measurement and minimizing the contact time. The calibration station consisted of four plastic bottles containing the different dielectric reference media arranged on a workbench. The bottle with the glass beads was placed on a vibration machine in order to maintain the same packing density and not affect the calibration of the 10HS sensors. The other three bottles were placed on magnetic stirring devices to avoid demixing of the reference media. They were also covered with a lid to prevent evaporation. In addition, a bottle of water was used to clean the sensors after each measurement. Bogena et al. (2017) provided a more detailed description of the set-up of the calibration workbench.

The sensor response (ν) was related to the dielectric permittivity (K_a) using an empirical sensor response permittivity (SRP) model. In this study, the sensor response was related to the apparent dielectric permittivity using the following empirical model:

$$K_a = \gamma + 1 / (\alpha + \beta / \nu) \quad \text{(Eq. 2)}$$

where ν was the sensor response (voltage, V) and α, β and γ were fitting parameters. The RMSE between the predicted K_a and the reference permittivity, ε_{ref}, was used to express the accuracy of the SRP model. Empirical SRP models were already successfully applied to relate sensor readings of low-cost sensors to dielectric permittivity in several studies to account for sensor-to-sensor variability of various SWC sensors (Rosenbaum et al., 2010; Qu et al., 2013). In addition, we investigate the decrease in accuracy when using a universal SRP model that ignores sensor-to-sensor variability of the 10HS sensors.

2.3.2. Permittivity-soil water content relationships

To obtain soil-specific relationships between dielectric permittivity and SWC for the Menàrguens and Mollerussa test sites, we took 16 undisturbed samples using Kopecky rings with a length of 7.7 cm and a diameter of 5 cm. We took 4 samples at 20 cm depth and 4 samples at 50 cm depth from the Menàrguens test site and 4 samples at 15 cm and 4 samples at 30 cm depth from the Mollerussa test site. In the laboratory, we saturated the samples with deionized water and let them evaporate at room temperature. The volumetric SWC was determined twice a day from the weight of the sample, the known sample volume and the dry weight of sample determined at the end of the experiment by oven drying (65°C, 48 h). The apparent dielectric permittivity of each sample was determined from measurements with a CS 640-L 3-rod TDR probe attached to a TDR-100 device (Campbell Scientific Inc., Logan, UT). We used the internal TDR-100 algorithm to analyse the TDR measurements. One sample had to be discarded because shrinkage caused a significant decrease in volume. Therefore, the final data set consisted of dielectric permittivity and SWC measurements for 15 soil samples with known bulk density and porosity as provided in Table 3.

It should be noted that there is a difference in operating frequency between the 10HS sensor (70 MHz) and the effective frequency of TDR (100 to 500 MHz), although the latter is poorly defined and depends on the measurement set-up and TDR waveform analysis approach (Chung et al., 2008). For the low-salinity and loamy soils investigated here, it is assumed that the operating frequency of 70 MHz for the capacitance sensors is sufficiently high to avoid effects of low-frequency polarization losses (Kizito et al., 2008). Therefore, the difference in measured apparent permittivity between the capacitance sensors and TDR is expected to be low. The alternative approach where 10HS sensors are used for soil-specific calibration would overcome possible differences in frequency

but has the disadvantage that sensor- and soil-specific calibration are convoluted. Therefore, we prefer not to use this latter approach.

Table 3. Properties of the samples for the topsoil and subsurface soil

Menàrguens				Mollerussa			
Sample name	Depth cm	Bulk density g cm^{-3}	Porosity %	**Sample name**	Depth cm	Bulk density g cm^{-3}	Porosity %
S1-Men	~20	1.40	47	**S1-Moll**	~15	1.56	41
S2-Men		1.33	50	**S2-Moll**		1.41	47
S3-Men		1.37	48	**S3-Moll**		1.41	47
S4-Men		1.36	49	**S4-Moll**		1.50	43
S5-Men	~50	1.72	35	**S5-Moll**	~30	1.57	41
S6-Men		1.60	40	**S6-Moll***		1.47	44
S7-Men		1.75	34	**S7-Moll**		1.46	45
S8-Men		1.70	36	**S8-Moll**		1.50	43

*Sample was discarded due to shrinkage

Five empirical and semi-theoretical model variants were evaluated using the root mean square error (RMSE) between measured and predicted SWC. The first model was the empirical Topp model (Topp et al., 1980):

$$\text{SWC (vol.\%)} = \left(-5.3 \times 10^{-2} + 2.92 \times 10^{-2} \times K_a - 5.5 \times 10^{-4} \times K_a^2 + 4.3 \times 10^{-6} \times K_a^3\right) \times 100 \qquad \text{(Eq. 3)}$$

In addition, we used four different variants of the complex refractive index model (CRIM) (Bircharck et al., 1974):

$$\text{SWC (vol.\%)} = 100 \times \frac{K_a^{\beta} - (1 - \eta) \times K_s^{\beta} - \eta K_{air}^{\beta}}{K_w(T)^{\beta} - K_{air}^{\beta}} \qquad \text{(Eq. 4)}$$

where K_a is the measured apparent dielectric sensor permittivity, K_s is the dielectric permittivity of the solid phase and η is the porosity. The value of the shape factor β was set to 0.5 (Pepin et al., 1995). The dielectric permittivity of air, K_{air}, was assumed to be 1 and the temperature dependent dielectric permittivity of water, K_w, was assumed to be 78.54 at 25 °C (Weast et al., 1986). In the first variant (CRIM-1), we used the averaged measured porosity for all samples (η = 43%) and assumed that the dielectric permittivity of the solid phase, K_s, was 4.4 based on the value for quartz (Robinson et al., 2004). In the second variant (CRIM-2), we again used the measured average porosity (η = 43%) but fitted K_s to the data. In the third variant (CRIM-3), we used the mean porosity per soil and depth (Menàrguens: η = 48% and 36% at 15 cm and 50 cm depth, respectively; Mollerussa: η = 44% and 43% at 15 cm and 30 cm depth, respectively) and fitted K_s again. In the fourth and final variant (CRIM-4), we again used the mean porosity per soil and depth and now fitted the dielectric permittivity of the solid phase for each soil and depth.

2.3.3. Sandbox experiment

In order to compare the accuracy of the factory calibration provided by the manufacturer with the two-step calibration developed in this study, a sandbox experiment was performed. The experiment was carried out in a box (length: 36.8 cm, width: 26.7 cm, height: 17.2 cm) which was filled with 15 kg of quartz sand, with a grain size diameter between 0.1 and 0.4 mm (F32, Quartzwerke Frechen, Germany). To cover soil water contents between 0 and 35 vol. %, we added 0.5 dm^3 of demineralized water in seven steps. Each time, the sand was thoroughly mixed with a blender before refilling into the box to achieve best possible soil homogeneity. During the refilling process, the soil material was carefully compacted to achieve similar soil density. The sand height and weight were measured to determine soil volume and soil density. Three 10HS sensors were installed in the central part of the box (see Figure 2) ensuring that the measurements were only affected by the sand inside the box. The ProCheck device (Meter Group Inc., USA) was used to determine the raw sensor response and the soil water content based on the factory calibration. For the two-step calibration, the universal SRP model determined using the reference media was used to convert the sensor response to permittivity, and the Topp equation (Topp et al., 1980) was used to determine SWC from permittivity. Additional corrections for the effect of electrical conductivity and temperature were not required here because of the use of demineralized water with low conductivity and the controlled temperature during the experiment.

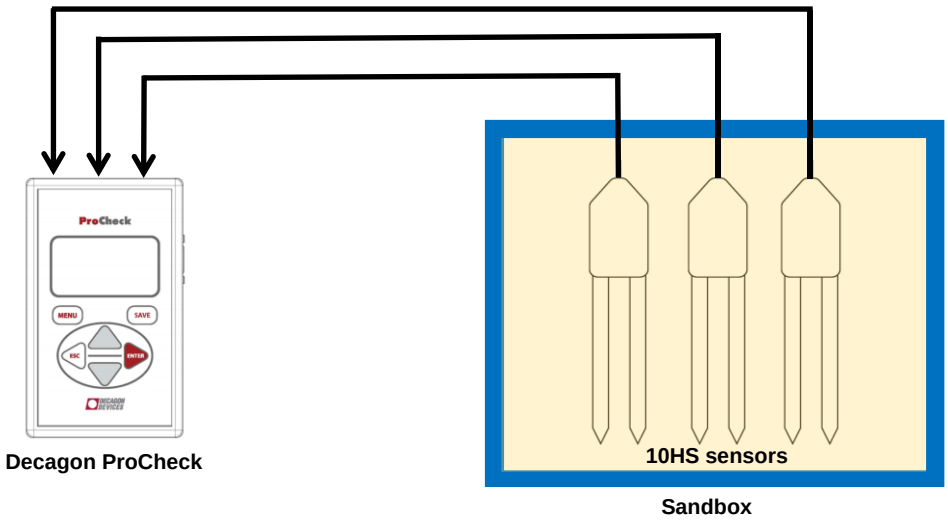

Figure 2. Top view of the sandbox experiment with three 10HS sensor connected to Decagon ProCheck device.

3. Results and Discussion

3.1. Sensor response – permittivity (SRP) calibration for the 10HS sensor

The statistical results of the sensor response measurements in the different reference media for the two immersion variants are summarized in Table 4. It can be seen that

mean sensor response increased with increasing permittivity and that the 10HS sensors showed considerable sensor-to-sensor variability as indicated by the average standard deviation and coefficient of variation of 13.8 mV and 1.41 %, respectively. This sensor-to-sensor variability is the consequence of intrinsic factors, such as subtle variations in the electrical components and probe geometry affecting the electromagnetic wave propagation characteristics (Rosenbaum et al., 2010). It can also be seen that the sensor readings are affected by the immersion depth of the sensor into the reference media. Our experimental results indicate that with increasing permittivity, the 10HS sensor becomes increasingly affected by the depth of immersion. For the reference media M1-M3, only minor differences were found. However, significant differences were found for M4 and M5 with differences in mean sensor response of 0.02 V and 0.05 V, respectively.

Table 4. Statistical result of the sensor response measurements using 10HS sensors in calibration media.

Calibration Medium	Incompletely immersed sensors in calibration medium			Fully immersed sensors in calibration medium		
	Mean Sensor Response	Standard Deviation	Coefficient of Variation	Mean Sensor Response	Standard Deviation	Coefficient of Variation
	V	V	%	V	V	%
M1	0.50	0.009	1.84	0.50	0.009	1.84
M2	0.80	0.017	2.10	0.79	0.016	2.08
M3	1.32	0.011	0.86	1.32	0.011	0.86
M4	1.41	0.017	1.23	1.43	0.016	1.12
M5	1.47	0.015	1.01	1.52	0.017	1.10

Table 5. Fitting parameters and root mean square error (RMSE) between measured and predicted dielectric permittivity when the sensors are incompletely immersed and fully immersed in calibration media.

	α	β	γ	RMSE
Equation (2) incompletely immersed	-0.200	0.335	-1.227	0.518
Equation (2) fully immersed	-0.118	0.220	-2.456	0.412

In order to test how the differences in sensor response of the two immersion variants affect the sensor calibration, we fitted the SRP model (Eq. 2) to both calibration data sets. The fitted SRP models are presented in Figure 3 and the fitting parameters and the associated RMSE are provided in Table 5.

The difference between the two SRP models is clearly visible in Figure 3. In the case of incomplete immersion in the reference media, the slope is much steeper in wet soil. This has the following implications for the measurement accuracy of the 10HS sensor. First, the use of a calibration strategy based on incomplete immersion will overestimate permittivity in the range between 0.20-0.65 V and 1.35-160 V and will underestimate it in the range between 0.65-1.35 V ranges when the sensor is completely buried in the soil during the field experiments. Second, the sensor reading is less sensitive to changes SWC

in the range between 1.35-1.60 V due to the steeper slope. In our field experiment, the 10HS sensors were completely buried in the soil. Therefore, we prefer the SRP model obtained from the fully immersed calibration data to describe sensor response-permittivity relationship of the 10HS sensors in the following.

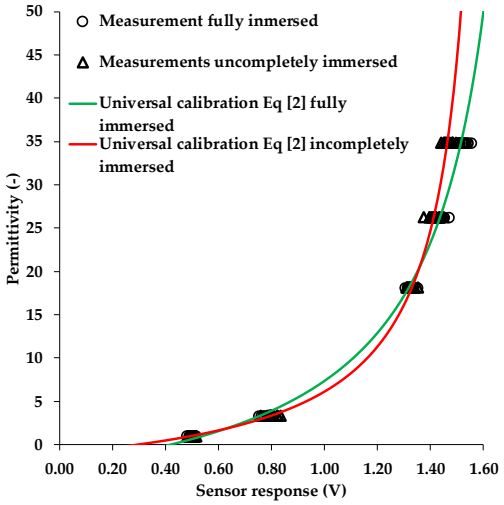

Figure 3. The response of 16 10HS sensors in five reference media for the two cases "incompletely immersed" and "fully immersed" as well as the corresponding universal SRP models.

3.2. Universal versus sensor-specific calibration

The 10HS sensor exhibited considerable sensor-to-sensor variability (Figure 3). Therefore, we tested to which degree the 10HS sensors would benefit from a sensor-specific calibration. The comparison between universal and sensor-specific calibration of each of 16 sensors is presented in Figure 4. The RMSE between the reference permittivity (Table 2) and the apparent dielectric permittivity estimated using the fitted SRP model (fully immersed case) was used to evaluate to what extent a sensor-specific calibration could improve the accuracy of the permittivity estimates (Table 6). To put the results into perspective, the permittivity was converted to equivalent SWC using the Topp model (Topp et al., 1980).

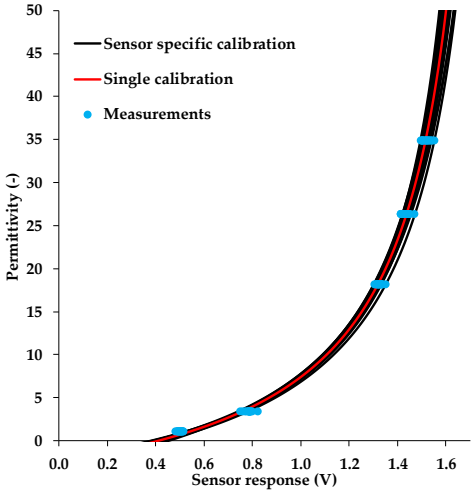

Figure 4. Universal SRP model fitted to the whole data set of every sensor and sensor-specific SRP models fitted to the sensor response measurement of each 10HS sensor.

Table 6. RMSE between apparent dielectric permittivity (K_a) and reference permittivity for sensor-specific and universal calibration, as well as the corresponding equivalent SWC (θ_{eq}) RMSE estimated using the Topp empirical permittivity-SWC relationship (Topp et al., 1980).

Calibration Standard	Sensor-Specific Calibration		Universal Calibration Function	
	RMSE K_a	RMSE θ_{eq} (Vol. %)	RMSE K_a	RMSE θ_{eq} (Vol. %)
M1	0.349	-	0.350	-
M2	0.398	1.014	0.426	1.083
M3	0.397	0.528	0.684	0.901
M4	0.608	0.571	1.424	1.317
M5	0.207	0.135	2.324	1.471
Total	0.427	0.642	1.421	1.213

In case a universal calibration function was used to relate sensor response to permittivity, the RMSE between estimated and reference permittivity increased considerably with increasing medium permittivity. The overall RMSE for K_a determined using a universal calibration function was 1.421 (θ_{eq}: 1.213 vol. %). Rosenbaum et al. (2010) obtained similar RMSE values of 1.5 and 1.2 for the EC-5 and 5TE sensors (METER Group Inc., USA), respectively. Bogena et al. (2017) found lower errors (RMSE K_a: ~0.87, RMSE (θ_{eq}: ~0.95 vol. %) for the low-cost SMT100 sensor (Truebner GmbH, Germany).

The use of sensor-specific calibration decreased the overall RMSE of K_a to 0.427 (θ_{eq}: ~0.642 vol. %). Sakaki et al. (2008) obtained a similar accuracy for dry sand (±0.5 vol. %) and a lower accuracy for saturated sand (±2.8 vol. %) in case of the EC-5 sensor. Rosenbaum et al. (2010) also investigated the EC-5 sensor and found a lower accuracy for a sensor-specific calibration (~0.8, 1.4 vol. %). Finally, Qu et al. (2013) investigated sensor-specific calibration for the SPADE sensor (Sceme.de, Germany), and obtained a higher accuracy of 0.226 (0.4 vol. %). Given the standardised calibration process that reduced side effects such as variations in glass beads density as well as medium contamination to a minimum (Bogena et al., 2017), we attribute the observed differences mainly to sensor-to-sensor variability which has been often observed for this kind of low-cost SWC sensors (Rosenbaum et al., 2010).

3.3. Permittivity-soil water content relationships

The relationship between the apparent dielectric permittivity and SWC of 15 undisturbed soil samples from Menàrguens (20 cm and 50 cm depth) and Mollerussa (15 cm and 30 cm depth) is shown in Figure 5a. It can be observed that the data were slightly different depending on location and depth.

In a first step, the accuracy of the relationship proposed by Topp et al. (1980) was evaluated. This empirical relationship resulted in a RMSE of 2.94 vol.% (Figure 5a, Table 7), which indicates a reasonably good match considering that the Topp model 1980 is a "universal function" derived from experiments with limited variation in soil properties.

Table 7. RMSE between soil water content measured and predicted by different models.

Model	RMSE (vol. %)
Topp	2.94
Complex Refractive Index Model 1 (CRIM-1)	3.54
Complex Refractive Index Model 2 (CRIM-2)	1.90
Complex Refractive Index Model 3 (CRIM-3)	1.43
Complex Refractive Index Model 4 (CRIM-4)	1.37

The first variant of the CRIM model (CRIM-1) considered the average porosity for all samples (43%) and a literature value for K_s (4.40 for quartz (Robinson et al., 2004)). The fit to the data is shown in Figure 5b and the resulting RMSE was 3.54 vol. % (Table 7). This indicates that the use of the CRIM-1 model based on measured average porosity and literature values for the permittivity of the solid phase resulted in a somewhat lower accuracy than the Topp model (Topp et al., 1980). In the next variant (CRIM-2), K_s was fitted. This resulted in a K_s value of 6.3 and a better fit to the data (Figure 5) with a RMSE of 1.90 vol. % (Table 7). The fitted K_s obtained with the CRIM-2 model is higher than that of the CRIM-1 model, which was based on the permittivity of quartz. Since most clay minerals have a higher permittivity than quartz (Robinson et al., 2004), this is not surprising considering the relatively high silt and clay fraction of the Menàrguens and Mollerussa test site (see Table 1).

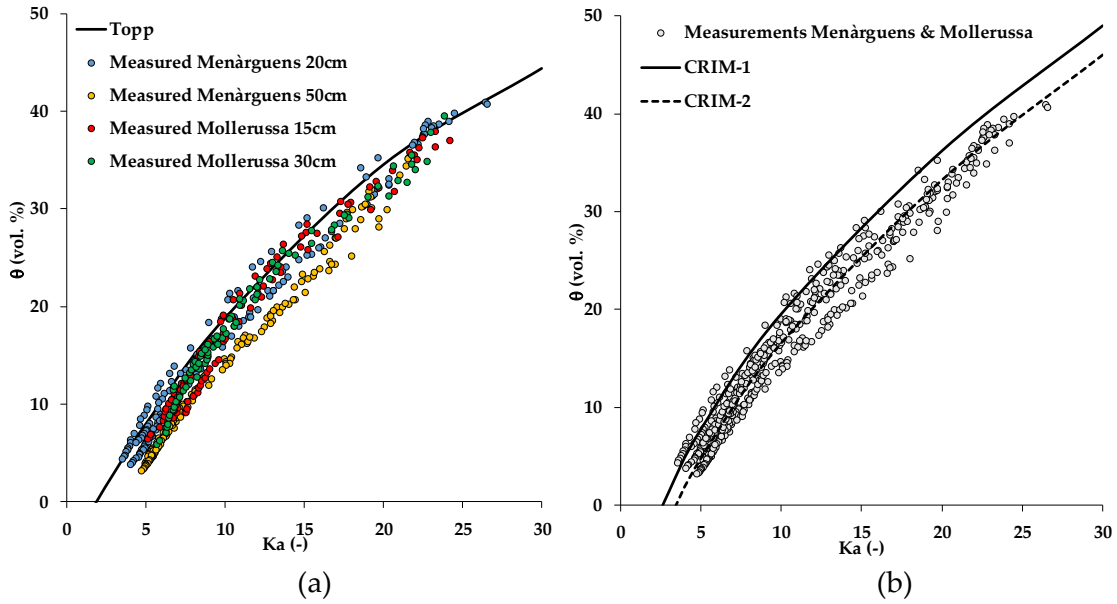

Figure 5. Relationship between apparent dielectric permittivity (K_a) and soil water content for all samples from the Menàrguens (20 cm and 50 cm depth) and Mollerussa (15 cm and 30 cm depth) test sites and the fit of Topp model (20) (a) and the CRIM-1 and CRIM-2 models (b).

In the next variant (CRIM-3), the variability in measured porosity was also considered. To this end, we averaged the porosity measurements per site and depth, resulting in a porosity of 48% and 36% for 20 and 50 cm depth, respectively, for the Menàrguens site and a porosity of 44% and 48% for 15 and 30 cm depth, respectively,

for the Mollerussa site. Again, a single value of K_s was fitted to the data, and this resulted in a K_s value of 6.3. The RMSE further decreased to 1.43 vol.%, indicating that porosity is an additional control of the apparent dielectric permittivity - soil water content relationship. Figure 6 shows the fit of the CRIM-3 model to the experimental data. For the Menàrguens site, the CRIM-3 model was significantly different for 20 and 50 cm depth due to the different porosity. At 50 cm depth, there was a zone of larger compaction due to the transition between the ridge and the original soil. Therefore, the undisturbed soil samples showed higher bulk density and lower porosity. For the Mollerussa site, the CRIM-3 model predictions were similar for 15 and 30 cm depth, since the bulk density and porosity of both depths were similar.

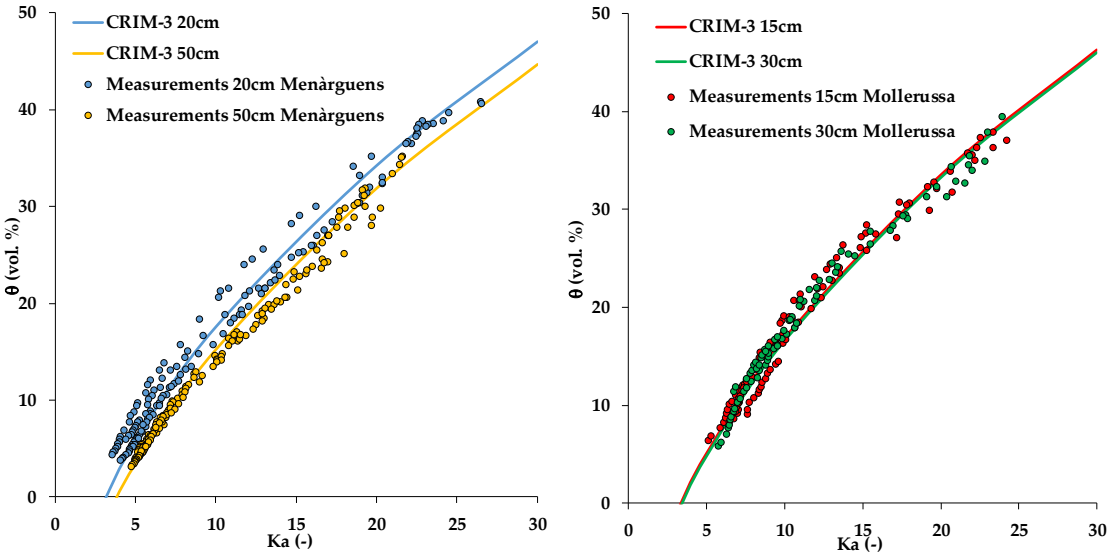

Figure 6. Apparent dielectric permittivity (K_a) - soil water content for all samples of the Menàrguens (20 cm and 50 cm depth) (a) and Mollerussa (15 cm and 30 cm depth) (b) test sites and the derived CRIM-3 model.

For the final variant (CRIM-4), both the dielectric permittivity of the solid phase (K_s) and average porosity varied per depth and site (Figure 7). In this variant, the RMSE further improved to 1.37 vol.%, although the improvement was only subtle compared to the variant CRIM-3 with only a single value for K_s. The fitted values for K_s are given in Table 8, and varied in a small range only. In comparison to other studies, this fit is excellent. For instance, Robinson et al. (1998), who evaluated the performance of several capacitive sensors including the Wet2 (Delta-T Devices), 5TE and 10HS sensors in well-characterized soils with variable texture, obtained accuracies that varied from 3.4 to 7.3 vol.%. Similar applications of the CRIM model by Rosenbaum et al. (2012) and Qu et al. (2016) resulted in RMSE values of 2.9 vol.% and 2.2 - 2.8 vol.%, respectively.

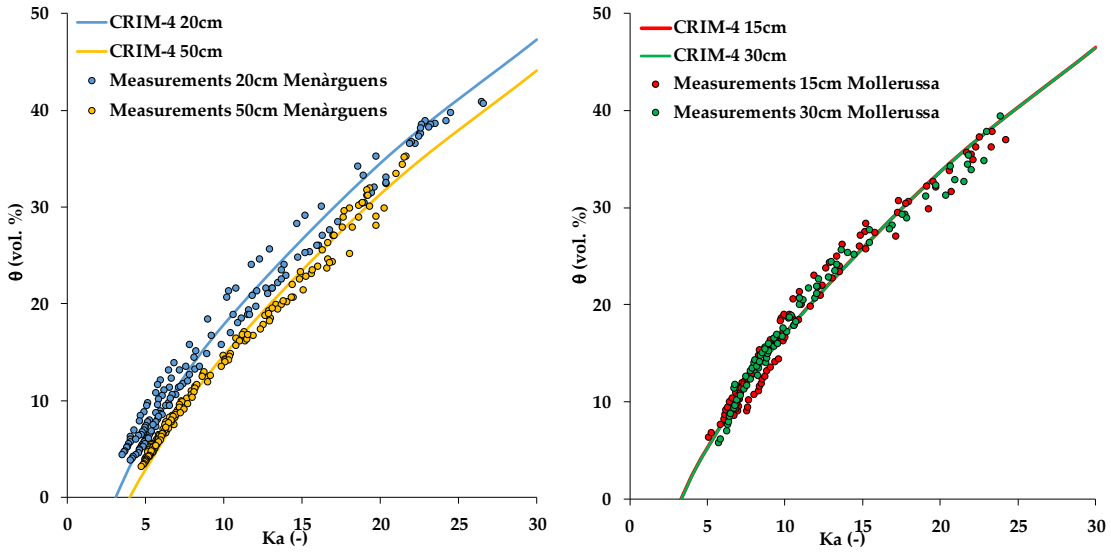

(a) (b)

Figure 7. Apparent dielectric permittivity (K_a) - soil water content for all samples of Menàrguens (20 cm and 50 cm depth) and Mollerussa (15 cm and 30 cm depth) test sites and the derived K_a-θ CRIM-4 model.

Table 8. Parameters of the CRIM-4 model for Menàrguens and Mollerussa sites.

	Menàrguens		**Mollerussa**	
Depth	**20cm**	**50cm**	**15cm**	**30cm**
K_{water}	78.54	78.54	78.54	78.54
K_{air}	1.00	1.00	1.00	1.00
K_{solid}	6.09	6.66	6.16	5.98
η	0.48	0.36	0.44	0.43

3.4. Comparison of factory and two-step calibration approach

In order to compare the two-step-calibration approach with the factory calibration, we combined both calibration steps (SRP and CRIM model) to obtain a sensor response - SWC relationship. In the following, we consider the calibration approach using the SRP model for a fully immersed sensor head and the CRIM-4 variant as the "reference" two-step calibration. Figure 8 shows that there was a substantial difference between factory calibration and the "reference" two-step calibration as well as the calibration variant using a combination of the SRP model and the Topp equation (Topp et al., 1980). For almost the entire range of relevant sensor response, the SWC predicted by the factory calibration was considerably higher than the SWC predicted by our two-step calibration. Spelman et al. 2013 reported a similar difference between the factory calibration of the 10HS sensor and soil-specific calibrations using agricultural soils.

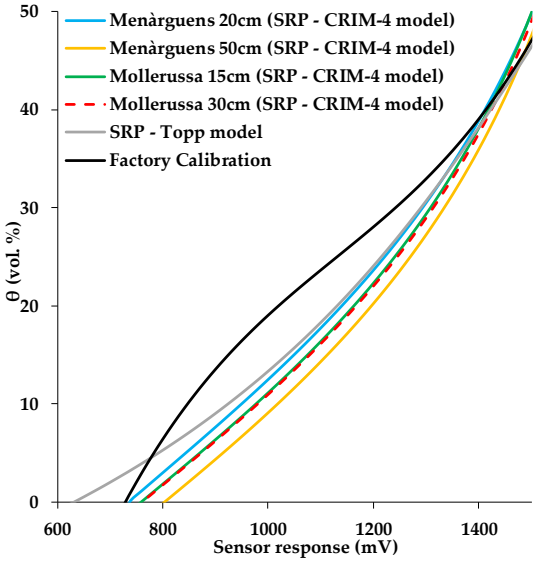

Figure 8. Comparison of the factory calibration and calibration curves for 10HS sensors obtained using the reference two-step calibration for soils samples from the Menàrguens and Mollerussa test sites. A calibration using the universal SRP model combined with the K_a-θ Topp model (Topp et al., 1980) is also presented

To further confirm this strong discrepancy, we conducted a sandbox experiment with three 10HS sensors. Figure 9 compares gravimetrically determined volumetric SWC with SWC determined with the 10HS sensors using the factory calibration and the universal SRP model combined with the Topp equation (Topp et al 1980). The factory calibration resulted in a relatively high RMSE of 5.33 vol. % (R^2=0.92), whereas the two-step calibration achieved a much better agreement (RMSE: 1.03 vol. %, R^2: 0.99). Fares et al. (2016), who studied the effect of soil organic matter on SWC measurements with 10HS sensors, obtained a similar RMSE using the factory calibration (RMSE ranged between 5.3-7.2 vol. %), but they obtained a somewhat lower accuracy for their soil-specific calibrations (RMSE ranged between 1.3-1.9 vol. %). Matula et al. 2016 found similar results for various ECH2O sensors (5TE, EC-5, EC-10 and EC-20) using two soil media with different bulk density (average RMSE of the factory calibration was 3.3 vol. %, while average of RMSE of the soil specific calibration was 1.3 vol. %). These results confirm the accuracy of the two-step calibration approach and highlight the limited accuracy of the factory calibration provided with the 10HS sensor.

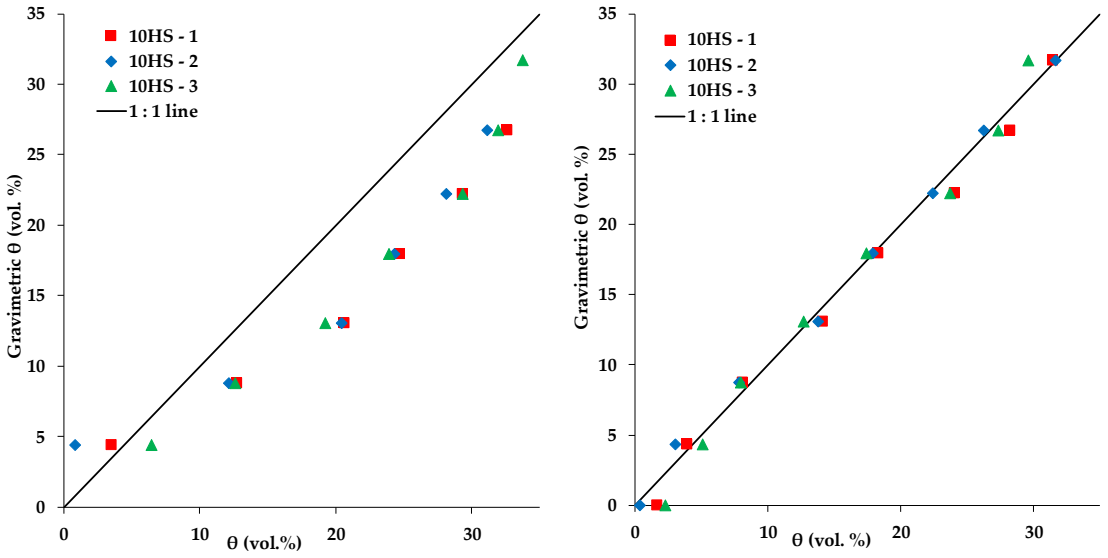

Figure 9. Comparison of the gravimetric soil water content with those measured with three 10HS sensors using either the factory calibration (a) or universal SRP model combined with K_a-θ Topp model (Topp et al., 1980) (b).

3.5. Analysis of field measurements

In a final step, we applied the factory calibration and different variants of the two-step calibration to the experimental field data used for irrigation scheduling in a period of intensive irrigation in July 2017 for both the Menàrguens and Mollerussa sites and the two measurements depths (Figure 10). The different SWC prediction variants based on the two-step calibration approach that were considered are: i) sensor-specific SRP models combined with the CRIM-4 model, ii) a universal SRP model combined with the CRIM-4 model, iii) a universal SRP model obtained with incompletely immersed sensor head combined with the CRIM-4 model, iv) and a universal SRP model combined with the Topp model (Topp et al., 1980). It should be noted that corrections for temperature and electrical conductivity were not yet considered here, and we only focus on differences in SWC predictions using different calibration strategies.

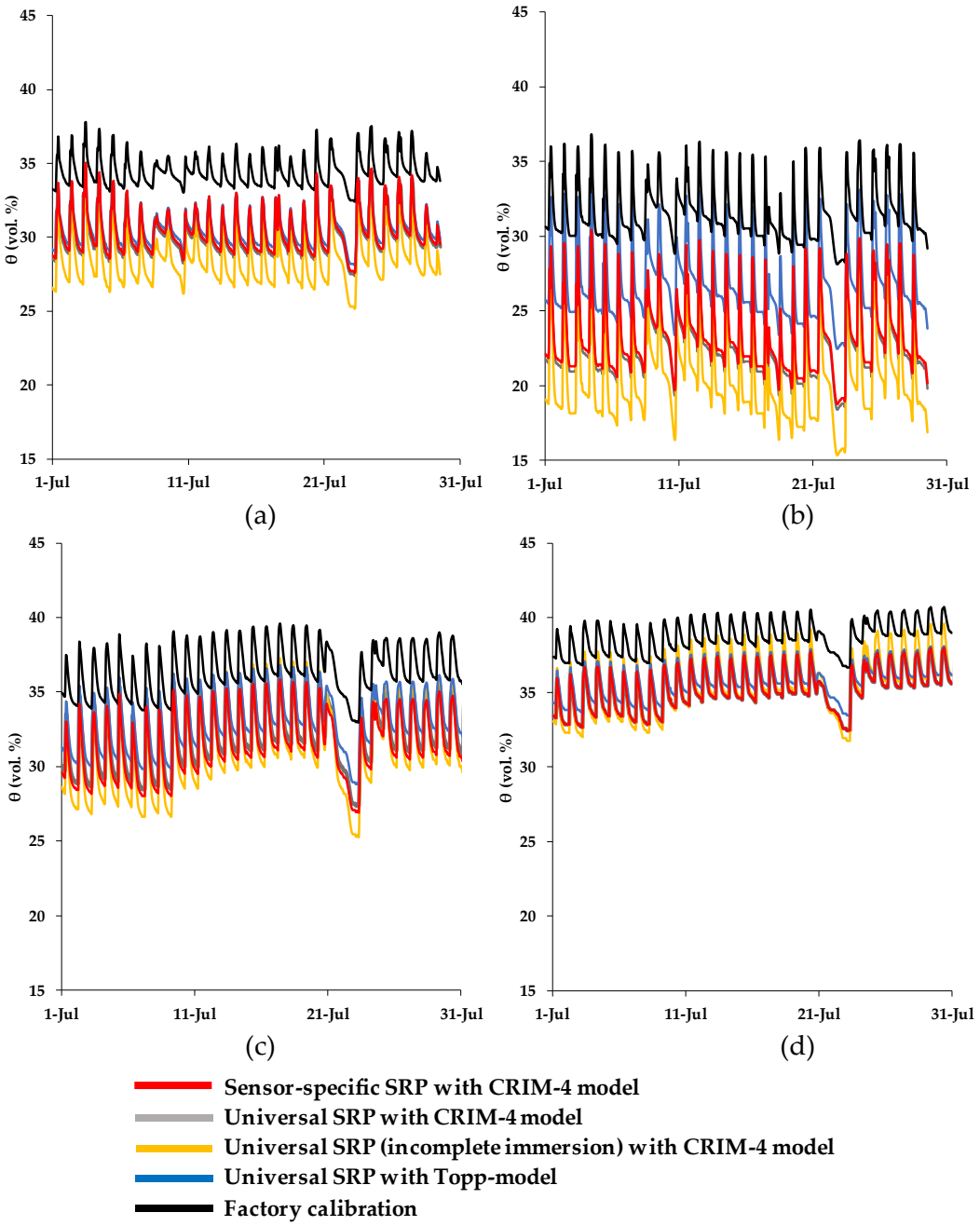

Figure 10. Soil water content measurements (vol. %) obtained from different calibration variants: (a) Menàrguens at 20 cm depth, (b) Menàrguens at 50 cm depth, (c) Mollerussa at 15 cm depth and (d) Mollerussa at 30 cm depth.

In the following, the sensor-specific SRP models combined with the CRIM-4 model were used as a reference because this combination provided the best results for the two-step calibration approach (RMSE: 1.37 vol.%). To quantify the differences in terms of SWC predictions made with the sensor-specific SRP and the CRIM-4 model and other variants, the root mean square error (RMSE) and the mean difference were calculated (Table 9 and 10, respectively). The results show that the use of a universal instead of a sensor-specific SRP model in combination with the CRIM-4 model resulted in a small difference in SWC predictions with an RMSE of 0.25 vol.% and a mean difference of 0.24

vol.%. When the universal SRP model derived from calibration measurements with incompletely immersed sensor heads was used, the RMSE and the mean difference increased substantially to 1.53 vol.% and 1.31 vol.%, respectively. This increase in RMSE suggests that the effect of immersion depth is important for this particular case study. However, this is likely not generally the case since the differences between the two immersion variants varied considerably for different sensor response ranges (see Figure 3). When the CRIM-4 model was replaced with the Topp model (Topp et al., 1980), the differences in SWC predictions resulted in a RMSE of 1.51 vol.% and a mean difference of 1.49 vol.%. Therefore, it can be concluded that the consideration of the correct immersion variant of the sensor response calibration and an accurate soil-specific calibration are more important than the use of a sensor-specific SRP model. Finally, the SWC predictions based on the factory calibration resulted in even larger differences with an RMSE of 5.18 vol.% and a mean difference of 5.16 vol.%.

Table 9. Accuracy of the different calibration variants with respect to the reference calibration (sensor-specific SRP models combined with the CRIM-4 model).

Calibration variant	Menàrguens		Mollerussa		Mean RMSE (vol.%)
	20 cm	50 cm	15 cm	30 cm	
	RMSE (vol.%)				
Universal SRP with CRIM-4 model.	0.17	0.32	0.50	0.02	0.25
Universal SRP (incomplete immersion) with CRIM-4 model.	1.84	2.79	0.79	0.70	1.53
Universal SRP with Topp model.	0.30	3.57	1.54	0.65	1.51
Factory calibration.	4.09	8.23	4.90	3.51	5.18

Table 10. Mean difference (vol. %) between reference calibration (sensor-specific SRP models combined with the CRIM-4 model) and different calibration variants.

Calibration variant	Menàrguens		Mollerussa		Absolute Mean difference (vol.%)
	20 cm	50 cm	15 cm	30 cm	
	Mean difference (vol. %)				
Universal SRP with CRIM-4 model.	-0.17	-0.32	0.50	-0.01	0.25
Universal SRP (incomplete immersion) with CRIM-4 model.	-1.80	-2.73	-0.31	0.39	1.31
Universal SRP with Topp model.	0.28	3.57	1.52	0.61	1.49
Factory calibration.	4.07	8.21	4.87	3.49	5.16

The results obtained in this study can be used to improve irrigation scheduling. At the Menàrguens and Mollerussa test sites, the SWC predictions obtained by the two-step calibration approach were always below the predictions based on the factory calibration. Therefore, the factory calibration would have resulted in an underestimation of irrigation amounts for both the Menàrguens and Mollerussa sites. Although two-step calibration requires more time, it was worthwhile in this particular study since it increased the accuracy of the SWC measurements and thus allows for a proper applications of irrigation that matches the crop needs.

4. Conclusions

In this paper, we evaluated the sensor response of low-cost 10HS soil water content sensors using a two-step calibration procedure. First, we calibrated the sensor response of 10HS sensors to permittivity using a standard procedure based on five reference media with known dielectric permittivity. Here, the effect of immersion depth on the calibration results was also considered. Second, a site-specific relationship between permittivity and soil water content with soil samples from different sites and depths was established. It was found that the results of the calibration in reference media depended on the immersion depth of the sensor. Therefore, the calibration protocol should be adapted to the type of application of the 10HS sensor. For example, the sensor head is typically inserted into the soil in field applications. Therefore, the sensor should be calibrated with a fully immersed sensor head for this type of application. In addition, we compared the accuracy of the use of a universal calibration relationship between sensor response and permittivity with the accuracy of a sensor-specific calibration. Our results showed that the RMSE of the dielectric permittivity estimated decreased from 1.421 to 0.427 when a sensor-specific calibration was considered.

In a next step, undisturbed soil samples and time domain reflectometry (TDR) were used to establish a site-specific relationship between permittivity and soil water content. Five different model variants were used that relied on available data on porosity and fitting of the permittivity of the solid phase to a different extent. The model that considered both variations in porosity and solid-phase permittivity between sites and depths resulted in the highest accuracy (RMSE: 1.37 vol.%). However, a simplified model that considered a universal fitted value for the solid-phase permittivity and spatially variable porosity provided almost equal accuracy. Based on the two-step calibration, relationships between sensor response and soil water content were obtained that were compared to the factory calibration using measurements on sand with known water content. It was found that the relationship obtained using the two-step calibration approach provided much more accurate SWC predictions than the factory calibration provided with the 10HS sensor (RMSE: 5.33 vol.% versus 1.03 vol.%).

Finally, we applied the factory calibration and different variants of the two-step calibration approach to field measurements made with 10HS sensors during a period of irrigation in almond and apple orchards in Menàrguens and Mollerussa, respectively. The results showed that the time-average absolute difference was 5.16 vol.% and the RMSE was 5.18 vol.% when the factory calibration was used instead of the most advanced model obtained with the two-step calibration approach. The use of a universal instead of a sensor-specific sensor response model only resulted in a small difference and RMSE, thus indicating that the use of a universal sensor response model would have been possible in this particular case study. The use of the empirical equation of Topp et al. (1980) instead of a soil-specific calibration resulted in a moderate increase in the mean difference and RMSE. Since the factory calibration significantly overestimated SWC, it is

recommended to improve the accuracy of SWC measurements of the 10HS sensors using sensor- and soil-specific calibration in applications where accuracy is important.

Acknowledgments

This research was supported by the National Institute for Agricultural and Food Research and Technology (INIA) (RTA 2013-00045-C04-01) of the Ministry of Economy and Competitiveness of the Spanish government and by the European Social Fund. The authors would like to acknowledge the collaboration of Ms. Sirgit Kummer part of the staff of the Institute of Bio- and Geosciences, Agrosphere Institute (IBG-3), Forschungszentrum Jülich GmbH and Mr. Jordi Oliver part of the staff of the Efficient Use of Water in Agriculture Program for their support in implementing this activity.

Literature cited

Birchak, J. R.; Gardner, C. G.; Hipp, J. E. and Victor J. M. High dielectric constant microwave probes for sensing soil moisture. P. IEEE. 1974, 62, 93-98.

Bogena, H. R.; Huisman, J. A.; Oberdörster, C.; H. Vereecken. Evaluation of a low-cost soil water content sensor for wireless network applications. J. Hydrol. 2007, 344, 32–42.

Bogena, H. R.; Huisman, J. A.; Schilling, B.; Weuthen, A.; Vereecken, H. Effective calibration of low-cost soil water content sensors. Sensors 2017, 17, 208.

Chung, C. C.; Lin, C. P. Apparent dielectric constant and effective frequency of TDR measurements: Influencing factors and comparison. Vadose Zone J. 2008, 8, 548-556.

Fares, A.; Awal, R; Bayabil, H. Soil water content sensor response to organic matter content under laboratory conditions. Sensors 2016 16, 1239.

Hilhorst, M.A.; Dirksen,C, Dielectric water content sensors: time domain versus frequency domain. In Time domain reflectometry in environmental, infrastructure, and mining applications, KM O'Connor et al. (eds.). US Dept. Interior Bureau of Mines, Northwestern Univ., Evanston, Illinois. 1994; pp. 23-33.

Jones, S.B.; Blonquist, J.M.; Robinson, D.A.; Rasmussen, V.P.; Or D. Standardizing characterization of electromagnetic water content sensors. Part 1. Methodology. Vadose Zone J. 2005, 4, 1048–1058.

Kaatze, U., Kettler, M., Pottel, R. Dielectric relaxation spectrometry of mixtures of water with isopropoxy- and isobutoxyethanol. Comparison to unbranched poly (ethylene glycol) monoalkyl ethers. J Phys Chem. 1996, 100, 2360–2366.

Kizito, F.; Campbell, C. S.; Campbell, G. S.; Cobos, D. R.; Teare, B. L.; Carter, B.; Hopmans, J. W. Frequency, electrical conductivity and temperature analysis of a low-cost capacitance soil moisture sensor. J. Hydrol. 2008, 352, 367-378.

Kögler, S.; Wagner, N.; Zacharias, S.; Wollschläger, U. Characterization of reference materials for an economic calibration approach for low-cost soil moisture sensors. In Proceedings of the 10th International; Conference on Electromagnetic Wave Interaction with Water and Moist Substances (ISEMA 2016), Weimar, Germany, 2013; 6–11.

Kojima, Y.; Shigeta, R.; Miyamoto, N.; Shirahama, Y.; Nishioka, K.; Mizoguchi, M.; Kawahara, Y. Low-Cost Soil Moisture Profile Probe Using Thin-Film Capacitors and a Capacitive Touch Sensor. Sensors 2016, 16, 1-14.

Matula, S., Bát'ková, K.; Legese, W.L. Laboratory performance of five selected soil moisture sensors applying factory and own calibration equations for two soil media of different bulk density and salinity levels. Sensors 2016, 16, 1912.

Nolz, R.; Kammerer G.; Cepuder P. Calibrating soil water potential sensors integrated into a wireless monitoring network. Agr. Water Manage. 2013, 116, 12–20.

Pepin, S.; Livingston, N. J.; Hook, W. R. Temperature dependent measurement errors in time domain reflectometry determination of soil water. Soil Sci. Soc. Am. J. 1995. 59, 38–43.

Qu, W.; Bogena, H. R.; Huisman, J. A.; Schmidt, M.; Kunkel, R.; Weuthen, A.; Schilling, B.; Sorg, J.; Vereecken, H. The integrated water balance and soil data set of the Rollesbroich hydrological observatory. Earth Syst. Sci. Data 2016, 8, 517-529.

Qu, W.; Bogena, H. R.; Huisman, J. A.; Vereecken H. Calibration of a Novel Low-Cost Soil Water Content Sensor Based on a Ring Oscillator. Vadose Zone J. 2013, 12, 0.

Robinson, D. A. Measurement of the solid dielectric permittivity of clay minerals and granular samples using a time domain reflectometry immersion method. Vadose Zone J. 2004, 3, 705–713.

Robinson, D. A.; Jones S. B.; Wraith, J. M.; Or, D.; Friedman, S.P. A review of advances in dielectric and electrical conductivity measurement in soils using time domain reflectometry. Vadose Zone J. 2003, 2, 444-475.

Robinson, D. A; Gardner, C. M. K.; Evans, J.; Cooper, J. D.; Hodnett, M. G.; Bell, J. P. The dielectric calibration of capacitance probes for soil hydrology using an oscillation frequency response model, Hydrol. and Earth Syst. Sc. 1998, 2, 111-120.

Rosenbaum, U.; Bogena, H. R; Herbst, M.; Huisman, J. A.; Peterson, T. J.; Weuthen, A.; Western, A. H.; Vereecken, H. Seasonal and event dynamics of spatial soil moisture patterns at the small catchment scale. Water Resour. Res. 2012. 48,1-22.

Rosenbaum, U.; Huisman, J.A.; Vrba, J.; Vereecken, H.;Bogena, H. R. Correction of temperature and electrical conductivity effects on dielectric permittivity measurements with ECH$_2$O sensors. Vadose Zone J. 2011, 10, 582–593.

Rosenbaum, U.; Huisman, J.A.; Weuthen, A.; Vereecken H.; Bogena H. R. Sensor-to-Sensor Variability of the ECHO EC-5, TE, and 5TE sensors in dielectric liquids. Vadose Zone J. 2010, 9, 181-186.

Roth, K.; Schulin, R.; Fluhler, H.; Attinger, W. Calibration of time domain reflectometry for water-content measurement using a composite dielectric approach. Water Resour. Res. 1990, 26, 2267–2273.

Sakaki, T.; Limsuwat, A.; Smits, K. M.; Illangasekare, T. H. Empirical two-point α-mixing model for calibrating the ECH$_2$O EC-5 soil moisture sensor in sands. Water Resour. Res. 2008, 44.

Seyfried, M.S.; Murdock, M. D. Measurement of Soil Water Content with a 50-MHz Soil Dielectric Sensor. Soil Sci. Soc. Am. J. 2004, 68, 394.

Soulis, K. X.; Elmaloglou S. Optimum soil water content sensors placement for surface drip irrigation scheduling in layered soils. Comput. Electron. Agr. 2018, 152, 1–8.

Spelman, D.; Kinzli KD.; Kunberger T. Calibration of the 10HS soil moisture sensor for Southwest Florida Agricultural Soils. J. Irrig Drain. Eng. 2013, 139, 965-971.

Topp, G. C., Davis, J. L.; Annan, A. P. Electromagnetic determination of soil water content: measurements in coaxial transmission lines. Water Resour. Res. 1980, 16, 574–582.

Topp, G.C.; Zegelin, S.; White, I. Impacts of the real and imaginary components of relative permittivity on time domain reflectometry measurements in soils. Soil Sci. Soc. Am. J. 2000, 64, 1244.

Vaz, C. M. P.; Jones, S.; Meding, M.; Tuller, M. Evaluation of standard calibration functions for eight electromagnetic soil moisture sensors. Vadose Zone J. 2013, 12, 0.

Visconti, F.; de Paz, J. M.; Martínez, D.; Molina, M. J. Laboratory and field assessment of the capacitance sensors Decagon 10HS and 5TE for estimating the water content of irrigated soils. Agr. Water Manage. 2014, 132, 111–119.

Weast, R. C. Handbook of physics and chemistry. 67th ed.; CRC press: Florida, United Estates, 1986; pp. 1983-1984.

Chapter II: Soil water dynamics around the dripper

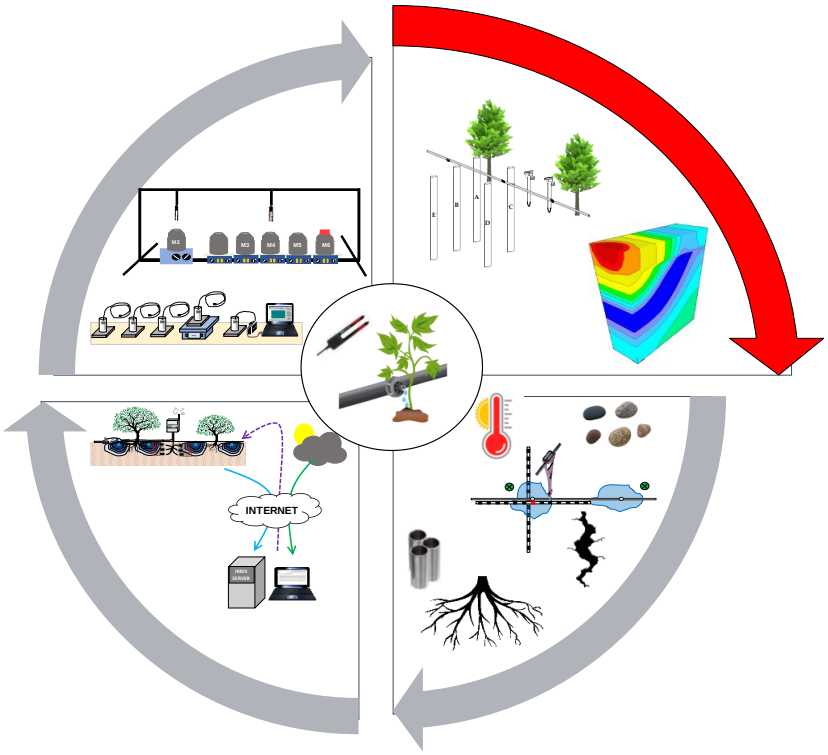

Parameterization of soil hydraulic parameters for HYDRUS-3D simulation of soil water dynamics in a drip-irrigated orchard

Jesús María Domínguez-Niño[1], Gerard Arbat[2], Iael Raij-Hoffman[3], Isaya Kisekka[3], Joan Girona[1], Jaume Casadesús[1]

[1] Programme on Efficient Use of Water in Agriculture, Institute of Agrifood Research and Technology (IRTA), Parc de Gardeny (PCiTAL), Fruitcentre, 25003, Lleida, Spain; jesus.dominguez@irta.cat; joan.girona@irta.cat; jaume.casadesus@irta.cat

[2] Department of Chemical and Agricultural Engineering and Technology, University of Girona, Campus Montilivi s/n, 17071 Girona, Spain; gerard.arbat@udg.edu

[3] Department of Land, Air and Water Resources/Biological and Agricultural Engineering, University of California Davis, One Shields Avenue, PES 1110, Davis, California, USA; iraij@ucdavis.edu; ikisekka@ucdavis.edu

Water (2020), 12-07, 1858 DOI: 10.3390/w12071858

Abstract

Although surface drip irrigation allows an efficient use of water in agriculture, the heterogeneous distribution of soil water complicates its optimal usage. Mathematical models can be used to simulate the dynamics of water in the soil below a dripper and promote: a better understanding, and optimization, of the design of drip irrigation systems, their improved management and their monitoring with soil moisture sensors. The aim of this paper was to find the most appropriate configuration of HYDRUS-3D for simulating the soil water dynamics in a drip-irrigated orchard. Special emphasis was placed on the source of the soil hydraulic parameters. Simulations parameterized using the Rosetta approach were therefore compared with others parameterized using that of HYPROP + WP4C. The simulations were validated on a seasonal scale, against measurements made using a neutron probe, and on the time course of several days, against tensiometers. The results showed that the best agreement with soil moisture measurements was achieved with simulations parameterized from HYPROP + WP4C. It further improved when the shape parameter n was empirically calibrated from a subset of neutron probe measurements. The fit of the simulations with measurements was best at positions near the dripper and worsened at positions outside its wetting pattern and at depths of 80 cm or more.

Keywords: HYDRUS-3D; simulation; soil water content; tensiometer; neutron probe; Rosetta; HYPROP; WP4C; soil wetting patterns.

1. Introduction

Agriculture is one of the activities that consumes most fresh water in the world approximately 70% (FAO, 2019). As population increases, so does the need for food and, as a consequence, the demand for water (Raij et al., 2016; Orzolez, 2017). It is therefore necessary to develop methods to improve the efficiently of water management (Kisekka et al., 2019). Drip irrigation is one of the most effective systems, since it gives irrigators a great deal of control over the amount of water that they use and helps to optimize parameters such as: the frequency and duration of irrigation, the discharge rate of the emitter, and the positioning of the emitters. This, in turn, helps to reduce water loss due to evaporation, percolation and runoff (Skaggs et al., 2004; Gärdenäs et al., 2005; Roberts et a., 2009).

Drip irrigation makes it possible to apply water at low rates and to match this, as closely as possible, to plant water uptake, thereby improving irrigation efficiency (Phogat et al., 2013). However, in the case of localized irrigation, the spatial distribution of water in the soil over time is complex and does not usually produce stable wetting patterns with respect to soil depth (Lin et al., 2006). The factors which can affect the resulting wetting patterns include soil characteristics, such as crop water uptake by the root system, soil surface evaporation, and the irrigation rate (Hao et al., 2007).

Wetting patterns can be studied using actual measurements taken in the field or simulations using mathematical models. Simulations allow us to analyze soil water dynamics both during and after irrigation and to provide relevant information about interacting processes. Models for estimating soil water distribution are tools for optimizing the design of irrigation systems. Once calibrated and validated, they make it possible to rapidly evaluate the spatial-temporal distribution of water, thereby saving time and money (Honari et al., 2017). The use of mathematical models also makes it possible to distinguish wet from dry soil (Arbat et al., 2013), describe the infiltration process, and provide an estimate of the water content of the wet pattern. In the latter case, it does this using the Richards equation, which describes the movement of water through unsaturated soils (Phogat et al., 2012; Elmaloglou et al., 2013).

Various mathematical models have been used to simulate soil water dynamics in drip irrigation systems, but unfriendly interfaces tend to complicate their use in the design of complex irrigation systems (Arbat et al., 2003). HYDRUS is one of the most widely used simulation models and makes it possible to simulate the movement of water, heat and solutes in a variety of saturated soil conditions. These include irregular boundaries and horizontal and vertical texture heterogeneity, in one, two or three dimensions (Simunek et al., 2016; Lu et al., 2019).

Given the stability of the HYDRUS model, this software can be used to investigate the distribution of soil water and its movement under the surface and subsurface of drip irrigation systems (Mailhol et al., 2011; Zhang et al., 2016; Lai et al., 2019; Sakaguchi et al.,

2019). It can also be used to design and evaluate the management of different irrigation systems, soils and crops (Egea et al., 2016; Garcia-Morillo et al., 2017; Tao et al., 2017). To simulate an orchard, it is more interesting to use HYDRUS-3D than HYDRUS-2D because it simultaneously solves transport problems on all three axes and provides more realistic calculations of soil water distribution around the dripper. For instance, a 3D representation makes it possible to consider neighboring drippers distributed along an irrigation dripline and at larger distances from neighboring driplines. Furthermore, a good level of accuracy can be achieved if the model is correctly calibrated for the soil hydraulic parameters in question (Arbat et al., 2008).

With an adequate soil characterization, it is possible to obtain results that are representative of reality. The soil hydraulic parameters that are required as inputs for the simulations can be obtained in different ways, such as applying the Rosetta method (Scaap et al., 2001), or a combination of the HYPROP (Schindler et al., 2016) and WP4C (Campbell et al., 2012) approaches. Rosetta is a model which uses pedotransfer functions (PTFs) to indirectly estimate the water retention parameters and the saturated and unsaturated hydraulic conductivity of a soil. It also estimates their probability distributions based on easily measured data such as soil texture and bulk density (Van Genuchten et al., 2003). On the other hand, combining HYPROP + WP4C offers a reliable experimental methodology that provides high resolution soil water retention (SWRC) and hydraulic conductivity (HCC) curves (Shokrana and Ghane, 2020).

In situ assessments of soil moisture can also be obtained by applying field approaches incorporating neutron probes and tensiometers (Robock et al., 2000). Neutron probes that have been previously calibrated for a specific location, measure representative volumes of soil and allow moisture levels to be measured at several different depths in order to obtain a profile of the moisture distribution (Zazueta et al., 1994). Tensiometers directly measure soil suction, with a good level of accuracy in well-watered crops, without the need to calibrate them for a specific soil type. They do, however, need periodic maintenance and may even show false variations in the soil water potential due to loss of contact with the soil (Heng and Evett, 2008; Migliaccio et al., 2015). Given the accuracy of the soil moisture measurements obtained using a neutron probe and tensiometers, they can be used to make comparisons with simulations and to analyze, calibrate and validate the performance of models.

The main goals of this study were to: (a) analyze and discuss the configuration of the HYDRUS-3D model for a drip irrigated apple orchard, especially regarding the sources of the soil hydraulic parameters; (b) analyze the sensitivity of the model to variations in the soil hydraulic parameters; and (c) obtain an adjusted model, which represents realistic soil water dynamics, and considers the three dimensions required to properly represent a drip-irrigated orchard. To achieve this, simulations were performed using different parameterization approaches and comparisons were made with measurements taken by

neutron probes and tensiometers at different soil depths and positions relative to the drippers.

2. Materials and Methods

2.1. Field experiment

The experiment was carried out at an apple orchard (*Malus domestica* Borkh. cv 'Golden Reinders'), which was planted in 2011 and grafted onto M-9 rootstock, at the IRTA-Lleida Experimental Station (Mollerussa, Lleida, Spain), over two crop seasons (2017-2018). The planting pattern was 3.63 m between rows and 1.2 m between trees, with a north-south orientation. Irrigation was automatically supplied by a surface drip system, which consisted of a single dripline, with drippers spaced at 0.60 m intervals, whose flowrate was 3.5 L h^{-1}. The climate in the area was semi-arid and characterized by hot, dry summers, and cool, wet winters, with annual rainfall and reference evapotranspiration (ET_O) of 290 and 1093 mm, respectively, for 2017 and 506 and 1040 mm, respectively, for 2018. The horizontal axis in Figure 1 corresponds to the years 2017 and 2018, when irrigation, rainfall, evaporation and transpiration were measured on a daily basis. Crop evapotranspiration (ET_C) was obtained by a weighing lysimeter located in the same orchard (Girona et al., 2004). The ET_C was divided into potential transpiration (T_P) and potential evaporation (E_P). It was experimentally determined in the lysimeter according to FAO (Allen et al., 1998). T_P was estimated as 90% of the ET_C and E_P was estimated as 10% of crop evapotranspiration, except on days following rain, when T_P was estimated as 90% of the ET_C and E_P was estimated as ET_O-T_P.

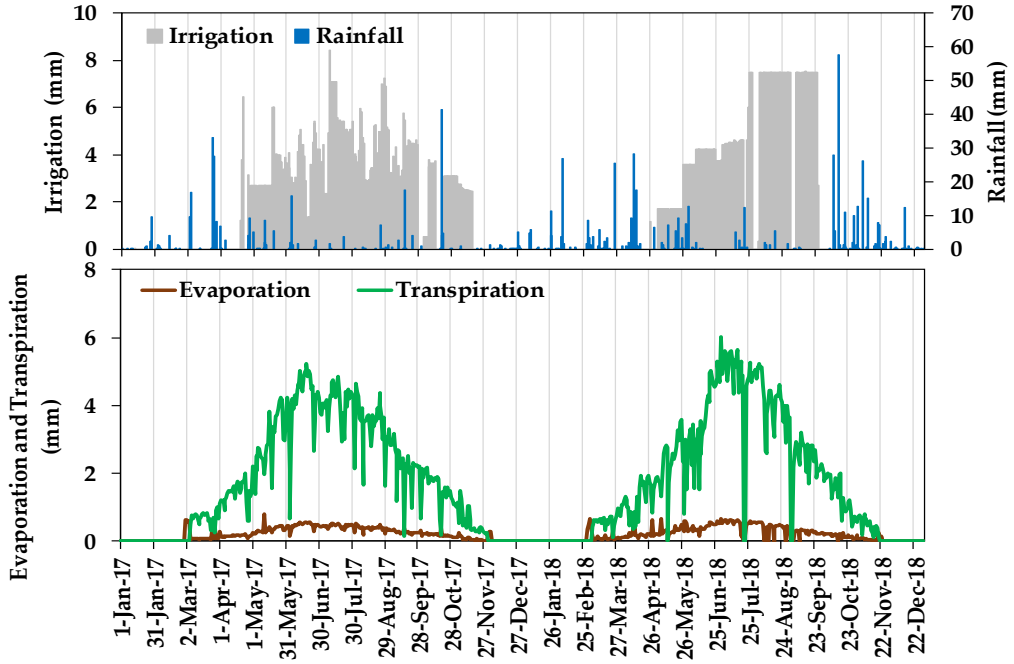

Figure 2. Irrigation, rainfall, evaporation and transpiration during the years 2017 and 2018

The orchard soil was classified as *Typic Calcixerepts, coarse-loamy, mixed and thermic* according to the Soil Survey Staff classification (Soil Survey Staff, 1999). Three soil layers were distinguished. The main difference between layers was due to the percentage of organic matter, which decreased with depth. Their physical properties are described in Table 1.

Table 11. Physical soil properties at the IRTA orchard in Mollerussa, at three depths

Depth (cm)	**0 - 20**	**20 - 40**	**40 -60**
USDA Soil Classification	Loamy	Loamy	Loamy
Sand (%)	35.80	35.50	36.00
Silt (%)	40.70	40.60	39.90
Clay (%)	23.50	23.90	24.10
Bulk density (g cm^{-3})	1.48	1.50	1.53
Organic Matter (%)	1.99	1.57	1.34

Throughout most of the study period, the apple trees were irrigated on a daily basis to meet crop water needs. This involved daily irrigation doses (DID) which were determined on a weekly basis, based on the FAO water balance (Allen et al., 1998):

$$DID = ET_O \times K_C \quad \text{(Eq. 1)}$$

where ETo was the reference evapotranspiration from the previous week, recorded by a weather station located on the same farm, and Kc was the crop coefficient determined in previous years by the weighing lysimeter in the same orchard (Girona et al., 2004). Modifications to this irrigation pattern were applied to challenge the simulations to reproduce some temporary unbalances in the soil water budget. This typically consisted of interrupting irrigation for a period of around a week. This was then followed by the recovery of the soil water content and also the application of arbitrary periods of overirrigation and drought. Irrigation was measured using digital water meters (model CZ3000 from Contazara, Zaragoza, Spain).

The dataset recorded in 2018, which covered most of the crop cycle, was used to analyse and calibrate the HYDRUS-3D model, while the dataset covering the whole of 2017 was used for its validation.

2.2. Measuring soil water content

The experimental design was monitored with a neutron probe and tensiometers. Six neutron probe access tubes were located at different points around a dripper (Figure 2). The volumetric soil water content in these access tubes was then monitored from May to October, using a neutron probe (Hydroprobe 503DR, Campbell Pacific Nuclear Corp., Martinez, CA, USA) which had previously been calibrated for this site. Measurements were taken at depths of between 0.20 and 1.00 m, at 0.20 cm intervals.

Six tensiometers (type RSU-C from Irrometer, Riverside, CA, USA) were installed at distances of less than 10 m from the access tubes. They were associated with equivalent trees, drippers and soil conditions and installed at depths of 30 cm and 60 cm. The locations

were at the mid-point position between two drippers (Figure 2- Tensiometer A) and placed 15 cm from the vertical of the dripper and perpendicular to the dripline (Figure 2- Tensiometer C). The tensiometers consisted of tubes filled with distilled water and fitted with porous ceramic tips, vacuum gauges and transducers. They measured the soil water tension within the range of 0 - 94 kPa. Measurements were taken every 10 seconds and the average reading over 5 minutes was stored in a model CR800 datalogger (Campbell Scientific Inc., Logan, UT, USA), which used a multiplexer (AM16/32, from Campbell Scientific Inc.) to increase the number of channels. The pressure head measured by the tensiometers was transformed to the soil water content using the HYPROP + WP4C soil water retention curve for undisturbed field soil samples from the same plot.

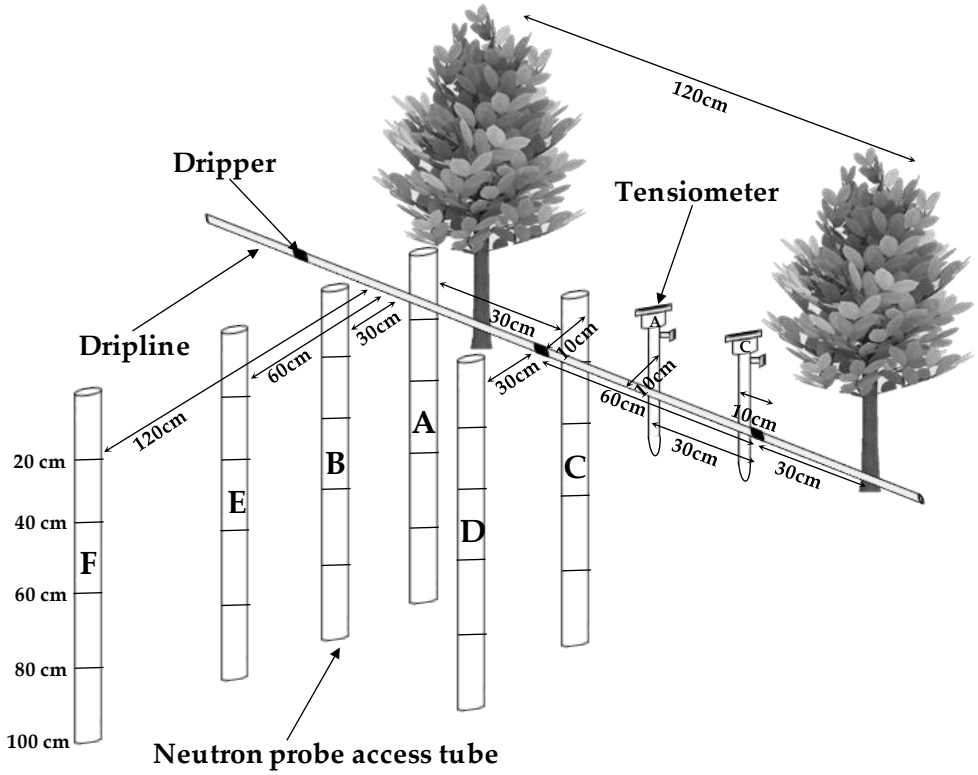

Figure 3. Relative positions and depths of the neutron probe access tubes and tensiometers.

The extent of the wetting pattern at the soil surface under the dripper was also characterized after an irrigation cycle lasting from June to August 2018. This was done using a Fieldscout TDR 300 (Spectrum Technologies INC., Aurora, IL, USA) with 12 cm-long rods. Soil water content measurements were made at 10 cm intervals. These were taken both parallel and perpendicular to the dripline. The wetted area perpendicular to the dripline was determined based on how far the wet region reached; the wetted area parallel to the dripline was determined as the point with the lowest soil water content located between the two drippers. Once the limits had been established, the wetted area was determined. The average wetted area per dripper was 0.316 ± 0.086 m^2 and included access tubes A, B, C and D.

2.3. Simulation with HYDRUS-3D

2.3.1. Soil water modelling

HYDRUS-3D (v. 2.05) is a three-dimensional, finite element model. It was used to simulate the soil water dynamics under a dripline (Simunek et al., 2016). The simulations with HYDRUS were carried during the irrigation seasons of the years 2017 and 2018. The soil water distribution was modelled using Richard's equation (Equation 2) for variable-saturated water flow. This includes a sink term (S) that represents root water uptake by plant roots. HYDRUS numerically solves Richard's equation (Eq. 2) using the Galerkin finite element method.

$$\frac{\partial \theta}{\partial t} = \frac{\partial}{\partial x}\left[K(h)\frac{\partial h}{\partial x}\right] + \frac{\partial}{\partial y}\left[K(h)\frac{\partial h}{\partial y}\right] + \frac{\partial}{\partial z}\left[K(h)\left(\frac{\partial h}{\partial z} + 1\right)\right] \text{-S} \qquad \text{(Eq. 2)}$$

where θ is the soil volumetric water content ($cm^3\ cm^{-3}$), t is time (days), K is hydraulic conductivity ($cm\ day^{-1}$), h is the soil water pressure head (cm), x and y are the horizontal space coordinates (cm), z is vertical space coordinate (cm), and S is the sink term ($cm^3\ cm^{-3}\ day^{-1}$).

In this study, the simulations were carried out with HYDRUS-3D. This symmetry made it possible to appropriately represent the actual dripper frame in an orchard. Along the same dripline, the dripper was located close to a neighboring dripper and as far as possible from parallel dripline drippers.

2.3.2. Flow domain, boundary and initial conditions.

Following this approach, the domain was defined as a parallel pipe whose dimensions were 180 cm long, 200 cm high and 60 cm wide (Figure 3). The domain was defined by 21 equally-spaced, horizontal planes and discretized using an unstructured, finite element mesh, with a total of 32,840 three-dimensional tetrahedral elements and 418,270 finite element nodes. Observation points, where measurements with neutron probe tubes and tensiometers were carried out, were located at depths of 20, 40, 60, 80 and 100 cm.

In line with field observations, irrigation was assumed to be applied to a wet semi-circular area with a radius of 30 cm. During the irrigation period, a variable flux condition (Eq. 3) was applied over an area of 1,399.92 cm^2: this area corresponded to the total soil surface wetted by the dripper. However, this wetted area is larger than the waterlogged area during irrigation, which would better represent the water inlet area in the soil but was not experimentally measured in this work (Figure 3). The flux, q, was estimated as:

$$q = \frac{\text{Emitter discharge flow rate } (cm^3\ h^{-1})}{\text{wetted surface area } (cm^2)} = \frac{3500\ cm^3 h^{-1}}{1399.92\ cm^2} = 2.5\ cm\ h^{-1} \qquad \text{(Eq. 3)}$$

Normal atmospheric conditions were imposed on the rest of the soil surface and the value of the minimum allowed pressure head at the soil surface was set at 10,000 cm. A no-

flux boundary condition was established at both the right and left edges of the profile, and a free drainage boundary condition was assumed at the bottom of the soil profile (Figure 3). The water table at the site is below the depth of 2 m, except on occasions of heavy rainfall, which did not occur during the simulated period. The simulations were run on an hourly basis, throughout the different irrigation seasons. The initial conditions were selected considering the initial soil water contents, based on measurements at field capacity, obtained from laboratory measurements using the HYPROP + WP4C system (METER Group, Pullman, CA, USA).

The use of the model required the sequencing of several simulations in which each one had different considerations: (i) simulations which considered three soil layers and whose soil hydraulic parameters were obtained from Rosetta using undisturbed soil samples in the field; (ii) simulations which considered two soil layers and whose soil hydraulic parameters were obtained from HYPROP + WP4C using undisturbed soil samples obtained in the field; (iii) simulations based on the soil hydraulic parameters obtained from HYPROP + WP4C, further adjusted by empirical calibration; and (iv) seasonal and hourly simulations, using the latter model for the period included in the validation dataset.

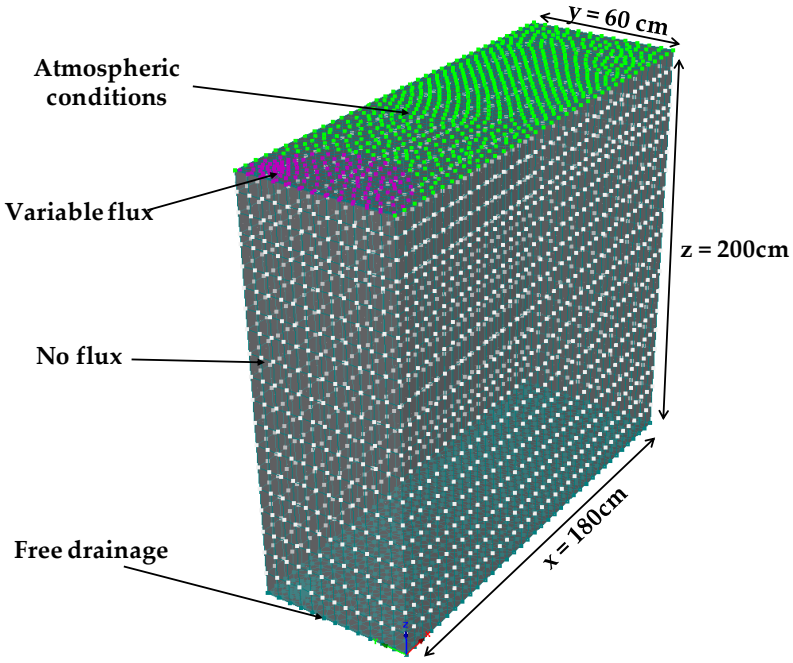

Figure 3. Flow domain and boundary conditions used in the HYDRUS-3D simulations.

2.3.3. Soil hydraulic parameters

2.3.3.1. Soil hydraulic parameters obtained from Rosetta

The Rosetta model (Schaap et al., 2001), which is integrated into the HYDRUS software, was used to obtain the soil hydraulic parameters in one group of simulations. Rosetta is a pedotransfer function software package that uses a neural network model to predict hydraulic parameters. In this study, four undisturbed soil samples were taken for each depth (20, 40 and 60 cm) using Kopecky rings (Eijkelkamp, Giesbeek, The Netherlands).

These rings were 5.1 cm long and 5.3 cm (top ring) and 5.0 cm (base ring) in diameter. A total of 12 samples were obtained. Bulk density (BD) and soil water content at -33 kPa and -1500 kPa were then determined using porous ceramic pressure plates with compressed air (Soil Moisture Equipment Corp., Santa Barbara, CA, USA) (Dane and Hopmans, 2002). The Rosetta inputs were soil texture, BD, soil water content at -33 kPa, and soil water content at -1500 kPa for each of the samples. Finally, the average soil hydraulic parameters obtained for each soil depth using Rosetta were used to carry out four simulations with HYDRUS-3D. Table 2 shows the average and standard deviations for each soil hydraulic parameter and soil depth.

Table 2. Soil hydraulic parameters obtained from Rosetta

Depth (cm)	θr ($cm^3 cm^{-3}$)	θs ($cm^3 cm^{-3}$)	α (cm^{-1})	*n* (-)	Ks (cm h^{-1})	*l* (-)
0-20	0.071 ± 0.003	0.454 ± 0.004	0.020 ± 0.004	1.303 ± 0.014	1.189 ± 0.091	0.500 ± 0.000
20-40	0.070 ± 0.005	0.445 ± 0.004	0.022 ± 0.006	1.308 ± 0.019	1.037 ± 0.052	0.500 ± 0.000
40-60	0.067 ± 0.003	0.446 ± 0.007	0.017 ± 0.004	1.319 ± 0.025	0.967 ± 0.112	0.500 ± 0.000

θ_r (cm^3 cm^{-3}) = residual water content; θ_s (cm^3 cm^{-3}) = saturated water content; K_s (cm h^{-1}) = saturated hydraulic conductivity; α (cm^{-1}), *n* and *l* are Van Genuchten shape parameters.

2.3.3.2. Soil Hydraulic Parameters Obtained from HYPROP and WP4C

Four undisturbed soil samples were extracted from depths of 0-20 cm and 20-40 cm using 250 cm^3 sampling rings. Soil hydraulic parameters such as θr, θs, α, *n*, Ks and *l* were described with Van Genuchten-Mualem relationships using HYPROP and WP4C (METER Group, Pullman, CA, USA) and are presented in Table 3. The HYPROP system, which works at suctions of between 0 and -85 kPa, can be used to determine the water potential and water content of an undisturbed soil sample. This permitted the subsequent calculation of moisture retention and unsaturated hydraulic conductivity curves. Combining HYPROP with WP4C, which is a dew point hygrometer, made it possible to extend the range up to -300 MPa. The equipment measured simultaneously the changes in weight and matric tension of a soil sample while it slowly dried at room conditions, thus producing a soil water retention curve. In addition, variations from -10% to +10% in each of these parameters were also considered in order to assess the uncertainty of the simulations. This variation range was considered appropriate in order to not alter the original parameter value too much.

Table 3. Soil hydraulic parameters obtained with HYPROP + WP4C

Depth (cm)	θr ($cm^3 cm^{-3}$)	θs ($cm^3 cm^{-3}$)	α (cm^{-1})	*n* (-)	Ks (cm h^{-1})	*l* (-)
0-20	0.023	0.388	0.012	1.259	1.553	0.500
20-40	0.029	0.400	0.019	1.275	1.444	0.500

θ_r (cm^3 cm^{-3}) = residual water content; θ_s (cm^3 cm^{-3}) = saturated water content; K_s (cm h^{-1}) = saturated hydraulic conductivity; α (cm^{-1}), *n* and *l* are all Van Genuchten shape parameters.

2.3.4. Root distribution and water uptake.

Vertical root distribution was defined according to the Vrugt model (Vrugt et al., 2001) (Eq.4)

$$\Omega(x,y,z)=\left(1-\frac{x}{X_m}\right)\left(1-\frac{y}{Y_m}\right)\left(1-\frac{z}{Z_m}\right)e^{-\left(\frac{P_x}{X_m}|x^*-x|+\frac{P_y}{Y_m}|y^*-y|+\frac{P_z}{Z_m}|z^*-z|\right)} \quad \text{(Eq. 4)}$$

where Ω (x,y,z) is the three dimensional spatial distribution of root water uptake; x_m, y_m and z_m are the maximum rooting lengths (cm) in directions x, y and z, respectively; x*, y* and z* describe the location of the maximum root water uptake in directions x, y and z, respectively, and p_x, p_y and p_z are empirical coefficients.

In this work, the distribution of roots in the simulated geometry was parameterized based on measurements of root water uptake in the year 2016. The raw data were the measurements of SWC by neutron probe at the different access tubes and depths before and after a period of one week without irrigation, with the soil covered with a plastic sheet to minimize evaporation from the soil surface. Then the root distribution functions available in HYDRUS-3D were parameterized to match the observed pattern of soil water extraction by roots characterized from those measurements. Based on these measurements, the root parameters for the simulations were set horizontally as x_m = 180 cm and y_m = 180 cm, and vertically as z_m = 60 cm. The maximum horizontal and vertical root water uptakes were x^* = 60 cm, y^* = 60 cm and z^* = 50 cm, respectively. The plots presented no salinity problems and the eventual reduction in root water uptake was modelled as described Feddes et al. (Feddes et al., 1978), as described in equation 5, although there was no evidence of tree water stress in the simulated periods.

$$S(h,z) = \alpha(h)S_{max}(h,z) \quad \text{(Eq. 5)}$$

where α is a dimensionless water stress reduction factor expressed as a function of pressure head h (cm), whose values were taken from Taylor and Ashcroft (1972) for deciduous fruit trees. S_{max} ($cm^3\ cm^{-3}\ day^{-1}$) is the maximum possible root water extraction rate when soil water is not a limiting factor, and z is the soil depth (cm).

2.4. Statistical analysis

Statistical indicators were used for analysing the goodness-of-fit between predictions by HYDRUS-3D simulations and the soil water content measurements obtained using the neutron probe and the tensiometers. The indicators were the coefficient of determination (R^2, Eq. (6)), Root Mean Square Error (RMSE, Eq. (7)) and the Nash-Sutcliffe model efficiency coefficient (NSE, Eq. (8)) (Nash and Sutcliffe, 1970).

$$R^2 = \frac{\left[\sum_{i=1}^{N}(O_i - \bar{O})(S_i - \bar{S})\right]^2}{\sum_{i=1}^{N}(O_i - \bar{O})^2 \cdot \sum_{i=1}^{N}(S_i - \bar{S})^2} \quad \text{(Eq. 6)}$$

$$RMSE = \sqrt{\frac{\sum_{i=1}^{N}(O_i - S_i)^2}{N}} \quad \text{(Eq. 7)}$$

$$NSE = 1 - \frac{\sum_{i=1}^{N}(S_i - O_i)^2}{\sum_{i=1}^{N}(O_i - \bar{O})^2} \quad \text{(Eq. 8)}$$

Where N refers to the number of compared values, Oi the ith observation point, Si the ith simulation and $\bar{O}$ the observed mean value

The R^2 indicates the degree of linear correlation between observed and predicted values as it varies from 0 to 1. Values closer to 1 indicate better agreement with the model. The RMSE measures the amount of error between two data sets. Unlike R^2, the error is expressed in the same units as the variable. Lower RMSE values indicate a better fit. The NSE is used to assess the predictive power of hydrological models. NSE ranges from -∞ to 1.0 (perfect fit).

For seasonal comparisons, we based our analyses on the daily minimum soil water content, which was obtained as the driest value between two irrigation cycles. The daily minimum soil water content was considered because it is a practical indicator that is used for irrigation management. It summarizes the outcome of the daily cycle after irrigation, redistribution and uptake by the roots have taken place (Casadesus et al., 2012, Domínguez-Niño et al., 2020).

3. Results

3.1. Seasonal soil water content comparisons between neutron probe measurements and HYDRUS-3D simulations, using soil hydraulic parameters obtained from Rosetta.

HYDRUS-3D simulations configured with the soil hydraulic parameters obtained from Rosetta were compared with the dataset of soil water content measured in 2018 using neutron probes, for each access tube and depth. The level of agreement between the simulations and measurements by neutron probe are summarized in Table 4, which shows some indicators of the quality of the fit (R^2, RMSE and NSE) and their variation (SD) for the study plot. The R^2 varied between access tubes and depths and was, in general, higher than 0.6, while the RMSE was greater than 0.044 $cm^3\ cm^{-3}$ and the NSE was less than -1.8. Higher R^2 were observed in access tubes near the dripper (access tubes A, B, C and D) and at depths of 40-60 cm. The best correlations were therefore observed in the subset of depths between 40 and 60 cm, in access tubes A, B, C and D (R^2 = 0.944).

Table 4. Summary of the fit between soil water content ($cm^3\ cm^{-3}$) measured using neutron probes in 2018 and HYDRUS-3D simulations using soil hydraulic parameters obtained from Rosetta

Subset of SWC Measurements	R^2 (-)	RMSE (cm^3cm^{-3})	NSE (-)
All access tubes and depths	0.631 ± 0.018	0.062 ± 0.004	-1.837 ± 0.376
All access tubes at a depth of 20 cm	0.760 ± 0.039	0.044 ± 0.005	-1.894 ± 0.674
All access tubes at depths of 40 and 60 cm	0.922 ± 0.016	0.059 ± 0.003	-2.643 ± 0.384
All access tubes at depths of 80 and 100 cm	0.719 ± 0.029	0.072 ± 0.005	-1.835 ± 0.400
Access tubes A, B, C and D at all depths	0.828 ± 0.015	0.059 ± 0.006	-4.778 ± 1.104
Access tubes E and F at all depths	0.234 ± 0.033	0.067 ± 0.003	-1.846 ± 0.254
Access tubes A, B, C and D at depths of 40 and 60 cm	0.944 ± 0.005	0.062 ± 0.004	-5.707 ± 0.939

A comparison between the simulations and measurements (Figure 4) showed that, in general, the simulations followed a pattern that was related to the measured values, though these tended to be overestimated, except in the case of access tube F, which was located farthest from the dripper, in which some simulations underestimated the soil water content.

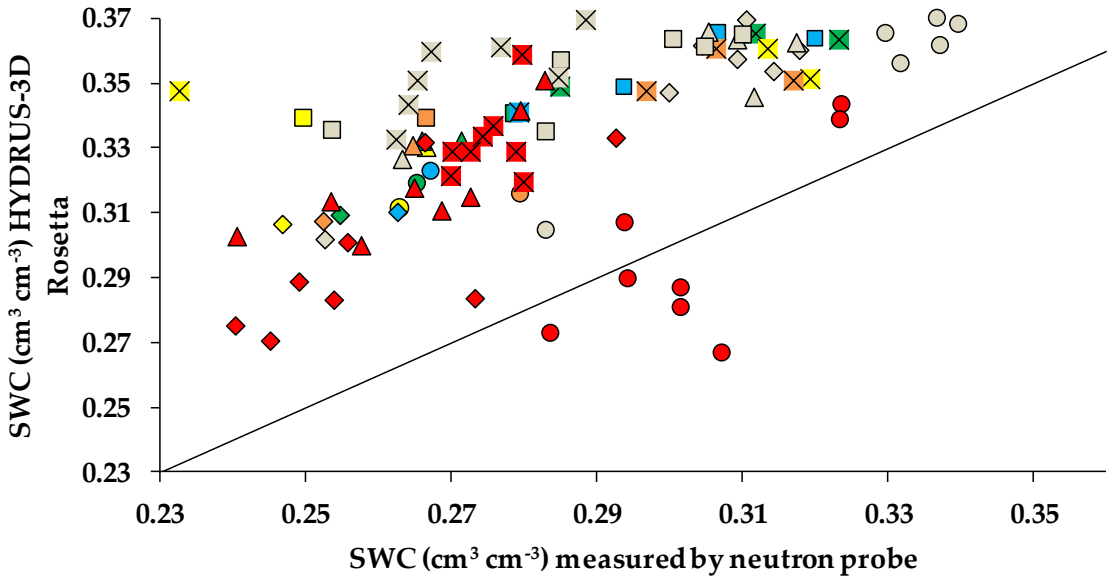

Figure 4. Soil water content (SWC) simulated with HYDRUS-3D parameterized from Rosetta versus average measurements by neutron probe on 8 different dates in the 2018 irrigation season. Colors indicate access tubes (green = A, yellow = B, blue = C, orange = D, grey = E and red = F) and shapes indicate different depths (◯ = 20cm, ◇ = 40cm, Δ = 60cm, □ = 80cm and × = 100cm).

3.2. Seasonal soil water content comparisons between neutron probe measurements and HYDRUS-3D simulations, using soil hydraulic parameters obtained from HYPROP + WP4C

The quality of fit between simulations based on HYPROP + WP4C and measurements using neutron probes are summarized in Table 5. All the indicators: R^2, RMSE and NSE, showed improvements compared with the simulations parameterized from Rosetta. The best agreement corresponded to the depth of 20 cm in almost all the access tubes. Overall, the R^2 either remained stable or improved, with the highest R^2 for the set of access tubes A,

B, C and D corresponding to depths of 40-60 cm (0.942). The worst agreements were at depths of 80 and 100 cm and in access tubes E and F, which were farthest from the dripper. The value of RMSE improved in all cases and, in contrast with to the results obtained with Rosetta, RMSE was acceptable when the whole set of access tubes and depths was considered (0.031 cm^3 cm^{-3}). Interestingly, RMSE also improved at depths of 80-100 cm (0.050 cm^3 cm^{-3}) and for access tubes in positions E and F (0.046 cm^3 cm^{-3}). Finally, NSE showed overall improvement for various depths and access tubes, with the exception of access tubes E and F. For the whole set of access tubes located at a depth of 20 cm, NSE reached 0.885.

Table 5. Summary of the fit between soil water content (cm^3 cm^{-3}) measured by neutron probe in 2018 and HYDRUS-3D simulations using soil hydraulic parameters obtained from HYPROP + WP4C

Subset of SWC Measurements	R^2 (-)	RMSE (cm^3cm^{-3})	NSE (-)
All access tubes and depths	0.692	0.031	0.277
All access tubes at a depth of 20 cm	0.923	0.009	0.885
All access tubes at depths of 40 and 60 cm	0.933	0.023	0.434
All access tubes at depths of 80 and 100 cm	0.698	0.050	0.094
Access tubes A, B, C and D at all depths	0.814	0.020	0.359
Access tubes E and F at all depths	0.409	0.046	-0.374
Access tubes A, B, C and D at depths of 40 and 60 cm	0.942	0.019	0.369

The comparisons between simulations parameterized from HYPROP + WP4C and the neutron probe measurements for 2018 are illustrated in Figure 5. Overall, the reduction in scatter evident in Figure 5 compared with Figure 4 illustrates a better fit of the simulations when using soil hydraulic parameters obtained from HYPROP + WP4C.

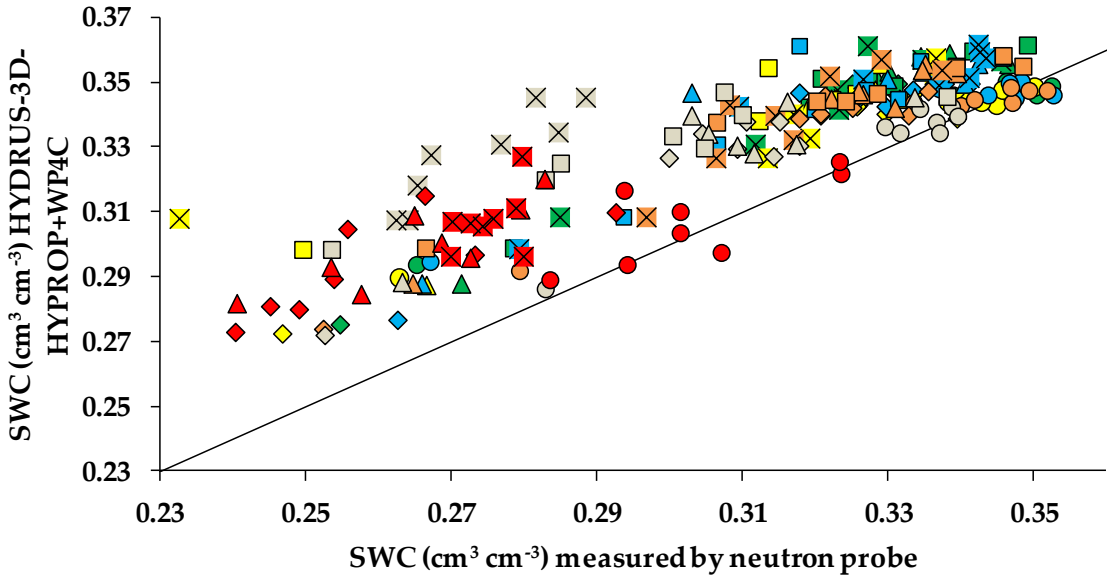

Figure 5. Soil water content (SWC) simulated with HYDRUS-3D parameterized from HYPROP + WP4 versus average measurements by neutron probe on 8 different dates in the 2018 irrigation season. Colors indicate access tubes (green = A, yellow = B, blue = C, orange = D, grey = E and red = F) and shapes indicate depths (◯ = 20cm, ◇ = 40cm, Δ = 60cm, □ = 80cm and × = 100cm).

Given the high R^2, the low RMSE and the NSE values close to 1.0 for all the access tubes at a depth of 20 cm, the soil hydraulic parameters obtained from HYPROP + WP4C could be considered to provide an appropriate soil parameterization for the simulations. However, at all the other depths, a systematic overestimation of SWC was still appreciated (Figure 5), with RMSE and NSE values being respectively higher and lower than optimal (Table 5). This suggested that there was still room for improvement in the simulations.

3.3. Seasonal soil water content comparison between neutron probe measurements and HYDRUS-3D simulations which consider variations in the soil hydraulic parameters obtained from HYPROP + WP4C

A sensitivity analysis was performed as a basis for empirical calibration and in order to characterize how variations in the soil hydraulic parameters influenced the level of agreement of the simulations with the soil moisture determinations obtained with the neutron probes. For the sake of simplicity, these parameters were analyzed independently of each other. In each set of simulations, only one of the parameters was varied by between -10% and +10% around the value obtained from HYPROP + WP4C. A total of 40 simulations were carried out, with each including the whole season for the year 2018.

Table 6 summarizes the sensitivity of the fit between the simulations and measurements regarding the variations in the soil hydraulic parameters. The table shows the best variation in each of the soil hydraulic parameters, which has been defined here as the value of that parameter which provided the highest NSE. Overall, the quality of the fit varied according to depth and the access tubes considered. For the whole set of depths and tubes, the R^2 increased from 0.692 to a range of between 0.700 and 0.773, depending on the parameter, with the best fit being for +8%*n*. RMSE improved from 0.031 to 0.020 cm^3 cm^{-3} when θs was reduced, or to 0.018 when *n* was increased, while NSE respectively improved from 0.277 to 0.704 and 0.760 with these same variations.

Sensitivity varied with soil depth. For all the access tubes at a depth of 20 cm, the original soil hydraulic parameters provided a sufficiently good level of agreement, with this only being slightly improved when θs was modified by -10%. For the depths of 40 and 60 cm, the R^2 was also high, suggesting a good level of agreement in the pattern of seasonal variation of SWC. However, RMSE was larger, which suggested a systematic bias in the simulations, which improved with the variation in +6%*n*. The worst fit was at depths of 80 and 100 cm, although this also improved when parameter *n* increased.

Regarding differences between access tubes, those closest to the dripper (A, B, C and D) showed much better levels of agreement than those outside the influence of the irrigation wetting pattern (E and F). The simulations that considered the access tubes near the dripper (A, B, C and D) had a good level of agreement when a -6% θs or +6% *n* was applied and it produced an NSEs of up to 0.867 and 0.863 respectively. In both simulations and neutron probe measurements, Tubes E and F produced their own seasonal patterns, which received little, or even no, influence from the wetting pattern caused by irrigation. Nevertheless, the

degree of agreement was low in these positions, even when the best variations in θs and *n* were applied whose respective NSE values were 0.410 and 0.561.

For the subset focused at depths of 40 and 60 cm with access tubes A, B, C and D, the original R^2 was already high, while the RMSE and NSE improved with a variation of +6%*n*, reaching values of 0.006 $cm^3\ cm^{-3}$ and 0.931, respectively.

Table 6. Variations in the fit between simulations parameterized from HYPROP + WP4C and measurements of SWC ($cm^3\ cm^{-3}$) by neutron probe, when each soil hydraulic parameter was varied between -10% to +10% around the original value. The average measurements were obtained on 8 different dates in the 2018 irrigation season.

Subset of SWC Measurements		Original	Best Variation θr		Best Variation θs		Best Variation Ks		Best Variation α		Best Variation *n*	
All access tubes and depths	R^2	0.692	0.700		0.736		0.697		0.7159		0.773	
	RMSE	0.031	0.030	-10%θr	0.020	-8%θs	0.029	+10%Ks	0.030	+10%α	0.018	+8%n
	NSE	0.277	0.335		0.704		0.384		0.332		0.760	
All access tubes at a depth of 20cm	R^2	0.923	0.922		0.932		0.921		0.920		0.914	
	RMSE	0.009	0.008	+8%θr	0.008	-10%θs	0.008	+10%Ks	0.008	-10%α	0.009	+4%n
	NSE	0.885	0.898		0.910		0.905		0.909		0.888	
All access tubes at depths of 40 and 60cm	R^2	0.933	0.933		0.928		0.925		0.932		0.941	
	RMSE	0.023	0.022	-10%θr	0.009	-6%θs	0.020	+10%Ks	0.022	+10% α	0.008	+6%n
	NSE	0.434	0.496		0.908		0.574		0.511		0.936	
All access tubes at depths of 80 and 100cm	R^2	0.698	0.696		0.685		0.693		0.703		0.720	
	RMSE	0.050	0.048	-10%θr	0.034	-8%θs	0.047	+10%Ks	0.048	+10%α	0.029	+10%n
	NSE	0.094	0.154		0.578		0.190		0.156		0.696	
Access tubes A, B, C and D at all depths	R^2	0.814	0.821		0.875		0.826		0.801		0.869	
	RMSE	0.020	0.019	-10%θr	0.009	-6%θs	0.017	+10%Ks	0.019	-10%α	0.009	+6%n
	NSE	0.359	0.431		0.867		0.526		0.430		0.863	
Access tubes E and F at all depths	R^2	0.409	0.423		0.550		0.416		0.452		0.572	
	RMSE	0.046	0.045	-10%θr	0.030	-8%θs	0.044	+10%Ks	0.044	+10%α	0.026	+10%n
	NSE	-0.374	-0.280		0.410		-0.227		-0.257		0.561	
Access tubes A, B, C and D at depths of 40 and 60cm	R^2	0.942	0.942		0.941		0.934		0.939		0.940	
	RMSE	0.019	0.018	-10%θr	0.007	-6%θs	0.016	+10%Ks	0.018	+10%α	0.006	+6%n
	NSE	0.369	0.437		0.922		0.560		0.434		0.931	
Best variation of the soil hydraulic parameter		**-**	**-10% θr**		**-6% θs**		**+10% Ks**		**+10% α**		**+6% *n***	

The fit of the simulations was most sensitive to the hydraulic parameters θs and *n*, whose variations were used to show improvements in RMSE and NSE, while variations in θr, Ks and *α* had less effect and produced negligible improvements. More specifically, according to these indicators, the best fit was obtained by either a decrease in the saturated water content of 6% or by an increase in the *n* parameter of 6%. The saturated water content refers to the maximum amount of water that a soil can store, while *n* is a shape parameter that refers to the pore-size distribution index.

Given the previously commented sensitivity, for the empirical calibration of the hydraulic parameters, we decided to keep the original parameters for the soil layer above a depth of 20 cm and to increase *n* by 6% for all other depths. Faced with the choice of adjusting either θs or *n*, we opted to adjust parameter *n*. The original value of *n* was obtained from an indirect estimation based on the shape of the curve obtained by HYPROP + WP4C. The estimation of θs, obtained from the same curve, was more straightforward. Table 7 shows the soil hydraulic parameters that were set after this empirical calibration. Some authors, including Singh et al. (2006); Marković et al. (2015); and Rai et al. (2019), also considered making adjustments to the shape parameters in simulations conducted with HYDRUS or other models.

Table 7. Soil hydraulic parameters based on HYPROP+WP4C and further refined by empirical calibration of *n*.

Depth (cm)	θr (cm^3cm^{-3})	θs (cm^3cm^{-3})	α (cm^{-1})	*n* (-)	Ks ($cm\ h^{-1}$)	*l* (-)
0-20	0.023	0.388	0.012	1.259	1.553	0.500
20-60	0.029	0.400	0.019	*1.351*	1.444	0.500

θ_r = residual water content; θ_s = saturated water content; K_s = saturated hydraulic conductivity; **α**, ***n*** and **l** are Van Genuchten shape parameters. The data in italics refer to parameter *n*, which was empirically calibrated.

A new set of simulations was then obtained using the soil hydraulic parameters from HYPROP + WP4C and further calibrated. In this parameterization, *n* was set at *1.351* for all soil positions and depths below 20 cm (Table 7). The use of this calibrated parameter improved the fit between the simulations and measurements made using a neutron probe. R^2 slightly increased across the whole set of access tubes and depths, while RMSE and NSE experienced significant improvements, especially for the access tubes which had most influence on the wetting pattern: access tubes A, B, C and D at depths of 40 and 60 cm (RMSE = 0.006 $cm^3\ cm^{-3}$ and NSE = 0.931) (Table 8 and Figure 7).

Table 8. Summary of the fit between soil water content (cm^3 cm^{-3}) measured by neutron probe in 2018 and HYDRUS-3D simulations using soil hydraulic parameters obtained from HYPROP + WP4C, with *n* empirically calibrated.

Subset of SWC measurements	R^2 (-)		RMSE (cm^3cm^{-3})		NSE (-)	
	Origin.	Adj.	Origin.	Adj.	Origin.	Adj.
All access tubes and depths	0.692	0.768	0.031	0.020	0.277	0.717
All access tubes at a depth of 20 cm	0.923	0.909	0.009	0.009	0.885	0.884
All access tubes at depths of 40 and 60 cm	0.933	0.941	0.023	0.008	0.434	0.936
All access tubes at depths of 80 and 100 cm	0.698	0.710	0.050	0.035	0.094	0.562
Access tubes A, B, C and D at all depths	0.814	0.869	0.020	0.009	0.359	0.863
Access tubes E and F at all depths	0.409	0.542	0.046	0.031	-0.374	0.374
Access tubes A, B, C and D at depths of 40 and 60cm	0.942	0.940	0.019	0.006	0.369	0.931

Origin. Refers to simulations parameterized from HYPROP + WP4C (Table 3), while **Adj.** refers to simulations parameterized from HYPROP + WP4C, except for *n*, which was empirically calibrated (Table 7).

Figure 6 shows a comparison between the simulations and measurements after the empirical calibration of parameter *n* was applied. Overall, agreement improved at all positions and for all depths with respect to Figure 5, which used the original soil hydraulic parameters from HYPROP + WP4C.

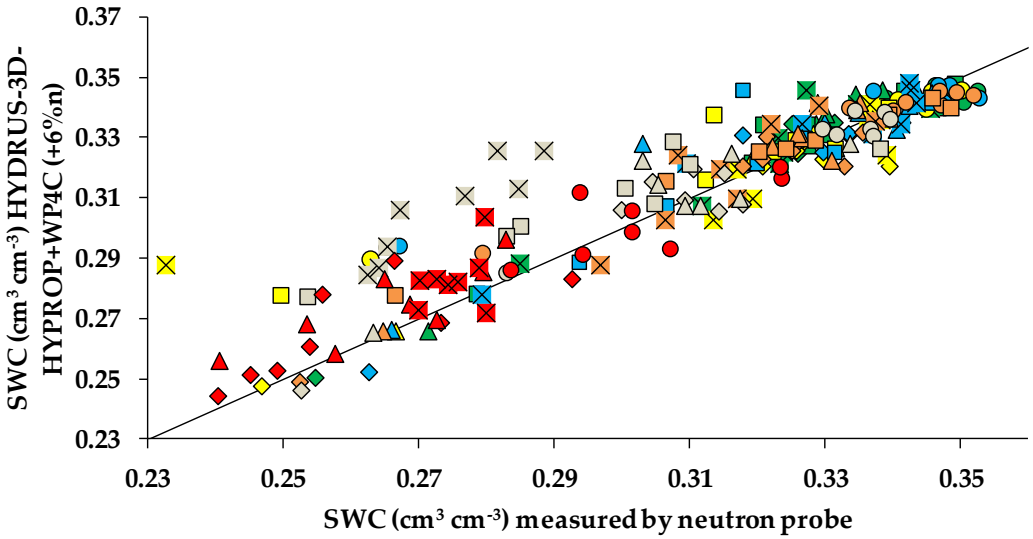

Figure 6. Soil water content (SWC) simulated with HYDRUS-3D parameterized from HYPROP + WP4 and further calibrated, versus average SWC measured by neutron probe on 8 different dates in the 2018 irrigation season. Colors indicate access tubes (green = A, yellow = B, blue = C, orange = D, grey = E and red = F) and shapes indicate depths (◯ = 20cm, ◇ = 40cm, Δ = 60cm, □ = 80cm and × = 100cm).

Figure 7 shows the seasonal soil water dynamics at depths of 20, 40 and 60 cm for neutron probe access tubes A, B, C, D, E and F. At a depth of 20 cm, the parameter *n* was maintained at its original value, with the simulations only slightly noticing the effects of calibration at other depths. At a depth of 20 cm, the simulations already matched both the seasonal pattern and the absolute value of SWC prior to calibration. At depths of 40

and 60 cm, the simulations with the original soil hydraulic parameters followed the measured seasonal SWC pattern, but were biased to approximately 0.019 cm^3 cm^{-3} based on the neutron probe measurements. This bias was removed with the calibration of shape parameter *n*.

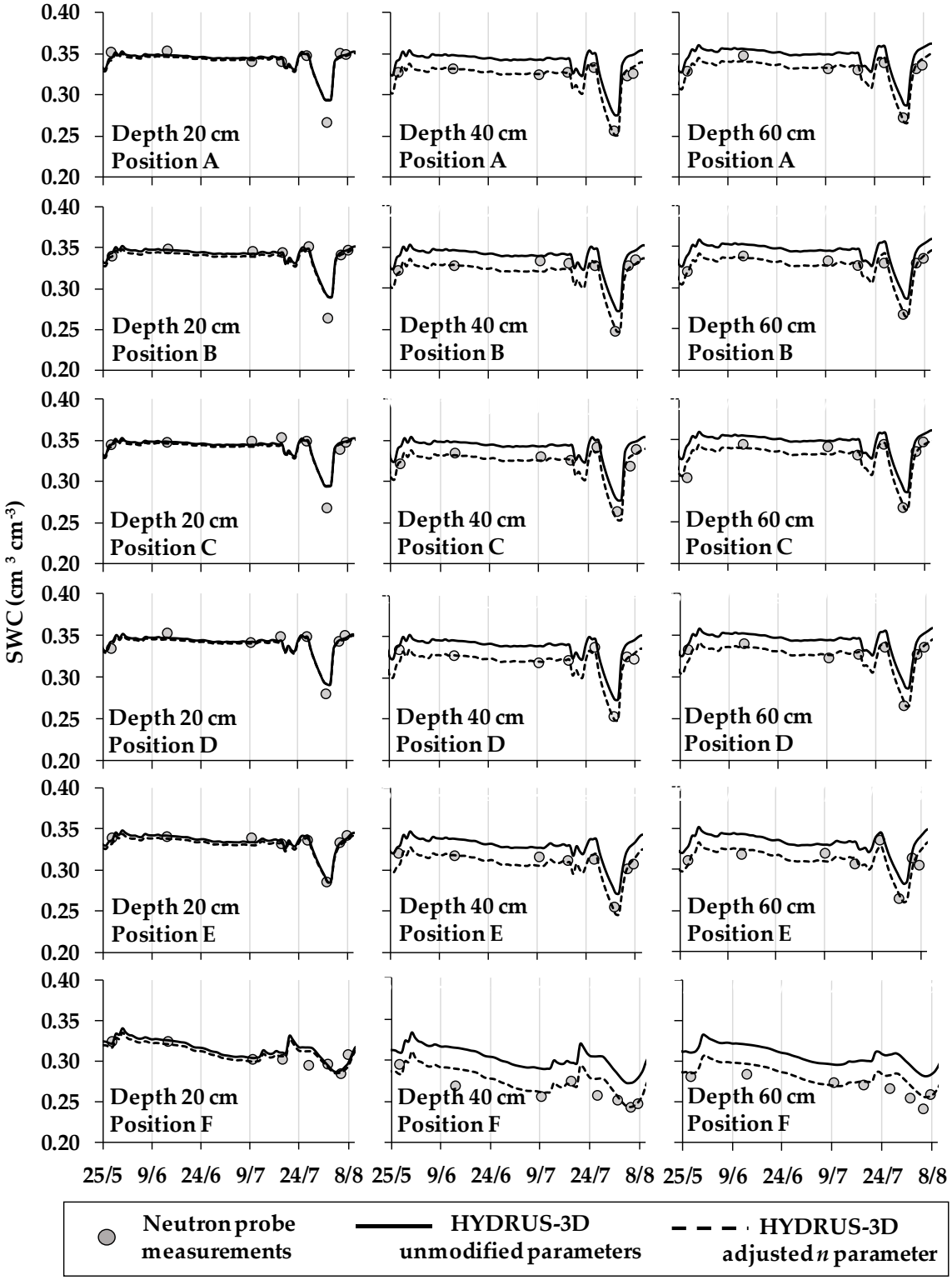

Figure 7. Soil water content (cm^3 cm^{-3}) simulated with HYDRUS-3D versus measurements by neutron probe in 2018 (dots) in different access tubes and at different depths. Continuous lines

are simulations using the hydraulic parameters obtained from HYPROP + WP4C. Dashed lines are simulations after the calibration of parameter *n*.

3.4. Validation of seasonal HYDRUS-3D simulations by comparison with the dataset of neutron probe measurements in 2017 for different access tubes and depths

The dataset of neutron probe measurements for 2017 (data not included in the previous sections) was compared with the HYDRUS-3D simulations using three different hydraulic parameterizations: a) that obtained from Rosetta (Table 2), b) that obtained from HYPROP + WP4C (Table 3) and c) that obtained from HYPROP + WP4C, except for the calibrated *n* value for depths below 20 cm (Table 7). All these simulations used the inputs for irrigation, rainfall, evaporation and transpiration registered in 2017 (Figure 1).

The quality of the agreements between the simulations and measurements obtained using neutron probes in the validation dataset is summarized in Table 9. In the case of the simulations parameterized from Rosetta, the fit with regard to general trends was acceptable. This was shown by their R^2, particularly relating to the access tubes most influenced by irrigation (A, B, C and D) and to all the access tubes at depths of between 20 and 60 cm. For the subset of access tubes A, B, C and D, at depths of 40 and 60 cm, the R^2 was 0.91, the RMSE values were 0.07 cm^3 cm^{-3}, and the NSE had a value of less than -17.00. On the other hand, when the parameterization was based on HYPROP + WP4C, the indicators of agreement between the simulation and the measurements improved substantially compared to that obtained from Rosetta. The R^2 remained almost unchanged, but the other indicators improved, with RMSE reaching 0.02 cm^3 cm^{-3} and the NSE producing values above -3.00. Using the shape parameter *n* as calibrated in the other dataset further improved the agreement. This improvement applied to all the access tubes and depths and it was especially noticeable for the access tubes located near the wetting pattern (A, B, C and D) and at depths of 40 and 60 cm.

In general, with the use of the calibrated parameter *n*, the statistical analysis improved. The R^2, remained similar or improved slightly, the RMSE halved its value and the NSE reached values greater than 0.80. The improvement occurred when access tubes A, B, C and D and depths of 40 and 60 cm were considered. The fit was particularly good for all access tubes at a depth of 20 cm. Despite maintaining the original soil hydraulic parameters at a depth of 20 cm, the adjustment of *n* at other depths resulted in a slight improvement, with the NSE rising to 0.411. At depths of 40 and 60 cm in all tubes, R^2 improved slightly to around 0.89, while RMSE improved notably: reaching 0.01 cm^3 cm^{-3}, and the NSE was 0.83. For tubes A, B, C and D, the adjusted simulation improved the statistics at all depths. The statistical analyses obtained were: R^2 = 0.781, RMSE = 0.011 cm^3 cm^{-3} and NSE = 0.612. These results were close to the soil water dynamics measured by the neutron probes. The combination of access tubes A, B, C and D and depths of 40 and 60 cm produced the best fit with values of R^2 = 0.92, RMSE = 0.01 cm^3 cm^{-3} and NSE = 0.87. On the other hand, at the access tubes and at depths with little influence from the

wetting pattern (access tubes E and F, at depths greater than 60 cm), the RMSE improved to 0.02 cm^3 cm^{-3}, but R^2 remained around 0.45 - 0.55 and NSE was negative: between -0.32 and -0.03, indicating the low reliability of the model used to reproduce the measurements provided by the neutron probes.

Table 9. Summary of the fit between soil water content (cm^3 cm^{-3}) measured by neutron probe in 2017 and HYDRUS-3D simulations using three different sets of soil hydraulic parameters: a) those estimated from Rosetta (Ros.); b) those estimated from HYPROP + WP4C (Orig.); and c) those estimated from HYPROP + WP4C, except for *n*, which was calibrated with the dataset for 2018 (Adj.).

Subset of SWC Measurements	R^2 (-)			RMSE (cm^3cm^{-3})			NSE (-)		
	Ros.	Orig.	Adj.	Ros.	Orig.	Adj.	Ros.	Orig.	Adj.
All access tubes and depths	0.55	0.59	0.69	0.07	0.03	0.02	-10.64	-1.02	0.46
All access tubes at a depth of 20 cm	0.74	0.73	0.72	0.05	0.02	0.01	-10.39	0.14	0.41
All access tubes at a depth of 40 and 60	0.88	0.88	0.89	0.07	0.03	0.01	-11.39	-0.76	0.83
All access tubes at depths of 80 and 100 cm	0.55	0.56	0.55	0.08	0.04	0.02	-14.02	-2.29	-0.03
Access tubes A, B, C and D, at all depths	0.66	0.63	0.78	0.07	0.03	0.01	-15.01	-1.09	0.61
Access tubes E and F, at all depths	0.17	0.33	0.45	0.07	0.04	0.02	-14.63	-2.86	-0.32
Access tubes A, B, C and D at 40 and 60 cm depth	0.91	0.91	0.92	0.07	0.02	0.01	-17.31	-1.03	0.87

Simulated soil water content, using calibrated parameterization, fitted reasonably well with measurements made by neutron probes in the validation dataset (Figure 8). In general, the level of agreement between the measured and simulated soil water contents was relevant at depths of 20, 40 and 60 cm, in the access tubes closest to the dripper (A, B, C and D). On the other hand, for access tubes located farther from the dripper (E and F), and at greater depths (80 and 100 cm), showed a worse fit with the measurements. This was probably because the HYDRUS-3D simulations overestimated the SWC measured by the neutron probes.

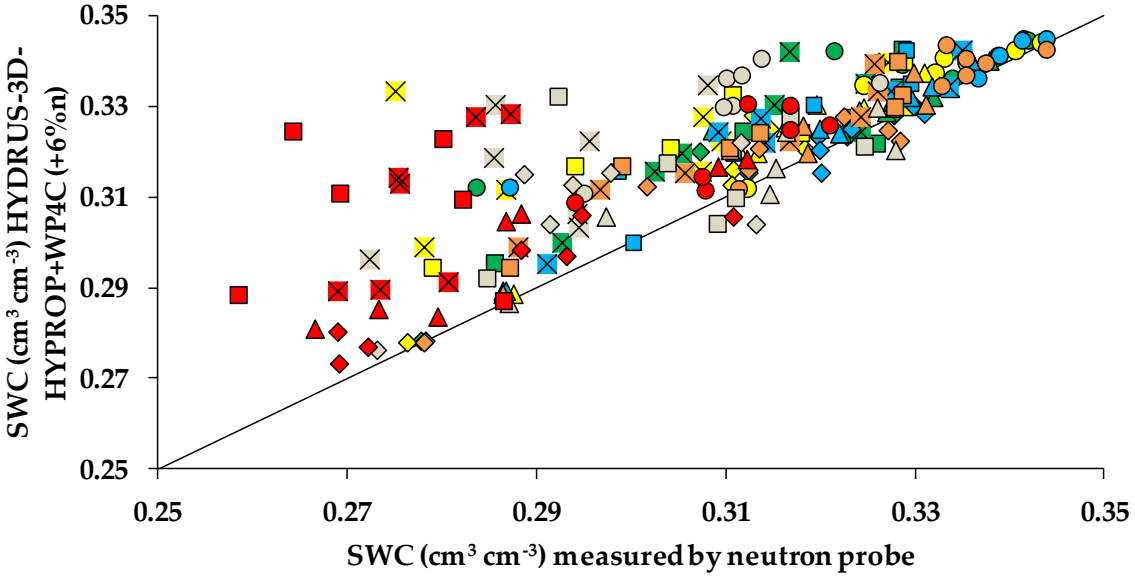

Figure 8. Soil water content **(**SWC) simulated with HYDRUS-3D parameterized from HYPROP + WP4, except for n, which was calibrated with the dataset of 2018, versus average measurements by neutron probe on 8 different dates in the 2017 irrigation season. Colors indicate access tubes (green = A, yellow = B, blue = C, orange = D, grey = E and red = F) and shapes indicate depths (◯ = 20cm, ◇ = 40cm, Δ = 60cm, □ = 80cm and × = 100cm).

Figure 9 represents the seasonal soil water content at depths of 20, 40 and 60 cm, for all the neutron probe access tubes (A, B, C, D, E and F). The original parameter *n*, which was obtained from HYPROP + WP4C, was maintained, at a depth of 20 cm and in all the access tubes. This showed a significant level of agreement between the measured and simulated SWC. This agreement improved slightly when the parameter *n* was increased by 6% at depths greater than 20 cm. At the depths of 40 and 60 cm, when the simulations considered the original parameter *n*, the SWC overestimated the neutron probe measurements by approximately 0.03 cm^3 cm^{-3}. When HYDRUS-3D used the adjusted parameter *n* +6%, the simulated SWC pattern shifted to lower values and its agreement with SWC measured by the neutron probes improved significantly.

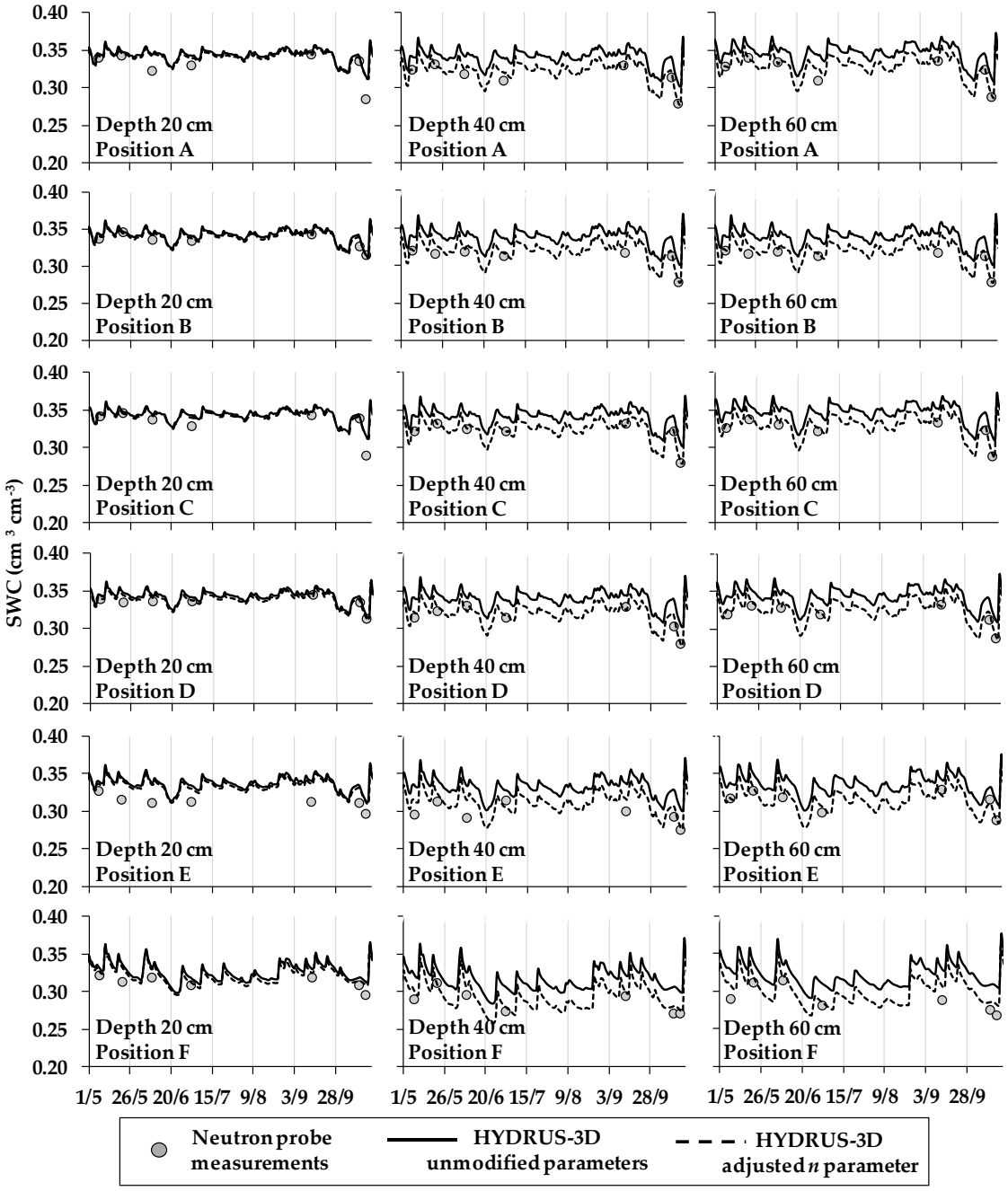

Figure 9. Comparison between soil water dynamics in the validation dataset relating to 2017, simulated with HYDRUS-3D and measured using neutron probes. The simulations were based on HYPROP + WP4C parameterization. This was either unmodified or modified with parameter *n* empirically adjusted in line with the dataset for 2018.

3.5. Validation of the soil water dynamics over the course of a day, simulated by HYDRUS-3D, as compared with measurements using tensiometers

While the neutron probe method provided a reliable assessment of the seasonal dynamics of SWC, it was unsuitable for continuous measurements over the course of several days. Tensiometers offered a more practical alternative at this time scale. The evolution over the course of a day of SWC estimated from tensiometers over one month in 2017, was compared with HYDRUS-3D simulations for the same period. The

simulations were the same as those described in the previous sections, but they were now analyzed at a finer time resolution. Table 10 summarizes the quality of the fit between the HYDRUS-3D simulations and tensiometer measurements. When the empirically adjusted parameter *n* was used in the simulations, the fit improved for all depths and positions, providing coefficients of determination of above 0.980. A particularly good prediction was observed at the depth of 30 cm at positions A and C, where the adjusted simulation and tensiometer data matched very well, with an R^2 of 0.993 for both positions, RMSEs of 0.016 $cm^3\,cm^{-3}$ and 0.013 $cm^3\,cm^{-3}$, respectively, and NSEs of 0.438 and 0.578 for the two positions. At the depth of 60 cm depth, the fit also improved at position A, reaching $R^2 = 0.980$, RMSE = 0.012 $cm^3\,cm^{-3}$ and NSE = -0.038.

Table 10. Summary of the fit between soil water content ($cm^3\,cm^{-3}$) estimated from tensiometers during July 2017 and HYDRUS-3D simulations parameterized from HYPROP + WP4C (Orig.), and simulations parameterized from HYPROP + WP4C, with the exception of *n*, which was calibrated from the 2018 dataset (Adj.).

Subset of SWC Measurements	R^2 (-)		RMSE ($cm^3\,cm^{-3}$)		NSE (-)	
	Orig.	Adj.	Orig.	Adj.	Orig.	Adj.
Tensiometer A at a depth of 30 cm	0.646	0.993	0.024	0.016	-0.311	0.438
Tensiometer A at a depth of 60 cm	0.702	0.980	0.017	0.012	-1.353	-0.038
Tensiometer C at a depth of 30 cm	0.889	0.993	0.023	0.013	-0.393	0.578

The graphical comparison of hourly values between the simulation and tensiometer measurements is shown in Figure 10. Overall, the simulations with the original parameters obtained from HYPROP + WP4C provided a slight overestimation of SWC. However, the estimations improved considerably when the adjusted parameter n, calibrated with neutron probe measurements for a different period, was used. This fit was also maintained in the scenario of a two-day interruption in irrigation.

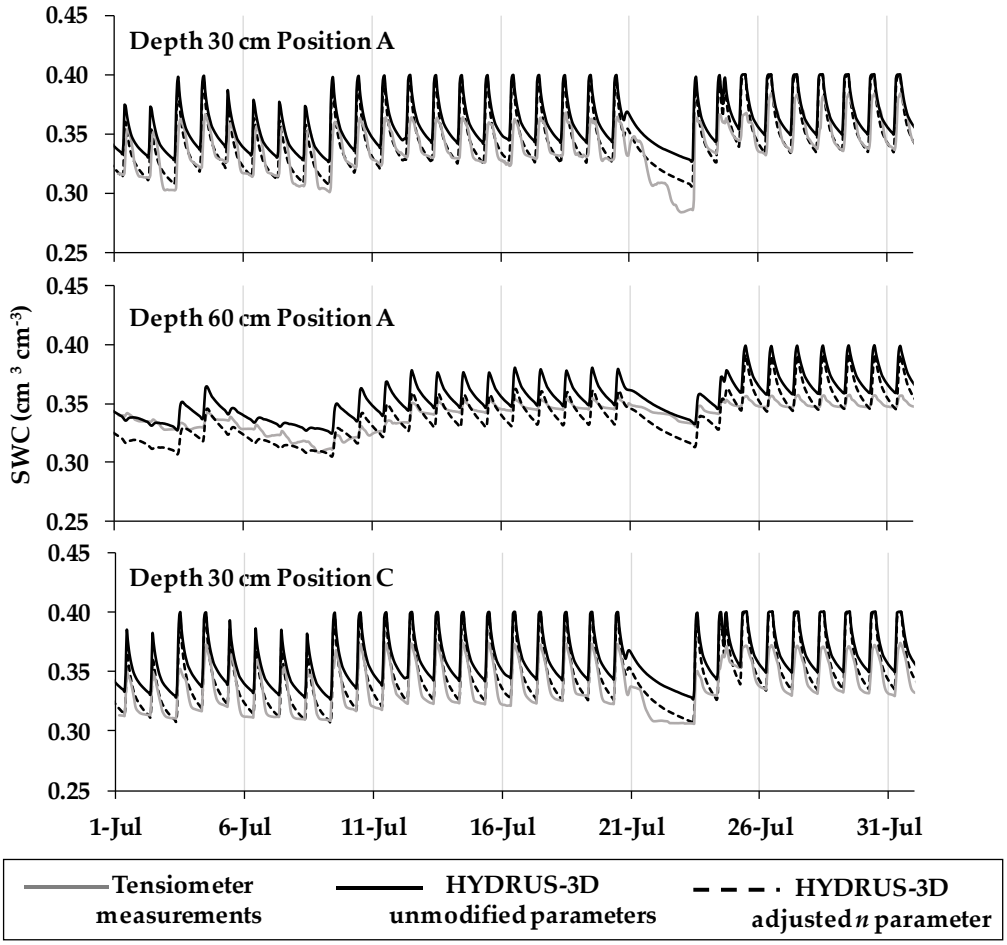

Figure 10. Comparison between soil water dynamics over several days in July 2017, simulated with HYDRUS-3D and measured by tensiometers. The simulations were parameterized from HYPROP + WP4C. They were either unmodified, or run with parameter *n* empirically adjusted in line with the dataset for 2018. The soil water content (SWC) was calculated from tensiometers located at positions A and C, at depths of 30 and 60 cm.

4. Discussion

In general, this study configured the HYDRUS-3D software to simulate a 3D soil scenario corresponding to a drip-irrigated orchard. Measurements made using neutron probes and tensiometers, located at different positions relative to the dripper and at different depths, were used to calibrate and validate the system over two different growing seasons. The simulation inputs were irrigation, rainfall, evaporation, transpiration and soil hydraulic parameters, which were obtained either from Rosetta (Schaap et al., 2001) or from HYPROP + WP4C (METER Group, Pullman, CA, USA).

Rosetta estimates soil hydraulic parameters from pedotransfer functions, based on soil textures, field capacity, wilting point and bulk density. One weakness of these estimations is that they do not consider the structure and mineralogy of the soil and, instead, assume that soils of similar textures have similar soil hydraulic properties (Carsel and Parrish, 1988, Wösten et al.,1999). When we used the Rosetta model, a porous ceramic pressure plate was required for the determination of the soil water content at

field capacity and at the wilting point. These data were used as input in the Rosetta model to estimate the soil hydraulic parameters necessary to carry out the simulation with HYDRUS-3D. In order to obtain these two inputs using porous ceramic pressure plates, the soil samples had to be sieved, which modified their structure. The soil water content readings at field capacity and at the wilting point obtained using porous ceramic pressure plates may therefore have differed from what would have been their actual values in the field. Furthermore, the reliability of the Rosetta databases cannot be guaranteed for the soil studied here, which was from a semi-arid region. Rosetta was designed and tested in soils from temperate regions, so it can only be used with confidence for a limited range of soils and climatic conditions (Bastet et al., 1999; Ottoni et al., 2019). Relationships between soil hydraulic properties and soil texture are therefore not easily transferable from one climatic zone to another (O'Connell et al., 2002). In this work, we noted that the simulations that used soil hydraulic parameters obtained from Rosetta overestimated the soil water content measured by the neutron probes for all positions and depths. One particular soil hydraulic parameter which may have been responsible for the observed bias was the saturated hydraulic conductivity, Ks, which is a key parameter for the quantitative determination of soil water dynamics (Saunders et al., 1979). The hydraulic conductivity and the capacity to retain bound water is related to particle shape (Zieba, 2017). Particle shape determines the effective porosity, which is crucial for soil hydraulic conductivity (Brook and Corey, 1964; Robin et al., 2016). For this reason, when soil samples used in porous ceramic pressure plates are sieved, their structures are broken and their size and the space between their particles decreases, resulting in a reduction in their hydraulic conductivity (Sasal et al., 2006; Tran et al., 2006). Hence, when the HYDRUS-3D simulations used soil hydraulic parameters from Rosetta, they probably underestimated Ks, thereby predicting slower drainage and SWCs that were closer to saturation. This was in line with the observed overestimation of SWC in these simulations.

Given the weaknesses of Rosetta, the HYPROP + WP4C method seemed a reasonable alternative for assessing the soil hydraulic properties, particularly as it is directly based on measurements of water-retention and conductivity pairs over a wide range of pressure head values in an undisturbed soil sample (Peters and Durner, 2008; Bezerra-Coelho et al., 2018). The combination of HYPROP + WP4C allowed us to determine soil hydraulic functions in the range between saturation and (close to) the wilting point (Schindler et al., 2015). The use of soil hydraulic parameters obtained from HYPROP + WP4C in HYDRUS-3D simulations produced a better fit with measurements obtained from the neutron probes and tensiometers. Nevertheless, to improve accuracy, it was decided to calibrate the model by modifying the soil hydraulic parameters. The best parameters to calibrate were α and/or n because they are empirical parameters that determine the shape of the water retention curve and they are usually estimated by fitting the experimental data. Some authors, such as Markovic et al. (2015), worked with HYDRUS-1D and estimated the initial values of α and n from measured water retention

data using RETC (Van Genuchten et al., 1991) and subsequently optimized them by inverse modelling, using the Van Genutchen-Mualem single-porosity model. Kanzari et al. (2018) used HYDRUS-1D to simulate soil water dynamics and assess environmental risks due to the salination process by adjusting the shape parameter α. Wang et al. (2018) evaluated the performance of HYDRUS-1D and inversely calibrated the α and n parameters until the observed data were sufficiently well-fitted to the simulated values. Kadyampakeni et al. (2018), calibrated HYDRUS-2D in drip irrigation systems, modifying Ks and n, since they are the most sensitive soil hydraulic parameters for the prediction of water movement. Rai et al. (2019) used the HYDRUS-2D model to predict soil water and energy balance components under different conservation agriculture practices when working with pigeon pea and optimized them by inversely modelling the α and n parameters. Mashayekhi et al. (2016) worked with HYDRUS 2D/3D and optimized the α, n, and Ks parameters using the infiltration data and field capacity and demonstrated that the simulation error could be reduced by reducing the number of hydraulic parameters involved in the optimization process. She also showed that the adjustment of the shape parameters could be carried out in other models. Singh et al. (2006), who used the SWAP (soil-water-atmosphere-plant) model to analyze the productivity of irrigation water, simultaneously optimized both the α and n parameters, thereby obtaining a low coefficient of variation for the n parameter due to its greater sensitivity to soil water flow. Furthermore, in our simulations with HYDRUS-3D, a model capable of representing the soil water dynamics was obtained by simply calibrating the shape parameter n which was valid for different depths and positions in a drip-irrigated orchard.

Overall, we obtained a satisfactory level of agreement between the SWC simulated with HYDRUS-3D which considered both the adjustment of parameter n and the SWC measured by the neutron probes. The simulations and measurements had notably better fits for depths and positions in the tree space that were close to the dripper. This is where the wet bulb develops and the root water uptake is greatest. Access tubes A, B, C and D, which were located near the wetting pattern, were therefore more affected by the irrigation dynamics and drying cycles and showed a better level of agreement than access tubes E and F, which were respectively located 60 and 120 cm from the dripper. Our results were consistent with Soulis et al. (2015), who observed that a distance of 11 cm from the dripline was the most suitable position for representing the water dynamics of the wet bulb. Our results also agreed with Tawutchaisamongdee et al. (2018), who studied distribution patterns in sandy clay loam soils under drip irrigation and observed that the maximum soil moisture width was 30 cm, measured horizontally. Given the distance of the tubes E and F from the drippers, irrigation and absorption by the tree roots was not as relevant. One possible explanation for the worse fit for these tubes could have been the water uptake by weeds (Bravdo and Proebsting, 1993). The degree of uncertainty associated with these phenomena may have been large. The initial moisture conditions were also assumed to be at field capacity. Any departure in the actual

conditions from this assumption would have had a higher impact on these access tubes than on those near the dripper. The access tubes close to the dripline would have eventually been hydrated by irrigation.

Regarding the effect of depth, we observed differences in the patterns of agreement between simulations and measurements at depths of 0-20 cm, although these did not require calibration. After calibration, the best degree of agreement was found at depths of 40 and 60 cm, while the level of agreement worsened at greater depths. The depth effect at 0-20 cm could be explained by the measurements by HYPROP + WP4C. At depths of 0-20 cm, the soil had lower θs and higher Ks than at 20-40 cm. This resulted in soil saturation with a lower soil water content and in greater infiltration to the lower layers. In addition, the measurements made by the neutron probe at the depth of 20 cm, could have been affected by proximity to the soil surface. This could have been due to the area of sensitivity of the neutron probe. This sensitivity is presumed to be within a 20 cm radius and to cover larger areas under drier soil conditions (Kramer and Boyer, 1995). On the other hand, at depths greater than 60 cm, the soil hydraulic parameters used in the simulations may have been less representative of the actual soil than those taken a shallower depths, since the simulations assumed the same soil hydraulic characteristics that had been determined by HYPROP + WP4C for depths of 40 and 60 cm. Furthermore, the results may have been influenced by the initial soil conditions at the beginning of the simulation. These were taken as being equivalent to field capacity, but this may not have been the case at that situation, as indicated in other studies (Márquez et al., 2017). Our results differed from those of Rizqui et al. (2019), who recommended that the best depth in a drip irrigation system is within 10 cm of the ground surface. Likewise, Soulis et al. (2015) indicated that the most suitable measurement position was 10 cm below the soil surface, although this position could vary according to the specific soil hydraulic properties, meteorological conditions, and configuration of the irrigation system.

According to our results, the positions and depths most accurately simulated by HYDRUS-3D were located in the vicinity of the dripper and at depths of 40 - 60 cm. In this area, our results were: $R^2 > 0.92$, RMSE < 0.01 $cm^3\ cm^{-3}$ and NSE > 0.87. This finding is relevant because this is the part of the soil of greatest interest for drip irrigation, according to Soulis and Elmaloglou, (2018), who determined that the optimum sensor positions for drip irrigation in a layered soil were at a horizontal distance of 7 cm and a depth of 16 cm in the upper layer, and at a horizontal distance of 11 cm and 34 cm depth in the lower layer.

Regarding to the hourly SWC measurements, HYDRUS-3D simulation reached a good agreement with the tensiometers, in particular when using parameterization calibrated with neutron probe, which reached $R^2 > 0.98$. These results improved on the results obtained by the likes of Arbat et al. (2008), who reported R^2 values of between 0.520 and 0.825 when comparing soil water content simulated by an hourly adjusted HYDRUS model, using measurements obtained from granular matrix sensors.

5. Conclusions

HYDRUS-3D was used with different parameterisation approaches to simulate soil water dynamics and the findings were compared with measurements made using neutron probes and tensiometers located at different positions relative to a dripper. The results obtained showed that soil hydraulic parameters estimated with the Rosetta model were useful for predicting general trends, but the simulations were not accurate enough to fit well with soil water contents measured using neutron probes at different points in the crop season. A site-specific determination of the soil hydraulic parameters conducted with HYPROP + WP4C provided better agreement with measurements taken by neutron probes at different soil positions in a drip-irrigated apple orchard. Further improvement was obtained following the empirical calibration of parameter n, based on neutron probe measurements. With such a configuration, the simulations produced a much finer fit with the measurements, both when comparing daily values at the seasonal scale, and also when comparing hourly values over the course of several days.

The 3D domain represented in these simulations is common in tree orchards, where wet bulbs from consecutive drippers arranged in a line may partly overlap and are clearly separated from neighboring drip lines. This work shows that the 3D simulations agreed with measurements of seasonal dynamics in the planes following and running perpendicular to the dripline. The simulations with the three-dimensional version of HYDRUS provided a good level of explanation and prediction of the overall water balance of the dripper domain, including both the area within the influence of the wetting pattern and the soil beyond it. Nevertheless, the fit was better for the regions of the soil domain within the influence of the dripper. These coincided with the region of greatest interest for managing irrigation, whereas the fit worsened in deeper and more peripherical soil regions.

Modelling water dynamics in localized irrigation with HYDRUS-3D, considering soil hydraulic properties, specific crop characteristics, and the irrigation system provide a useful base from which to improve the design of irrigation systems and to define efficient irrigation strategies to prevent water losses through percolation and leaching. In addition, these simulations allow a better understanding of the patterns of soil moisture that can be measured by sensors installed at different depths and in different positions relative to a dripper. This, in turn, provides valuable knowledge which helps to optimize the installation, processing and interpretation of soil moisture sensors.

Acknowledgments

The authors would like to acknowledge the collaboration of Jordi Oliver, Carles París, Mercè Mata, Jesús del Campo and Jordi Virgili, as part of the staff of the programme on Efficient Use of Water in Agriculture for their support in implementing this activity.

Literature cited

Allen, R.G.; Pereira, L.S.; Raes, D.; Smith, M. Crop evapotranspiration. Guidelines for Computing

Crop Water Requirements. FAO Irrigation and Drainage Paper 56, 1998, Rome.

AQUASTAT database. Available online: http://www. fao.org/nr/aquastat (accessed July 2019).

Arbat, G.; Barragán, J.; Puig, J.; Poch, R.; Ramírez de Cartagena, F. Evaluación de los modelos numéricos de flujo de agua en el suelo HYDRUS- 2D y SIMDAS en riego localizado. Alvarez-Benedí, J. y Marinero, P. (ed) Estudios de la zona no saturada del suelo, 2003,6, 279–288.

Arbat, G.; Puig-Bargués, J.; Barragán, J.; Bonany, J.; Ramírez de Cartagena, F. Monitoring soil water status for micro-irrigation management versus modelling approach. Biosyst. Eng. 2008, 100, 286–296.

Arbat, G.; Puig-Bargués, J.; Duran-Ros M.; Barragán, J.; De Cartagena, F. R. Drip-Irriwater: Computer software to simulate soil wetting patterns under surface drip irrigation. Comput. Electron. Agric. 2013, 98, 183-192.

Bastet, G.; Bruand, A.; Voltz, M.; Bornand, M.; Que´tin, P. Performance of available pedotransfer functions for predicting the water retention properties of French soils. In Proceedings of the International Workshop on Characterization and Measurement of the Hydraulic Properties of Unsaturated Porous Media; Riverside, CA, 22–24 October 1997, University of California, Riverside, CA, USA, 1999; pp. 981–992.

Bezerra-Coelho, C. R.; Zhuang, L.; Barbosa, M. C.; Soto, M. A.; Van Genuchten, M. T. Further tests of the HYPROP evaporation method for estimating the unsaturated soil hydraulic properties. J. Hydrol. Hydromech. 2018, 66, 161-169.

Bravdo, B.; Proebsting, E. L. Use of drip irrigation in orchards. HortTechnology. 1993, 3, 44-49.

Campbell, C. S.; Cobos, D. R.; Rivera, L. D.; Dunne, K. M.; Campbell, G. S. Constructing fast, accurate soil water characteristic curves by combining the Wind/Schindler and vapor pressure techniques; Springer, Berlin, Germany, 2012; pp. 55-62.

Carsel, R. F.; Parrish, R. S. Developing joint probability distributions of soil water retention characteristics. Water Resour. Res. 1988, 24, 755-769.

Casadesús, J.; Mata, M.; Marsal, J.; Girona, J. A general algorithm for automated scheduling of drip irrigation in tree crops. Comput. Electron. Agric. 2012, 83, 11–20.

Dane, J.H.; Hopmans, J.W. Water retention and storage. In: Dane, J.H., Topp, G.C. (Eds.), Methods of Soil Analysis. Part 4, SSSA Book Series No. 5. 2002, Soil Science Society of America Journal, Madison WI.

Domínguez-Niño, J.M.; Oliver-Manera, J.; Girona, J.; Casadesús, J. Differential irrigation scheduling by an automated algorithm of water balance tuned by capacitance-type soil moisture sensors. Agric. Water Manag. 2020, 228, 105880.

Egea, G.; Diaz-Espejo, A.; Fernández, J. E. Soil moisture dynamics in a hedgerow olive orchard underwell-watered and deficit irrigation regime: Assessment, prediction and scenario analysis. Agric. Water Manag. 2016, 164, 197–211.

Elmaloglou, S.; Soulis, K. X.; Dercas, N. Simulation of soil water dynamics under surface drip irrigation from equidistant line sources. Water Resour. Manag. 2013, 27, 4131-4148.

Feddes R A; Kowalik P J; Zaradny H. Simulation of Field Water Use and Crop Yield. John Wiley and Sons, Inc. New York, USA, 1978 pp. 16-30

García Morillo, J.; Rodríguez Díaz, J. A.; Camacho, E.; Montesinos, P. Drip irrigation scheduling using HYDRUS 2-D numerical model application for strawberry production in south-west Spain. Irrig. Drain Syst. 2017, 66, 797–807.

Gärdenäs, A. I.; Hopmans, J. W.; Hanson, B. R.; Šimůnek, J. Two-dimensional modeling of nitrate leaching for various fertigation scenarios under micro-irrigation. Agric. Water Manag. 2005, 74, 219–2

Girona, J.; Marsal, J.; Mata, M.; del Campo, J. Pear crop coefficients obtained in a large weighing lysimeter. Acta Hortic. 2004, 664, 277-281

Hao, A.; Marui, A.; Haraguchi, T.; Nakano, Y. Estimation of wet bulb formation in various soil during drip irrigation. J. Fac. Agric. Kyushu Univ. 2007, 52, 187.

Heng, L.K.; Evett, S., Field estimation of soil water content. A practical guide to methods, instrumentation and sensor technology. Direct and Surrogate Measures of Soil Water Content Ed. IAEA. Training Course Series No. 30, Vienna, 2008; pp.131

Honari, M.; Ashrafzadeh, A.; Khaledian, M.; Vazifedoust, M.; Mailhol, J. C. Comparison of HYDRUS-3D soil moisture simulations of subsurface drip irrigation with experimental observations in the south of France. J. Irrig. Drain. Eng., 2017, 143, 04017014.

Kadyampakeni, D. M.; Morgan, K. T.; Nkedi-Kizza, P.; Schumann, A. W.; Jawitz, J. W. Modeling Water and Nutrient Movement in Sandy Soils Using HYDRUS-2D. J. Environ. Qual. 2018, 47, 1546-1553.

Kanzari, S.; Nouna, B. B.; Mariem, S. B.; Rezig, M. Hydrus-1D model calibration and validation in various field conditions for simulating water flow and salts transport in a semi-arid region of Tunisia. Sustain. Environ. Res. 2018. 28, 350-356.

Kisekka, I.; Kandelous, M. M.; Sanden, B.; Hopmans, J. W. Uncertainties in leaching assessment in micro-irrigated fields using water balance approach. Agric. Water Manag. 2019, 213, 107-115.

Kramer, P.J.; Boyer, J.S. Soil and Water. In Water relations of plants and soils, X ed.; Academic Press, Orlando, USA, 1995; pp. 84-114.

Lai, X.; Liu, Y.; Zhou, Z.; Zhu, Q.; Liao, K. Investigating the spatio-temporal variations of nitrate leaching on a tea garden hillslope by combining HYDRUS-3D and DNDC models. J. Plant Nutr. Soil Sci. 2019, 000, 1–12.

Lin, H. Temporal stability of soil moisture spatial pattern and subsurface preferential flow pathways in the Shale Hills Catchment. Vadose Zone J. 2006, 5, 317-340.

Lu, P.; Zhang, Z.; Sheng, Z.; Huang, M.; Zhang, Z. Assess effectiveness of salt removal by a subsurface drainage with bundled crop straws in coastal saline soil using HYDRUS-3D. Water. 2019, 11, 943.

Mailhol, J. C.; Ruelle, P.; Walser, S.; Schütze, N.; Dejean, C. Analysis of AET and yield predictions under surface and buried drip irrigation systems using the Crop Model PILOTE and Hydrus-2D. Agric. Water Manag. 2011, 98, 1033-1044.

Marković, M.; Filipović, V.; Legović, T.; Josipović, M.; Tadić, V. Evaluation of different soil water potential by field capacity threshold in combination with a triggered irrigation module. Soil Water Res. 2015, 10, 164-171.

Márquez, D.; Faúndez, C.; Aballay, E.; Haberland, J.; Kremer, C. Assesing the vertical movement of a nematicide in a sandy loam soil and its correspondence using a numerical model (HYDRUS 1D). J. Soil Sci. Plant Nutr. 2017, 17, 167-179.

Mashayekhi, P.; Ghorbani-Dashtaki, S.; Mosaddeghi, M. R.; Shirani, H.; Nodoushan, A. R. M. Different scenarios for inverse estimation of soil hydraulic parameters from double-ring infiltrometer data using HYDRUS-2D/3D. Int. Agrophys. 2016, 30.

Migliaccio, K. W.; Olczyk, T.; Li, Y.; Muñoz-Carpena, R.; Dispenza, T. Using Tensiometers for Vegetable Irrigation Scheduling in Miami-Dade County. Agricultural and Biological Engineering Department, University of Florida, Institute of Food and Agricultural Sciences Extension, 2015.

Nash, J. E.; Sutcliffe, J. V. River flow forecasting through conceptual models part I-A discussion of principles. J. Hydrol, 1970, 10, 282-290.

O'Connell, D. A.; Ryan, P. J. Prediction of three key hydraulic properties in a soil survey of a small forested catchment. Soil Res. 2002, 40, 191-206.

Orzolek, M. Guide to the Manufacture, Performance, and Potential of Plastics in Agriculture, 1st ed.; Matthew Deans, USA, 2017; pp. 1-18

Ottoni, M. V.; Ottoni Filho, T. B.; Lopes-Assad, M. L. R.; Rotunno Filho, O. C. Pedotransfer functions for saturated hydraulic conductivity using a database with temperate and tropical climate soils. J. Hydrol. 2019, 575, 1345-1358.

Peters, A.; Durner, W. Simplified evaporation method for determining soil hydraulic properties. J. Hydrology, 2008, 356, 147-162.

Phogat, V.; Mahadevan, M.; Skewes, M.; Cox, J. W. Modelling soil water and salt dynamics under pulsed and continuous surface drip irrigation of almond and implications of system design. Irrig. Sci. 2012, 30, 315-333.

Phogat, V.; Skewes, M. A.; Mahadevan, M.; Cox, J. W. Evaluation of soil plant system response to pulsed drip irrigation of an almond tree under sustained stress conditions. Agric. Water Manag. 2013, 118, 1–11.

Rai, V.; Pramanik, P.; Das, T. K.; Aggarwal, P.; Bhattacharyya, R.; Krishnan, P.; Sehgal, V. K. Modelling soil hydrothermal regimes in pigeon pea under conservation agriculture using Hydrus-2D. Soil Till. Res. 2019, 190, 92-108.

Raij, I.; Simunek, J.; Ben-Gal, A.; Lazarovitch, N. Water flow and multicomponent solute transport in drip-irrigated lysimeters. Water Resour. Res., 2016, 52, 6557-6574.

Roberts, T.; Lazarovitch, N.; Warrick, A. W.; Thompson, T. L. Modeling Salt Accumulation with Subsurface Drip Irrigation Using HYDRUS-2D. Soil Sci. Soc. Am J. 2009, 73, 233.

Robin, V.; Sardini, P.; Mazurier, A.; Regnault, O.; Descostes, M. Effective porosity measurements of poorly consolidated materials using non-destructive methods. Eng.Geol. 2016, 205, 24-29.

Robock, A.; Vinnikov, K. Y.; Srinivasan, G.; Entin, J. K.; Hollinger, S. E.; Speranskaya, N. A.; Namkhai, A. The global soil moisture data bank. B. Am. Meteorol. Soc, 2000, 81, 1281-1300.

Sakaguchi, A.; Yanai, Y.; Sasaki, H. Subsurface irrigation system design for vegetable production using HYDRUS-2D. Agric. Water Manag. 2019, 219, 12-18.

Sasal, M. C.; Andriulo, A. E.; Taboada, M. A. Soil porosity characteristics and water movement under zero tillage in silty soils in Argentinian Pampas. Soil Till. Res. 2006, 87, 9-18.

Saunders, L. C. U.; Libardi, P. L.; Reichardt, K. Condutividade hidráulica da terra roxa estruturada em condições de campo. Rev. Bras. Ciênc. Solo. 1979, 23, 3.

Schaap, M. G.; Leij, F. J.; Van Genuchten, M. T. Rosetta: A computer program for estimating soil hydraulic parameters with hierarchical pedotransfer functions. J. Hydrol. 2001, 251, 163-176.

Schindler, U.; Mueller, L.; Unold, G. V.; Durner, W.; Fank, J. Emerging measurement methods for soil hydrological studies; Springer: Berlin, Germany, 2016; pp. 345-363.

Schindler, U.; von Unold, G.; Durner, W.; Mueller, L. Recent progress in measuring soil hydraulic properties. In Proceedings of the International Conference on Environment and Civil Engineering, Pattaya, Thailand, 2015; pp. 24-25.

Shokrana, M. S. B.; Ghane, E. Measurement of soil water characteristic curve using HYPROP2. MethodsX. 2020, 100840.

Simunek, J.; Van Genuchten, M. T; Sejna, M. Recent developments and applications of the HYDRUS computer software packages. Vadose Zone J. 2016, 15, 25.

Singh, R.; Van Dam, J. C.; Feddes, R. A. Water productivity analysis of irrigated crops in Sirsa district, India. Agric. Water Manag. 2006, 82, 253-278.

Skaggs, T. H.; Trout, T. J.; Simunek, J.; Shouse, P. J. Comparison of HYDRUS-2D Simulations of Drip Irrigation with Experimental Observations. J. Irrig. Drain. Eng. 2004, 130, 304–310.

Soil Survey Staff. Soil Taxonomy. A basic System for Making and Interpreting Soil Surveys. 2nd ed.; United States Department of Agriculture, National Resources Conservation Service, USA, 1999; pp. 869.

Soulis, K. X.; Elmaloglou, S.; Dercas, N. Investigating the effects of soil moisture sensors positioning and accuracy on soil moisture based drip irrigation scheduling systems. Agric. Water Manag. 2005, 148, 258-268.

Soulis, K. X.; Elmaloglou, S. Optimum soil water content sensors placement for surface drip irrigation scheduling in layered soils. Comput. Electron. Agric. 2018, 152, 1-8.

Tao, Y.; Wang, S.; Xu, D.; Yuan, H.; Chen, H.J.A.W.M. Field and numerical experiment of an improved subsurface drainage system in Huaibei plain. Agric. Water Manag. 2017, 194, 24–32.

Taylor, S. A.; Ashcroft, G. L. Physical Edaphology: the physics of irrigated and non irrigated soils. W. H. Freeman., San Francisco, USA; 1972; pp. 532.

Tawutchaisamongdee; Wonprasaid, S.; Horkaew, P.; Machikowa, T. Moisture distribution patterns in loamy sand and sandy clay loam soils under drip irrigation system. Proceedings of ISER 124th International Conference, Tokyo, Japan, 29th -30th April 2018, Pages: 86-89.

Tran, T. D.; Cui, Y. J.; Tang, A. M.; Audiguier, M.; Cojean, R. Effects of lime treatment on the microstructure and hydraulic conductivity of Héricourt clay. J. Rock Mech. Geotech. Eng. 2014, 6, 399-404.

Van Genuchten, M.T.; Leij, F.J.; Yates, S.R. The RETC Code for Quantifying the Hydraulic Functions of Unsaturated Soils. Salinity Laboratory, Riverside, USA; 1991

Van Genuchten, M. T.; Simunek, J.; Schaap, M. G.; Skaggs, T. H. Unsaturated Zone Parameter Estimation Using the HYDRUS and Rosetta Software Packages. Multimedia Environmental Models, 2003, 41.

Vrugt, J.; Hopmans, J.; Simunek, J. Calibration of a two-dimensional root water uptake model. Soil Sci. Soc Am. J. 2001, 65, 1027–1037.

Wang, X.; Li, Y.; Wang, Y.; Liu, C. Performance of HYDRUS-1D for simulating water movement in water-repellent soils. Can. J. Soil Sci. 2018, 98, 407-420.

Wösten, J. H. M.; Lilly, A.; Nemes, A.; Le Bas, C. Development and use of a database of hydraulic properties of European soils. Geoderma. 1999, 90, 169-185.

Zazueta, F. S.; Xin, J. Soil moisture sensors. Soil Sci. 1994, 73, 391-401.

Zhang, Y.; Wu, P.; Zhao, X.; Zhao, W. Measuring and modeling two-dimensional irrigation infiltration under film-mulched furrows. Sci. Cold Arid. Reg. 2016, 8, 419-431.

Zięba, Z. Influence of soil particle shape on saturated hydraulic conductivity. J. Hydrol. Hydromech. 2017, 65, 80-87.

Chapter III: Actual sensor performance in the field

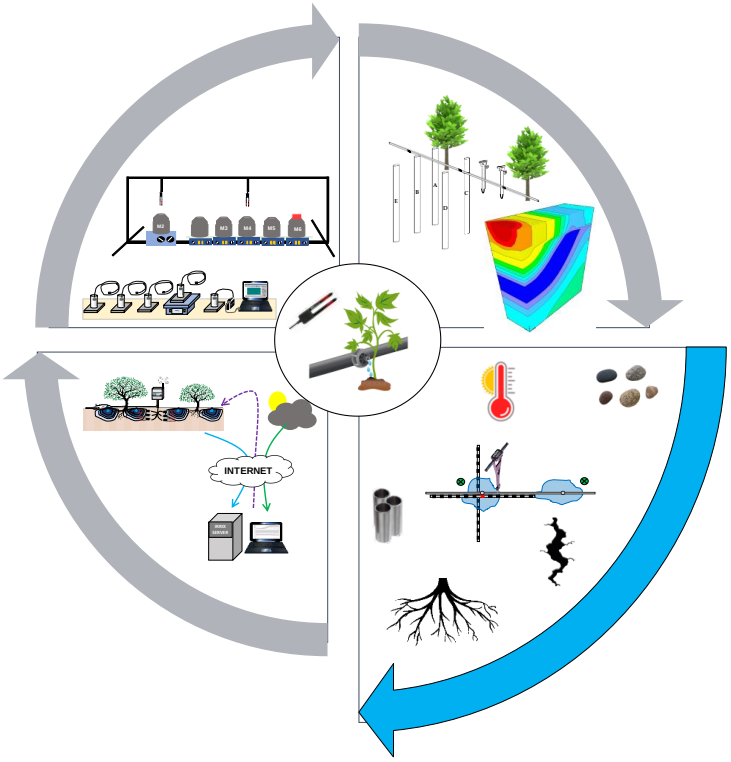

Analysis of the variability in soil moisture measurements by capacitance sensors in a drip-irrigated orchard

Jesús María Domínguez-Niño[1]*, Jordi Oliver-Manera[1], Gerard Arbat[2], Joan Girona[1]; Jaume Casadesús[1]

[1] Efficient Use of Water in Agriculture Program, Institute of Agrifood Research and Technology (IRTA), Parc de Gardeny (PCiTAL), Fruitcentre, 25003, Lleida, Spain; jesus.dominguez@irta.cat; jordi.oliver@irta.cat; joan.girona@irta.cat; jaume.casadesus@irta.cat

[2] Department of Chemical and Agricultural Engineering and Technology, University of Girona, Campus Montilivi s/n, 17071 Girona, Spain; gerard.arbat@udg.edu

Sensors (2020), 20, 5100 DOI: 10.3390/s20185100

Abstract

Among the diverse techniques for monitoring soil moisture, capacitance-type soil moisture sensors are popular because of their low cost, low maintenance requirements and acceptable performance. However, although in laboratory conditions the accuracy of these sensors is good, when installed in the field they tend to show large sensor-to-sensor differences, especially in drip irrigation. This complicates decisions on the design of sensor deployment and the interpretation of the recorded data. The aim of this paper is to study the variability involved in the measurement of soil moisture by capacitance sensors in a drip-irrigated orchard and, using this information, find ways to optimize their usage to manage irrigation. For this purpose, the study examines the uncertainties in the measurement process plus the natural variability in the actual soil water dynamics. Measurements were collected by 57 sensors, located at 10 combinations of depth and position relative to the dripper. Our results showed large sensor-to-sensor differences, even when installed at equivalent depth and coordinates relative to the drippers. In contrast, differences among virtual sensors simulated using a HYDRUS-3D model at those soil locations were one order of magnitude smaller. Our results highlight as a possible cause for the sensor-to-sensor differences in the measurements by capacitance sensors the natural variability in size, shape, and centring of the wet area below the drippers, combined with the sharply defined variation in water content at the soil scale perceived by the sensors.

Keywords: capacitance sensor; HYDRUS-3D; soil water content; soil wetting patterns; soil temperature; two-steps calibration.

1. Introduction

The increase in the world's population and the consequent increase in water consumption necessitates the proper and efficient management of water resources (Ashofteh et al., 2015). In agriculture, drip irrigation is one of the most important solutions for the efficient use of limited water resources (Kilic, 2020). Drip irrigation provides water to a limited volume of soil in the region where the greatest water extraction by plants occurs, reducing losses by surface evaporation and deep percolation (Rajput and Neelam, 2006; Liao et al 2008; Naglic et al., 2014). The distribution of moisture within a volume of wet soil is known as the wet bulb (Arraes et al., 2019). Its formation is affected by a number of factors, including the physical properties of the soil (texture, bulk density, initial water content…), absorption of the crops by the root system, soil surface evaporation and the intensity of the irrigation rate (Hao et al., 2007; Kandelous et al., 2011).

Real-time monitoring of soil moisture can provide useful information for optimizing the amount and timing of irrigation (Nolz et al., 2016; Soulis and Elmaloglou, 2018). Soil moisture can be measured using electromagnetic methods, such as time domain reflectometry (TDR) (Ledieu et al., 1986) and capacitance sensors (Zotarelli et al., 2011), or using electrical resistance blocks (Cummings and Chandler, 1941), neutron probes (Chanasyk and Naeth, 1996) or tensiometers (Muñoz-Carpena et al., 2005). Among the range of different soil water sensing technologies, capacitance-type soil moisture sensors (Kojima et al., 2016; Bogena et al., 2017) are the most popular because of their cost, reasonable robustness and precision, low power consumption and low maintenance requirements (Jones et al., 2005, Spelman et al., 2013, Visconti et al., 2014; Rosenbaum et al., 2011). While their adoption by farmers remains low, their use is increasing not only for the visual supervision of the dynamics of soil water content (SWC) with irrigation, but also as a potential way of providing input data for decision support systems (DSS) that help to determine when to irrigate and how much water to apply on a plot (Fares and Alva, 2000; Gallardo et al., 2020).

However, although these sensors give good accuracy in laboratory conditions (Rosenbaum et al., 2010; Spelman et al., 2013; Bogena et al 2017), in field conditions they show large sensor-to-sensor variability, especially in drip irrigation (Nolz and Loiskandl, 2017). One explanation for this variability is that they only perceive a small volume of soil (in the order of 1 dm^3 (Cobos, 2008; Sakaki et al., 2008)), which makes them very sensitive to local variations in, for example, gravel content, bulk density, soil salinity, the existence of macropores and shrinkage cracks, the proximity of plant roots and small-scale surface features (Waugh et al., 1996; Dane and Hopmans, 2002). Some of these factors vary little over time and, hence, once a sensor is installed their effect is permanent. In addition, there are other factors that influence sensor variability which are dynamic in nature. These include soil temperature (Adla et al., 2020) and soil apparent electrical conductivity (Scudeiro et al., 2012). The SWC pattern around a

dripper is also dynamic and its change over time can be simulated with mathematical models. In this respect, HYDRUS (Simunek et al., 2016) is a well-known software package for the simulation of water and solute movement in soils of one-, two- or three-dimensions, for different combinations of initial and boundary conditions (Badni et al., 2018; Fan et al., 2018). Some authors (Skaggs et al., 2004; Abou Lila et al., 2012; García et al., 2017; Domínguez-Niño et al., 2020) have used HYDRUS modelling to simulate surface drip irrigation. These and other works have demonstrated the ability of HYDRUS to simulate the space-time dynamics of soil water in drip irrigated crops. Simulations with HYDRUS can indicate whether the observed differences between sensors can be attributed to the expected dynamics of the wet bulbs or, alternatively, whether other factors need to be considered.

Despite the difficulties described above, capacitance-type soil moisture sensors are successfully being used for irrigation management, including in scenarios of drip-irrigated orchards (Millán et al., 2019; Domínguez-Niño et al., 2020). A better understanding of the uncertainty of these measurements and of the variability in the actual soil conditions should provide clues about how to improve their performance, their effectivity and, ultimately, their practical utility in real orchard conditions.

The objective of this study is to analyse why capacitive sensors provide accurate measurements of SWC in laboratory conditions but, when installed in a real drip-irrigated orchard, show large sensor-to-sensor differences. The study consisted of analysing the performance, during two consecutive irrigation seasons, of 57 capacitive-type soil moisture sensors installed in 10 soil locations around the drippers of an apple orchard under semi-arid conditions. The effect was considered of potentially disturbing factors such as variability in the soil area wetted by the dripper and the influence of soil temperature and sensor calibration. In addition, virtual sensor readings, obtained from simulations of soil water dynamics with HYDRUS-3D, were used to assess how much of the observed differences can be explained by the expected soil moisture dynamics of an idealized wet bulb.

2. Materials and Methods

2.1. *Experimental orchard*

The research was carried out in the irrigation seasons of 2017 and 2018 in two experimental plots (Plot I and Plot II) of an apple orchard (*Malus domestica* Borkh. cv 'Golden Reinders') planted in 2011 and grafted on M-9 rootstock located at the IRTA-Lleida Experimental Station (Mollerussa, Lleida, Spain). The planting pattern was 3.50 m x 1.63 m with a north-to-south tree row orientation. The climate of the area is Mediterranean, with annual rainfall and evapotranspiration rates of 290 mm and 1093 mm, respectively, for the year 2017, and 506 mm and 1040 mm, respectively for the year 2018.

Irrigation water was supplied by a drip irrigation system (3.5 L h^{-1}) with a 0.6 m separation between drippers. During the irrigation season, the water was applied at 8:00 a.m., except in the months of August and September 2017 when variations in irrigation schedules were applied. In general, these plots were irrigated, on a daily basis, with a daily irrigation dose (DID) to meet crop water needs based on the FAO water balance (Allen et al., 1998) (Eq. 1).

$$DID = ET_O \times K_C \quad \text{(Eq. 1)}$$

where ET_O is the reference evapotranspiration from the previous week, recorded by a weather station located on the same farm, and Kc is the crop coefficient determined in previous years in the same orchard using the weighing lysimeter method (Girona et al., 2004). However, arbitrary irrigation doses were imposed in certain periods in order to test sensor response to soil water input/output imbalances. Furthermore, each plot was irrigated independently and, therefore, different doses of water were applied. Electrical conductivity of the irrigation water was 0.309 dS m^{-1}, and NPK fertigation was applied (100 kg N, 30 kg P_2O_5 and 108 K_2O) from May to June (90%) and in September (10%).

The soil of the orchard was classified as *Typic Calcixerepts, coarse-loamy, mixed and thermic* according to the Soil Survey Staff classification (Soil Survey Staff, 1999). Soil samples were taken at different depths and their texture, bulk density and organic matter were determined. The results obtained are shown in Table 1.

Table 112. Physical soil properties at three depths

Depth (cm)	0 - 20	20 - 40	40 -60
Sand (%)	35.80	35.50	36.00
Silt (%)	40.70	40.60	39.90
Clay (%)	23.50	23.90	24.10
USDA soil classification	loamy	loamy	loamy
Bulk density (g cm^{-3})	1.48	1.50	1.53
Organic matter (%)	1.99	1.57	1.34

2.2. Soil water content measurements

The soil moisture sensors used in this study, EC-5 and 10HS, are capacitance and frequency domain reflectometry (FDR)-type sensors (Meter Group Inc., Pullman, WA, USA). These sensors measure the dielectric constant or permittivity of the soil to calculate its moisture content. The EC-5 sensor is 5 cm long and has an approximate theoretical measurement volume of 0.3 L (Rosenbaum et al., 2011). The 10HS sensor is 10 cm long and can measure 1 L of soil volume (Visconti et al., 2014). Both sensors measured the SWC every 10 seconds, and the average of 5 minutes was stored in the dataloggers CR800 and CR1000 (Campbell Scientific Inc., Logan, UT, USA), which used a multiplexer AM16/32 to increase the number of channels. The moisture sensors were deployed in two plots, with one sensor type in each plot. Three repetitions of 9 or 10 sensors were installed in each plot in different positions and depths around the dripper

(Fig. 1). The experiment ended in September 2018 when the sensors were removed from the soil and taken to the laboratory for two-step calibration under specific conditions described in a previous study (Domínguez-Niño et al., 2019).

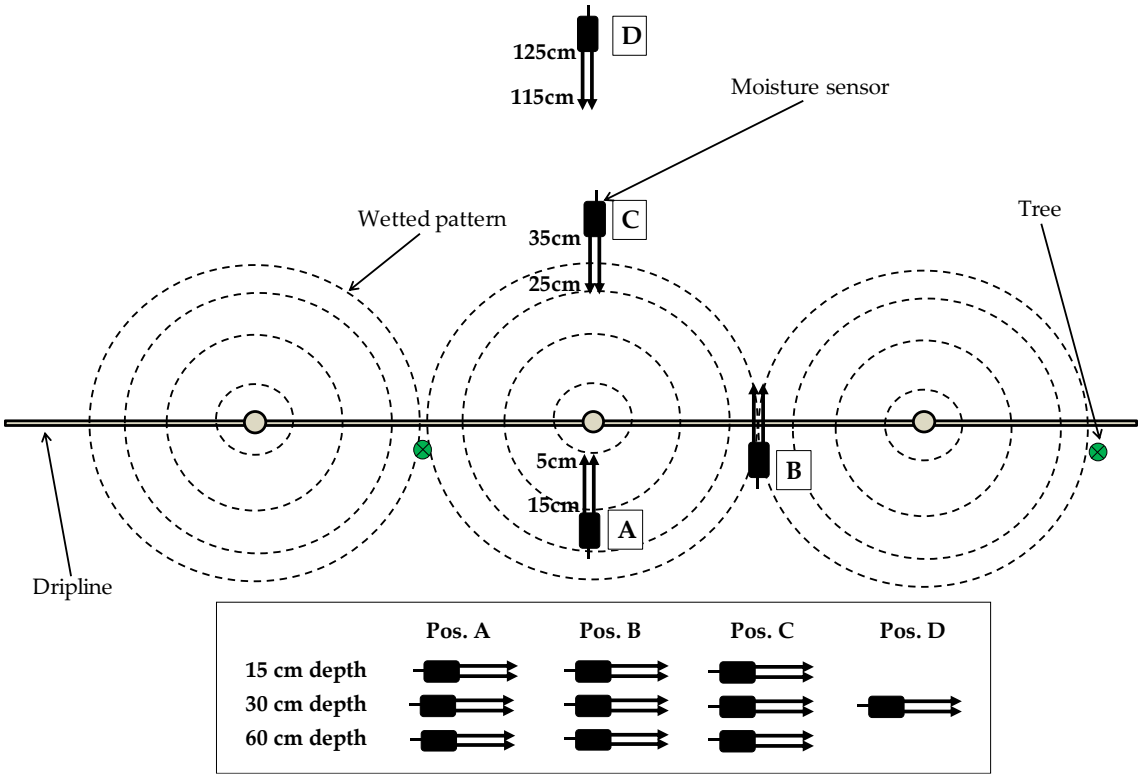

Figure 1. EC-5 and 10HS moisture sensors installed at three depths (15, 30 and 60 cm) in four positions relative to the dripper (Pos. A: centre of wet bulb, Pos. B: mid-point between two drippers (30 cm), Pos. C: perimeter of the wet area, Pos. D: outside the influence of the dripper.

The EC-5 sensors of Plot I were installed in 2013 and deployed in positions A, B and C at 15, 30 and 60 cm depths, with 3 repetitions each around a different dripper. All repetitions were within the same tree row and separated by a distance of less than 5 m. The 10HS sensors of Plot II, which were installed in 2016 and deployed in equivalent positions and depths as in Plot I, additionally included position D at a depth of 30 cm (Table 2).

Table 2. Deployment of 10HS sensors in the study plot

Position	Distance to dripper (cm)	Depth (cm)
A: centre of wet bulb	5-15	15, 30 and 60
B: mid-point between two drippers	25-35	15, 30 and 60
C: wet area perimeter	25-35	15, 30 and 60
D: outside the influence of the dripper	115-125	30

A total of nine temperature probes (Omega HSTH-44000, 2252 Ohm) were also installed in 2013 in Plot I, at soil locations equivalent to those of the EC-5 sensors. Probe readings were recorded using the same datalogger as for the EC-5 sensors , through a dedicated multiplexer AM16/32 (Campbell Scientific Inc., Logan, UT, USA). Soil

temperature measurements ended in early 2016 when the multiplexer was damaged by a flood. The dataset of soil temperatures analysed in this work corresponds to the 2015 season, when soil temperature and soil moisture were recorded simultaneously. Figure 2 shows a temporal scheme that indicates the most relevant moments related to the installation of soil moisture and temperature sensors, calibration and simulation with HYDRUS-3D.

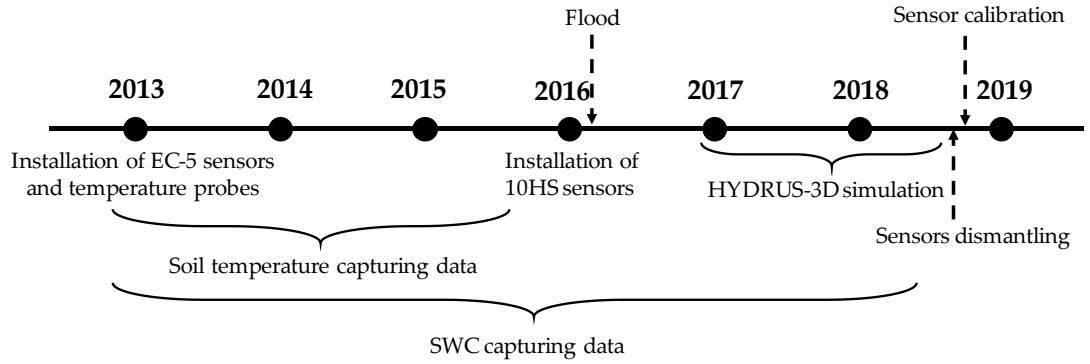

Figure 4. Temporal sequence where the most relevant moments are indicated. Recording of soil temperature ended in early 2016 when the setup was damaged by flood. The SWC measurements analyzed in this paper focus on the irrigation seasons of 2017 and 2018, which were also simulated with HYDRUS. At the end of this period, all 10HS sensors were dismantled and calibrated in laboratory.

The extent and position of the area wetted by drippers was characterized in this site in order to standardize the positions of the sensor in relationship to the wet bulbs. The measurements were done at the end of an irrigation pulse, in July-August 2018, using a portable Fieldscout TDR 300 soil moisture instrument (Spectrum Technologies INC., Aurora, IL, USA) with 12 cm-long rods (Fig. 3). The characterization of the extent of the wetted area consisted in measuring the SWC at intervals of 10 cm, parallel and perpendicular to the dripline. The position of the wetting pattern was referred to the centring of the wet bulb relative to the dripper and was determined as the point with the highest SWC between two drippers. To determine the variability in the extent and position of the wetted area, a "reference wetting pattern" was defined as the wetting pattern most frequently observed during the measurements. Then, all transects included in the dataset were compared with this "reference wetting pattern".

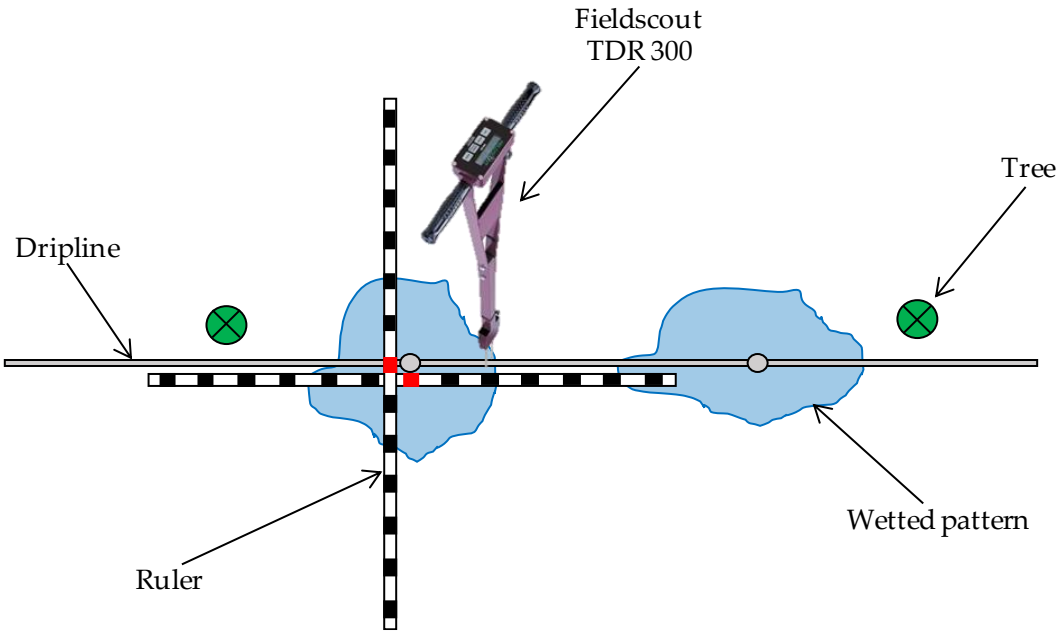

Figure 3. Characterization of the wetting patterns around drippers using the Fieldscout TDR 300.

SWC at Plot I was measured periodically using a neutron. Twelve access tubes were installed in 2013 at positions A, B, C, D, relative to the drippers, and repeated in three drippers as described in Domínguez-Niño et al. (2020). The volumetric soil water content in these access tubes was measured using a neutron probe (Hydroprobe 503DR, Campbell Pacific Nuclear Corp., Martinez, CA, USA) which had previously been calibrated for this site. Measurements were taken at depths between 0.20 m and 1.00 m, at intervals of 20 cm depth, on a total of 15 days in the periods from May to October of 2017 and 2018.

2.3. HYDRUS-3D model

The HYDRUS-3D model (v. 2.02) was used to simulate the soil water movement in a three-dimensional domain and hourly scale (Simunek et al., 2016). The water movement was simulated for 2017 and 2018. The Richards equation (Eq. 2) governs the movement of water flow in an unsaturated soil, with a sink term, S (cm^3 cm^{-3} day^{-1}), incorporated to consider water absorption by the root system.

$$\frac{\partial \theta}{\partial t} = \frac{\partial}{\partial x}\left[K(h)\frac{\partial h}{\partial x}\right] + \frac{\partial}{\partial y}\left[K(h)\frac{\partial h}{\partial y}\right] + \frac{\partial}{\partial z}\left[K(h)\left(\frac{\partial h}{\partial z} + 1\right)\right] - S \qquad \text{(Eq. 2)}$$

where θ represents the volumetric water content (cm^3 cm^{-3}), h is soil water pressure head (cm), t is time (days), x and y are the horizontal space coordinates (cm), z is the vertical space coordinate (cm), and K is hydraulic conductivity (cm day^{-1}). In HYDRUS, the S term represents the volume of water extracted by the roots in a soil volume unit per unit of time. It uses a complex function proposed by Feddes (Feddes et al., 1978) (Eq. 3).

$$S(h,z) = \alpha(h) S_{max}(h,z) \quad \text{(Eq. 3)}$$

where α is a dimensionless water stress reduction factor expressed as a function of pressure head h (cm), whose values were taken from Taylor and Ashcroft (Taylor and Ashcroft, 1972) for deciduous fruit trees. S_{max} ($cm^3\ cm^{-3}\ day^{-1}$) is the maximum possible root water extraction rate when soil water is not a limiting factor, and z is the soil depth (cm).

The HYDRUS model solves the Richards equation using van Genuchten's parametric function (van Genuchten, 1980), which relates moisture and soil water potential through Eq. 4:

$$\theta(h) = \begin{cases} \theta_r + \dfrac{\theta_s - \theta_r}{[1 + |\alpha \cdot h|^n]^m} & h < 0 \\ \theta_s & h \geq 0 \end{cases} \quad \text{(Eq. 4)}$$

where θs ($cm^3\ cm^{-3}$) is saturated water content, θr ($cm^3\ cm^{-3}$) is residual water content, and m, n and α are empirical values that affect the shape of the retention curve (for purposes of simplification it is assumed that $m = 1 - (1/n)$). Unsaturated hydraulic conductivity, $K(h)$ (cm day^{-1}), is determined through Eq. 5 (Mualen, 1976).

$$K(h) = K_s S_e^l \left[1 - (1 - S_e^{1/m})^m\right]^2 \quad \text{(Eq. 5)}$$

where Se is the dimensionless effective water content, Ks is the saturated hydraulic conductivity of the soil and l is an empirical parameter related to the conductivity between the pores.

The soil hydraulic parameters and root distribution used for the purposes of the present study were obtained from a previous work (Domínguez-Niño et al., 2020) in which the most appropriate HYDRUS-3D configuration was defined and the soil water dynamics in a drip irrigated orchard were simulated. However, in contrast with the previous work, here the initial conditions were established from the SWC measured by the capacitance sensors at the beginning of the year. We also assumed a semi-circular area with a radius of 10 cm, which was the waterlogged area during the irrigation. Accordingly, the flux, q (Eq. 6), was estimated as:

$$q = \frac{\text{Emitter discharge flow rate } (cm^3\ h^{-1})}{\text{wetted surface area } (cm^2)} = \frac{3500\ cm^3 h^{-1}}{157\ cm^2} = 22.29\ cm\ h^{-1} \quad \text{(Eq. 6)}$$

Virtual sensors were defined within the simulated geometry in order to monitor the soil water dynamics from equivalent locations to those where the capacitance-type soil moisture sensors had been installed in the field. Three virtual sensors were defined for

each of the 10 soil locations of interest, one centred at the position of interest and the other two displaced 10 cm closer to and further from the dripper, respectively.

HYDRUS-3D model is characterized by simulating soil water dynamics in a homogeneous soil and root distribution where ideal, symmetric and centred wet bulbs develop around the dripper. However, HYDRUS-3D neither represent heterogeneous soil and root distributions, or macropores and soil irregularities among other phenomena that usually take place in a real soil where wet bulbs are generated.

2.4. Analysis of sensor performance

Sensor performance was analysed using quantitative indicators for several aspects of interest, which were calculated as follows:

- **Repeatability between sensors:** refers to the variability between sensors installed at equivalent depth and position relative to the dripper. They were quantified as the root mean square error (RMSE) between those repetitions, using the dataset composed of the daily values of Plot I and Plot II in 2017 and 2018. In the case of the HYDRUS-3D simulations, the repetitions came from the 3 virtual sensors defined for each of the 10 locations of interest.

- **Sensitivity to the soil water balance:** refers to the dependence of the SWC at a given sensor location on the balance of water inputs/outputs to the soil. This indicator was quantified through a regression that modelled the sensor measurement of any given day as a function of the sensor measurement 7 days earlier, the balance that day and the aggregated balance of the previous 7 days.

$$SWCd_d = Coef_0 \cdot SWCd_{d-7} + Coef_1 \cdot bal_d + Coef_2 \cdot \Sigma bal_{d-7\ldots d} \quad \text{(Eq. 7)}$$

where:

- $SWCd_d$: the driest SWC measured by the sensor on day d, $cm^3\ cm^{-3}$.
- $SWCd_{d-7}$: the driest SWC measured by the sensor 7 days earlier (d-7), $cm^3\ cm^{-3}$.
- bal_d: the balance of water inputs and outputs ($DID_d + PPT_d - ET_d$), mm.
- DID_d: the daily irrigation dose on day d, mm.
- PPT_d: the daily rainfall dose on day d, mm.
- ET_d: the daily irrigation dose on day d, mm.
- $\Sigma bal_{d-7\ldots d}$: the aggregated balance of water inputs and outputs in the previous 7 days ($\Sigma(DID_d + PPT_d - ET_d)$), mm.
- $Coef_0$, $Coef_1$ and $Coef_2$: the regression coefficients.

To focus on water balance variations related with irrigation, the analysis included only days in the irrigation season and excluded rainy days and the day following rain.

This linear regression model was analysed using the Python package statsmodels (Seabold, and Perktold, 2010).

2.5. Statistical calculations.

In order to facilitate their comparison, in this study both the uncertainties in the measurement process and the variability of the measured data were expressed in terms of Root Mean Square Error (RMSE). In accordance with their usage in diverse disciplines (Morgan and Henrion, 1990; Frey and Rubin, 1992; Huijbregts, 1998; Van Belle, 2008), here, uncertainty refers to the degree of precision with which a quantity is measured, while variability refers to the natural variation in some quantity. We use the term variability to refer to the measured data and, also, to refer to the presumed real quantity, since we have no way to distinguish between them.

The coefficient of determination (R^2) and the RMSE which were used for the statistical analysis were calculated as follows.

The R^2 (Eq. 8) value explains how much of the variability of a factor can be caused or explained by its relationship to another factor. It is computed as a value between 0 and 1. Values close to 1 indicate a good agreement of the model.

$$R^2 = \frac{\left[\sum_{i=1}^{N}(O_i - \bar{O})(S_i - \bar{S})\right]^2}{\sum_{i=1}^{N}(O_i - \bar{O})^2 \cdot \sum_{i=1}^{N}(S_i - \bar{S})^2} \quad \text{(Eq. 8)}$$

The RMSE (Eq. 9) measures how much error there is between two data sets. It compares a predicted value and an observed value. Values close to 0 indicate a better fit of the model.

$$RMSE = \sqrt{\frac{\sum_{i=1}^{N}(O_i - S_i)^2}{N}} \quad \text{(Eq. 9)}$$

where N refers to the number of compared values, O_i the *ith* observation point, S_i the *ith* simulation and $\bar{O}$ the observed mean value.

3. Results

3.1. Variability in the soil conditions around a dripper

3.1.1. Centring and extent of the wetted area

The extent of the soil surface wetted by the drippers and the alignment of the centres of these areas with the drippers were studied in order to obtain a clue to the variability in a real orchard of the size, shape and centring of the wet bulbs. The measured SWC transects around drippers, following the dripline and perpendicular to it, are illustrated

in Figure 4. The width of the wetted area following the dripline was 64.5 ± 8.9 cm, which partly overlapped with the area wetted by the neighbouring dripper. In the axis perpendicular to the dripline, the width was 87.6 ± 13.7 cm. The centring of the wet bulb was displaced westwards by 13.6 ± 7.5 cm from the emitter, towards the centre of the tree line.

Compared with this range of variabilities in the wetted area, the separation between sensor positions A-B and A-C was 30 cm. The volume of sensitivity of sensor EC-5 is around 0.3 L, which corresponds, approximately, to a horizontal cylinder of 5 cm diameter and 9 cm length. For sensor 10HS the volume of sensitivity is around 1 L, which corresponds, approximately, to a horizontal cylinder of 9 cm diameter and 21 cm length. These volumes of sensitivity suggest a fine spatial resolution which, for positions B and C, may fall in a soil region with variable inclusion within the wetted area. Based on the measurements of these wetted areas, the RMSE values of the SWC at positions A, B and C were 0.039, 0.075, and 0.095 cm^3 cm^{-3}, respectively.

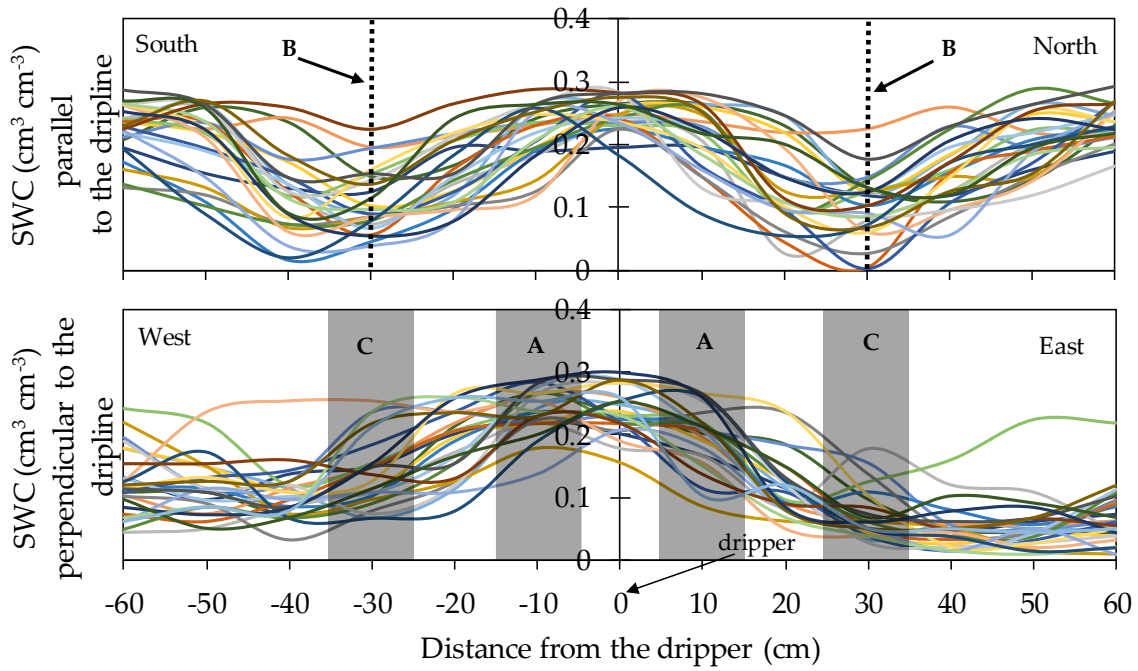

Figure 4. SWC measurements variability parallel and perpendicular to the dripline using the Fieldscout TDR 300. The different colours represent the repetitions.

3.1.2. Pattern of temperature in a soil wet bulb

Soil temperature at the locations where the studied moisture sensors were located varied following both a seasonal pattern and a daily pattern. Soil temperature measurements ended accidentally in early 2016. We considered that the simultaneous recording of soil temperature and soil moisture by EC-5 probes in 2015 was sufficient to assess the magnitude of the effect of temperature on the measurements of soil moisture and that this magnitude was also representative for 2017 and 2018. Over the irrigation

season, the daily mean soil temperature ranged between 19 and 27 °C, with instantaneous maximum and minimum values of 16 and 34 °C respectively. The amplitude of the daily pattern varied with position and depth, with location C15 showing the widest daily amplitude of up to 6 °C (Fig. 5). Weather conditions were observed to affect temperature, with rainfall producing sudden drops in temperature at all positions and depths, of as much as 8 °C, and progressive recovery in the following days.

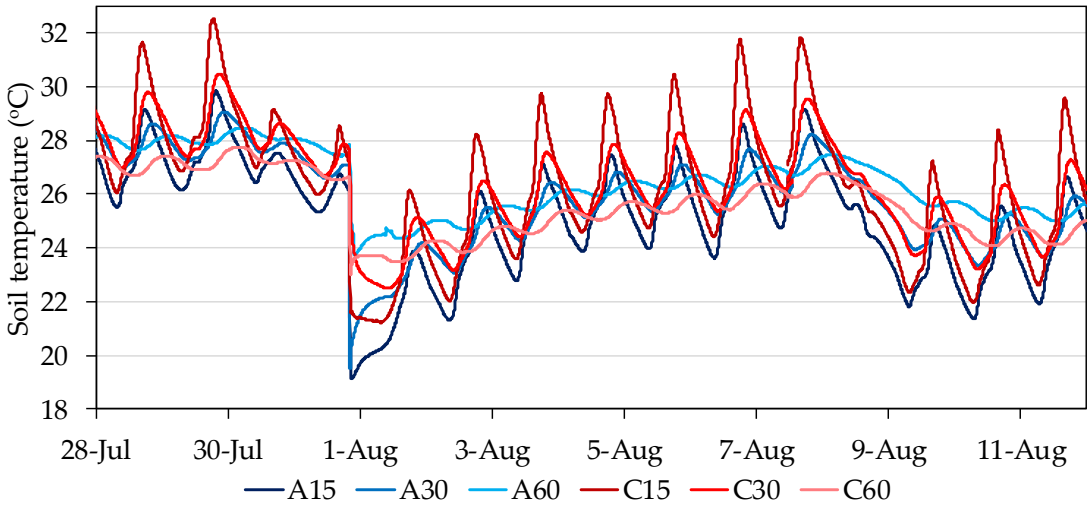

Figure 5. Sample of daily fluctuations in soil temperature at the studied positions and depths in Plot I in July – August 2015.

At the sensor locations with the widest fluctuations in soil temperature, the SWC readings were checked for signs of temperature effects (Fig. 6). EC5 sensors at C15 showed a daily pattern with minimum and maximum values synchronized with minimum and maximum values of soil temperature. The relationship between measurements by those sensors during the night and simultaneous measurements of soil temperature showed a significant slope of up to 0.002 $cm^3\ cm^{-3}$ per °C. On the other hand, measurements by 10HS sensors did not show such clear signs of being influenced by temperature, though some of the sensors recorded a nocturnal decrease in SWC, parallel to the decrease in soil temperature, with a slope that in all cases was lower than 0.001 $cm^3\ cm^{-3}$ per °C. Considering a range of fluctuation in soil temperature of up to 8 °C, caused either by weather or the diurnal cycle, a high estimate of its potential impact on SWC measurements would be a deviation smaller than 0.016 and 0.008 $cm^3\ cm^{-3}$ for EC5 and 10HS, respectively. This high estimate would correspond to position C15, with lower potential impacts in other sensor locations.

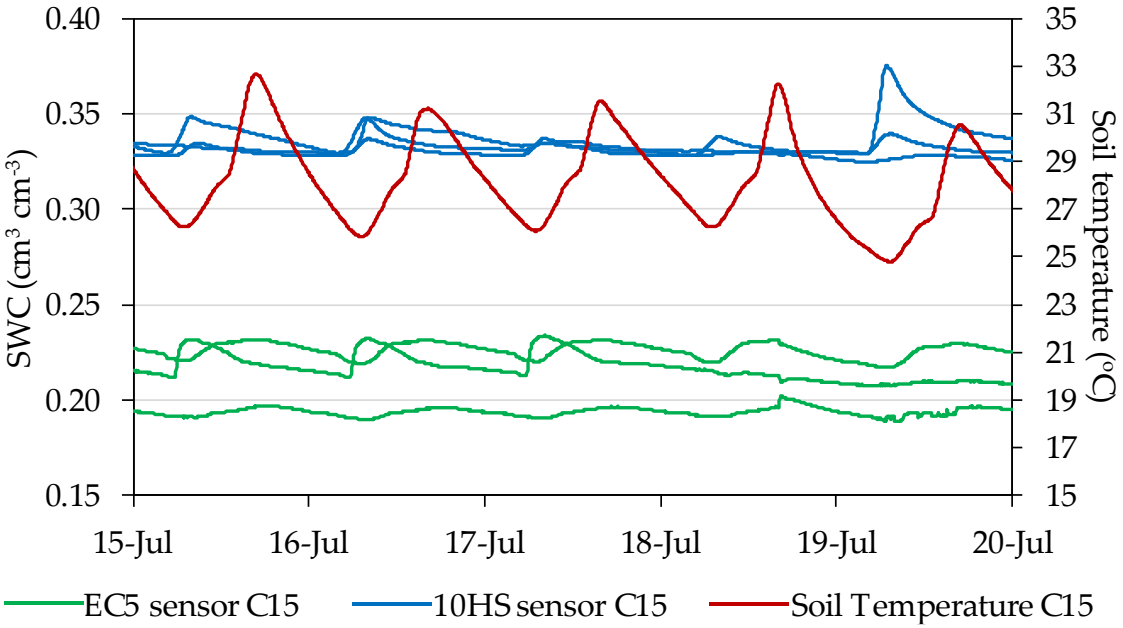

Figure 6. Comparison of daily fluctuations in soil temperature and SWC at position C, 15 cm depth in Plot I in July 2015.

3.2. Overall response of the sensors

The SWC data were recorded from 57 moisture sensors deployed in two plots during 20 consecutive months in 2017 and 2018. After this period, the sensors were recovered and characterized in the laboratory (Domínguez-Niño et al, 2019). Different patterns of sensor response were observed, both over the course of a day and at a seasonal scale, among the depth and positions where the sensors were located. Generally, over the course of a day (Fig. 7), in position A for each of the depths, the sensors were the most sensitive to irrigation and responded quickly to the irrigation cycles as well as to the lack of irrigation. In this location, the sensors showed high sensor-to-sensor differences and a wide daily amplitude of SWC between the minimum before irrigation and the maximum following irrigation. In position B, the sensors followed a similar pattern to that of position A, but their response to irrigation was more delayed in time. The sensors installed in this position tended to show a smaller amplitude between SWC before and after irrigation, especially at the depth of 60 cm. In position C, some of the installed sensors followed a seasonal pattern with only a faint effect of the irrigation cycles. In position D, the sensors followed a seasonal pattern related with occasional rains and overall drying in the periods of high ET_o, with no perceptible effects of the irrigation cycles.

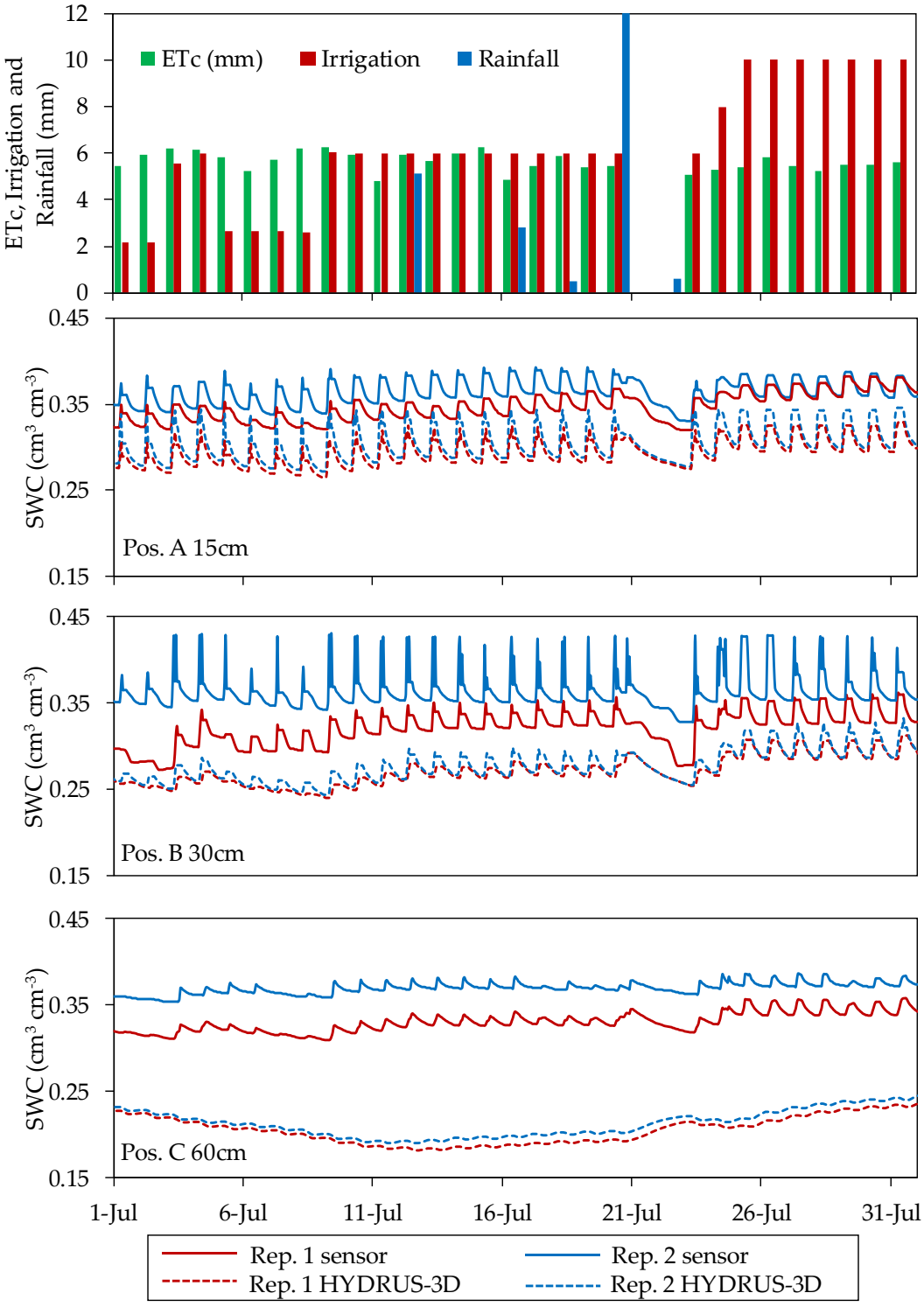

Figure 7. Example of daily behaviour of humidity sensors located in position A at the depth of 15 cm, B at the depth of 30 cm, and C at the depth of 60 cm in Plot II in July 2018.

The amplitude of the daily oscillation of SWC between its minimum before an irrigation cycle and its maximum after an irrigation cycle was calculated both in capacitance sensors and in HYDRUS-3D during and outside the irrigation season (Fig. 8).

According to the results, during the irrigation season the capacitance sensors at soil location A15 showed a wide oscillation during the irrigation cycle, with a median of 0.027 cm^3 cm^{-3} and an 80^{th} percentile as high as 0.069 cm^3 cm^{-3}. These amplitudes were approximately halved at A30, B15 and B30 and were much further reduced at 60 cm depth. In position C, the median amplitude was in the order of 0.004 cm^3 cm^{-3} or smaller but with a large variability, as shown by an 80^{th} percentile of up to 0.029 cm^3 cm^{-3} in C30. All amplitudes were much smaller outside the irrigation season, with all medians below 0.003 cm^3 cm^{-3} and the 80^{th} percentiles at 0.01 cm^3 cm^{-3} or smaller.

For their part, the HYDRUS-3D simulations showed in Figure 8 a similar order of amplitude to that of the sensors for locations A30, A60, B30. However, the median amplitude at A15 simulated by HYDRUS-3D was only 0.0089 cm^3 cm^{-3}, one third of that observed by sensors, and also with less variability, with an 80^{th} percentile of 0.0143 cm^3 cm^{-3}. The wider oscillation with sensors at A15 consisted of a more intense drop of SWC before irrigation compared with simulation. At this position, after irrigation and redistribution, the simulation measurements tended to decrease less with water uptake by roots. At C15 and C30, the median amplitude simulated by HYDRUS-3D was three times higher than that observed by the sensors, but with less variability. Overall, at C positions most sensors only showed a faint oscillation with irrigation cycles, whereas the oscillations produced by irrigation were clearer and more intense in the simulations. Hence, the soil water dynamics reproduced in the HYDRUS-3D simulations may explain the patterns of daily amplitude observed in sensors at A30, A60 and B30, but do not explain either the large amplitude observed at A15 or the much more attenuated C position amplitudes. In this respect, it seems that the simulations considered a more even distribution of soil water and also of water uptake by roots among the different positions. Compared to the sensors, the simulations were less variable, underestimated uptake at A15, and overestimated the influx of irrigation water at positions C.

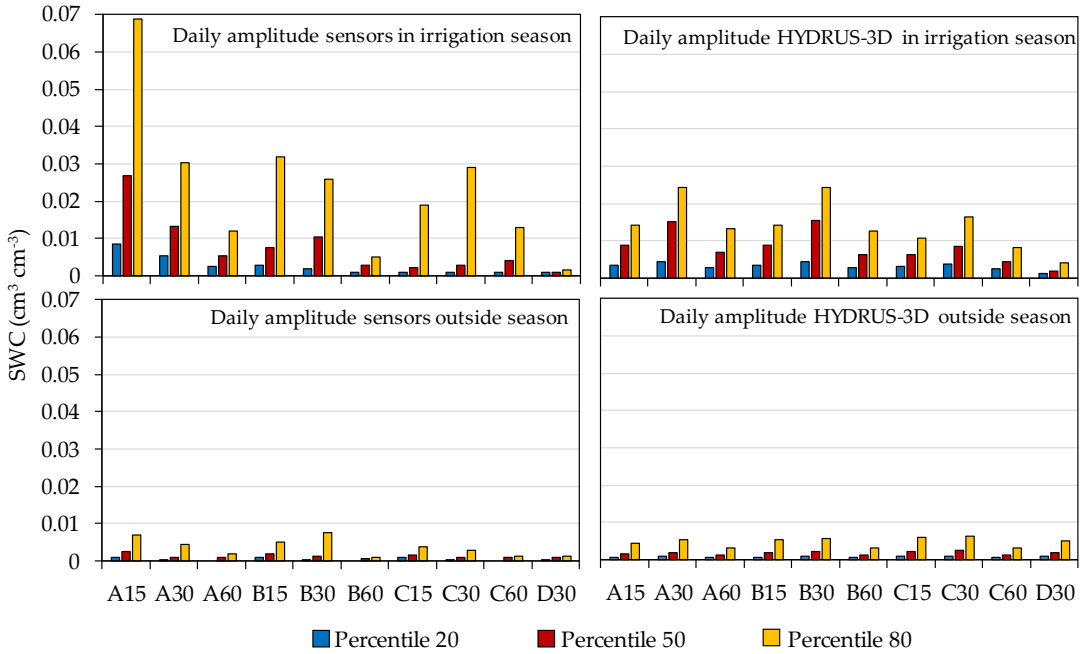

Figure 8. Daily amplitude of the measured and simulated soil water contents at different position and depth.

The timing of irrigation affected the SWC pattern over the course of a day. Figure 9 illustrates the dynamics of SWC when irrigation was in the morning, split between morning and afternoon, and in the afternoon, showing the sensor-recorded data at different locations in the soil together with the corresponding HYDRUS-3D simulation in the 2017 season. At position A15, irrigation in the morning produced a steep drop of SWC shortly after irrigation, with SWC during the night at the lower end of the daily range. At the other extreme, irrigation in the afternoon resulted in an attenuated drop after irrigation, with SWC remaining high, near field capacity, overnight, and dropping the following day before irrigation. With irrigation split in two pulses per day, SWC remained high for a longer period per day and, in this particular case, dropped to its daily minimum before the second pulse. The effect of the timing of irrigation on the SWC value at night justifies usage of the minimum daily SWC as a summary of the daily cycle, rather than the average daily SWC which would be much more affected by the timing of irrigation. The daily patterns described by the HYDRUS-3D simulations agreed with those described by the sensors at A15 in the rise of SWC during irrigation but differed in that, following irrigation, the relaxation of SWC was smoother and without a clear drop at the hours of higher ET. The patterns at other sensor locations in the soil were more attenuated both when measured by sensors and when simulated.

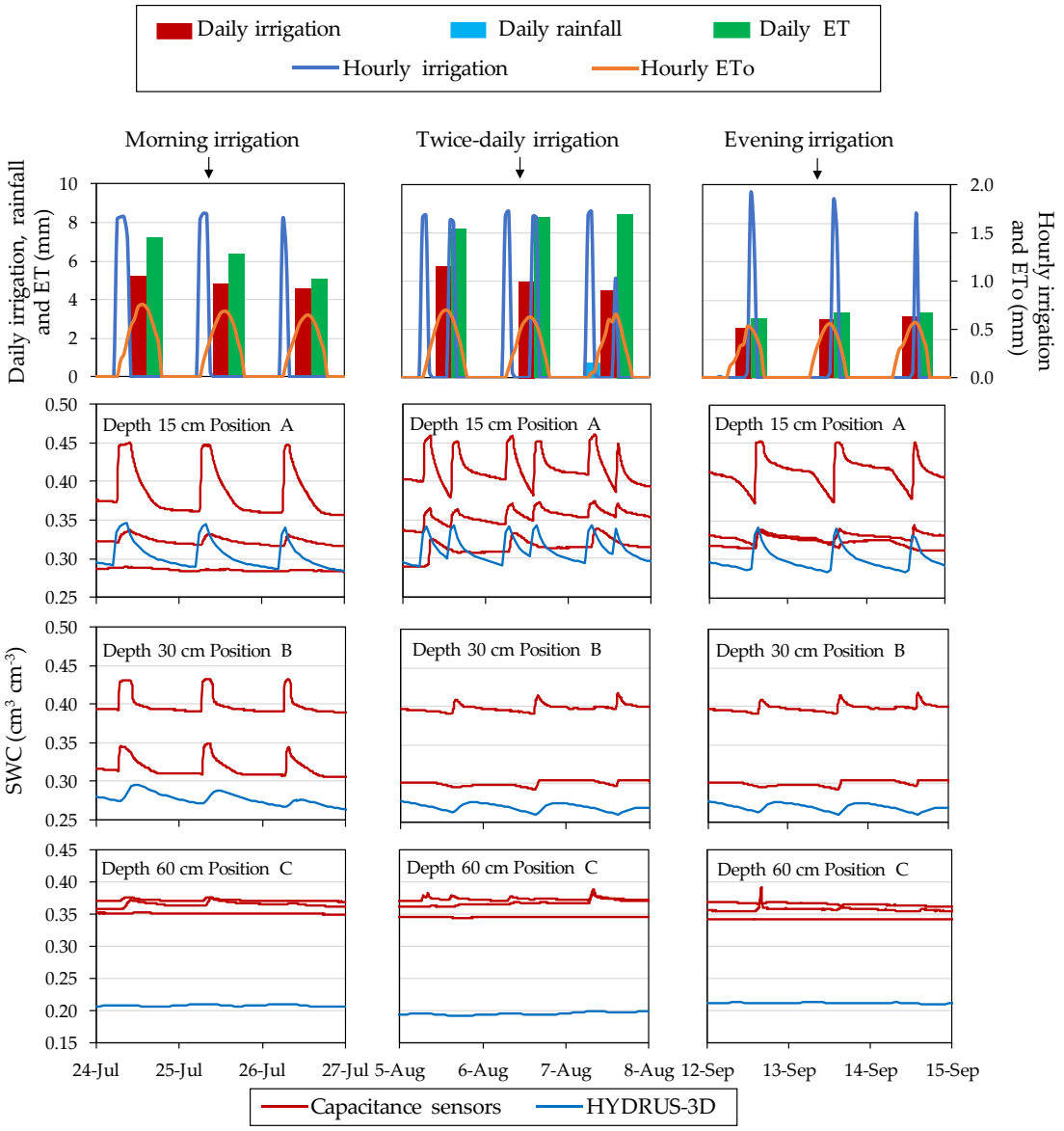

Figure 9. Relationship between the daily shape of the SWC curve and the moment of the day of irrigation in Plot II in 2017. In red are represented sensor moisture repetitions and in blue is represented the model.

3.3. Variability between sensors at seasonal scale

3.3.1. Repeatability between sensors

Sensors installed at the same depth and position relative to the dripper tended to show synchronized patterns in terms of their response to irrigation cycles. However, the series of SWC measurements tended to fluctuate within a particular range for each individual sensor. In order to quantify sensor-to-sensor differences, we calculated the RMSE between measurements taken at the same time by sensors installed in equivalent locations with respect to depth and position relative to the dripper. This indicator was calculated from the daily values t including both plots and both irrigation seasons -i.e. excluding the periods of the year without irrigation-. The results are shown in Figure 10, together with the equivalent indicators calculated from the HYDRUS-3D simulations. Overall, sensor-to-sensor repeatability depended on the location where the sensors were

installed, ranging between 0.020 cm^3 cm^{-3} and 0.050 cm^3 cm^{-3}. In general, the closer to the dripper, either in position or in depth, the higher the RMSE. Sensors located in position A had the lowest repeatability, in particular at the depth of 15 cm (0.050 cm^3 cm^{-3}), while repeatability improved at the depth of 60 cm (0.035 cm^3 cm^{-3}). Sensors located in position B showed greater repeatability than sensors located in position A. In particular, the depths of 15 cm and 30 cm showed greater repeatability (0.027 cm^3 cm^{-3} and 0.037 cm^3 cm^{-3}) than the depth of 60 cm (0.022 cm^3 cm^{-3}). In position C, sensors located at the depth of 15 cm had lower repeatability (0.047 cm^3 cm^{-3}) than the rest of the depths, while the sensors located at the depths of 30 and 60 cm showed greater repeatability than sensors located at the depth of 15 cm (0.024 cm^3 cm^{-3} and 0.021 cm^3 cm^{-3}, respectively).

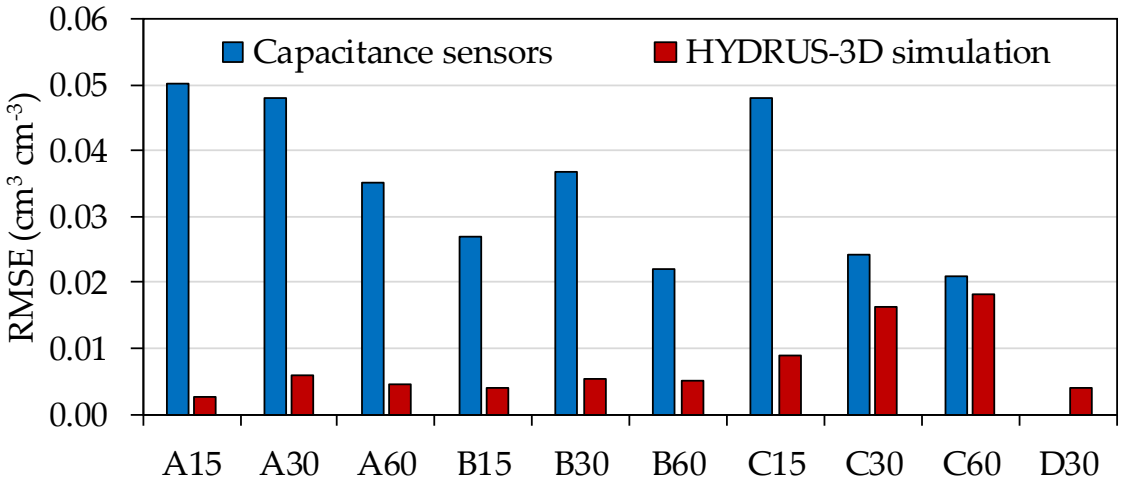

Figure 10. Sensor-to-sensor differences in SWC measured by capacitance sensors and by HYDRUS-3D simulations at the same soil positions +- 10 cm in the direction to the dripper.

In contrast with sensors, the RMSE between simulations where the horizontal position of the virtual sensor was displaced 10 cm to either side, was always below 0.020 cm^3 cm^{-3} in all locations and below 0.006 cm^3 cm^{-3} in A and B positions at all depths. This would suggest that variability in the alignment between wet bulb and dripper, alone, cannot explain the observed variability between sensors. In addition, in position C, the simulated RMSE results for the depths of 30 and 60 cm were close to the RMSE of the sensors, with values of 0.016 cm^3 cm^{-3} and 0.018 cm^3 cm^{-3}, respectively.

3.4. Seasonal pattern at each sensor location in soil

Over the course of the two monitored irrigation seasons, the data recorded by the capacitance soil moisture sensors displayed different seasonal patterns of response to irrigation depending on the location of the sensor in the soil. Figures 11 and 12 show the seasonal soil water dynamics at the different sensor locations measured with capacitance sensors and simulated HYDRUS-3D model, irrigation, rainfall and ET measured by the weighing lysimeter in the years 2017 and 2018. The observed seasonal patterns differed between the two monitored plots. In general, although more evident in Plot I, sensor data from different positions and depths tended to be closer after rain and in periods of

over-irrigation and more separated in periods with drier conditions. In periods of higher water deficit, variability between sensor locations increased. In Plot I under this situation, both the HYDRUS-3D and neutron probe SWC measurements were higher than those from the capacitance sensors.

During the irrigation season, irrigation cycles affected capacitance sensor measurements in differing ways depending on sensor location. Compared with measurements by neutron probe, EC5 sensor measurements in Plot I underestimated SWC in all positions and depths. Despite this bias, irrigation cycles as well as the lack of irrigation produced an immediate response in sensor measurements, especially in positions A. In contrast, in the other positions the SWC decreased more slightly over time. At the depth of 30 cm, the seasonal variability was less pronounced. The positions closest to the dripper (position A) tended to respond quickly to irrigation cycles, evapotranspiration and consumption by the crop on the same day. The response at positions B and C tended to be slower and more progressive. At the depth of 60 cm, especially in positions away from the dripper, the sensors recorded less variation in response to the irrigation cycles. In position D, the sensors showed a slowly varying trend throughout the season, except for some peaks associated with rainfall.

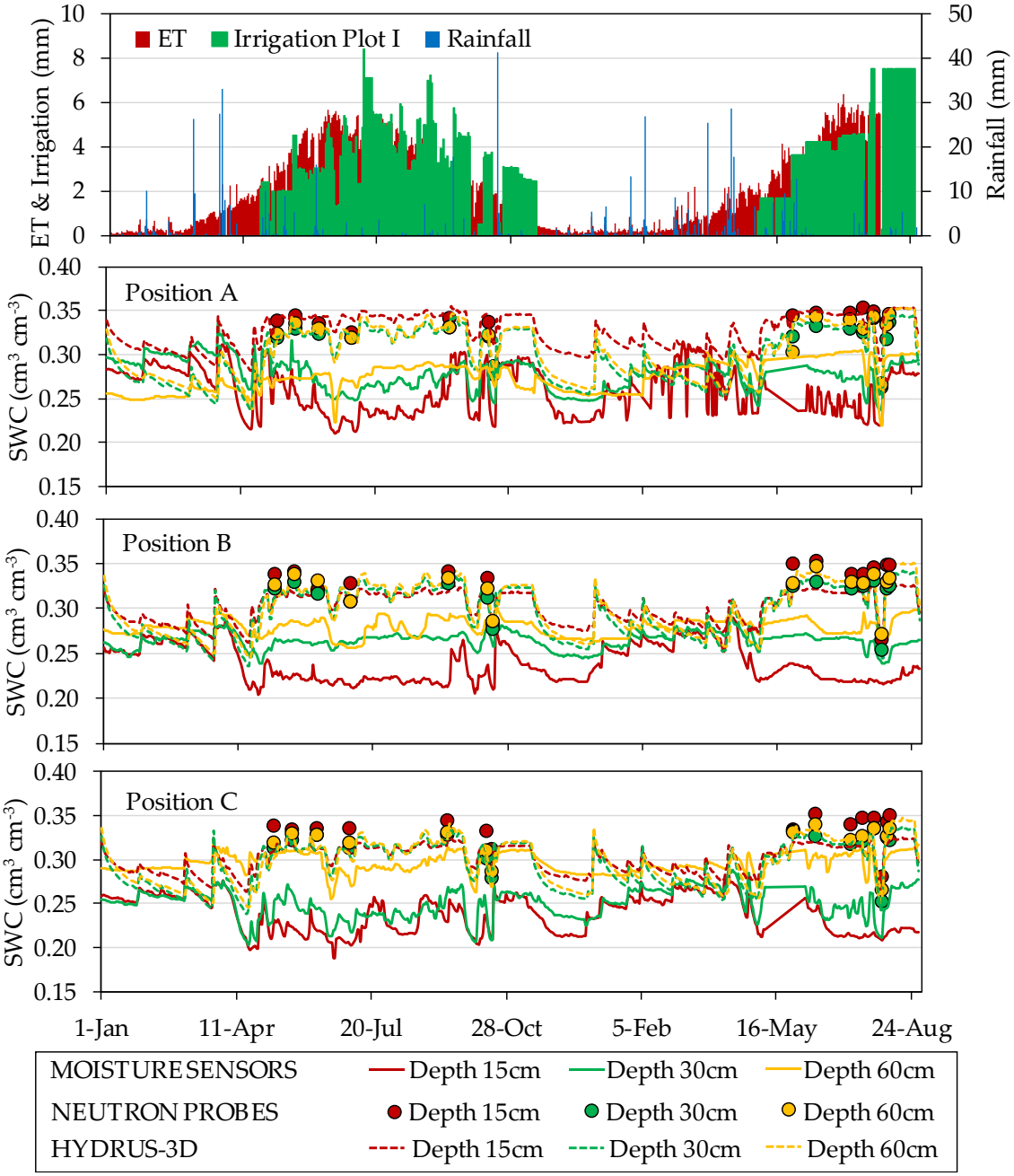

Figure 11. Seasonal variations in soil water content (represented by the series of daily minimum values, $cm^3\ cm^{-3}$) measured by EC-5 capacitance soil moisture sensors, neutron probes and HYDRUS-3D simulations in different positions and depths in the years 2017 and 2018 in Plot I. Irrigation, rainfall and ET measured by the weighing lysimeter is detailed at the top of the figure.

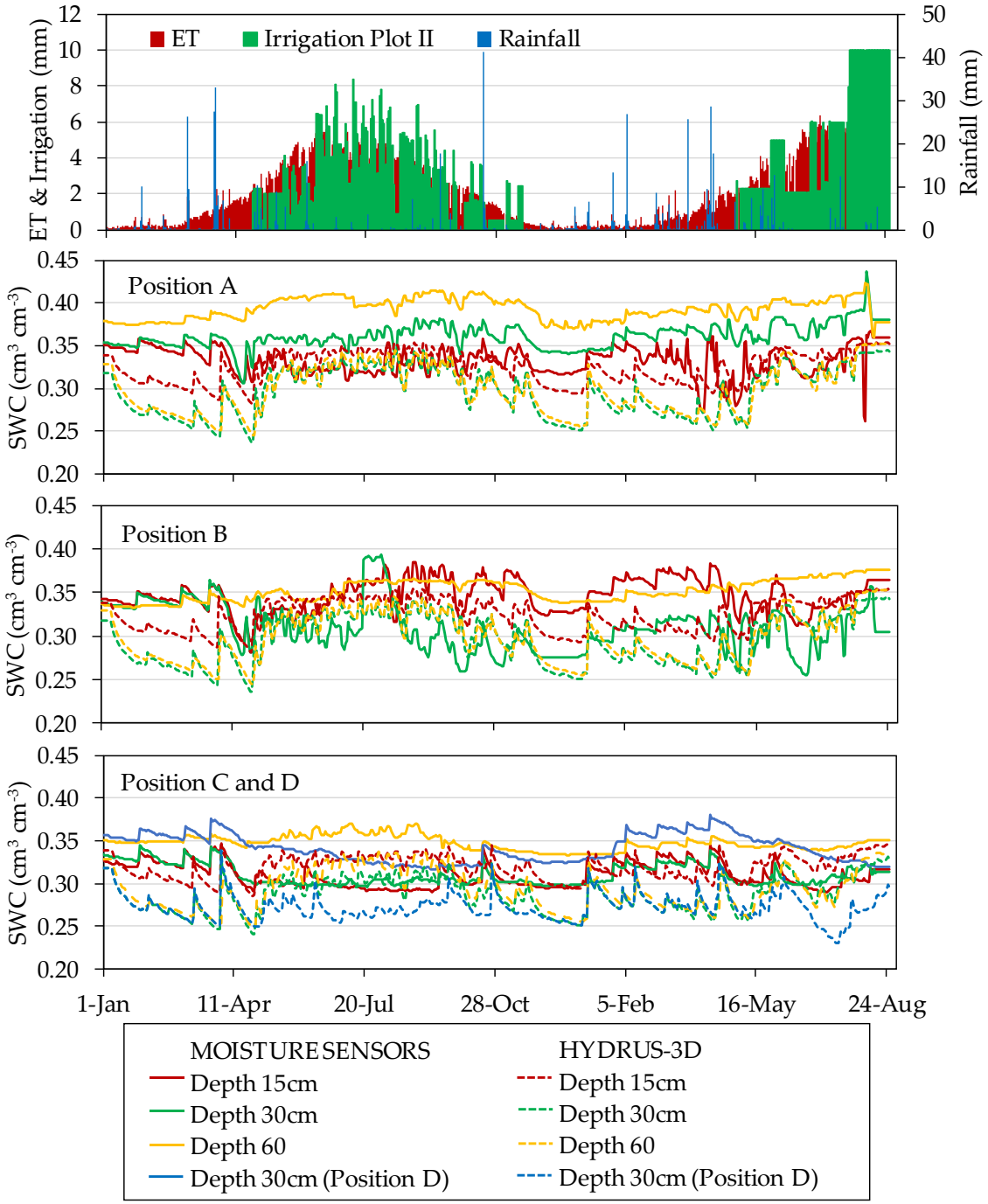

Figure 12. Seasonal soil water content ($cm^3\ cm^{-3}$) measured by 10HS moisture sensors and HYDRUS-3D simulations in different positions and depths in the years 2017 and 2018 in Plot II. Irrigation, rainfall and ET measured by the weighing lysimeter is detailed at the top of the figure.

3.5 Comparisons between capacitance sensor measurements and HYDRUS-3D simulations.

All the results reported thus far correspond to the use of capacitance-type sensors with their factory calibration for mineral soils, which is their most expected usage in commercial farms. In order to determine whether the results would improve with a calibration specific for the soil at that orchard, a previously developed two-steps

calibration (Domínguez-Niño et al., 2019) was performed. Overall, the R^2 varied between sensor positions and depths regardless of the calibration used. In general, higher R^2 were observed in the sensor locations that were deepest and farthest from the dripper. In general, the RMSE between measurements by capacitance sensors and neutron probe decreased with the two-step calibration, except for the depth of 15 cm, where it increased.

Figure 13 shows the effect of calibration on the fit between measurements by 10HS sensors and simulations by HYDRUS-3D. The data shown corresponds to one measurement every 15 days for the whole studied period -both in and out of season- during 2017 and 2018. In general, with factory calibration the sensor-measured SWC was smaller than that of the simulations, except in the case of a few A, B and C positions at the depth of 15-30 cm. Overall, application of the soil-specific calibration did not reduce the scatter of the sensor measurements but did improve the adjustment of the whole cloud of sensor measurements to that of the simulations.

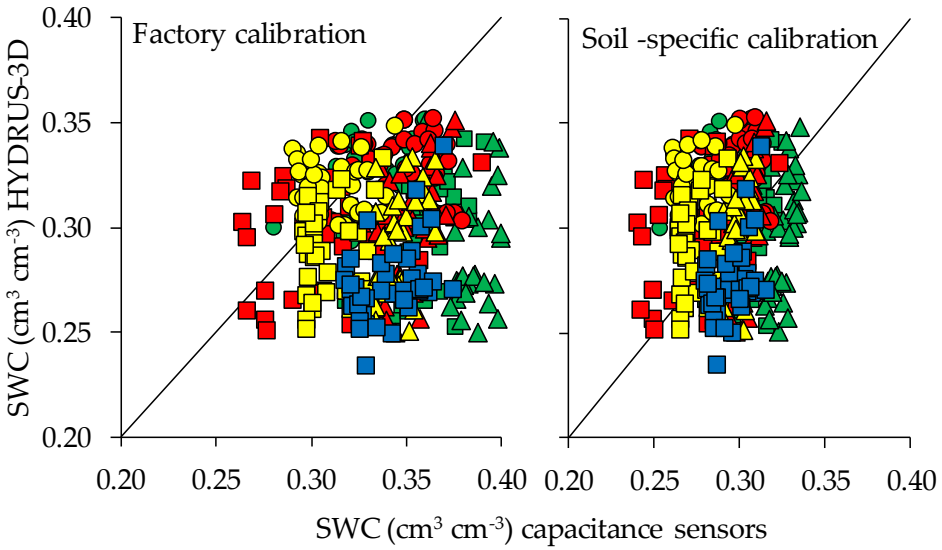

Figure 13. Fit between soil water content (SWC) measured by capacitance sensors and estimates by HYDRUS-3D, comparing factory calibration of the sensors with soil-specific calibration. Data includes one measurement every 15 days during the whole studied period. Colours indicate sensor position relative to dripper (green = A, red = B, yellow = C, blue = D) and shapes indicate depths (◯ = 15cm, □= 30cm, Δ = 60cm).

3.6. Sensor sensitivity at each location to fluctuations in the balance of water inputs/outputs

A feature of special interest when comparing different sensor locations is how sensitive each location is to the balance between water inputs/outputs to the soil. This information can be used to highlight candidate sensor positions to monitor the fit between irrigation dosage and crop water requirements. In addition, visual interpretation of the sensors can indicate which locations may respond swiftly to the latest irrigation cycle and which may respond more progressively to the outcome of a period including several irrigation cycles.

The dependence of sensor-measured SWC on the balance of water input/outputs is summarized in Table 3. The analysis consisted of checking how the SWC measured on a given day could be modelled as a function of the SWC measured a week earlier, the water balance of that day and the aggregated water balance of the previous week. The results show that this dependence varies according to the position and depth where the sensor is located. In all cases, the independent variable with the strongest effect was the measurement one week earlier, which highlights the relevance of the trends rather than the absolute values in the interpretation of SWC. As shown in the table, the response at positions A depended on the SWC measured the previous week and the water balance of the same day, especially at the depths of 15 cm and 30 cm. In this respect, sensors in position A responded as if they had no memory of the balance of the previous week. Meanwhile, the B positions depended on the SWC measured the previous week, the water balance of the same day (especially at depth of 30 cm) and the water balance of the whole week (especially at 30 cm). The C positions depended on the SWC measured the previous week, the water balance of the same day (in particular at the depths of 30 cm and 60 cm) and the water balance of the whole week (especially at depths of 15 cm). The D positions depended on the SWC measured the previous week, the water balance of the same day and especially the water balance of the whole week.

Table 3. Summary of dependence of soil water content (SWC) measured by sensors on the measurement of a week before (coef_SWC$_7$), the water input/output balance of the day (coef_bal) and on the water input/output balance of the whole previous week (coef_bal$_7$). N corresponds to the number of SWC measurements.

Position	depth (cm)	N	R^2_adj	coef_SWC$_7$		coef_bal		coef_bal$_7$	
A	15	514	0.994	1.0021	***	0.0036	***	0.0007	n.s
A	30	514	0.998	0.9968	***	0.0025	***	0.0000	n.s
A	60	514	0.999	0.9971	***	0.0009	**	0.0003	n.s
B	15	514	0.997	0.9876	***	0.0016	***	0.0021	***
B	30	514	0.982	0.9630	***	0.0039	***	0.0034	***
B	60	514	1.000	0.9973	***	0.0004	*	0.0013	***
C	15	514	0.998	0.9808	***	-0.0002	n.s	0.0034	***
C	30	514	0.998	0.9892	***	0.0018	***	0.0014	***
C	60	514	0.999	0.9963	***	0.0013	***	0.0009	**
D	30	260	1.000	0.9927	***	-0.0005	**	0.0013	***

n.s, *, **, *** are statistically non-significant, and statistically significant at P<0.05, 0.01 or 0.001, respectively.

Figure 14 illustrates an example of the distinct type of response to the soil water balance at different sensor locations. In this example, during several days in June 2018, in Plot II, the applied irrigation doses were reduced for experimental purposes. Measurements of SWC by capacitance sensors in the following days at locations A15, A30, B15 and B30 all revealed the occurrence of an irrigation deficit and, later on, the recovery of the soil moisture when irrigation doses were increased again. However, the

recovery of SWC at position A when irrigation doses were increased again may take place almost the same day (for instance sensor A30 in this example), as if the sensor had no memory of the preceding period of deficit. On the other hand, sensors at position B tended to have a longer period of response, thus aggregating the outcome of several irrigation cycles. Sensors at positions C and D were also affected by the deficit but took a much longer period to recover. Meanwhile, sensors at 60 cm depth showed a much fainter response to these changes in irrigation.

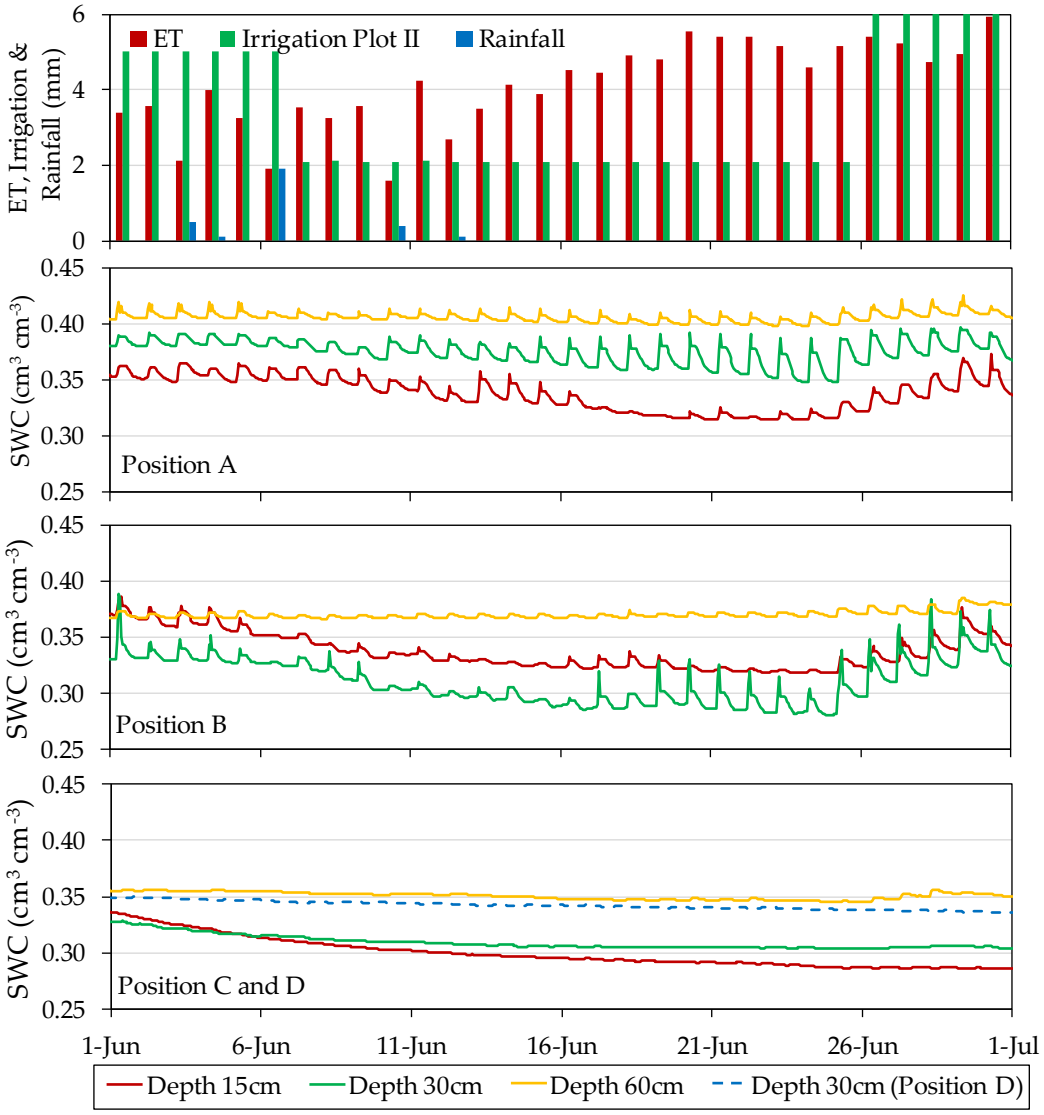

Figure 14. Moisture sensor sensitivity to irrigation in Plot II in June 2018. Sample of different types of sensor responses to the soil water balance, corresponding to different sensor locations in Plot II in June 2018.

The analysis of sensitivity of different sensor locations to the soil water balance was also performed with the HYDRUS-3D simulations and the results are summarized in Table 4. In the case of simulations, the SWC at all depths and positions depended on the SWC measured in the previous week and the water balance of that day (especially at the depth of 30 cm). Also, in positions A and B at the depth of 60 cm, there was a highly

significant dependence of the SWC on the water balance of previous week. Interestingly, at sensor locations A15, A30, B15 and B30 the balance of the previous week was not significant, thus suggesting that the lack of memory of the preceding period is a sound and repetitive feature at these locations, well represented in the soil water dynamics by HYDRUS-3D.

Table 4. Summary of dependence of soil water content (SWC) simulated by HYDRUS-3D on the simulation of a week before (coef_SWC$_7$), the water input/output balance of the day (coef_bal) and on the water input/output balance of the whole previous week (coef_bal$_7$). N corresponds to the number of SWC measurements.

Position	depth (cm)	N	R^2_adj	coef_SWC$_7$		coef_bal		coef_bal$_7$	
A	15	514	0.999	0.9979	***	0.0020	***	0.0004	n.s
A	30	514	0.996	0.9963	***	0.0032	***	0.0006	n.s
A	60	514	0.997	0.9934	***	0.0023	***	0.0019	***
B	15	514	0.999	0.9974	***	0.0021	***	0.0003	n.s
B	30	514	0.996	0.9951	***	0.0031	***	0.0007	n.s
B	60	514	0.997	0.9929	***	0.0022	***	0.0021	***
C	15	514	0.999	0.9936	***	0.0017	***	0.0010	***
C	30	514	0.997	0.9892	***	0.0024	***	0.0019	***
C	60	514	0.998	0.9893	***	0.0016	***	0.0030	***
D	30	260	0.999	0.9756	***	-0.0007	***	0.0051	***

n.s, *, **, *** are statistically non-significant, and statistically significant at a P<0.05, 0.01 or 0.001, respectively.

3.7. Components of the variability in the measurements by capacitive-type soil sensors

Regarding the performance of sensors in real orchard conditions, an issue of interest in this study was to compare the uncertainties in the measuring process with the observed variability in sensor data and with the natural variability in the soil environment. To this end, all them were expressed in the same terms, as RMSE. When comparing the output of several soil sensors, the observed differences between sensors can be caused by a combination of uncertainties in the measuring process and actual variability in the physical property being measured. In this study, the distinction between uncertainty in the process and variability in the data can offer clues in terms of directions for improvement in the usage of the sensors. However, in a practical application there may be no need to distinguish between them (Hofer, 1996) and the whole ensemble would contribute to the overall uncertainty of monitoring SWC in a drip-irrigated orchard. That is to say, when using a setup of several sensors, each of them reporting a different value of SWC, usage of these data for decision-making is faced with the uncertainty resulting from the combination of the measuring process and the natural variability in the actual values. The preceding sections described the observed variability in sensor measurements at different locations in the soil around a dripper. In order to better appraise its significance and gain clues as to its possible origin, the observed

variability can be compared with the uncertainties in different factors affecting the process of measuring SWC by capacitive-type sensors (Fig. 15).

First, the accuracy of SWC measurement by capacitive-type sensors can be decomposed into two steps (Robinson et al., 1998; Jones et al., 2005). The first step converts the sensor response to permittivity, regardless of the media- where it has been measured. The second step converts permittivity to SWC for a specific soil. The 10HS sensors used were, at the end of the study, calibrated specifically for the soil of the orchard (Domínguez-Niño et al., 2019). Comparing the output of the different options for sensor calibrations, the range of uncertainty[3] for the first and second steps, expressed as RMSE, were of 0.006 cm^3 cm^{-3} and 0.014 cm^3 cm^{-}, respectively. Here, the first step includes the variability between individual sensors and the second step the specific relationship between permittivity and SWC for that soil. In addition, soil temperature varies with depth and with position relative to tree shade and fluctuates over the course of a day, with potential effects on 10HS sensor measurements which we estimated as an uncertainty up to 0.008 cm^3 cm^{-3}.

Virtual sensors that monitored HYDRUS-3D simulations at the sensor locations +-10 cm in the direction to the dripper showed sensor-to-sensor differences of between 0.003 cm^3 cm^{-3} and 0.018 cm^3 cm^{-3}, depending on sensor location. In contrast, in this study, the observed differences between capacitive-type sensors in real drip-irrigated orchard conditions ranged between 0.021 cm^3 cm^{-3} and 0.050 cm^3 cm^{-3}, depending on sensor location. In addition, the range of uncertainty between positions A, B and C showed a range of differences between 0.048 cm^3 cm^{-3} and 0.091 cm^3 cm^{-3}.

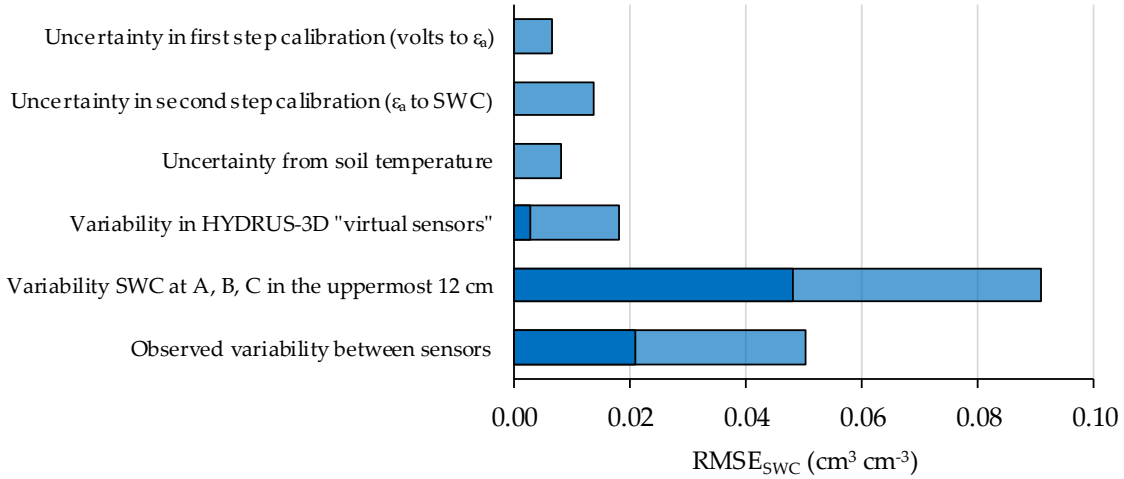

Figure 15. Ranges of uncertainty and variability in the measurement of soil water content (SWC) by capacitance sensors. Dark blue indicates least variability and light blue indicates maximum variability/uncertainty

This comparative range of variability suggests the possibility of ranking the factors to consider for optimizing the monitoring of soil moisture with capacitive-type sensors in a drip-irrigated orchard. In particular, it highlights the uncertainty derived from the arbitrary movement of water at the soil surface, between the dripper and the entrance

into the soil. In contrast, there seems to be little margin of improvement in direct sensor response, as two-step calibration improves measurement accuracy but is minimal compared to other sources of uncertainty unless it manages to integrate a much larger soil volume.

4. Discussion

4.1. Variability in the soil conditions

The performance of capacitance moisture sensors (EC-5 and 10HS) installed at different depths and positions relative to the dripper were evaluated for two years. In addition, it was evaluated the particular conditions of disturbance and the natural variability of soil water patterns in drip irrigation. In this type of scenario, the actual environment around a sensor can vary considerably, combining modellable and capricious patterns, and might, at least partly, cause the observed variability in sensor measurements. To some degree, sensor-to-sensor differences can be expected, given the small volume of influence of capacitance sensors and the highly heterogenous patterns of SWC expected in their vicinity. Virtual sensors were configured in the HYDRUS-3D model to monitor the simulated SWC at the locations where the real sensors were installed and, to check sensitivity to the precise position of the sensor, additional virtual sensors were displaced 10 cm from their original position in either direction relative to the dripper. Overall, the virtual sensors were much more repetitive and with slighter differences between soil locations compared to the real sensors. Our characterization of the soil area wetted by the drippers show that the size, shape and alignment of these areas have a large natural variability. Even at locations close to the vertical of the dripper (position A), measurements of SWC in the uppermost 12 cm show a large variability which suggests that the wet bulb is not always centred there. For locations presumably closer to the border of the wet bulb (positions B and C), SWC variability in the uppermost 12 cm was still larger. These measurements of the wetted area, close to the wet surface, are not a direct measurement of the wet bulb, which develops deeper. However, the observed variability in the wetted area may be indicative of the variability of the wet bulb, though as observed with sensors, up to a point, variability tends to diminish with depth.

Soil temperature in the wet bulb is also heterogeneous. First, it depends on depth, with shallower locations showing wider diurnal variations, with an amplitude in summer of up to 8 °C at 15 cm depth and 1 °C at 60 cm depth. Second, in our measurements it varied with the position relative to the dripper, with diurnal variation increasing with the distance from the dripline. This may be attributable to differences in shade (Aguiar et al., 2019). Differences in soil moisture might also imply thermal differences, either through soil evaporation or through the thermal conductivity of the soil, which is dependent on soil moisture (Evett et al., 2012). In our results, EC5 sensors showed clear signs of being affected by temperature, with a potential disturbance up to

+-0.02 cm^3 cm^{-3}. The effect of temperature on EC5 sensors has been described by other authors (Rosenbaum et al., 2011). There was less clear evidence of 10HS sensors being affected by temperature, though this cannot be discarded since temperature effects have been observed by other authors (Mittelbach et al., 2012). The dynamic behaviour of the two variables, soil temperature and SWC, in the context of a drip-irrigated orchard where they vary diurnally and in space within the dripper frame, can disguise their relationship. Laboratory characterization of 10HS sensors by other authors has shown that temperature effects depend on soil texture, with an increase of the measured SWC with temperature in soils with fine texture (Kargas and Soulis, 2012). Given the observed range of variability in soil temperature (between 1 and 25 °C through the year), the potential effect of soil temperature on the measurement of SWC at an annual scale can be as high as 0.028 cm^3 cm^{-3} comparing different extreme conditions through the year. Also, in other moisture capacitance sensors such as the SMT100 model, it has been reported that temperature has a significant influence on sensor output (Bogena et al., 2017). As stated above, this effect would be higher at shallow and sunlit positions and lower at deeper and shaded positions.

Regarding the diurnal pattern of SWC, we observed the widest amplitude at position A15, near the area where irrigation water enters the soil. The diurnal amplitude displayed by sensors at this soil location is much wider and more variable than expected according to HYDRUS simulations (Fig. 7). This difference might be attributable to the more idealized and smooth conditions at the soil surface represented in the simulations. In real orchard conditions, the soil surface presents an arbitrary microrelief which determines preferential pathways at the soil surface to water from the dripper and may produce arbitrary patches of waterlogged soil during irrigation (De Lima and Abrantes, 2014). This coexists with patches of differently shaded/sunlit soil spots, which in turn may determine heterogeneous patterns of evaporation at the soil surface. All this would determine a more arbitrary and sharply defined soil condition scenario compared with that represented in the simulations. Even so, the simulations coincided with sensors in terms of the ranges of diurnal amplitude at 30 cm depth in positions A and B, a region in the soil which is at the core of the daily cycles of hydration and water uptake by roots. The simulations also estimated a greater amplitude than observed by sensors at 60 cm depth, where they might overestimate root water uptake compared with sensor measurements, and at position C, where they might overestimate the arrival of water from the irrigation pulses. The range of diurnal fluctuations is much smaller offseason, where, except for rain events, the magnitude of the common water inputs and outputs to the soil are much smaller and, additionally, the wet bulbs disappear.

As expected, the patterns of diurnal fluctuation in SWC were affected by the timing of irrigation, particularly in relation to the daily curve of ET. Irrigation in the early morning produces steeper changes as the result of saturation during irrigation followed by redistribution and immediate uptake by roots. In contrast, when irrigation is in the afternoon, SWC remains high at night and drops the following day. Irrigation split into

two pulses, one in the morning and the other in the afternoon produces a less severe pattern for a longer period of time. Given the effect of the timing of irrigation on SWC at night and this, in turn, on the daily average, the driest daily measurement appears as a practical and robust summary of the preceding cycle of irrigation, redistribution and uptake by roots.

4.2. Repeatability between sensors

The characterization of capacitance-type soil moisture sensors in laboratory conditions has produced highly repetitive readings among sensors (Rosenbaum et al., 2010; Domínguez-Niño et al., 2019). Nevertheless, in field conditions, large differences in sensor measurements have been reported by many authors (Schmitz and Sourell, 2000; Kizito et al., 2008; Sakaki et al., 2008; Bogena et al., 2010; Nagahage et al., 2019). Our results show a large sensor-to-sensor differences, even though repeated sensors were installed precisely at the same soil locations in terms of depth and position relative to the dripper. We quantified these differences as RMSE and observed that it depended on sensor location. Broadly speaking, the RMSE between equivalent sensors seems to vary with depth, from 0.05 $cm^3\ cm^{-3}$ at 15 cm to 0.02 $cm^3\ cm^{-3}$ at 60 cm depth. At 30 and 60 cm depth, variability decreased from position A to positions B and C. A correspondence can be suggested between the positions with the largest diurnal amplitude and their sensor-to-sensor differences. In this sense, some sensor positions in the soil are more sensitive to the irrigation cycles, and any factor that may affect either hydration or water uptake at those locations would greatly contribute to sensor-to-sensor differences.

The HYDRUS-3D simulations were found to be much more repetitive, including between virtual sensors displaced 10 cm in either direction relative to the dripper. With the HYDRUS-3D simulations, an RMSE was calculated of around one order of magnitude smaller than that observed with the sensors in positions A and B, while it was similar to the sensor-based RMSE at position C at the 30 and 60 cm depths. That is, the simulations produced a more homogeneous SWC within the wet bulb than measured by sensors, and only in the periphery of the bulb were the simulations sensitive to the precise centring of the bulb.

In our measurements, even though we ensured the equivalent depth and position of the repeated sensors, our results in terms of variability in soil wetting patterns and the existence of heterogeneous SWC and soil temperature patterns suggest that the spatial coordinates of the sensor do not guarantee that they will encounter repeat conditions in terms of irrigation cycle dynamics. The reported 10HS sensor volume of sensitivity is around 1 L (Cobos, 2008; Spelman et al., 2013) and, furthermore, sensitivity is not homogeneous within this volume. Therefore, any soil property that may vary at this spatial scale would cause the immediate vicinity of a particular sensor to depart from the idealized properties considered in simulations. For instance, sensors would be sensitive to the presence of macropores and stones (Rowland et al., 2011), microvariations in soil bulk density (Parvin and Degré, 2016), uneven distribution of

roots (Kang et al., 2019), uneven temperature due to contrasts between shaded and sunlit soil surface (Gónzalez-Teruel et al., 2019), etc. Moreover, there may be additional interaction between these factors. In contrast, HYDRUS-3D simulations do not allow the input of a dynamic root system (Bufon et al., 2012) and do not consider that the soil structure may contain macro-pores or pores with less tortuosity and higher continuity (Xu et al., 2017). In addition, the simulations could be improved by implementing the possibility of simulating the formation of the wetted surface and its evolution over time (Arbat et al., 2003).

The two plots included in the study showed slightly different seasonal patterns. These would not necessarily be associated to the fact that the installed sensors corresponded to different models, since the two plots were managed separately and, at specific periods, received different irrigation doses. In Plot I, the sensors reported drier measurements, especially at 15 cm depth, than expected according to the HYDRUS-3D simulations. Neutron probe measurements supported the results of the simulations (Domínguez-Niño et al., 2020). A possible explanation for this divergence could be the thinner spatial resolution of sensors, together with a scenario of limited irrigation doses. In Plot II, the general agreement with the model was better but nonetheless the sensors still differed in terms of the precise response to all water input/output disruptions. To check the effect of specific soil calibration, the 10HS capacitive sensors installed in Plot II were specifically calibrated for this soil at the end of the study period (Domínguez-Niño et al., 2019). When the measured data were recalculated according to the specific soil calibration, the overall set of calibrated measurements centred around those of the simulations, but the same scatter persisted. Noticeably, measurements at some specific locations systematically increased or decreased when the soil-specific calibration was applied. Compared with the simulations, the sensors tended to give drier measurements at A60 and wetter ones at B30 and C30. This could be because the root water uptake reached higher depths than assumed in the simulations.

4.3. Sensor sensitivity at each location

Despite the complexity involved in discriminating between relevant trends and the noise introduced by variability between sensors, there is no doubt that important information for irrigation control can be derived from sensor response to irrigation cycles. These responses vary with sensor position and depth and must be taken into account both when designing sensor deployment and later on when interpreting the recorded data. Among other things, the effect of sensor position varies according to the soil hydraulic properties, meteorological conditions and the irrigation configuration (Soulis et al., 2015).

A feature of interest for the usage of soil moisture sensors is their ability to indicate the balance of water inputs and outputs to the soil. We observed that, depending on their location, they are more sensitive either to the recent balance of the last irrigation cycle or to the aggregated balance of several cycles. In particular, the sensors located in position

A responded to the water balance of the same day and were especially more sensitive at the depths of 15 cm and 30 cm. Importantly, the sensors installed in these positions were not sensitive to the water balance of the previous week. This suggests that, at these locations, sensors tend to respond to irrigation rapidly and intensely, with little memory of the soil water trends of a few days earlier. The sensors installed in position B at all depths were sensitive to both the water balance of that day and to that of the previous week, especially at the 30 cm depth. The sensitivity at this location, B30, can be explained in terms of the progressive effect of the water balance over the course of several days on the SWC at this point through the overlapping or recession of two neighbouring wet bulbs. The sensors located at C15 were sensitive to the balance of the previous week but not to that of the last day. Also, sensors located at the 30 cm depth and, to a lesser extent, sensors located at the 60 cm depth retained a memory of the water balance of that day and the previous week. This may be because the sensors in these positions were located on the perimeter of the wet area and were only affected by the dynamics of a single wet bulb.

Overall, this different sensitivity, either to the last cycle or to the aggregated period, is also observed in the simulations. The difference is that the B15 and B30 sensors seem more sensitive to the aggregated balance than the simulations. Compared to the simulations, some sensor locations (B60, C15, D30) are less sensitive to the last irrigation cycle and more sensitive to the aggregated balance. This may be due to the actual noise of the irrigation cycles at these positions, while the effect of the accumulated balance is more straightforward.

4.4. Contributions of different factors to sensor-to-sensor differences

Measurements of SWC by capacitance-type soil sensors show a large difference between sensors. Factors such as the calibration applied, the effect of soil temperature and the variability in the area wetted by drippers can contribute individually and in an accumulative way to differences in the measured SWC values. Comparing the potential range of uncertainty by each of these contributory factors could provide clues as to the relative importance of each of them for ensuring the quality of the measurements.

The calibration applied has a minor effect on the variability of the SWC measured by sensors. The potential effect of soil temperature, even if detectable in EC5 sensors, was also limited. The measurements of the virtual HYDRUS-3D sensors can be used to explain a small part of the differences between real sensors. A large part of the impaired repeatability of the sensors may be attributable to the variability observed in the wetted area. In the HYDRUS-3D simulations, this wetted area variability is even larger than that of the sensor measurements, which might be explained by the trend, observed in our data, of the variability increasing as the distance to the soil surface decreases. The results suggest that most of the variability observed in the sensor measurements is caused by the arbitrariness of the shape and the positioning of the wet bulbs. In other words, the variability in a drip-irrigated orchard may be caused by the co-occurrence of a sharply

defined nature of the actual distribution of soil water and a small volume perceived by each capacitance sensor.

Sensor performance in laboratory conditions suggests that their lack of repeatability in the field is not a fault of the sensors but a consequence of the actual complexity of the soil environment in drip-irrigated orchards. Capacitance sensors perceive a smaller soil volume than desirable to compensate for small-scale soil variability, as these sensors are too sensitive to local variations in soil texture, and the presence of gravel, stones, roots, macropores or small compacted soil parts (Hignett and Evett, 2008). In addition, wet bulbs may coexist with patches of differently shaded/sunlit soil spots. Roots may be more clustered and unpredictable than in annual crops. At the same time, macropores and differences in soil bulk density may develop more easily than in arable crops.

4.5. Recommended location for capacitance sensors in drip irrigation

Despite the accuracy of capacitance-type soil moisture sensors in laboratory conditions, in actual drip-irrigated orchards their usage is complicated by both their low repeatability and the dependence of their performance on their location in the soil. The non-uniform distribution patterns make soil water sensor placement a key factor in automated irrigation scheduling (Coelho and Or, 1996). The plant root architecture around the drippers also complicates the decision as to where to place moisture sensors (Or, 1995). As a result, in drip-irrigated orchards, the approach when using these sensors cannot be the same as in scenarios of more homogeneous soil water distribution, such as in rainfed or sprinkler-irrigated field crops. In particular, any approach relying on an accurate assessment of the SWC or its projection to the volume of available water can be unreliable. Instead, an alternative is to use an approach which focuses more on the SWC trends by individual sensors (Casadesús et al., 2012).

The optimal location of capacitance-type moisture sensors for SWC monitoring depends on the type of crop, soil texture, salinity and irrigation system, among other things. Various authors, including Soulis and Elmaloglou (Soulis and Elmaloglou, 2015) have investigated the effects of sensor position and accuracy on drip irrigation scheduling. These same authors (Soulis and Elmaloglou, 2016) introduced the time stable representative position (TSRP) concept and proposed general guidelines for sensor placement in soil moisture–based surface and subsurface drip irrigation scheduling systems (28 cm below the soil surface and 15 cm from the dripline). In a subsequent study (Soulis and Elmaloglou, 2018), they complemented their previous work by considering the representativity of SWC readings and the TSRP in two layered soil profiles. They determined that optimum sensor positions for drip irrigation in a layered soil were at a horizontal distance of 7 cm and a depth of 16 cm in the upper layer, and at a horizontal distance of 11 cm and 34 cm depth in the lower layer.

Regarding the results of this study, attributes that are of interest for irrigation management include sensor-to-sensor repeatability, the extent to which sensor position represents the overall soil water availability to the crop, and the ability of the sensor

location to match applied irrigation doses and actual irrigation needs. Our results indicate each of these attributes has its own pattern of response at different sensor locations, and that probably there is no single location that best reflects these attributes. Moreover, the optimal trade-off between these attributes may depend on the precise purpose and type of usage of the sensors in the farm in question. In this respect, the criteria for sensor deployment intended for visual supervision of soil water may prioritize obtaining a wide and clear view of the whole soil, whereas sensor deployment intended for automated irrigation scheduling may prioritize robustness and sensitivity to changes in the soil water budget.

Nevertheless, when used for irrigation control, the criteria for selecting sensor locations would also depend on the control algorithm used. In this respect, if the control algorithm is based on thresholds for activating/deactivating irrigation pulses (Muñoz-Carpena et al., 2005; Dukes et al., 2010) the criteria may differ from when the algorithm is based on a water balance approach and tuned through sensor feedback (Casadesus et al., 2012; Domínguez-Niño et al., 2020). Therefore, the optimal choice of sensor location will depend on the intended usage. Some authors (Silva et al., 2018), in a study on banana crops, established that the optimal position of the sensors for irrigation scheduling purposes varied according to the crop growth stage. Other authors (Lea-Cox et al., 2010; Casadesús et al., 2012; Mittelbach et al., 2012) used two or more depths to monitor SWC. Alternatively, rather than combining different depths, for automated irrigation it makes sense to ensure measurement robustness by focussing on repetitive positions where there is more root activity (Hignett and Evett, 2008; Domínguez-Niño., 2020). Our study suggests that, to provide feedback to an irrigation scheduling algorithm based on water balance tuned by sensors (Domínguez-Niño., 2020), the combination of sensors close to the vertical of the dripper (location A30) with others in the middle between two neighbouring drippers (location B30) provide useful and complementary information. Moisture sensors aligned with the dripper provide an immediate response to the cycles of irrigation and water uptake by roots, while sensors between two drippers tend to display a slower dynamic which better represents the cumulative balance of the preceding period of several days. In our results, the best performing depth of 30 cm coincides with peak root activity. Other depths seem less favourable, with sensors at 15 cm being the least repeatable and sensors at 60 cm the least responsive to the irrigation cycles.

Our proposals for capacitive-sensor location for irrigation control are in line with other authors who used tensiometers on drip irrigated crops. Hodnett et al. (1990) recommended installing tensiometers along the dripline, below the root zone and inside the wet zone. Thompson et al. (2002), who considered the subsurface drip-irrigation of broccoli, suggested placing tensiometers midway between two plants located in the same row at a depth of 30 cm. However, Dabach et al. (2015), using HYDRUS 2D/3D to evaluate the optimum tensiometer location with ψ measurements in heterogeneous soil, determined that the optimal location was near the subsurface dripper. In addition, Nolz

et al. (2016), who monitored the soil water in a vineyard with Watermark sensors, determined that the representative measurement depth of water absorption by plants was 30 cm.

5. Conclusions

This study describes the variability in the measurements of SWC collected by capacitance-type soil moisture sensors in conditions of drip-irrigated orchards and analyses them in terms of uncertainty of the measurement process and possible variability of the actual quantities. The observed differences in sensor measurements were compared with the estimated potential perturbation as the result of factors such as the variability in the wetted area below the drippers, soil temperature, sensor calibration and the gradients of SWC within a wet bulb expected by simulations. The results obtained show that moisture sensors installed in the field experience more variability than the simulations. Our results suggest that the main source of uncertainty involved in these measurements is the exact positioning of the sensor within the actual wet bulbs, as these vary in size, shape and alignment with respect to the dripper in a magnitude that may explain the observed sensor-to-sensor differences. For its part, uncertainty in the measurements resulting from sensor calibration is only a fraction of the observed variability in data collected by sensors. This indicates that an increased accuracy in SWC measurements is considerably less relevant compared to the variability associated with the wetting pattern. The effect of temperature, with variation throughout the day and according to the position of the dripper, was especially notable in the EC5 sensors. The soil water dynamics represented by the HYDRUS-3D simulation could only explain a small part of the differences observed in the real sensors. These simulations probably correspond to an ideal wet bulb, symmetric and centred around the dripper with homogeneous soil characteristics and root distribution, in contrast with the arbitrary and sharply defined variations in these conditions that can occur in actual wet bulbs.

According to the sensor response to irrigation, sensors closer to the dripper in position and depth (A15) respond quickly, have the highest amplitude and lowest repeatability and are sensitive to the water balance of the same day. For their part, the sensors positioned at greater depth and further away from the dripper (C60) respond slightly, have the lowest amplitude and highest repeatability and are sensitive to the water balance of the whole previous week.

The analysis of the soil water dynamics allows the definition of candidate regions for monitoring. Positions and depths that provide more information for automated irrigation scheduling in a drip-irrigated orchard are also of interest to better understand the soil water dynamics. Given the variability of the system, it is convenient to locate sensors in repeat positions to make the interpretation more robust. In the context of automated irrigation scheduling based on the water balance tuned by soil moisture sensors , the recommended sensor locations could be a combination of sensors close to

the vertical of the dripper (position A) and other sensors midway between neighboring drippers (position B), both at 30 cm depth.

Acknowledgments

The authors would like to acknowledge the collaboration of Carles París, Mercè Mata, Jesús del Campo, Jordi Virgili and Alexandre Escolà, as part of the staff of the program on Efficient Use of Water in Agriculture for their support in implementing this activity.

Literature cited

Abou Lila, T. S.; Balah, M. I.; Hamed, Y. A. Solute infiltration and spatial salinity distribution behavior for the main soil types at El-Salam Canal project cultivated land. Port Said Eng. Res. J. 2005, 9, 242-253.

Adla, S.; Rai, N. K.; Karumanchi, S. H.; Tripathi, S.; Disse, M.; Pande, S. Laboratory calibration and performance evaluation of low-cost capacitive and very low-cost resistive soil moisture sensors. Sensors. 2020, 20, 363.

Aguiar, A. C.; Robinson, S. A.; French, K. Friends with benefits: The effects of vegetative shading on plant survival in a green roof environment. PloS One, 2019, 14, e0225078.

Allen, R.G.; Pereira, L.S.; Raes, D.; Smith, M. Crop evapotranspiration. Guidelines for Computing Crop Water Requirements. FAO Irrigation and Drainage Paper 56, 1998, Rome.

Arbat, G.: Puig-Bargués, J.; Duran-Ros, M.; Barragán, J.; De Cartagena, F. R. Drip-Irriwater: Computer software to simulate soil wetting patterns under surface drip irrigation. Comput. Electron. Agric. 2013, 98, 183-192.

Arraes, F. D.; Miranda, J. H. D.; Duarte, S. N. Modeling soil water redistribution under surface drip irrigation. Eng. Agricola, 2019, 39, 55-64.

Ashofteh, P. S.; Haddad, O. B.; Akbari-Alashti, H.; Marino, M. A. Determination of irrigation allocation policy under climate change by genetic programming. J. Irrig. Drain. Eng. 2015, 141, 04014059.

Badni, N.; Hamoudi, S.; Alazba, A. A.; Elnesr, M. N. Simulations of Soil Moisture Distribution Patterns Between Two Simultaneously-Working Surface Drippers Using Hydrus-2D/3D Model. International Journal of Engineering and Technology. 2018, 10, 586-595.

Bogena, H. R.; Huisman, J. A.; Schilling, B.; Weuthen, A.; Vereecken, H. Effective calibration of low-cost soil water content sensors. Sensors. 2017, 17, 208.

Bogena, H. R.; Herbst, M.; Huisman, J. A.; Rosenbaum, U.; Weuthen, A.; Vereecken, H. Potential of wireless sensor networks for measuring soil water content variability. Vadose Zone J. 2010, 9, 1002-1013.
Bufon, V. B.; Lascano, R. J.; Bednarz, C.; Booker, J. D.; Gitz, D. C. Soil water content on drip irrigated cotton: comparison of measured and simulated values obtained with the Hydrus 2-D model. Irrig. Sci. 2012, 30, 259-273.

Casadesús, J.; Mata, M.; Marsal, J.; Girona, J. A general algorithm for automated scheduling of drip irrigation in tree crops. Comput. Electron. Agric. 2012 83, 11–20.

Chanasyk, D. S., Naeth, M. A. Field measurement of soil moisture using neutron probes. Can. J. Soil Sci. 1996, 76, 317-323.

Cobos, D. 10HS Volume of Sensitivity. Application Note 13900-01, Decagon Devices, 2008, Pullman, WA.

Coelho, E.F.; Or, D. Flow and uptake patterns affecting soil water sensor placement for drip irrigation management. Trans. ASAE. 1996, 39, 2007-2016.

Cummings, R. W.; Chandler, R. F. A Field Comparison of the Electrothermal and Gypsum Block Electrical Resistance Methods with the Tensiometer Method for Estimating Soil Moisture in Situ 1. Soil Sci. Soc. Am. J. 1941, 5, 80-85.

Dabach, S.; Shani, U.; Lazarovitch, N. Optimal tensiometer placement for high-frequency subsurface drip irrigation management in heterogeneous soils. Agric. Water Manag. 2015, 152, 91-98.

Dane, J.H.; Hopmans, J.W. Water retention and storage. In: Dane, J.H., Topp, G.C. (Eds.), Methods of Soil Analysis. Part 4, SSSA Book Series No. 5. 2002, Soil Science Society of America Journal, Madison WI.

De Lima, J. L. M. P.; Abrantes, J. R. C. B. Can infrared thermography be used to estimate soil surfacemicrorelief and rill morphology? Catena. 2014, 113, 314-322.

Domínguez-Niño, J.M.; Oliver-Manera, J.; Girona, J.; Casadesús, J. Differential irrigation scheduling by an automated algorithm of water balance tuned by capacitance-type soil moisture sensors. Agric. Water Manag. 2020, 228, 105880.

Domínguez-Niño, J. M.; Arbat, G.; Raij-Hoffman, I.; Kisekka, I.; Girona, J.; Casadesús, J. Parameterization of Soil Hydraulic Parameters for HYDRUS-3D Simulation of Soil Water Dynamics in a Drip-Irrigated Orchard. Water. 2020, 12, 1858.

Domínguez-Niño, J. M.; Bogena, H. R.; Huisman, J. A.; Schilling, B.; Casadesús, J. On the Accuracy of Factory-Calibrated Low-Cost Soil Water Content Sensors. Sensors. 2019, 19, 3101.

Dukes, M. D.; Zotarelli, L.; Morgan, K. T. Use of irrigation technologies for vegetable crops in Florida. Horttechnology. 2010, 20, 133-142.

Evett, S. R.; Agam, N.; Kustas, W. P.; Colaizzi, P. D.; Schwartz, R. C. Soil profile method for soil thermal diffusivity, conductivity and heat flux: Comparison to soil heat flux plates. Adv. Water Resour, 2012, 50, 41-54.

Fan, Y. W.; Huang, N.; Zhang, J.; Zhao, T. Simulation of soil wetting pattern of vertical moistube-irrigation. Water. 2018, 10, 601.

Fares, A.; Alva, A. K. Evaluation of capacitance probes for optimal irrigation of citrus through soil moisture monitoring in an entisol profile. Irrig. Sci. 2000, 19, 57-64.

Feddes R A; Kowalik P J; Zaradny H. Simulation of Field Water Use and Crop Yield. John Wiley and Sons, Inc. New York, USA, 1978 pp. 16-30.

Frey, H.C.; E.S. Rubin. Evaluate Uncertainties in Advanced Process Technologies. Chem. Eng. Progress. 1992, 88,63-70.

Gallardo, M.; Elia, A.; Thompson, R. B. Decision support systems and models for aiding irrigation and nutrient management of vegetable crops. Agr. Water Manage. 2020, 106209.

García Morillo, J.; Rodríguez Díaz, J. A.; Camacho, E.; Montesinos, P. Drip Irrigation Scheduling Using Hydrus 2-D Numerical Model Application for Strawberry Production in South-West Spain. Irrig. Drain. 2017, 66, 797-807.

Girona, J.; Marsal, J.; Mata, M.; del Campo, J. Pear crop coefficients obtained in a large weighing lysimeter. Acta Hortic. 2004, 664, 277-281.

González-Teruel, J. D.; Torres-Sánchez, R.; Blaya-Ros, P. J.; Toledo-Moreo, A. B.; Jiménez-Buendía, M.; Soto-Valles, F. Design and calibration of a low-cost SDI-12 soil moisture sensor. Sensors. 2019, 19, 491.

Hao, A.; Marui, A.; Haraguchi, T.; Nakano, Y. Estimation of wet bulb formation in various soil during drip irrigation. J. Fac. Agr. Kyushu U. 2007, 52, 187.

Hignett, C.; Evett, S. Direct and surrogate measures of soil water content. In S.R. Evett et al. (ed.). Field Estimation of Soil Water Content. A practical guide to methods, instrumentation and sensor technology. International Atomic Energy Agency, Vienna, Austria 2008, pp. 1-21.

Hodnett, M. G.; Bell, J. P.; Koon, P. A.; Soopramanien, G. C.; Batchelor, C. H. The control of drip irrigation of sugarcane using "index" tensiometers: some comparisons with control by the water budget method. Agric. Water Manag. 1990, 17, 189-207.

Hofer, E. When to separate uncertainties and when not to separate. Reliab. Eng. Syst. Safe. 1996, 54, 113-118.

Huijbregts, M. A. Application of uncertainty and variability in LCA. Int. J. Life Cycle Ass. 1998, 3, 273-280.

Jones, S.B.; Blonquist, J.M.; Robinson, D.A.; Rasmussen, V.P.; Or, D. Standardizing characterization of electromagnetic water content sensors. Part 1. Methodology. Vadose Zone J. 2005, 4, 1048–1058.

Kandelous, M. M.; Simunek, J.; Van Genuchten, M. T.;Malek, K. Soil water content distributions between two emitters of a subsurface drip irrigation system. Soil Sci. Soc. Am. J. 2011, 75, 488-497.

Kang, S.; van Iersel, M. W.; Kim, J. Plant root growth affects FDR soil moisture sensor calibration. Scientia Hortic. 2019, 252, 208-211.

Kargas, G.; Soulis, K. X. Performance analysis and calibration of a new low-cost capacitance soil moisture sensor. J. Irrig. Drain. Eng. 2012, 138, 632-641.

Kilic, M. A new analytical method for estimating the 3D volumetric wetting pattern under drip irrigation system. Agric. Water Manag. 2020, 228, 105898.

Kizito, F.; Campbell, C. S.; Campbell, G. S.; Cobos, D. R.; Teare, B. L.; Carter, B.; Hopmans, J. W. Frequency, electrical conductivity and temperature analysis of a low-cost capacitance soil moisture sensor. J Hydrol, 2008, 352, 367–378.

Kojima, Y.; Shigeta, R; Miyamoto, N.; Shirahama, Y.; Nishioka, K.; Mizoguchi, M.; Kawahara, Y. Low-cost soil moisture profile probe using thin-film capacitors and a capacitive touch sensor. Sensors. 2016, 16, 1292

Lea-Cox, J.D.; Kantor, G.F.; Bauerle, W.L.; van Iersel, M.W.; Campbell, C.; Bauerle, T.L.; Ross, D.S.; Ristvey, A.G.; Parker, D.; King, D.M.; Bauer, R.; Cohan, S.M.; Thomas, P.A.; Ruter, J.M.; Chappell, M.; Lefsky, M.; Kampf, S.; Bissey, L. A specialty crops research project: Using wireless sensor networks and crop modeling for precision irrigation and nutrient management in nursery greenhouse and green roof systems. Proc. Southern Nursery Assn. Res. Conf. 2010, 55, 211–215

Ledieu, J.; De Ridder, P.; De Clerck, P.; Dautrebande, S. A method of measuring soil moisture by time-domain reflectometry. J. Hydrol. 1986, 88, 319-328.

Liao L; Zhang L; Bengtsson L. Soil moisture variation and water consumption of spring wheat and their effects on crop yield under drip irrigation. Irrigat. Drain. Syst. 2008, 22, 253-270.

Millán, S.; Casadesús, J.; Campillo, C.; Moñino, M. J.; Prieto, M. H. Using soil moisture sensors for automated irrigation scheduling in a plum crop. Water. 2019, 11, 2061.

Mittelbach, H.; Lehner, I.; Seneviratne, S. I. Comparison of four soil moisture sensor types under field conditions in Switzerland. J. Hydrol. 2012, 430, 39-49.

Morgan, M.G.; M. Henrion. Uncertainty: a guide to dealing with uncertainty in quantitative risk and policy analysis. Cambridge University Press, New York, NY, USA, 1990.

Mualem, Y. A new model for predicting the hydraulic conductivity of unsaturated porous media. Water Resour. Res. 1976, 12, 513–522.

Muñoz-Carpena, R.; Li, Y. C.; Klassen, W.; Dukes, M. D. Field comparison of tensiometer and granular matrix sensor automatic drip irrigation on tomato. Horttechnology. 2005, 15, 584-590.

Nagahage, E. A. A. D.; Nagahage, I. S. P.; Fujino, T. Calibration and validation of a low-cost capacitive moisture Sensor to integrate the automated soil moisture monitoring system. Agriculture. 2019, 9, 141.

Naglič, B; Kechavarzi, C; Coulon, F; Pintar, M. Numerical investigation of the influence of texture, surface drip emitter discharge rate and initial soil moisture condition on wetting pattern size. Irrig. Sci. 2014, 32, 421-436.

Nolz, R.; Loiskandl, W. Evaluating soil water content data monitored at different locations in a vineyard with regard to irrigation control. Soil Water Res. 2017, 12, 152-160.

Nolz, R.; Cepuder, P.; Balas, J.; Loiskandl, W. Soil water monitoring in a vineyard and assessment of unsaturated hydraulic parameters as thresholds for irrigation management. Agr. Water Manage. 2016, 164, 235-242.

Or, D. Stochastic analysis of soil water monitoring for drip irrigation management in heterogeneous soils. Soil Sci. Soc. Am. J. 1995, 59, 1222-1233.

Parvin, N.; Degré, A. (2016). Soil-specific calibration of capacitance sensors considering clay content and bulk density. Soil Res. 2016, 54, 111-119.

Rajput, T. B. S.; Patel, N. Water and nitrate movement in drip-irrigated onion under fertigation and irrigation treatments. Agric. Water Manag. 2006, 79, 293-311.

Robinson, D.A.; Gardner, C.M.K.; Evans, J.; Cooper, J.D.; Hodnett, M.G.; Bell, J.P. The dielectric calibration of capacitance probes for soil hydrology using an oscillation frequency response model. Hydrol. Earth Syst. Sci. Discuss. 1998, 2, 111–120.

Rosenbaum, U.; Huisman, J. A.; Weuthen, A.; Vereecken, H.; Bogena, H. R. Sensor-to-sensor variability of the ECH2O EC-5, TE, and 5TE sensors in dielectric liquids. Vadose Zone J. 2010, 9, 181-186.

Rosenbaum, U.; Huisman, J. A.; Vrba, J.; Vereecken, H.; Bogena, H. R. Correction of temperature and electrical conductivity effects on dielectric permittivity measurements with ECH2O sensors. Vadose Zone J. 2011, 10, 582-593.

Rowland, R.; Pachepsky, Y. A.; Guber, A. K. Sensitivity of a Capacitance Sensor to Artificial Macropores. Soil Sci. 2011, 176, 9-14.

Sakaki, T.; Limsuwat, A.; Smits, K. M., Illangasekare, T. H. Empirical two-point α-mixing model for calibrating the ECH2O EC-5 soil moisture sensor in sands. Water Resour. Res. 2008, 44.
Scudiero, E.; Berti, A.; Teatini, P.; Morari, F. Simultaneous monitoring of soil water content and salinity with a low-cost capacitance-resistance probe. Sensors. 2012, 12, 17588-17607.

Schmitz, M.; Sourell, H. Variability in soil moisture measurements. Irrigation Sci. 2000, 19, 147-151.

Seabold, S.; Perktold, J. Statsmodels: Econometric and statistical modeling with python. In Proceedings of the 9th Python in Science Conference; Austin, TX, 28 June – 3 July 2010; pp. 61.

Silva, A. J. P. D.; Coelho, E. F.; Coelho Filho, M. A.; Souza, J. L. D. Water extraction and implications on soil moisture sensor placement in the root zone of banana. Sci Agr. 2018, 75, 95-101.

Simunek, J.; Van Genuchten, M. T; Sejna, M. Recent developments and applications of the HYDRUS computer software packages. Vadose Zone J. 2016, 15, 25.

Skaggs, T. H.; Trout, T. J.; Simunek, J.; Shouse, P. J. Comparison of HYDRUS-2D simulations of drip irrigation with experimental observations. J. Irrig. Drain. Eng. 2004, 130, 304-310.

Soil Survey Staff. Soil Taxonomy. A basic System for Making and Interpreting Soil Surveys. 2nd ed.; United States Department of Agriculture, National Resources Conservation Service, USA, 1999; pp. 869.

Soulis, K. X.; Elmaloglou, S. Optimum soil water content sensors placement in drip irrigation scheduling systems: concept of time stable representative positions. J Irrig. Drain Eng. 2016, 142, 04016054.

Soulis, K. X.; Elmaloglou, S.; Dercas, N. Investigating the effects of soil moisture sensors positioning and accuracy on soil moisture based drip irrigation scheduling systems. Agric. Water Manag., 2015, 148, 258-268.

Soulis, K. X.; Elmaloglou, S. Optimum soil water content sensors placement for surface drip irrigation scheduling in layered soils. Comput. Electron. Agric. 2018, 152, 1-8.

Spelman, D.; Kinzli, K. D.; Kunberger, T. Calibration of the 10HS soil moisture sensor for southwest Florida agricultural soils. J Irrig. Drain Eng. 2013, 139, 965-971.

Taylor, S. A.; Ashcroft, G. L. Physical Edaphology: the physics of irrigated and non irrigated soils. W. H. Freeman., San Francisco, USA; 1972; pp. 532.

Thompson, T. L.; Doerge, T. A.; Godin, R. E. Subsurface drip irrigation and fertigation of broccoli: I. Yield, quality, and nitrogen uptake. Soil Sci. Soc. Am. J. 2002, 66, 186-192.

Van Belle, G. Statistical Rules of Thumb (2nd edition), John Wiley and Sons, Hoboken, 2008, New Jersey.

Van Genuchten, M. T. A closed-form equation for predicting the hydraulic conductivity of unsaturated flow, Soil Sci. Soc. Am. J. 1980, 44, 892-898.

Visconti, F.; de Paz, J. M.; Martínez, D.; Molina, M. J. Laboratory and field assessment of the capacitance sensors Decagon 10HS and 5TE for estimating the water content of irrigated soils. Agr. Water Manage. 2014, 132, 111-119.

Waugh W.J.; Baker D.A.; Kastens M.K.; Abraham J.A. Calibration precision of capacitance and neutron soil water content gauges in arid soils. Arid Soil Res. and Rehabil. 1996, 10, 391-401.

Xu, X.; Kalhoro, S. A.; Chen, W.; Raza, S. The evaluation/application of Hydrus-2D model for simulating macro-pores flow in loess soil. Int. Soil Water Conse. 2017, 5, 196-201.

Zotarelli, L.; Dukes, M. D.; Scholberg, J. M. S.; Femminella, K.; Muñoz-Carpena, R. Irrigation scheduling for green bell peppers using capacitance soil moisture sensors. J. Irrig. Drain. Eng. 2011, 137, 73-81.

Chapter IV: Integration in irrigation control

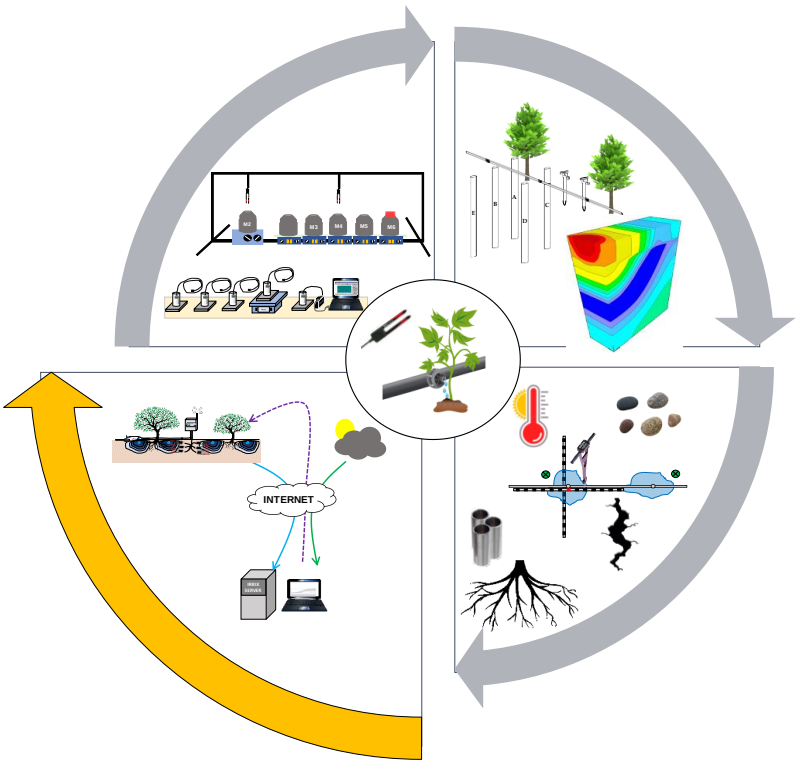

Differential irrigation scheduling by an automated algorithm of water balance tuned by capacitance-type soil moisture sensors

Jesús María Domínguez-Niño[1], Jordi Oliver-Manera[1], Joan Girona[1], Jaume Casadesús[1]

[1] Programme on Efficient Use of Water in Agriculture, Institute of Agrifood Research and Technology (IRTA), Parc de Gardeny (PCiTAL), Fruitcentre, 25003, Lleida, Spain; jesus.dominguez@irta.cat; jaume.casadesus@irta.cat

Agricultural Water Management (2020), 228, 105880 DOI: 10.1016/j.agwat.2019.105880

Abstract

Automated software tools are required to undertake the routine tasks and decision-making involved in scheduling irrigation. A key issue in this topic is how to integrate sensors in the scheduling approach. The objectives of this research were to test, in the context of drip-irrigated orchards: (a) the suitability of FAO's water balance method, locally adjusted by sensors, as the basis for the scheduling algorithm, (b) the suitability of capacitance-type soil moisture sensors, and an approach for their automated interpretation, for providing feedback to the scheduling algorithm, and (c) the performance of these combined approaches in the autonomous scheduling of irrigation in an apple orchard with heterogeneous vigour. The trial consisted of applying for two years the proposed approaches using an experimental web application, IRRIX, which scheduled irrigation of two irrigation sectors, which differed in tree size. The automated system was compared with manual scheduling by a classical water balance and with the actual evapotranspiration determined by a weighing lysimeter located in the same orchard. Results show that the irrigation applied by the automated approach in the sector of larger trees agreed with the ET determined by the lysimeter and, overall, with the scheduling by an experienced irrigator using a classical water balance. Meanwhile, as a result of a different feedback from soil moisture sensors, the same system reduced irrigation in the sector of smaller trees by a similar amount to that expected from the differences between the two sectors in the fraction of photosynthetically active radiation. This study illustrates that the method of water balance complemented with capacitance-type soil moisture sensors provides a sound basis for automated irrigation scheduling in orchards.

Keywords: Irrigation control, drip irrigation, 10HS sensor, Internet of things, orchard automation, precision agriculture.

1. Introduction

At the plot level, an appropriate irrigation scheduling promotes benefits such as saving water, decreasing environmental impacts and generating sustainable agriculture (Smith et al., 1996). In this context, the paradigm of precision irrigation emphasizes the variable-rate application of water according with the variability in weather, soil, crop properties and topography (Daccache et al., 2015). In practice, the variety of factors to take into account, together with the sequence of routine steps involved in scheduling irrigation, requires of farmers too much dedication, perseverance and expertise for conducting an optimized irrigation strategy. Consequently, digital tools are required to alleviate those requirements and enable commercial orchards apply precision irrigation with a feasible effort.

As a basis for determining the irrigation schedules, the most common method for calculating irrigation requirements follows the approach of FAO's soil water balance, where the water inputs in the soil-plant system are compared with the outputs (Doorenbos and Pruit, 1977). The major output is the evapotranspiration by the crop (ET_C), which, under non-stress conditions, can be predicted from $ET_C = ET_O \times K_C$, where the evapotranspiration of a reference crop (ET_O) is estimated by the Penman-Monteith method and K_C is the crop coefficient characteristic of each crop (Allen et all., 1998). However, in horticultural crops, this approach can be quite uncertain since for a given crop species its K_C may vary with factors such as spacing and orientation of the rows (Intrieri et al., 1998), the plant variety (Higgins et al., 1992), crop load (Wünsche et al., 2000; Naor et al., 2008) and the size and shape of the canopy (Wünsche et al., 1995; Ayars et al., 2003; Girona et al., 2011; Marsal et al., 2014). In particular, the dependence of K_C on the solar radiation intercepted by the canopy has previously being studied in apple orchards (Girona et al., 2011; Auzmendi et al., 2011; Marsal et al., 2013). Furthermore, automated dosing of irrigation proportional to the daily amount of solar radiation intercepted by the canopy has experimentally been tested in apple (Casadesús et al., 2011). On the other hand, given the practical difficulties for a precise parameterization of the water balance, sensors can be used for an empirical site-specific adjustment. A simple approach is to set in the irrigation automata a general irrigation program, based on a conservative water balance and then, an automated system suppresses irrigation when the soil moisture exceeds a determined threshold (Muñoz-Carpena et al., 2005; Cáceres et al., 2008). A more elaborated approach is to determine irrigation doses by water balance but using the feedback from sensors for the empirical adjustment of Kc (Bacci et al., 2008; Casadesús et al., 2012). This combination of water balance and sensors sums up the ability to calculate irrigation volumes by water balance with the site-specific adaptive response to sensors.

The choice of the sensing method for providing feedback must trade-off its reliability with the feasibility of its usage in farms. One of the most widely used types of sensors for irrigation management are soil water sensors of capacitance type (Kojima et

al., 2016; Bogena et al., 2017; Domínguez-Niño et al., 2019). Their functioning relies on the determination of the dielectric permittivity of the soil around the sensor, which mostly depends on the soil water content. Capacitance sensors have the advantage of being low cost and require little maintenance (Campbell, 1990; Kizito et al., 2008; Visconti et al., 2014). However, the response of these sensors varies with soil texture, presence of coarse elements, macropores, roots and soil compaction (Hignett and Evett, 2008). Furthermore, the dielectric permittivity is influenced by the temperature and by the electrical conductivity of the medium (Kizito et al., 2008; Kargas and Soulis, 2019). An additional complication in scenarios of localized irrigation is the heterogeneous distribution of soil water. In contrast with flood and sprinkler irrigation, where the water infiltrates on the most or all soil surface, in localized irrigation infiltration takes place directly in the area around the emitter (Cote et al., 2003; Irmak et al., 2016). This creates wet bulbs in the soil whose size and shape depend on many factors such as the soil hydraulic characteristics, the absorption by the roots, the evaporation from the soil surface, as well as the irrigation depth, relative position of the dripper, drip line sources spacing and quantity and frequency of the irrigation (Lazarovitch et al., 2007; Nafchi et al., 2011; Elmaloglou et al., 2013; Hao et al., 2016). All of these factors lead to one of the major difficulties in using capacitance sensors, which is the high variability between sensors even if installed at equivalent positions in the soil (Intrigliolo and Castel, 2004). Nevertheless, once a sensor has been installed, the effects associated with its exact position, including the properties of the soil around it, will be nearly constant (Rolston et al., 1991). Hence, one approach to deal with the variability between sensors is to field calibrate each individual sensor after installation (Evett et al., 2008; Evett et al., 2009; Mittelbach et al., 2012; Singh et al., 2018). A simplified field calibration approach for practical use in irrigation is to rescale the measurements by each sensor as relative to the measurements recorded by the same sensor under conditions of soil water at field capacity. In addition, to simplify dealing with the daily pattern of soil water content, the interpretation can focus in the driest measurement recorded each day (Casadesús et al., 2012). The trend of this value, between consecutive days, has been proposed as an indicator of the resulting water balance in that period and has been used for tuning the water balance in an algorithm of automated irrigation scheduling (Casadesús et al., 2012).

The overall goal of this research was to demonstrate the feasibility of automated scheduling irrigation in orchards, where, in practice, size and structure of the canopy can be a common source of variation. In particular, this study focused at testing: (a) the suitability of water balance locally tuned by sensors as the basis for irrigation scheduling in drip-irrigated orchards, (b) the unmanned interpretation of soil moisture measured by capacitance sensors as a source of feedback for the scheduling algorithm, and (c) the performance of these combined approaches in the autonomous scheduling of irrigation in an apple orchard with heterogeneous vigour. The study was conducted with an experimental web application, IRRIX, which implements the proposed algorithms and the methods for unmanned interpretation of capacitance sensors. On an apple orchard

with heterogeneous vigour, sectors with larger and smaller trees were scheduled during two seasons by the automated system using capacitance sensors. The trial looked at how the automated system behaved on sectors with different tree vigour and whether, with identical configuration, it was able to provide differential irrigation according to the differences in tree vigour. Additionally, the automated system was compared with manual scheduling by a classical water balance and with the actual evapotranspiration determined by a weighing lysimeter located in the same orchard.

2. Materials and Methods

2.1. Experimental design and irrigation treatments

The apple orchard (*Malus domestica* Borkh. cv 'Golden Reinders') was located at the IRTA-Lleida Experimental Station in Mollerussa (41.6° N, 0.8° E, 260 m above sea level), Lleida, Spain, with a dry continental mediterranean climate. Apple trees had been planted in 2011, spaced at 3.63 m x 1.2 m oriented north-south. Irrigation was provided by means of a single pipe with drippers every 0.6 m, whose delivery rate was 3.5 $dm^3 h^{-1}$. Some properties of the soil are shown in Table 1. One fraction of this plantation had been replanted after a previous apple plantation and, in this area, the trees were homogeneously smaller than in the rest of the orchard because of the apple tree replant disease (Laurent et al., 2010; Singh et al., 2017). The average Trunk Cross Sectional Area (TCSA) in the unaffected area was 40.55 cm^2 while in the affected area it was 27.94 cm^2. The trial consisted of the automated scheduling of two independent irrigation sectors, one in the area of larger trees (AUTO-L) and the other in an area with smaller trees (AUTO-S). These were compared with two sectors scheduled manually following a classical water balance, one with larger trees (MANUAL-L) and the other with smaller trees (MANUAL-S).

Table 1. Soil properties sampled in the experimental site at two depths.

Depth (m)	0 - 0.2	0.2 - 0.4
Silt (0.002 < d < 0.05 mm) %	40.70	40.60
Clay (d < 0.002 mm) %	23.50	23.90
Sand (0.05 < d < 2mm) %	35.80	35.50
USDA Soil Classification	Loamy	Loamy
Soil Water content at field capacity (33 KPa) m^3m^{-3}	0.38	0.37
Soil water content at wilting point (-1500 KPa) m^3m^{-3}	0.17	0.17
Apparent density (Kg m^{-3})	1480	1500

Manual irrigation scheduling consisted of the application of the FAO's water balance (Allen et al., 1998), on a weekly basis, by an experienced irrigator, using ET_O from the previous week recorded by a weather station located in the same farm and crop coefficients (K_C) determined in previous years by the weighing lysimeter included in the same orchard. In these sectors, irrigation was controlled by solenoid valves operated by a commercial automata, Agronic 4000 (Sistemes Electrònics Progrés, Palau d'Anglesola, Lleida, Spain) which was programmed remotely, every Monday, through the desktop

application provided by the manufacturer. All irrigation sectors were equipped with the same model of water meter, CZ3000 (Contazara, Zaragoza, Spain), that were recorded at least twice per week, apart from the scheduling application. The manual scheduling made no distinction between MANUAL-L and MANUAL-S and applied a homogeneous irrigation program to the whole orchard, based on the estimated requirements of the larger trees, which mirrors the expected practice in a commercial farm.

2.2. Deployment and management of the automated scheduling

One datalogger, model CR800 (Campbell Scientific, INC., Logan, UT, USA) was used in the automated sectors for both recording sensors and commanding irrigation valves. The datalogger was equipped with a multiplexer AM16/32 (Campbell Scientific, INC., Logan, UT, USA), to increase the number of sensor channels, which were measured every 15 seconds and the average of 5 minutes was stored. A 3G modem MTX-3G-JAVA (MTX, Flexitron Group, Madrid, Spain), allowed remote communication through Internet Protocol. In addition, a four-channel latching relay LR4 (Campbell Scientific, INC., Logan, UT, USA) enabled the datalogger open and close the irrigation valves of the AUTO sectors, model ¾" AquaNet Plus (Netafim). The program in the datalogger, written in CR Basic (Campbell Scientific, INC., Logan, UT, USA), implemented the functionalities of an irrigation automata. Four times per day, the web application polled the datalogger for new sensor data and once per day, typically at 02:30 GMT, IRRIX sent to the datalogger the irrigation doses of each sector, in mm, for the new day. Communication between the IRRIX server and the datalogger used the API PackBus SDK (Campbell Scientific, INC., Logan, UT, USA). During the day, independently for each sector, at the appointed time, 8:00 AM, the datalogger started irrigation and ended it when it had measured the scheduled dose.

Each automated sector was equipped with six capacitance-type soil moisture sensors, 10HS (METER Group, Pullman, WA, USA), which were recorded by the datalogger in units of soil water content ($m^3\ m^{-3}$) using the general calibration for mineral soils proposed by the manufacturer. These sensors have one body with two 14.5 cm long prong, spaced 3.3 cm, which gives an apparent permittivity measurement volume of around 1 dm^3 (Sakaki et al., 2008). All soil sensors were installed at 30 cm depth, three of them centered 15 cm from the vertical of the dripper, perpendicular to the irrigation pipe, and the other three at the mid-point between two drippers. Each automated sector was equipped with a water meter with a resolution of one pulse per litter, model Multijet M15 (Arad Group, Dalia, Israel), which were used by the datalogger for controlling the delivery of the appointed doses. In addition, a temperature sensor, model VP3 (METER Group, Pullman, WA, USA), provided a continuous measurement of air temperature that was used by IRRIX for the estimation of ET_O using Hargreaves equation (Hargreaves and Samami, 1985).

The settings of AUTO-L and AUTO-S in the automated scheduling application were exactly the same, while they were equipped with separate sets of soil moisture sensors

which would provide independent feedback to the scheduling algorithm.

2.3. Web platform for irrigation control: IRRIX

IRRIX is a custom-made software for research on sensor-based irrigation scheduling. It can operate autonomously during the whole irrigation season, with a daily routine that includes uploading sensor data from the field, analysing those data, updating the water balance, deciding the next irrigation doses at each plot and transmitting them to the automata in the field. The scheduling approach used by IRRIX consists of estimating the crop water requirements by the method of water balance (Allen et al., 1998) and use the feedback from sensors for adjusting empirically the irrigation doses of each sector (Casadesús et al., 2012). Basically, the daily irrigation doses (DID), in mm, were determined on a daily basis as:

$$DID = ET_0 \times K_X \quad \text{(Eq. 1)}$$

Where ET_O was the reference evapotranspiration estimated by the Hargreaves equation using as input the air temperature recorded by the datalogger. K_X was initialized as a crop coefficient and, later on, independently for each sector, it was iteratively adjusted on a daily basis from feedback by the sensors.

In order to provide a seasonal vision of irrigation, and to enable in other studies the application of certain types of irrigation strategies, IRRIX requires the definition of a seasonal plan. The seasonal plans of IRRIX specify, for every day of the irrigation season, the acceptable ranges for (a) the accumulated irrigation; (b) the weekly water unbalance; and (c) the range of crop's water comfort in terms of the monitored Normalized Soil Water Content (NSWC). In the seasonal plan for this trial, the range of accumulated irrigation and the weekly balance were set sufficiently wide to avoid limiting the response to sensors (Figure 1). Sectors AUTO-L and AUTO-S were configured exactly with the same seasonal plan, which was also the same for 2017 and 2018.

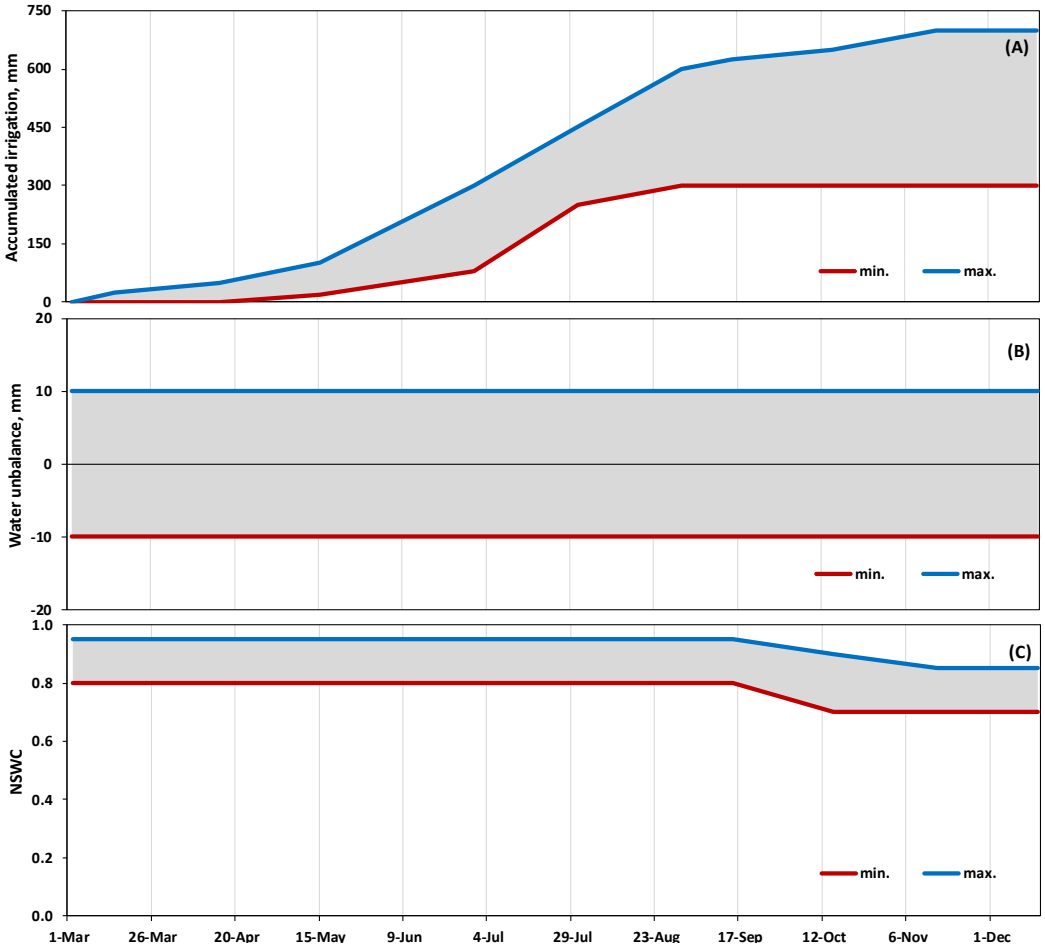

Figure 1. Seasonal plan configured in IRRIX for AUTO-L and AUTO-S. The plan specifies (A) acceptable range of irrigation, (B) acceptable weekly water unbalance and (C) crop's water comfort in terms of the NSWC recorded by sensors.

Interpretation of the soil moisture sensors by IRRIX focused at the trend, between consecutive days, of the driest measurement of each day, SWC_d. In order to manage the variability between sensors, IRRIX normalized those values between the measurable range of each individual sensor as defined by its actual reading at field capacity and the presumed wilting point for that soil textural class. Hence, the NSWC, dimensionless, was calculated as:

$$NSWC = \frac{(SWC_d - SWC_{WP})}{(SWC_{FC} - SWC_{WP})} \quad \text{(Eq. 2)}$$

Where SWC_d was the driest soil water content measured by the sensor at given day (m^3 m^{-3}), SWC_{FC} was the highest daily minimum of the soil water content (SWC_d) recorded by a sensor in a period of reference at the start of the season, under conditions near field capacity. In this context, the purpose of SWC_{FC} is just to provide an empirical reference for that sensor near its high end of scale. Figure 2 shows an example of the empirical setting of SWC_{FC} for one sensor. Since normal growing conditions were far from wilting point, SWC_{WP} was not empirically based but set at the typical SWC at wilting point for

that soil textural class. Table 2 shows the references set to the different sensors involved in this study.

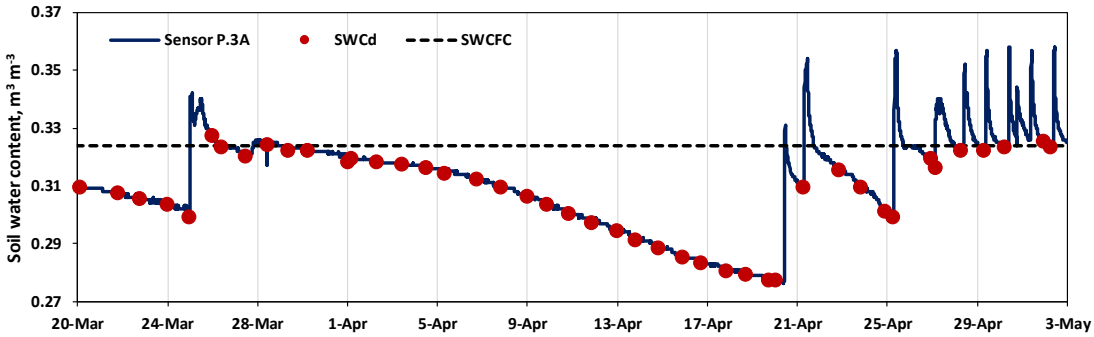

Figure 2. Example of setting the reference of a sensor at field capacity, SWC_{FC}. Following rainfall (33 mm) on March 24th, the daily driest measurement on March 28th was taken as the SWC_{FC} for this sensor. Irrigation started in April 20th. The continuous line is the data recorded by the sensor. Dots are the driest measurement each day, SWC_d.

Table 2. References used by IRRIX for normalizing the daily driest measurements to the span between SWC_{WP} and SWC_{FC} for each sensor. The values of SWC_{FC} were assigned empirically in March 2017 as shown in Figure 3. The values for SWC_{WP} were set to the presumed soil water content at wilting point for this soil texture.

sensor	AUTO-L		AUTO-S	
	SWC_{WP}	SWC_{FC}	SWC_{WP}	SWC_{FC}
1A	0.15	0.363	0.15	0.356
1B	0.15	0.364	0.15	0.347
2A	0.15	0.368	0.15	0.318
2B	0.15	0.360	0.15	0.338
3A	0.15	0.392	0.15	0.324
3B	0.15	0.384	0.15	0.345

In order to enforce its tolerance to sensor failures, the daily analysis of sensor data by IRRIX included rating the reliability of each sensor. These automated ratings started assigning to each sensor a reliability of 1.0 and when IRRIX detected values out of range, noise or abnormal patterns, the reliability of the sensor was penalized, which could decrease its value down to 0.0. The advantage of this method is that, if a sensor is broken or disconnected for any reason, IRRIX can automatically detect this situation, assign it a reliability of 0.0 and keep the aggregated value safe from its influence. To obtain a single value to summarize the state of an irrigation sector, IRRIX aggregated the NSWC obtained by the six sensors installed on a sector through a weighted average. In this trial, the weight of each sensor was its current rating of reliability, updated with the same set of data being summarized.

In order to provide feedback to the scheduling algorithm, IRRIX evaluates every day the state of an irrigation sector as either "to dry", "to wet" or "fitted". From the current value of aggregated NSWC and its trend in the last 3 days, it calculates the projected value after 3 days, $NSWC_{+3d}$. If $NSWC_{+3d}$ is below the comfort zone specified in the seasonal plan, then the state of that sector is evaluated as "too dry" and the response of

IRRIX consists of increasing K_X by the estimated amount to fill in three days the soil wet bulbs up to the water content corresponding to the midst of the comfort zone. If $NSWC_{+3d}$ is above the comfort zone, it is evaluated as "too wet" and the response aims at reaching the midst of the comfort zone at the wet bulbs in 7 days. In either case, the change in K_X is conditioned to fulfil the conditions of accumulated irrigation and water unbalance specified in the seasonal plan.

2.4. Measurement of ETC by weighing lysimeter

The same orchard where this trial was conducted is equipped with two weighing lysimeters that provide a continuous measurement of crop evapotranspiration (Girona et al., 2004). These lysimeters contain four apple trees each, grown in equivalent conditions than the rest of the plantation. The ET_O used in the lysimeter was the Penman-Monteith evapotranspiration, determined by an automated meteorological station, located next to the orchard, operated by the Catalan Meteorological Service. Due to maintenance operations, in the period from March to July 2017 the lysimeters were not operative and the daily ET values for that period were estimated from the K_C values determined in 2018 corrected by the ratio between K_C measured in August of both years, as:

$$ET_{d2017} = ETo_{d2017} \times Kc_{d2018} \times \frac{Kc_{August2017}}{Kc_{August2018}} \quad \text{(Eq. 3)}$$

2.5. Physiological and agronomical measurements.

Stem water potential (SWP) was determined once a week using a pressure chamber (3005-series portable plant water status console, Soil Moisture Equipment Corp., Model 3005, Santa Barbara, CA, USA) following the method described by McCutchan and Shakel (1992) procedure. Measurements were made at solar noon on shaded leaves located close to the main trunk. Previously, leaves were covered with plastic sheathes with aluminium foil bags to minimize transpiration and keep in balance with the xylem of the tree.

The differences in vigour between the large and small trees were quantified in terms of fraction of photosynthetically active radiation intercepted by the canopies (FIPAR) along the whole day. The measurement method was similar to the Fisheye Photography described by Wünsche et al. (1995) and consisted on taking hemispheric photos from below the tree, following a pattern that covered the entire planting space. The photographs were taken with a digital camera Nikon D70 and a 10-17 mm AT-X Tokina fish-eye lens on a self-leveling support that held the camera 10 cm above ground. The photographs were processed to calculate the daily solar path on each picture and analyse the fraction between treetop pixels and background -i.e. blue sky- at the different sun positions along the day.

To determine yield and its components, the central five apple trees of each plot were individually harvested and the collected fruits counted and weighted to determine total yield (kg of fruits per tree) (Yield) and after passing the fruits for a grade, and removing fruits smaller than 70 mm, the remaining ones were used to determine Commercial Yield (kg·tree^{-1} and t·ha^{-1}) (CY). Yield Index (YI) (kg of total yield·CTSA^{-1}) (kg·cm^{-2}) and Commercial Yield Index (CYI) (kg of commercial yield·CTSA^{-1}) (kg·cm^{-2}) were also determined to compare the effects of treatments in fruit production. Because of the location and distribution of the different plots within the orchard, each individual tree was used as a repetition resulting a strip plot design. Statistical analyses were carried out with SAS (SAS Institute, Cary, NC, USA, version 9.4).The effects of treatments were analysed by means of the general linear model (GLM) procedure, and differences among means were compared with the LSmeans followed by Tukey-Kramer adjustment, with the statistical significance established at $P \leq 0.05$.

3. Results and discussion

3.1. IRRIX performance and interpretation of sensor data

The trees in sectors AUTO-S and MANUAL-S had, through the duration of the trial, a visually lower vigour than those in the rest of the plot, including AUTO-L, MANUAL-L and the lysimeter. The ratio between $FIPAR_{AUTO\text{-}S}$ and $FIPAR_{AUTO\text{-}L}$ was persistently around 0.88 during the whole period of study (Figure 3).

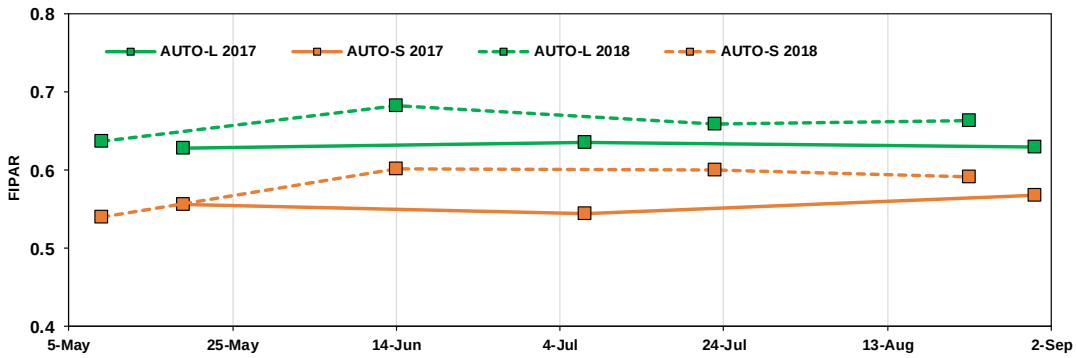

Figure 3. Fraction of intercepted photosynthetically active radiation (FIPAR) in the irrigation sectors with large (L) and smaller (S) trees during the years 2017 and 2018.

Interaction of the research team with the web application IRRIX concentrated in 2017 before season, when the seasonal plan was established and the references for each sensor were set. During the irrigation seasons of 2017 and 2018 IRRIX operated autonomously and the participation of the research team consisted in supervising the normal development of the irrigation plan, by connecting once/twice per week to IRRIX and checking for common anomalies that would require a physical repair, such as malfunction of the irrigation system or the sensors.

Data recorded by soil moisture sensors used to show clear responses to irrigation, rain and water uptake by the crop, as illustrated in Figure 4, which shows a period that

includes rain events and an interruption in water supply. As shown in Figure 4a, at the daily scale the timing of irrigation was programmed to concur with ET_O. However, irrigation did not necessarily fluctuate between days with ET_O, because the control algorithm may vary at any time the proportionality between irrigation and ET_O. The soil water content recorded by sensors showed a clear daily pattern, with a peak during irrigation, followed by a decrease that may be attributed to the redistribution of water in soil plus uptake by roots. In days without irrigation, sensors showed a clear decrease in water content during transpiration hours and still values at night. Most rain events could be observed as a rise in soil water content unaligned with irrigation.

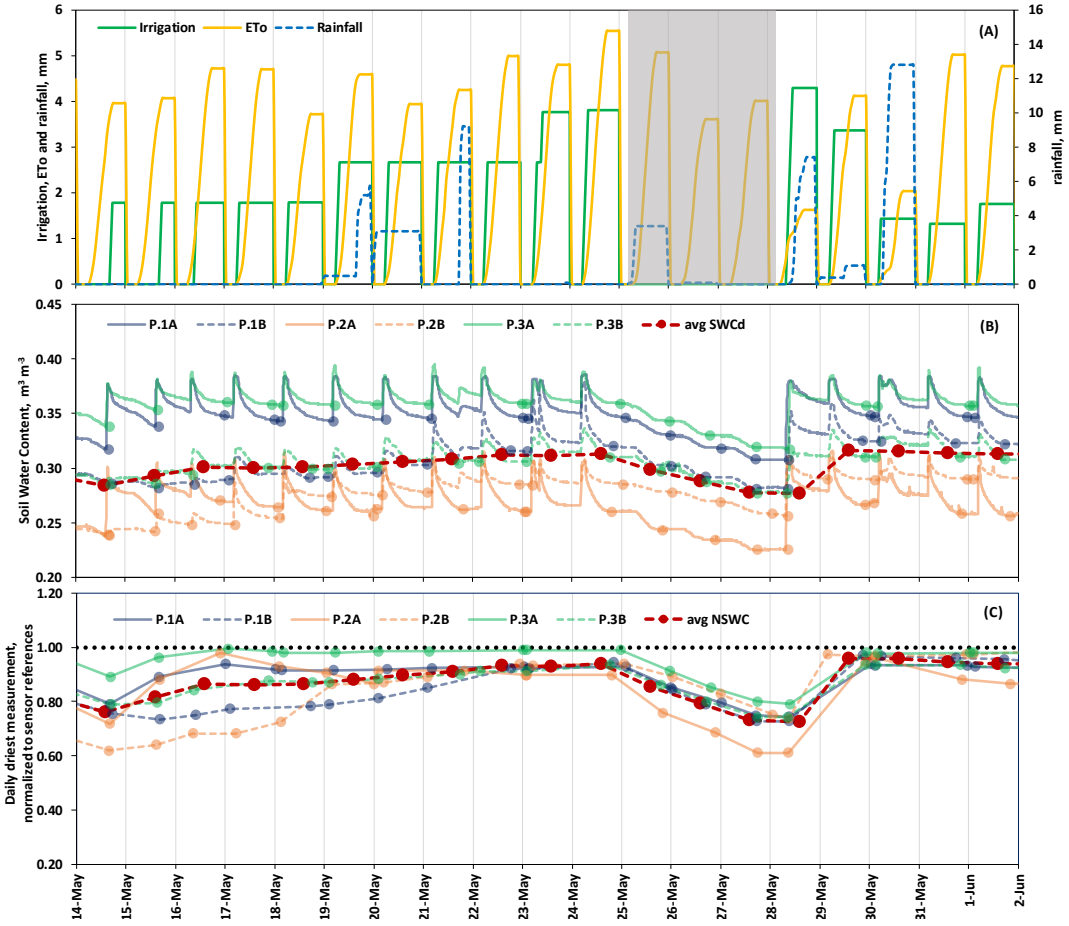

Figure 4. Example of sensor data for the sector AUTO-S in an early part of the season of 2018. (A): irrigation, ET_O and rainfall, and how they accumulate each day. Notice an interruption of irrigation for three days due to an external anomaly, marked in grey. (B): the original soil water content, SWC, recorded by the six soil moisture sensors installed in AUTO-S. On each line, a dot indicates the daily driest measurement, SWC_d. (C): the SWC_d of each sensor normalized to the span between its readings at wilting point and field capacity, NSWC.

Despite the coherent responses of individual sensors to irrigation, rain and water uptake by the crop, a large variation was observed between sensors, which fluctuated with similar patterns but shifted at different positions in the scale of soil water content (SWC). As shown in Figure 4b, the scatter between sensors in SWC was twice as large as the typical fluctuation of a sensor in a daily cycle and, also, larger than the effect of

suppressing irrigation for several days. Sensor-to-sensor variability in the soil moisture recorded by capacitance-type sensors has frequently been reported (Intrigliolo and Castel 2004; Hignett and Evett, 2008; Kizito et al., 2008; Kargas and Soulis, 2011). Such variation could partially be explained by the small volume of soil perceived by a capacitance sensor, around 1 dm^3 in sensor 10HS (Sakaki et al., 2008), whereas the soil electrical permittivity at that scale of observation may vary at different spots as affected by macropores, soil density or stones (Hignett and Evett, 2008). In addition, under conditions of localized irrigation wet bulbs develop below the emitters, determining a very heterogeneous pattern of soil moisture (Samadianfard et al., 2012). To cope with such variability, some authors recommend installing sensors at two or more depths or positions (Dursun and Ozden, 2011; Casadesús et al., 2012; Lea-Cox et al., 2013; Soulis et al., 2015; Domínguez-Niño et al., 2019).

Regarding the interpretation of sensor data, an approach for handling the variability between sensors is to look at the dynamics rather than the absolute readings. IRRIX focuses on the trend of SWC_d (Figure 4b), with the assumption that the driest situation after a cycle of irrigation, redistribution and uptake by roots summarizes the aggregate outcome of those processes. Moreover, the trends of SWC_d in consecutive days may follow the soil water balance and be used for rating the fit between irrigation and the crop water requirements (Casadesús et al., 2012). Besides its dynamics, another informative trait of SWC_d is its relative position within the particular span of measurements by that sensor, which can be specified by normalizing the value of SWC_d between the readings of that sensor at wilting point and field capacity (Figure 4c). Hence, one normalized, the dataset including different sensors can offer a more straightforward view of the soil water dynamics than the original readings, whose overall pattern may be partly obscured by the variability in the baseline of each sensor. Additionally, as it can be observed in this example, variability between sensors was highest when the average soil moisture was lowest, and that the variability was reduced at higher soil moisture, specially following rain. This observation may endorse the interpretation that, under localized irrigation, short irrigation doses can cause larger variability because while some spots can still be wetted, the shrunk wet bulbs leave some spots outside the wetted volume. Swelled bulbs may re-include those spots and the sensors there and, hence, reduce their variability. Accordingly, aggregation of the different sensors once normalized may offer a sounder basis for decision making compared with the direct readings.

3.2. Applied irrigation

Overall, the seasonal amount of irrigation applied in AUTO-L was similar to that applied by an expert using water balance in the MANUAL treatment, and similar also to the ET_C measured by the lysimeter, while AUTO-S applied 24 % less irrigation (Figure 5). In 2017, AUTO-L applied a total irrigation volume of 666.0 mm, similar to MANUAL (only differed by a 1.0%), while in 2018, AUTO-L irrigated 724.7 mm, 4.9 % more than

MANUAL. In both years, AUTO-S applied lower doses than AUTO-L (23.7 % and 27.2 % less in 2017 and 2018, respectively) and MANUAL (24.5 % and 23.4 % less in the year 2017 and 2018, respectively). The seasonal amount of irrigation applied in AUTO-L was in agreement with the ET_C measured by the lysimeter (differences of 6.1 % and 0.9 % in the years 2017 and 2018 respectively), while the irrigation in AUTO-S was considerably lower than the ET_C at the lysimeter (-18.7 % and -27.9 % for the year 2017 and 2018 respectively). Figure 5 shows how those volumes accumulated along the season.

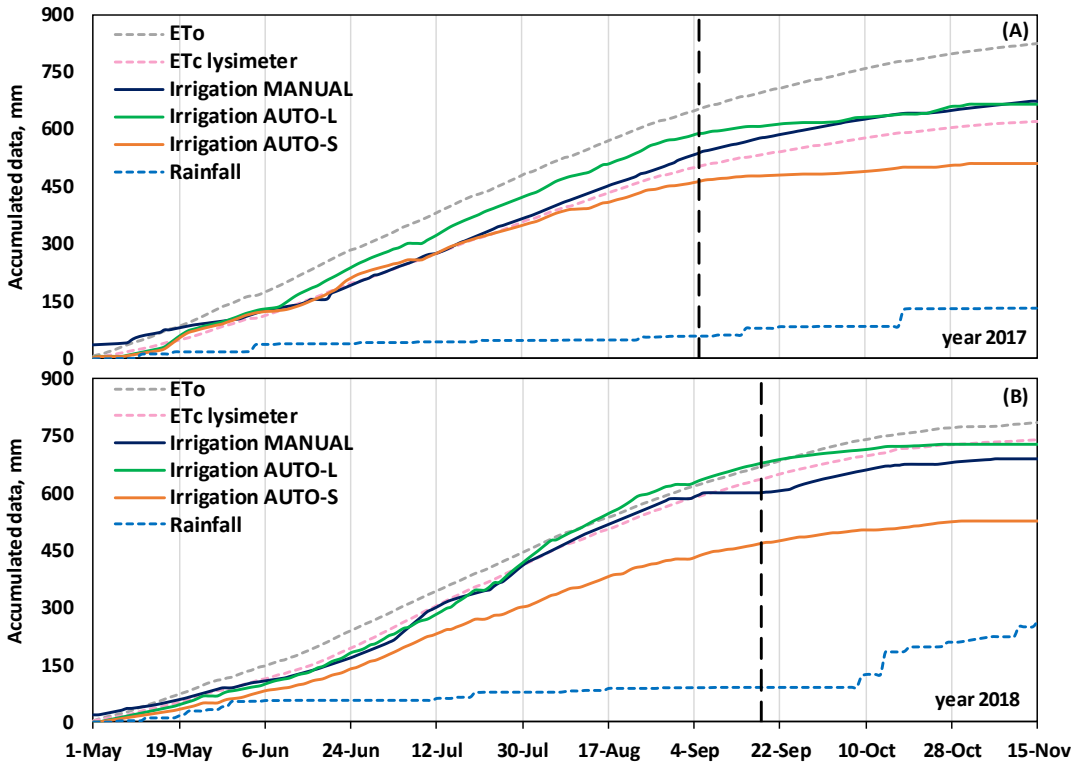

Figure 5. Seasonal accumulated values of ET_O, rain, ET_C and irrigation in 2017 (A) and 2018 (B).

3.3. Response of the automated irrigation scheduling

With a greater detail, the functioning of the automated scheduling is illustrated in Figure 6. The span of time shown in the figure corresponds to the part of the season in 2018 where the irrigation requirements were highest. In that period, the measured ET_O fluctuated between 3.4 and 6.1 mm and ET measured by the lysimeter was slightly higher than ET_O, with an average K_C of 1.03. In both AUTO-L and AUTO-S, IRRIX tried to keep the soil moisture, here expressed as NSWC, within the comfort zone specified in the seasonal plan. However, the observed pattern of soil moisture response to irrigation by these two sectors was different, which caused that they required different adjustments to maintain the comfort zone. AUTO-L used to remain in the lower part of the comfort zone and several times it decreased below the lower limit of comfort. Hence, IRRIX often evaluated that the state of the soil, or its projection for the next days, was "too dry" and it adjusted the irrigation coefficient of AUTO-L upwards. On the other hand, AUTO-S used to remain easily in the upper part of the comfort zone and several

times its moisture level surpassed the upper limit of comfort. Consequently, in those occasions where IRRIX evaluated that the state of the soil, or its projection in the next days, were "too wet", IRRIX adjusted the irrigation coefficient downwards. As a result, within that period, the average irrigation coefficient for AUTO-L was 0.97, and 47.2 % of the time it was above the presumed K_C value. Meanwhile, the irrigation coefficient for AUTO-S was on average 0.75, and most of the time below 1.0, which was the presumed K_C at the time of preparing the seasonal plan. All those adjustments of the irrigation coefficients produced different irrigation doses in the two automated sectors, with average daily doses of 5.6 mm and 4.4 mm in AUTO-L and AUTO-S, respectively, and 73.6 % of the time AUTO-S with a lower irrigation dose than AUTO-L.

Incidentally, within the period shown in Figure 6, a power cut following a small storm in July 20th produced an interruption of irrigation for two days, which triggered different responses in the two automated sectors. In AUTO-L, the lack of irrigation immediately produced a decrease in soil moisture, which stimulated the irrigation coefficient and helped in approaching the comfort zone after the incident. In contrast, in AUTO-S, the soil moisture was maintained probably because the rainfall could compensate the missing irrigation and, furthermore, the next irrigation after this event raised the soil moisture above the comfort zone, causing a decrease in the irrigation coefficient some days later.

These results show how the control algorithm of IRRIX, without using information of tree vigour, applied a differential irrigation because the moisture sensors perceived that soil water was depleted faster in AUTO-L than in AUTO-S. Previous studies at the same site had looked at the effect of tree canopy on irrigation requirements. In particular, lysimeter data from a previous apple plantation showed a strong relationship between FIPAR and K_C (Girona et al., 2011). Using the relationship described in Girona et al. (2011) with the FIPAR measured in this trial, we estimate that K_C at AUTO-S would be 21% below the K_C at AUTO-L. This value fits closely with the response of the automated algorithm in the present study, where the amount of irrigation applied to AUTO-S was 23% lower than the amount applied to AUTO-L.

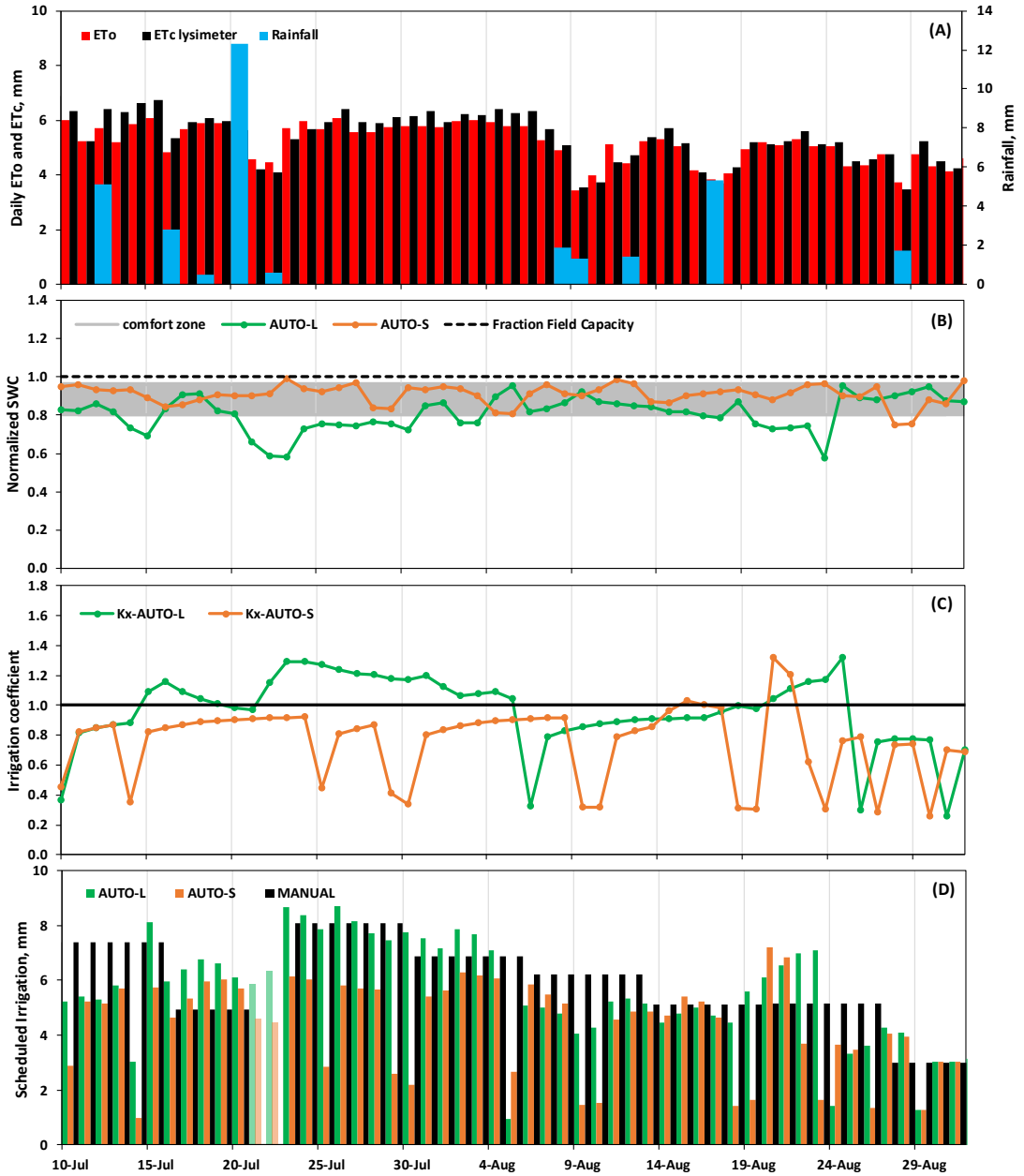

Figure 6. Example of the adaptive response of the automated irrigation scheduling during the period of highest irrigation demand in 2018. (A): ET_O, rainfall and ET_C by a weighing lysimeter with large trees. (B): soil moisture in the two automated sectors, normalized to sensor-specific references, with a grey band indicating the comfort zone configured in IRRIX. (C): response of IRRIX, modulating the irrigation coefficient K_X in the automated sectors. (D): irrigation doses scheduled on each automated sector and by a manual water balance. In 21st and 22nd July the schedules were not applied because of a power cut in the farm. Labels L and S indicate large and small trees, respectively

3.4. Physiological and agronomical results

Measurements of stem water potential were aligned with the values obtained by Girona et al. (2010) (between -0.8 MPa and -1.3 MPa). The measured stem water potential showed slightly more negative values in the smaller trees, regardless of whether irrigation was scheduled automatically or manually (Figure 7). More precisely, during

the year 2017, in MANUAL-L and AUTO-L, the stem water potential remained between -1.3 MPa and -0.7 MPa and in MANUAL-S and AUTO-S they were between -1.5 MPa and -0.7 MPa. During the year 2018, in MANUAL-L and AUTO-L, the stem water potential remained between -1.2 MPa and -0.7 MPa and in MANUAL-S and AUTO-S they were between -1.3 MPa and -0.7 MPa. In the manual treatment, it can be noticed that, even though MANUAL-S received the same irrigation than MANUAL-L, their stem water potential used to be lower. This may be explained by the diagnosed cause of their smaller size, the apple replant disease. That disease affects the root system (Laurent et al., 2010; Singh et al., 2017) and the lower SWP may be a consequence of the limited hydraulic conductance of their root system. Therefore, taking into account the measured SWP and the effect of this disease, the data suggests that trees in AUTO-S were not water-limited by irrigation.

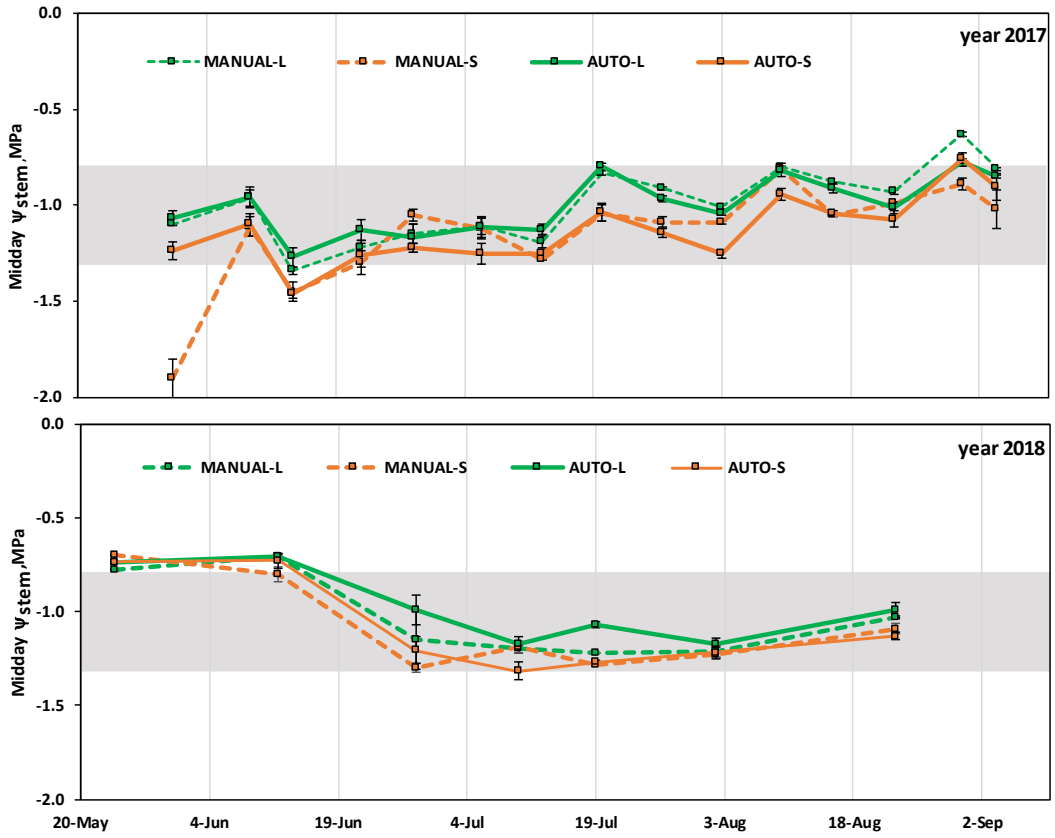

Figure 7. Stem water potential on the different irrigation sectors in 2017 and 2018. AUTO sectors were automated with IRRIX. MANUAL sectors were scheduled by classical water balance. Labels L and S indicate large and small trees, respectively. Error bars indicate the standard deviation. Grey band indicate the acceptable range of stem water potential in non-water limited conditions.

The yield of this apple orchard (Table 3) showed a large variation between the two years of the study, mainly attributed to a poor fruit set in 2017, which was also clearly identified in the whole area. However, no statistical differences were found between treatments for the main productivity indicators when analysing the harvest data for the whole experimental period (Table 3). Because of the commercial thinning practices, no

differences were observed on yield between large and small tress, and more important no statistical significant differences were found on CYI (commercial yield index) and YI (yield index). Therefore, it can be stated that no negative effects of the automated management were observed on yield, either in the larger trees, which were irrigated a similar amount to classical water balance, or in smaller trees, where the automated algorithm saved 23 % of irrigation volume.

Table 3. Analysis of Variance and Mean Separation summary for the orchard yield parameters whole experiment (two years).

		Variables					
	df	**CY**	**FL**	**FFW**	**YI**	**CYI**	**TCSA**
		Signification (Pr > F)					
Model	12	0.0386	0.0461	0.1388	0.0343	0.0856	0.0059
Treatments	3	0.5544	0.0876	0.0077	0.6764	0.1537	0.0001
REP	4	0.9400	0.9855	0.9446	0.5946	0.4044	0.2255
Year	1	0.0001	0.0003	0.3956	0.0001	0.0018	-
Rep * Year	4	0.9034	0.9029	0.4846	0.9889	0.9554	-
		TRT Mean Separation					
MANUAL-L		41826	163	176.6 b	0.648	0.445	40.93 a
AUTO-L		39771	105	213.3 a	0.560	0.435	40.17 a
MANUAL-S		37496	112	177.4 a	0.692	0.588	28.50 b
AUTO-S		34089	96	173.9 b	0.709	0.628	27.38 b
		Year Mean Separation					
2017		28815 b	79 b	181.6	0.431 b	0.401 b	-
2018		47763 a	160 a	188.9	0.873 a	0.648 a	-

CY = Commercial yield (kg·ha^{-1}); **FL** = Fruit Load (fruits·tree^{-1}); **FFW** = Fruit Fresh Weight (kg); **YI** = Yield Index (Total production·CTSA^{-1})(kg·cm^{-2}); **CYI** = Commercial Yield Index (YI·CTSA^{-1}) (kg·cm^{-2}); **TCSA** = Trunk Cross Sectional Area (cm^2); **df** = degrees of freedom; Means within column (within treatments or years) followed by different letters were significantly different at P ≤ 0.05 using Tukey-Kramer adjustment.

3.5. Irrigation scheduling approach

Overall, this study tested the performance of scheduling irrigation through an automated water balance approach tuned by capacitance-type soil moisture sensors. Here, we observed how the adaptive response allowed spontaneous adjustment to a component of the water balance, in this case the low ET associated to low vigour, that had not been considered in the original configuration of the water balance. This experience may exemplify the capacity of this approach to confront site-specific conditions that would be difficult to parameterize in a deterministic model. As another example, a previous version of the algorithm showed a spontaneous adaptation to the presence of groundwater (Casadesús et al., 2014), which would otherwise be omitted in the management of irrigation.

Regarding the choice for a base scheduling method, the water balance approach provides an effective method for fitting irrigation to the encountered weather conditions (Allen et al., 1998). While irrigation controllers based on water balance are commercially

available for turfgrass (Davis and Dukes, 2014), their application to orchards would be more complicated because of the much larger uncertainty of crop coefficients. That uncertainty was solved here through feedback from sensors, which provided an empirical site-specific adjustment of the ratio of irrigation to ET_O. Other alternative sensor-based approaches use predefined thresholds either to trigger irrigation when the soil is too dry (Dukes and Scholberg, 2005; Osroosh et al., 2016; Vera et al., 2019) and/or to bypass a timer-triggered irrigation when the soil is too wet (Smajstrla and Locascio, 1996; Cáceres et al., 2007; Muñoz-Carpena et al., 2008). Some advantages of water balance tuned by sensors are that its response is smoother and more predictable than occasional switching on/off valves. Additionally, it allows modulating the daily irrigation depth of each sector without disturbing the hydraulic scheme for the whole farm, while irrigation triggered directly by sensors can switch valves on at arbitrary times, complicating the operation of the farm's hydraulic system.

4. Conclusions

The results of this trial show the feasibility of automated sensor-based scheduling of irrigation in orchards. The algorithm, based on the approach of water balance and tuned locally through feedback from sensors, provided precise irrigation doses along the season, adapting itself to weather conditions and to the seasonal vegetation cycle of the crop.

Capacitance sensors have successfully been used to provide automated feedback to the scheduling algorithm. In spite of the observed sensor-to-sensor variability – comparable with that reported by other authors – the approach followed here allows a consistent mechanism for their unmanned interpretation and integration with decision-making. First, the summarization of the daily fluctuation of soil water content on the daily driest measurement focuses the analysis on a simple parameter whose day-to-day dynamics retains much of the information on the fit between irrigation and the crop water demand. Second, the sensor-specific normalization of those daily values reduces the scatter between sensors and brings a more intelligible dataset on which to base automate control. This trial shows how the irrigation doses determined by the algorithm are aligned with the ET measured on the same orchard by a weighing lysimeter. The irrigation doses applied by the automated approach are also comparable with those by a skilled irrigation technician though requiring less labour effort. Furthermore, the tested algorithm adapts itself to heterogeneous tree vigour, applying less irrigation to sectors with smaller trees in a proportion that fits previous lysimeter studies on the relationship between K_C and FIPAR. Therefore, this indicates that the algorithm could be suitable for horticultural application, where adaptation to site-specific vigour are a common concern.

Acknowledgments

This research was supported by the Spanish National Institute for Agricultural and Food Research and Technology (INIA) (RTA2013- 00045-C04-01 and RTI2018-099949-R-C21) of the Ministry of Economy and Competitiveness of the Spanish government and by the European Social Fund. The authors are grateful to Mercè Mata and Jesús del Campo, part of the staff of the Efficient Use of Water in Agriculture Program, for their support in implementing this activity.

Literature cited

Allen, R. G.; Pereira, L. S.; Raes, D.; Smith, M. Crop evapotranspiration. Guidelines for computing crop water requirements. FAO irrigation and drainage paper 56, 1998. Rome.

Auzmendi, I.; Mata, M.; Lopez, G.; Girona, J.; Marsal, J. Intercepted radiation by apple canopy can be used as a basis for irrigation scheduling. Agric. Water Manag. 2011, 98, 886-892.

Ayars, J. E.; Johnson, R. S.; Phene, C. J.; Trout, T. J.; Clark, D. A.; Mead, R. M. Water use by drip-irrigated late-season peaches. Irrigation Sci. 2003, 22, 187-194.

Bacci, L.; Battista, P.; Rapi, B. An integrated method for irrigation scheduling of potted plants. Sci. Hortic. 2008, 116, 89-97.

Bogena, H.; Huisman, J.; Schilling, B.; Weuthen, A.; Vereecken, H. Effective calibration of low-cost soil water content sensors. Sensors 2017, 17, 208.
Cáceres, R.; Casadesús, J.; Marfà, O. Adaptation of an automatic irrigation-control tray system for outdoor nurseries. Biosyst. Eng. 2007, 96, 419-425.

Campbell, J. E. Dielectric properties and influence of conductivity in soils at one to fifty megahertz. Soil Sci. Soc. Am. J. 1990, 54, 332-341.

Casadesús, J.; Mata, M.; Marsal, J.; Girona, J. Automated irrigation of apple trees based on measurements of light interception by the canopy. Biosyst. Eng. 2011, 108, 220-226.

Casadesús, J.; Mata, M.; Marsal, J.; Girona, J. A general algorithm for automated scheduling of drip irrigation in tree crops. Comput. Electron. Agric. 2012, 83, 11-20.

Casadesús, J.; Mata, M.; Marsal, J.; Girona, J. Spontaneous accommodation of irrigation scheduling to groundwater through feedback from soil water sensors in drip irrigated peach. Acta Hortic. 2014, 1038, 207-213.

Cote, C. M.; Bristow, K. L.; Charlesworth, P. B.; Cook, F. J.; Thorburn, P. J. Analysis of soil wetting and solute transport in subsurface trickle irrigation. Irrig. Sci. 2003, 22, 143-156.

Daccache, A.; Knox, J. W.; Weatherhead, E. K.; Daneshkhah, A.; Hess, T. M. Implementing precision irrigation in a humid climate–Recent experiences and on-going challenges. Agric. Water Manag. 2015, 147, 135-143.

Davis, S. L.; Dukes, M. D. Methodologies for successful implementation of smart irrigation controllers. J. Irrig. Drain. Eng. 2014, 141, 04014055.

Domínguez-Niño, J.M.; Bogena, H.R.; Huisman, J.A.; Schilling, B.; Casadesús, J. On the accuracy of factory-calibrated low-cost soil water content sensors. Sensors 2019, 19, 3101.

Doorenbos, J.; Pruitt, W. O. Guidelines for predicting crop water requirements. FAO irrigation and drainage Paper 24, 1997, Rome.

Dukes, M.D.; Scholberg, J.M. Soil moisture controlled subsurface drip irrigation on sandy soils. Appl. Eng. Agric. 2005, 21, 89-101.

Dursun, M.; Ozden, S. A wireless application of drip irrigation automation supported by soil moisture sensors. Sci. Res. Essays. 2011, 6, 1573-1582.

Elmaloglou, S.; Soulis, K. X.; Dercas, N. Simulation of soil water dynamics under surface drip irrigation from equidistant line sources. Water Resour. Manag. 27, 4131-4148.Evett, S. R.; Heng, L. K.; Moutonnet, P.; Nguyen, M.L., 2008. Field estimation of soil water content: A practical Guide to methods, instrumentation and sensor technology, IAEA, Direct and surrogate measures of soil water content, 2013, Vienna, pp. 1-21.

Evett, S. R.; Schwartz, R. C.; Tolk, J. A.; Howell, T. A. Soil profile water content determination: Spatiotemporal variability of electromagnetic and neutron probe sensors in access tubes. Vadose Zone J. 2009, 8, 926-941.

Girona, J.; Marsal, J.; Mata, M.; del Campo, J. Pear crop coefficients obtained in a large weighing lysimeter. Acta Hortic. 2004, 664, 277-281

Girona, J.; Behboudian, M. H.; Mata, M.; Del Campo, J.; Marsal, J. Exploring six reduced irrigation options under water shortage for 'Golden Smoothee' apple: responses of yield components over three years. Agr. Water Manage. 2010, 98, 370-375.

Girona, J.: Del Campo, J.; Mata, M.; Lopez, G.; Marsal, J. A comparative study of apple and pear tree water consumption measured with two weighing lysimeters. Irrig. Sci.

2011, 29, 55-63.

Hao, A.; Marui, A.; Haraguchi, T.; Nakano, Y. Estimation of wet bulb formation in various soil during drip irrigation. J. Fac. Agr. Kyushu U. 2007, 52, 187.

Hargreaves, G. H.; Samani, Z. A. Reference crop evapotranspiration from temperature. Appl. Eng. Agric. 1985, 1, 96-99.

Higgins, S. S.; Larsen, F. E.; Bendel, R. B.; Radamaker, G. K.; Bassman, J. H.; Bidlake, W. R.; Al Wir, A. Comparative gas exchange characteristics of potted, glasshouse-grown almond, apple, fig, grape, olive, peach and Asian pear. Scientia Hortic. 1992, 52, 313-329.

Hignett, C.; Evett, S. Field Estimation of Soil Water Content. A Practical Guide to Methods, Instrumentation and Sensor Technology, in: IAEA, Eds., Direct and surrogate measures of soil water content**.** Training Course Series No. 30, 2008, Vienna, pp. 1-22.

Intrieri, C.; Poni, S.; Rebucci, B.; Magnanine, E. Row orientation effects on whole-canopy gas exchange of potted and field-grown grapevines. Vitis. 1998, 37, 147-154.

Intrigliolo, D. S.; Castel, J. R. Continuous measurement of plant and soil water status for irrigation scheduling in plum. Irrig. Sci. 2004, 23, 93-102.

Irmak, S.; Djaman, K.; Rudnick, D. R., 2016. Effect of full and limited irrigation amount and frequency on subsurface drip-irrigated maize evapotranspiration, yield, water use efficiency and yield response factors. Irrig. Sci. 34, 271-286.

Kargas, G.; Soulis, K. X. 2011. Performance analysis and calibration of a new low-cost capacitance soil moisture sensor. J. Irrig. Drain. Eng. 138, 632-641.

Kargas, G.; Soulis, K. X., 2019. Performance evaluation of a recently developed soil water content, dielectric permittivity, and bulk electrical conductivity electromagnetic sensor. Agric. Water Manag. 213, 568-579.

Kizito, F.; Campbell, C. S.; Campbell, G. S.; Cobos, D. R.; Teare, B. L.; Carter, B.; Hopmans, J. W. Frequency, electrical conductivity and temperature analysis of a low-cost capacitance soil moisture sensor. J. Hydrol. 2008, 352, 367-378.

Kojima, Y.; Shigeta, R.; Miyamoto, N.; Shirahama; Y.; Nishioka, K.; Mizoguchi, M.; Kawahara, Y. Low-cost soil moisture profile probe using thin-film capacitors and a capacitive touch sensor. Sensors 2016, 16, 1292.

Laurent, A. S.; Merwin, I. A.; Fazio, G.; Thies, J. E., Brown, M. G. Rootstock genotype succession influences apple replant disease and root-zone microbial community composition in an orchard soil. Plant Soil 2010, 337, 259-272.

Lazarovitch, N.; Warrick, A. W.; Furman, A.; Šimůnek, J. Subsurface water distribution from drip irrigation described by moment analyses. Vadose Zone J. 2007, 6, 116-123.

Lea-Cox, J. D.; Bauerle, W. L.; van Iersel, M. W.; Kantor, G. F.; Bauerle, T. L.; Lichtenberg, E.; King, D.M.; Crawford, L. Advancing wireless sensor networks for irrigation management of ornamental crops: An overview. HortTechnology 2013, 23, 717-724.

Marsal, J.; Girona, J.; Casadesús, J.; Lopez, G.; Stöckle, C. O. Crop coefficient (K_C) for apple: comparison between measurements by a weighing lysimeter and prediction by CropSyst. Irrig. Sci. 2013, 31, 455-463.

Marsal, J.; Johnson, S.; Casadesús, J.; Lopez, G.; Girona, J.; Stöckle, C. Fraction of canopy intercepted radiation relates differently with crop coefficient depending on the season and the fruit tree species. Agric. For. Meteorol. 2014, 184, 1-11.

McCutchan, H.; Shackel, K.A. Stem water potential as a sensitive indicator of water stress in prune trees (Prunus domestica L. cv. French.). J. Am. Soc. Hortic. Sci. 1992, 117, 607-611.

Mittelbach, H.; Lehner, I.; Seneviratne, S. I. Comparison of four soil moisture sensor types under field conditions in Switzerland. J. Hydrol. 2012, 430, 39-49.

Muñoz-Carpena, R.; Dukes, M. D.; Li, Y. C.; Klassen, W. Field comparison of tensiometer and granular matrix sensor automatic drip irrigation on tomato. Horttechnology, 2005, 15, 584-590.

Nafchi, R. F.; Mosavi, F.; Parvanak, K. Experimental study of shape and volume of wetted soil in trickle irrigation method. Afr. J. Agr. Res. 2011, 6, 458-466.

Naor, A.; Naschitz, S.; Peres, M.; Gal, Y. Responses of apple fruit size to tree water status and crop load. Tree Physiol. 28, 2008, 1255-1261.

Osroosh, Y.; Peters, R. T.; Campbell, C. S.; Zhang, Q. Comparison of irrigation automation algorithms for drip-irrigated apple trees. Comput. Electron. Agric. 2016, 128, 87-99.

Rolston, D.E.; Biggar, J.W.; Nightingale, H.I. Temporal persistence of spatial soil-water patterns under trickle irrigation. Irrig. Sci. 1991, 12, 181–186.

Sakaki, T.; Limsuwat, A.; Smits, K. M.; Illangasekare, T. H. Empirical two-point α-mixing model for calibrating the ECH2O EC-5 soil moisture sensor in sands. Water Resour. Res. 2008, 44.

Smajstrla, A.G.; Locascio S.J. Tensiometer-controlled drip irrigation scheduling of tomato. Appl. Eng. Agr. 1996, 12, 315–319.

Samadianfard, S.; Sadraddini, A. A.; Nazemi, A. H.; Provenzano, G.; Kisi, O. Estimating soil wetting patterns for drip irrigation using genetic programming. Span. J. Agric. Res. 2012, 1155-1166.

Singh, J.; Lo, T.; Rudnick, D. R.; Dorr, T. J.; Burr, C. A.; Werle, R.; Shaver, T.M.; Muñoz-Arriola, F. Performance assessment of factory and field calibrations for electromagnetic sensors in a loam soil. Agric. Water Manag. 2018, 196, 87-98.

Singh, N.; Sharma, D. P.; Kumar, V. Managing apple replant disease: the effect of rootstocks and soil treatments on tree performance and biological activities. J. Pharmacogn. Phytochem. 2017, 6, 2554-2559.

Smith, M.; Pereira, L.S.; Berengena, J.; Itier, B.; Goussard, J.; Ragab, R.; Tollefson, L. Van Hoffwegen, P. (Eds.). Irrigation Scheduling: From Theory to Practice. FAO Water Report 8, FAO, 1996, Rome, 384 pp.

Soulis, K. X.; Elmaloglou, S.; Dercas, N. Investigating the effects of soil moisture sensors positioning and accuracy on soil moisture based drip irrigation scheduling systems. Agric. Water Manag. 2015, 148, 258-268.

Vera, J.; Conejero, W.; Conesa, M. R.; Ruiz-Sanchez, M. C. Irrigation factor approach based on soil water content: A nectarine orchard case study. Water 2019, 11, 589

Visconti, F.; de Paz, J. M.; Martínez, D.; Molina, M. J. Laboratory and field assessment of the capacitance sensors Decagon 10HS and 5TE for estimating the water content of irrigated soils. Agric. Water Manag. 2014, 132, 111-119.

Wu̇nsche, J. N.; Lakso, A. N.; Robinson, T. L. Comparison of four methods for estimating total light interception by apple trees of varying forms. HortScience 1995, 30, 272-276.

Wu̇nsche, J. N.; Palmer, J. W; Greer, D. H. Effects of crop load on fruiting and gas-exchange characteristics of 'Braeburn'/M. 26 apple trees at full canopy. J. Am. Hortic. Sci. 2000, 125, 93-99

GENERAL DISCUSSION

In the present PhD thesis the soil water dynamics in localized irrigation and the response of capacitance soil moisture sensors were characterized in order to understand and optimize the use of these sensors in irrigation scheduling.

Chapter I evaluated the suitability of performing sensor and soil-specific calibrations instead of using the factory calibration. The two-step calibration approach allowed the soil water content measured by the 10HS capacitance sensors to be more accurate than the factory calibration.

In the first calibration step, sensor response was related with dielectric permittivity using media with well-defined permittivity and an appropriate sensor response permittivity (SRP) model. When we used a universal SRP model, the overall RMSE for the apparent dielectric sensor permittivity, K_a, and equivalent soil water content, θ_{eq}, were 1.42 and 1.21 vol.% When we used a universal SRP model, the overall RMSE for the apparent dielectric sensor permittivity, K_a, and equivalent soil water content, h_e, were 1.42 and 1.21 vol.% respectively. Rosenbaum et al. (2010) obtained a similar RMSE for K_a with values between 1.2 and 1.5 for 5TE and EC-5 capacitance sensors, respectively. However, Bogena et al. However, Begena et al. (2017), who used SMT-100 sensors, improved the results with an RMSE for K_a of 0.87 and an RMSE for θ_{eq} of 0.95 vol.%. When we used a specific calibration, the RMSE improved to respective values of 0.43 and 0.64 vol.%. Other authors such as Sakaki et al. (2008), who used EC-5 sensors, found a similar accuracy for dry sand (RMSE = ± 0.5 vol.%) and a lower accuracy for saturated sand (RMSE = ± 2.8 vol.%), whereas Rosembaum et al. (2010) found a lower accuracy with an RMSE of 0.80 and 1.40 vol.%. However, Qu et al. (2013) managed to improve results to an RMSE of 0.23 and 0.40 vol.% when using SPADE sensors.

In the second calibration step, the apparent dielectric permittivity and soil water content were related using undisturbed soil samples and TDR measurements. The Topp model (Topp et al., 1980) was used, which only considers the measured apparent dielectric permittivity (K_a), as well as different variants of the CRIM model (Birchak et al., 2014), which additionally considers the dielectric permittivity of solid phase (K_s), porosity (η), the dielectric permittivity of the air (K_{air}) and the temperature dependent dielectric permittivity of water (K_w). The best option was the CRIM model variant which considers mean porosity per soil and depth and fits the K_s for each soil and depth, achieving an RMSE of 1.37 vol.%. These results improved the accuracy of the results obtained by Robinson et al. (1998), who evaluated Wet2, 5TE and 10HS sensors in soil with variable texture and obtained an RMSE between 3.4 and 7.3 vol.%. In addition, other authors who used the CRIM model such as Rosenbaum et al. (2012) and Qu et al. (2016) obtained higher RMSE values of 2.9 vol.% and 2.2-28 vol.%. After the two calibration steps had been carried out separately, they were combined (SRP model + CRIM model)

to obtain sensor response-SWC relationships and the results were then compared with those of factory calibration. As in Spelman et al. (2013), the predicted factory SWC was substantially higher than the SWC obtained using the two-step calibration. To confirm this difference, an experiment was conducted to compare the volumetric SWC determined gravimetrically with the SWC determined by 10HS sensors using factory calibration and the SRP model combined with the Topp equation (Topp et al., 1980). According to the results we obtained, the factory calibration RMSE was five times higher than that obtained by a two-step calibration (5.33 vol.% versus 1.03 vol.%). Fares et al. (2013), who studied the effect of organic matter on SWC by 10HS sensors, obtained factory calibration results (RMSE = 5.3 – 7.2 vol. %) in agreement with our results, although when they used the two-step calibration they obtained a lower accuracy than us (RMSE = 1.3-1.0 vol.%). Matula et al. (2016), who used soil media with different bulk density, also found similar results for various ECH$_2$O sensors (RMSE factory calibration = 3.3 vol.% and RMSE two-step calibration = 1.3 vol.%). These comparisons confirmed the high accuracy of the two-step calibration method and the limited accuracy of factory calibration for 10HS sensors.

The two-step sensor calibration produces repetitive readings between sensors (Domínguez-Niño et al., 2019, Rosenbaum et al., 2010) and improves SWC measurement accuracy. However, when the sensors are installed in a drip-irrigated orchard, even if arranged in equivalent positions, the improvement due to calibration is minimal because the SWC readings are affected by other factors of higher variability (Nagahage et al., 2019). In our study, as indicated in ***Chapter III,*** measurements with the TDR Fieldscout 300 were one of the factors that generated fluctuations in the SWC readings in a drip-irrigated orchard of the wet area under the dripper, which had variability in its size, shape and alignment to the dripper (RMSE: 0.05 $cm^3\ cm^{-3}$ at the depth of 15 cm and 0.02 $cm^3\ cm^{-3}$ at the depth of 60 cm). Soil temperature, both in depth and in relative distance to the dripper, also affected the sensor readings. This effect was higher at shallow and sunlit positions and lower at deeper and shaded positions. As Rosenbaum et al. (2011) also observed, in our work the temperature differences mainly affected the readings of the EC-5 sensors, whereas the effect on the 10HS sensors was less clear. In addition, with a sensitivity range of 10HS sensors of about 1 L, any spatial properties such as the presence of macropores and gravels (Rowland et al., 2011), microvariations in density (Parvin and Degré, 2016), uneven root distribution (Kang et al., 2019) or uneven soil temperature distribution (Gonzalez-Teruel et al., 2019) can cause variations in SWC measurements.

In ***Chapter II,*** the HYDRUS 3D model was parametrised using soil hydraulic parameters obtained from Rosetta and HYPROP + WP4C models from undisturbed soil

samples. Firstly, the model was adjusted on a daily basis using neutron probes located in different positions around the dripper and, later, the simulations were validated on a daily and hourly basis using a neutron probe and tensiometers.

The neutron probe SWC measurements in different moments of the year were compared with HYDRUS-3D simulations. First, the soil hydraulic parameters obtained from Rosetta were used and found to be valid for general trends, achieving good agreement especially in positions near the wetting pattern and at 40-60 cm depth (R^2 = 0.94). However, the simulations showed an overestimation of the SWC (RMSE = 0.62 cm^3 cm^{-3}) and low prediction of the model. Overall, when HYDRUS-3D simulations used the soil hydraulic parameters from Rosetta, the K_s was underestimated and resulted in slow water drainage and SWC closer to saturation. One of Rosetta's limitations was the imprecision of the soil hydraulic parameters obtained as the model was designed for temperate zone soils (Bastet et al., 1999) and gave more importance to the texture of the soil than to its structure and mineralogy (Carsel and Parrish, 1988, Wösten et al., 1999).

Secondly, the combination of the HYPROP + WP4 model was used to predict the soil hydraulic parameters. Even use of the uncalibrated model achieved high accuracy between the SWC measured by the neutron probe and predicted by HYDRUS-3D simulations. A high correlation was achieved in the wetting pattern zone influence at 40-60 cm depth (R^2 = 0.94), with a low RMSE = 0.02 cm^3 cm^{-3} but a low predictive power of the model (NSE = 0.37). To improve the results, a sensitivity analysis of the different soil hydraulic parameters was carried out. In principle, the best parameters for adjustment were the θ_s and the shape parameter *n*. However, it was decided not to modify the soil hydraulic parameter θ_s as it is a particular characteristic of the soil, but to modify the *n* parameter as it is related with the pore-size distribution (Marković et al., 2015). This parameter was obtained by fitting the experimental data. The fit of the *n* parameter resulted in a model capable of representing the soil water dynamics, valid for different depths and positions in drip-irrigated orchards, achieving an acceptable agreement between the simulated HYDRUS-3D SWC and the neutron probe-measured SWC. The best fit took place in the area close to the drippers, where the wet bulbs were generated and there was more root activity. This is in line with the results obtained in ***Chapter III,*** in which sensor repeatability was analysed and it was found that the HYDRUS-3D simulations had acceptable RMSE values in the centre of the wet bulb and in the mid-point between two drippers. This was due to HYDRUS-3D generating homogeneous SWC within the wet bulb and representing more idealized and smooth soil surface conditions. However, as we move away from the dripper, the fit between measured and simulated SWC values decreased. This may be due to other phenomena such as water uptake by weeds (Bravdo and Proebsting, 1993) or assuming the SWC to be at field capacity. As described in ***Chapters III*** and ***IV***, the SWC measurements with capacitance

sensors at the beginning of the year indicated a lower SWC in these positions. With respect to the effect of depth, between 0 and 20 cm HYDRUS-3D calibration was not required due to the good agreement between the SWC values of the HYDRUS-3D simulations and the neutron probe measurements. However, calibration was applied between the 40-100 cm depths, with the best agreement obtained between 40 and 60 cm. Deeper than 60 cm the agreement was lower, since at these depths the soil hydraulic properties were considered to be those determined with the HYPROP+WP4C model at the depths of 40 and 60 cm. The positions and depths most accurately simulated by HYDRUS-3D were located close to the dripper at the depths of 40-60 cm ($R^2 > 0.92$, RMSE < 0.01 cm^3 cm^{-3} and NSE > 0.87). This finding was relevant because later, as discussed in ***Chapter IV***, this will be the soil region of greatest interest for controlling drip irrigation.

Chapter III described the variability in the measurements by capacitance soil water sensors installed at different depths and positions in an actual orchard irrigated with drippers. First, it analyses the uncertainties in the measurement process in relation with the natural variability of the soil water dynamics in this type of scenario. Second, the HYDRUS-3D model calibrated and validated in Chapter II is used as a reference for the expected patterns of soil-water distribution. However, characterization of the soil area wetted by drippers reveals large variability of SWC at the uppermost 12 cm of the soil which, departs from the idealized patterns. This chapter compares those uncertainties and variabilities looking for an explanation for the observed sensor-to-sensor differences.

There was high variability in the SWC monitored with capacitance soil sensors. In contrast, the simulated wet bulbs are idealised as the model does not consider local variations including, amongst others, gravel content, macropores, shrinkage cracks or compacted soil fragments (Dane and Hopmans, 2002). However, the wet bulbs generated in the field are irregular. This was evidenced by the variability in the size, shape and alignment of the wetted areas. In addition, there was variability in the sensor measurements as a result of various factors such as sensor calibration, soil temperature and sensor location. Both sensors and simulations showed large SWC amplitude in the center of the wet bulb and at the mid-point position between two drippers at the depth of 30 cm. However, in the center of the wet bulb at the depth of 15 cm, the HYDRUS simulations results were one third of those recorded by the sensors, which had a more intense drop. In the perimeter of the wetted area most sensors showed a faint oscillation, whilst in the simulations the oscillations were more intense. In addition, the HYDRUS-3D model and the capacitance-type moisture sensors were affected by the timing of irrigation, and their SWC patterns varied depending on the time of the day when the irrigation was applied (morning, evening or split in two pulses).

The repeatability between sensors was high in laboratory conditions, whereas when

these sensors were installed in the field, the variability increased due to the factors mentioned above. In general, the HYDRUS simulations showed greater repeatability due to the homogeneous distribution of SWC in the wet bulb. Only the virtual sensors located in the perimeter of the wet bulb showed greater sensitivity.

Sensor sensitivity at the location where they are installed depends on soil hydraulic properties, meteorological conditions and the irrigation configuration (Soulis et al., 2015). The sensors installed in the center of the wet bulb position, especially at the depth of 15 and 30 cm, responded fast and intensively to the irrigation, with little memory of the soil water trends a few days earlier. These sensors responded to the water balance of the same day but were not sensitive to the water balance of the previous week. The sensors installed at the mid-point position between two drippers were sensitive to both the water balance of the day and that of the previous week, especially at the depth of 30 cm. This sensitivity may be explained by the effect of the water balance of several days or by the overlapping or recession of two neighboring wet bulbs. The sensors installed in the perimeter position of the wetted area at the depth of 15 cm were sensitive to the water balance of the previous week but not to that of the last day, while the sensors located at the depths of 30 and 60 cm retained a memory of the water balance of that day and the previous week. The sensors installed in the perimeter position of the wetted area at the depth of 15 cm were sensitive to the water balance of the previous week but not to that of the last day, while the sensors located at the depths of 30 and 60 cm retained a memory of the water balance of that day and the previous week. This situation may be attributable to the sensors in these positions being located on the periphery of the wetted area and only being affected by the dynamics of a single wet bulb. This difference in sensitivity was also observed in the HYDRUS-3D simulations. Actual sensor measurements at the mid-point position between two drippers at the depths of 15 and 30 cm seem more sensitive to the aggregated balance than simulations. When compared to simulations, some sensor locations (mid-point position between two drippers at the depth of 60 cm, perimeter of the wet area at the depth of 15 cm and outside the influence at the depth of 30 cm) are less sensitive to the last irrigation and more sensitive to the aggregated balance. This may be due to the actual noise of the irrigation cycles at these spots, while the effect of the accumulated balance is more straightforward.

In drip irrigation, the non-uniform distribution patterns make soil water sensor placement a key factor in automated irrigation scheduling (Coelho and Or, 1996). The plant root architecture around the drippers also complicates the decision about where to place moisture sensors (Or, 1995). Therefore, when installing capacitive-type moisture sensors, it is important to consider the following characteristics: sensor-to-sensor repeatability, the representativity of the overall soil water availability to the crop, and the ability of sensor location to match irrigation doses and actual irrigation needs. The

balance between these characteristics is dependent on the purpose and type of usage of these sensors in the orchard. In our particular case, as detailed in ***Chapter IV***, the sensors were used for automated irrigation scheduling and, in this particular case, prioritization was given to robustness and sensitivity to changes in the soil water budget. In addition, when sensors are used for irrigation control, the criteria for sensor location also depends on the control algorithms. In this respect, if the control algorithm is based on thresholds for activating/deactivating irrigation pulses (Dukes et al., 2010; Muñoz-Carpena et al., 2005) the criteria may differ from when the algorithm consists of a water balance tuned by sensors (Casadesus et al., 2012; Domínguez-Niño et al., 2020). Finally, our study suggests that, to provide feedback to an irrigation scheduling algorithm based on a water balance tuned by sensors (Domínguez-Niño., 2020), it is convenient to install one sensor close to the center of the wet bulb position at the depth of 30 cm and another at the mid-point position between two neighboring drippers at the depth of 30 cm to provide useful and complementary information. The moisture sensors aligned with the dripper provided an immediate response to the cycles of irrigation and water uptake by roots, whereas the sensors between two drippers tended to display a slower dynamic which better represents the aggregated balance of the preceding period of several days. In our results, the best performing depth of 30 cm coincided with the peak root activity. Other depths seem less favorable, with sensors at 15 cm being the least repeatable and sensors at 60 cm depth the least responsive to the irrigation cycles. These sensor locations were then used in ***Chapter IV*** to automate irrigation scheduling.

Chapter IV determined the feasibility of using capacitance soil sensors in automated irrigation scheduling in a drip-irrigated apple orchard. In this trial, the sensors were used as the only source of data for the spontaneous adjustment of a water balance model to the site-specific conditions of on orchard containing two plots that differed in tree vigour.

The automated system recorded soil moisture and weather data from the field. Later, the web platform for irrigation (IRRIX), designed by Casadesús et al. (2012), automatically interpreted the capacitance sensor data and used the feedback from sensors to adjust the irrigation doses of each plot according to the previously established seasonal plan. Basically, the automated interpretation of sensor data focused on the trend of the daily minimum and its distance to field capacity. An upward trend was interpreted as a positive water balance and a downward trend as a negative water balance. The results showed that without using information about tree vigour, IRRIX applied differential irrigation to the plots and provided 23% more irrigation to the trees with higher vigour because the moisture sensors perceived that the soil water content decreased faster than in the trees with lower vigour. Furthermore, despite the difference in vigour between treatments, there were no differences in stem water potential values,

which were in agreement with values obtained by Girona et al. (2010). On the other hand, in classical procedures for determining the irrigation schedule, it is necessary to know the ETo and the Kc, which is quite uncertain. Previous studies carried out by Girona et al. (2011), Auzmendi et al. (2011) and Marsal et al. (2013) established a high relationship between the crop coefficient and solar radiation intercepted by the canopy in the same apple orchard. In addition, Casadesus et al. (2011) evaluated the automated application of irrigation according to the daily amount of solar radiation intercepted by the canopy. Using the approach of Girona et al. (2011), it was found that the Kc of the low vigour trees was 21% lower than the high vigour trees, a similar value than that applied by IRRIX to the low vigour trees plot of our study, based exclusively on its response to the soil moisture sensors. Furthermore, the IRRIX web platform was used by Millán et al. (2019) and Millán et al. (2020) in a Japanese plum crop and hedgerow olive orchard, and the amount of manually and automatically applied irrigation was similar. In addition, in the olive orchard IRRIX was able to establish an RDI strategy and induced moderate-to-severe stress according to the vigour and apparent electrical conductivity (ECa) values, homogenizing the yield of plots and increasing production. The use of irrigation controllers based on the water balance is complex because of the uncertainty of the crop coefficients. Feedback with sensors can be used to solve this problem. Some authors, including Dukes and Scholberg (2005) Osroosh et al. (2016) and Vera et al. (2019), used the sensors to activate irrigation when the soil was too dry, while others, including Smajstrla and Locascio (1996), Cáceres et al. (2007) and Muñoz-Carpena et al. (2008), used them to avoid irrigation when the soil was too wet. Therefore, the water balance adjusted by moisture sensors allows modification of the daily irrigation of each plot and the maintenance of a coordinated hydraulic scheme for the whole orchard.

Literature cited

Auzmendi, I.; Mata, M.; Lopez, G.; Girona, J.; Marsal, J. Intercepted radiation by apple canopy can be used as a basis for irrigation scheduling. Agric. Water Manag. 2011, 98, 886-892.

Bastet, G.; Bruand, A.; Voltz, M.; Bornand, M.; Que´tin, P. Performance of available pedotransfer functions for predicting the water retention properties of French soils. In Proceedings of the International Workshop on Characterization and Measurement of the Hydraulic Properties of Unsaturated Porous Media; Riverside, CA, 22–24 October 1997, University of California, Riverside, CA, USA, 1999; pp. 981–992.

Birchak, J.R.; Gardner, C.G.; Hipp, J.E.; Victor, J.M. High dielectric constant microwave probes for sensing soil moisture. Proc. IEEE 1974, 62, 93–98.

Bogena, H.R.; Huisman, J.A.; Schilling, B.; Weuthen, A.; Vereecken, H. Effective calibration of low-cost soil water content sensors. Sensors 2017, 17, 208.

Bravdo, B.; Proebsting, E. L. Use of drip irrigation in orchards. HortTechnology. 1993, 3, 44-49.

Cáceres, R.; Casadesús, J.; Marfà, O. Adaptation of an automatic irrigation-control tray system for outdoor nurseries. Biosyst. Eng. 2007, 96, 419-425.

Carsel, R. F.; Parrish, R. S. Developing joint probability distributions of soil water retention characteristics. Water Resour. Res. 1988, 24, 755-769.

Coelho, E.F.; Or, D. Flow and uptake patterns affecting soil water sensor placement for drip irrigation management. Trans. ASAE. 1996, 39, 2007-2016

Casadesús, J.; Mata, M.; Marsal, J., Girona, J. Automated irrigation of apple trees based on measurements of light interception by the canopy. Biosyst. Eng. 2011, 108, 220-226.

Casadesús, J.; Mata, M.; Marsal, J.; Girona, J. A general algorithm for automated scheduling of drip irrigation in tree crops. Comput. Electron. Agric. 2012, 83, 11-20.

Dane, J.H.; Hopmans, J.W. Water retention and storage. In: Dane, J.H., Topp, G.C. (Eds.), Methods of Soil Analysis. Part 4, SSSA Book Series No. 5. 2002, Soil Science Society of America Journal, Madison WI.

Domínguez-Niño, J.M.; Oliver-Manera, J.; Girona, J.; Casadesús, J. Differential irrigation scheduling by an automated algorithm of water balance tuned by capacitance-type soil moisture sensors. Agric. Water Manag. 2020, 228, 105880.

Domínguez-Niño, J. M.; Bogena, H. R.; Huisman, J. A.; Schilling, B.; Casadesús, J. On the Accuracy of Factory-Calibrated Low-Cost Soil Water Content Sensors. Sensors. 2019, 19, 3101.

Dukes, M. D.; Zotarelli, L.; Morgan, K. T. Use of irrigation technologies for vegetable crops in Florida. Horttechnology. 2010, 20, 133-142.

Dukes, M.D; Scholberg, J.M. Soil moisture controlled subsurface drip irrigation on sandy soils. Appl. Eng. Agric. 2005, 21, 89-101.

Fares, A.; Awal, R.; Bayabil, H. Soil water content sensor response to organic matter content under laboratory conditions. Sensors 2016, 16, 1239.

Girona, J.; Behboudian, M. H.; Mata, M.; Del Campo, J.; Marsal, J. Exploring six reduced irrigation options under water shortage for 'Golden Smoothee' apple: responses of yield components over three years. Agr. Water Manage. 2010, 98, 370-375.

Girona, J.; Del Campo, J.; Mata, M.; Lopez, G.; Marsal, J. A comparative study of apple and pear tree water consumption measured with two weighing lysimeters. Irrig. Sci. 2011, 29, 55-63.

González-Teruel, J. D.; Torres-Sánchez, R.; Blaya-Ros, P. J.; Toledo-Moreo, A. B.; Jiménez-Buendía, M.; Soto-Valles, F. Design and calibration of a low-cost SDI-12 soil moisture sensor. Sensors. 2019, 19, 491.

Kang, S.; van Iersel, M. W.; Kim, J. Plant root growth affects FDR soil moisture sensor calibration. Scientia Hortic. 2019, 252, 208-211.

Marković, M.; Filipović, V.; Legović, T.; Josipović, M.; Tadić, V. Evaluation of different soil water potential by field capacity threshold in combination with a triggered irrigation module. Soil Water Res. 2015, 10, 164-171.

Marsal, J.; Girona, J.; Casadesús, J.; Lopez, G.; Stöckle, C. O. Crop coefficient (KC) for apple: comparison between measurements by a weighing lysimeter and prediction by CropSyst. Irrig. Sci. 2013, 31, 455-463

Matula, S.; Bát'ková, K.; Legese, W.L. Laboratory performance of five selected soil moisture sensors applying factory and own calibration equations for two soil media of di_erent bulk density and salinity levels. Sensors. 2016, 16, 1912.

Millán, S.; Casadesús, J.; Campillo, C.; Moñino, M. J.; Prieto, M. H. Using Soil Moisture Sensors for Automated Irrigation Scheduling in a Plum Crop. Water. 2019, 11, 2061.

Millán, S.; Campillo, C.; Casadesús, J.; Pérez-Rodríguez, J. M.; Prieto, M. H. Automatic Irrigation Scheduling on a Hedgerow Olive Orchard Using an Algorithm of Water Balance Readjusted with Soil Moisture Sensors. Sensors. 2020, 20, 2526.

Muñoz-Carpena, R.; Dukes, M. D.; Li, Y. C.; Klassen, W. Field comparison of tensiometer and granular matrix sensor automatic drip irrigation on tomato. Horttechnology, 2005, 15, 584-590.

Nagahage, E. A. A. D.; Nagahage, I. S. P.; Fujino, T. Calibration and validation of a low-cost capacitive moisture Sensor to integrate the automated soil moisture monitoring system. Agriculture. 2019, 9, 141.

Or, D. Stochastic analysis of soil water monitoring for drip irrigation management in heterogeneous soils. Soil Sci. Soc. Am. J. 1995, 59, 1222-1233.

Osroosh, Y.; Peters, R. T.; Campbell, C. S.; Zhang, Q. Comparison of irrigation automation algorithms for drip-irrigated apple trees. Comput. Electron. Agric. 2016, 128, 87-99.

Parvin, N.; Degré, A. Soil-specific calibration of capacitance sensors considering clay content and bulk density. Soil Res. 2016, 54, 111-119.

Qu, W.; Bogena, H.R.; Huisman, J.A.; Schmidt, M.; Kunkel, R.; Weuthen, A.; Schilling, B.; Sorg, J.; Vereecken, H. The integrated water balance and soil data set of the Rollesbroich hydrological observatory. Earth Syst. Sci. Data 2016, 8, 517–529.

Qu, W.; Bogena, H.R.; Huisman, J.A.; Vereecken, H. Calibation of a Novel Low-Cost Soil Water Content Sensor Based on a Ring Oscillator. Vadose Zone J. 2013, 12.

Rowland, R.; Pachepsky, Y. A.; Guber, A. K. Sensitivity of a Capacitance Sensor to Artificial Macropores. Soil Sci. 2011, 176, 9-14.

Robinson, D.A.; Gardner, C.M.K.; Evans, J.; Cooper, J.D.; Hodnett, M.G.; Bell, J.P. The dielectric calibration of capacitance probes for soil hydrology using an oscillation frequency response model. Hydrol. Earth Syst. Sci. Discuss. 1998, 2, 111–120.

Rosenbaum, U.; Bogena, H.R.; Herbst, M.; Huisman, J.A.; Peterson, T.J.; Weuthen, A.; Western, A.H.; Vereecken, H. Seasonal and event dynamics of spatial soil moisture patterns at the small catchment scale. Water Resour. Res. 2012, 48, 1–22.

Rosenbaum, U.; Huisman, J. A.; Vrba, J.; Vereecken, H.; Bogena, H. R. Correction of temperature and electrical conductivity effects on dielectric permittivity measurements with ECH2O sensors. Vadose Zone J. 2011, 10, 582-593.

Rosenbaum, U.; Huisman, J.A.; Weuthen, A.; Vereecken, H.; Bogena, H.R. Sensor-to-Sensor Variability of the ECHO EC-5, TE, and 5TE sensors in dielectric liquids. Vadose Zone J. 2010, 9, 181–186.

Sakaki, T.; Limsuwat, A.; Smits, K.M.; Illangasekare, T.H. Empirical two-point _-mixing model for calibrating the ECH2O EC-5 soil moisture sensor in sands. Water Resour. Res. 2008, 44.

Smajstrla, A.G.; Locascio S.J. Tensiometer-controlled drip irrigation scheduling of tomato. Appl. Eng. Agr. 1996, 12, 315–319.

Soulis, K. X.; Elmaloglou, S.; Dercas, N. Investigating the effects of soil moisture sensors positioning and accuracy on soil moisture based drip irrigation scheduling systems. Agric. Water Manag., 2015, 148, 258-268.

Spelman, D.; Kinzli, K.D.; Kunberger, T. Calibration of the 10HS soil moisture sensor for Southwest Florida Agricultural Soils. J. Irrig. Drain. Eng. 2013, 139, 965–971.

Tawutchaisamongdee; Wonprasaid, S.; Horkaew, P.; Machikowa, T. Moisture distribution patterns in loamy sand and sandy clay loam soils under drip irrigation system. Proceedings of ISER 124th International Conference, Tokyo, Japan, 29th -30th April 2018, Pages: 86-89.

Topp, G.C.; Davis, J.L.; Annan, A.P. Electromagnetic determination of soil water content: Measurements in coaxial transmission lines. Water Resour. Res. 1980, 16, 574–582.

Vera, J.; Conejero, W.; Conesa, M. R.; Ruiz-Sanchez, M. C. Irrigation factor approach based on soil water content: A nectarine orchard case study. Water 2019, 11, 589

Wösten, J. H. M.; Lilly, A.; Nemes, A.; Le Bas, C. Development and use of a database of hydraulic properties of European soils. Geoderma. 1999, 90, 169-185.

CONCLUSIONS

Based on the objectives proposed in this PhD thesis, the main conclusions drawn from its four chapters are the following:

- The two-step capacitance moisture sensor calibration under laboratory conditions improves the accuracy of SWC measurements. The RMSE involved in the first step of the calibration, once converted to SWC, is in the order of 0.006 $cm^3\ cm^{-3}$, which includes the differences between individual 10HS sensors in how their electronics perceive the dielectric permittivity of the surrounding media. The RMSE involved in the second step is up to 0.014 $cm^3\ cm^{-3}$, which refers to the conversion from dielectric permittivity to SWC for the specific soil used in this study.

- HYDRUS-3D allows prediction of SWC dynamics at different soil positions in a drip irrigated orchard. Parameterization of HYDRUS-3D with the soil hydraulic parameters obtained from the laboratory method of HYPROP + WP4C provided a good fit between the simulations and measurements by neutron probe and tensiometers. Parameterization could further be improved by calibration of parameter n using a subset of the neutron probe measurements.

- HYDRUS-3D simulations show that the expected soil water dynamics of the wet bulb can explain part of the difference in the SWC recorded by sensors located at equivalent depths and positions relative to the dripper. These differences are explained by the heterogeneous and fluctuating distribution of soil water produced by the dripper. According to the virtual sensors simulated by HYDRUS-3D, the estimated range of RMSE in the measurement of SWC explained by the predictable dynamics of the wet bulb is up to 0.02 $cm^3\ cm^{-3}$.

- In a real orchard, the soil surface wetted by individual drippers is irregular and varies in size, shape and centring relative to the dripper. In the vertical of the sensor installation positions, in the uppermost 12 cm of the soil, SWC is highly variable between individual drippers, with an RMSE of up to 0.085 $cm^3\ cm^{-3}$.

- The SWC recorded by capacitance soil moisture sensors installed in a drip-irrigated orchard shows large differences between sensors installed in equivalent locations in terms of depth and position relative to the dripper, with an RMSE of between 0.02 and 0.07 $cm^3\ cm^{-3}$, depending on the sensor location. This is much larger than the effect of sensor calibration and, thus, it reduces the practical significance of performing specific sensor calibration for their mainstream usage in commercial orchards.

- The observed differences between sensors are larger than expected by HYDRUS-3D simulations and smaller than measured between drippers in the uppermost 12 cm of the soil. This suggests that the observed differences between sensors result from the summation of two coexisting processes: first, from the predictable heterogeneity and fluctuations in SWC determined by the dynamics of the wet bulb; and second, from the unpredictable differences in the dimensions, shape and exact position of the wet bulbs caused by the arbitrary path followed by the irrigation water at the soil surface, between the dripper and infiltration into the soil.

- Rather than a fault of the measuring principle, the large sensor-to-sensor differences in the measurement of SWC by capacitive soil moisture sensors in drip-irrigated orchards is inherent to the actual soil water conditions there. Usage of the sensors in such scenario should be adapted to the practical limitations derived from a small volume of sensitivity on a sharply defined distribution of soil water.

- The cycles of irrigation, water distribution in the soil and uptake by roots produce different patterns in the measured SWC dynamics depending on the sensor depth and position relative to the dripper. Overall, close to the dripper the effects of irrigation cycles are faster and more intense. On the other hand, at the mid-point position between drippers the response to irrigation tends to be more attenuated but can better reflect the aggregated balance of water inputs and outputs of the preceding several days and not only that of the same day. In this study, the patterns of SWC with greater interest regarding their response to irrigation cycles were recorded at 30 cm depth, coinciding with the maximum root activity.

- Despite the described concerns with respect to the practical uncertainty in the SWC monitored by capacitive soil moisture sensors installed in drip-irrigated orchards, their usage for automated irrigation scheduling is feasible. Below are some recommendations for their usage in this kind of application:
    - ✓ Always locate the sensors in predefined positions relative to the dripper and use redundant sensors.
    - ✓ Sensor interpretation is based on the trend of the sequence of the daily driest measurements in the last few days. A positive slope is generally associated to positive soil water balance, and vice versa.
    - ✓ Irrigation prescriptions are based on an algorithm of water balance locally adjusted by feedback from the sensors.

ADVANCEMENT IN THE STATE OF THE ART

As reported in the Introduction, numerous studies have been published in the literature on the laboratory characterization of capacitance-type soil water sensors as well as on their use in field conditions, especially in scenarios where soil water content heterogeneity is not very large, such as in rainfed and sprinkler or flood-irrigated crops. However, drip-irrigated orchards are among the scenarios of greatest interest for the application of smart irrigation approaches and the conditions there pose certain challenges to the use of these sensors which justifies the need to search for more sophisticated approaches. Previous experiences in this type of scenario do exist and they typically report on the difficulties encountered because of the differences between sensors.

In this context, we believe that the main value of the present Thesis is that it focuses on the real problem that the conditions of such scenarios pose for attaining the opportunities of using soil-water sensors in irrigation control. Here, the sensors are not seen as a mere data source for some kind of soil monitoring purpose. Instead, they are analysed from the perspective of a precise role in the workflow of automated irrigation scheduling. This avoids an abstract evaluation, enables greater precision as to their relevant traits in terms of performance, and allows the conception of practical recommendations to compensate for their limitations. Chapter I quantifies the intrinsic uncertainties involved in the measuring principle. In the first step, where a given sensor model (Decagon's 10HS) perceives the dielectric permittivity of its surrounding media. In the second step, where this dielectric permittivity is related to the SWC of a specific soil. Independently from the sensors, Chapter II demonstrates an approach for configuring the HYDRUS-3D model to accurately simulate the soil water dynamics of the scenario of interest. With this calibrated model, the expected patterns of soil water dynamics below a dripper were obtained and validated at a coarse spatial resolution by neutron probe measurements. In Chapter III the patterns of SWC recorded by capacitance sensors were observed to be more sharply defined, irregular and variable than those expected by the HYDRUS-3D model, presumably because of the irregular and arbitrary patterns for irrigation distribution at the soil surface below a dripper. It is concluded that, because of that, and to a certain degree, variability in SWC measurement is unavoidable and representative of the real soil environment in drip-irrigated orchards. Therefore, when sensors are used in these conditions there is a need to be aware of the uncertainties in the SWC data collected. Chapter IV demonstrates that, despite the limitations described above, these sensors can effectively be used for controlling drip irrigation in orchards. The chapter describes specific approaches followed to compensate for the sensor limitations. Among these, special emphasis is given to the use of a scheduling algorithm based on the soil water balance tuned by sensors. In this case, the water balance strengthens the predictability and reliability of the irrigation prescriptions, whilst the sensors allow site-specific, spontaneous adaptation of the water balance model. In addition, sensor data is interpreted in terms of the fit between the irrigation doses and the actual water consumption by the crop, by looking at the trend of the driest

daily SWC measured in consecutive days. Robustness is ensured by automated rating of sensor reliability and aggregation of the sensors considering these reliabilities in a weighted average. In that trial, capacitance soil moisture sensors were the only data source for site-specific spontaneous adaptation of the IRRIX algorithm, which managed to provide differential irrigation to tree plots of different vigour, coherent with their irrigation requirements determined by other methods.

Overall, this Thesis concludes that the intrinsic performance of the sensors is adequate, though it could be improved if their volume of sensitivity was larger. However, the conclusions of this Thesis emphasize that, in drip-irrigated orchards, it is crucial to adapt the deployment of the sensors and the usage of their recorded data taking into account the practical limitations of the sensors.

In addition to the four scientific papers that have been published in the literature, the results and conclusions of this Thesis are expected to have an impact on the practical use of soil moisture sensors in orchards. Recommendations can be derived for sensor end users, sensor integrators in irrigation-support platforms and sensor manufacturers.

FUTURE WORK

Despite the advances made in this PhD thesis towards the optimization of the use of capacitance-type moisture sensors in automated irrigation scheduling, the automation and simulation of irrigation continues to constitute an opportunity for future research in the field of agriculture. Of particular interest is the applicability of irrigation automation in a real large-scale scenario and an evaluate of its efficacy and efficiency.

Based on the results obtained in this thesis, future lines of research can include:

- The application of automated irrigation scheduling in other crops and irrigation systems. An example would be to apply it in an orchard where different IRRIX-managed irrigation sectors were compared with different irrigation sectors managed by an expert irrigator based on meteorological data and crop coefficients.

- The application of the HYDRUS-3D model to manage the soil salinity and nutrients of different crops.

ABOUT THE AUTHOR

Biography

Jesús María Domínguez Niño (Valladolid, 1989) carried out his Environmental Sciences studies at Miguel de Cervantes European University (2007-2012) and his Environmental Engineering studies at Valladolid University (2013-2014), where he began his first steps in the world of research. In June 2016, he joined the Efficient Use of Water in Agriculture program headed by Dr. Jaume Casadesús in the Institute of Agrifood Research and Technology (IRTA). He was awarded a research contract by Spain's National Institute for Agricultural and Food Research and Technology (Spanish initials: INIA). His PhD studies have focussed on the characterization of capacitance soil moisture sensors for the automated scheduling of drip irrigation in orchards. Research for the PhD studies included a 3-month research stay in the Institute of Land, Water and Environment (Spanish initials: ITAMA) at the Universidad Nacional del Comahue in Neuquén (Argentina) under the supervision of Dr. Federico Horne and Dr. Gabriela Polla, a 3-month research stay in the Agrosphere Institute (IBG-3) at the Forschungszentrum Jülich, in Jülich (Germany) under the supervision of Dr. Heye Reemt Bogena and Dr. Johan Alexander Huisman, and a 3-month research stay in the Department of Land, Air, and Water Resources, at the University of California Davis in Davis (US) under the supervision of Dr. Isaya Kisekka and Dr. Iael Raij.

Publications in international journals

- **Domínguez-Niño, J. M**.; Bogena, H. R.; Huisman, J. A.; Schilling, B.; Casadesús, J. On the accuracy of factory-calibrated low-cost soil water content sensors. Sensors, 2019, 19, 3101.

- **Domínguez-Niño, J. M**., Oliver-Manera, J., Girona, J., Casadesús, J. Differential irrigation scheduling by an automated algorithm of water balance tuned by capacitance-type soil moisture sensors. Agricultural Water Management, 2020, 228, 105880.

- **Domínguez-Niño, J. M**.; Arbat, G.; Raij-Hoffman, I.; Kisekka, I.; Girona, J., Casadesús, J. Parameterization of soil hydraulic parameters for HYDRUS-3D simulation of soil water dynamics in a drip-irrigated orchard. Water, 2020, 12, 1858.

- **Domínguez-Niño, J. M**.; Oliver-Manera, J., Arbat, G., Girona, J., Casadesús, J. Analysis of the variability in soil moisture measurements by capacitance sensors in a drip-irrigated orchard. Sensors, 2020, 20, 5100.

Others scientific disseminations

- Casadesús, J; **Domínguez-Niño, J. M.** Lògica del control de reg. In technical dossier "Conceptes del reg de precisió".

- **Domínguez-Niño, J. M.**; Casadesús, J. Ús de sensors d'humitat per controlar el Reg. In Butlletí de l'Oficina del Regant (July 2020).

Contributions to conferences

- **Domínguez-Niño, J. M.**, Oliver-Manera, J., Casadesús, J. Monitorización de la humedad del suelo alrededor de un gotero. XXXV Congreso Nacional de Riegos. June 6-8th, 2017. Tarragona (Spain) **(Oral presentation).**

- Casadesús, J., **Domínguez-Niño, J. M.**, Oliver-Manera, J. IRRIX, una plataforma web para la supervisión y control automatizados del riego. XXXV Congreso Nacional de Riegos. June 6-8th, 2017. Tarragona (Spain) (**Oral presentation**).

- **Domínguez-Niño, J. M**., Oliver-Manera, J., Casadesús, J. Análisis de la humedad del suelo en riego localizado mediante sensores. Congreso Internacional de Aguas, Ambiente y Energía. October 11st-13th 2017. Mendoza (Argentina) (**Poster**).

- **Domínguez-Niño, J. M.**, Casadesús, J. Comparación de observaciones experimentales y simulaciones con HYDRUS 2D del riego por goteo aplicado en cultivo de manzanos. Jornada de Doctorandos 2018. April 16th, 2018. Lleida (Spain) (**Poster**).

- **Domínguez-Niño, J. M.**, Casadesús, J. Análisis comparativo de la humedad registrada por sensores en parcela de manzanos regada por goteo y simulaciones con HYDRUS 2D. XXXVI Congreso Nacional de Riegos. June 5-7th, 2018. Valladolid (Spain) (**Oral presentation**).

- **Domínguez-Niño, J. M.**, Casadesús, J., Bogena, H.R., Huisman, J.A. Fuentes de variabilidad que intervienen en la medición de contenido de agua en el suelo en parcelas de manzano regadas por goteo. XXXVII Congreso Nacional de Riegos. June 4-6th, 2018. Don Benito, Badajoz (Spain) (**Oral presentation**).

- **Domínguez-Niño, J. M.**, Casadesús, J., Bogena, H.R., Huisman, J.A. Reliability of capacitance type soil moisture sensors for their use in automated scheduling of drip irrigation orchards. IX International Symposium on Irrigation of Horticultural Crops. 17-20th, June 2019. Matera (Italy) (**Poster**).

- **Domínguez-Niño, J. M.**, Arbat, G., Raij, I., Kisekka, I., Casadesús, J. Ideal location of capacitance soil moisture sensors in a drip irrigated apple orchard. Irrigation Show 2019. December 2nd-6th, 2019. Las Vegas, Nevada (United States) (**Poster**).

- **Domínguez-Niño, J. M.**, Arbat, G., Bogena, H.R., Kisekka, I., Casadesús, J. Caracterización y simulación de la dinámica del agua en el suelo para la programación automatizada del riego por goteo en cultivos leñosos. XXXVIII Congreso Nacional de Riegos. June 2nd-4th, 2020 (postponed). Cartagena, Murcia (Spain) (**Oral presentation**).

Workshops

- International Irrigation Course. Programme of Efficient Use of Water in Agriculture. IRTA. October, 2016. Lleida (Spain).

- Uso de sensores para optimización del riego y la fertilización. Centro de Investigaciones Científicas y Tecnológicas de Extremadura y Cajamar. November, 2016. Guadajira, Badajoz (Spain).

- HYDRUS short course and workshop. Advanced modelling of water flow and contaminant transport in porous media using the HYDRUS and HPI software packages. Faculty of Agrobiology, Food and Natural Resources. Czech University of Life Sciences Prage. March, 2017. Prague (Czech Republic).

- Programació del reg amb sensors d'humitat del sòl. Departament d'Agricultura, Ramaderia, Pesca i Alimentació. November, 2017. Tárrega, Lleida (Spain).

- International Irrigation Course in the almond tree. programme of Efficient Use of Water in Agriculture. IRTA. January, 2019. Lleida (Spain).

Stays in national research centers

- Departament d' Enginyeria Quimica, Agraria i Tecnología Agroalimentaria. Universitat de Girona, Girona (Spain) (January, 2019)

Stays in international research centers

- Instituto de Tierras, Agua y Medio Ambiente (ITAMA), Universidad Nacional del Comahue, Neuquén (Argentina) (September-December, 2017).

- Agrosphere Institute (IBG-3), Forschungszentrum Jülich GmbH, Jülich (Germany) (September-December, 2018).

- Department of Land, Air, and Water Resources, University of California Davis, Davis, (United States of America) (September-December, 2019).